A NOVEL ELECTROMAGNETIC TECHNIQUE FOR REMOTE REPOSITIONING OF COOLANT TUBE SPACERS IN CANDU NUCLEAR REACTORS

By

YOUSSEF (JOSEPH) HANNA DABLEH

A Thesis

Submitted to the School of Graduate Studies

in Partial Fulfilment of the Requirements

for the Degree of

Doctor of Philosophy

McMaster University

EM REPOSITIONING OF COOLANT TUBE SPACERS IN CANDU REACTORS

DOCTOR OF PHILOSOPHY (1986)

McMASTER UNIVERSITY
(Electrical and Computer Engineering)
Hamilton, Ontario

TITLE: A Novel Electromagnetic Technique for Remote Repositioning of Coolant Tube Spacers In CANDU Nuclear Reactors

AUTHOR: Youssef Hanna Dableh, B.Sc.E. (University of New Brunswick)

M.Sc.E. (University of New Brunswick)

SUPERVISOR: Professor Raymond D. Findlay

NUMBER OF PAGES: xxii and 301

ABSTRACT

On August 1, 1983, a sudden failure of a coolant tube, known as a pressure tube, was experienced in one of the CANDU reactors at Pickering 'A' Nuclear Generating Station of Ontario Hydro. A contributing factor to the rupture of the tube was a contact for a period of several years between the tube and an outer coaxial tube, called the calandria tube. The contact between the pressure tube and calandria tube occurred because the annular spacers (garter springs), used to maintain the coaxial configuration when the uranium fuel bundles are loaded inside the pressure tube, had shifted out of their design locations during the construction stage and subsequent hot conditioning of the reactor. The displacement of the spacers was attributed to vibration induced by various sources and was determined to have taken place prior to loading the fuel bundles in the reactor.

Since the garter springs are not directly accessible by mechanical means, extensive dismantling of the fuel channels would have been necessary to reposition the springs in their designated locations. This Thesis describes a novel

electromagnetic method to reposition the garter springs without dismantling the fuel channels. The method consists of inserting an electromagnetic coil into the pressure tube to a location adjacent to the spacer and passing a time-varying electric current in the coil to induce secondary currents in the pressure tube and the spacer. The interaction between the induced current in the spacer and net magnetic field in the spacer region results in an electromagnetic force having an axial component large enough to displace the spacer in the required direction. In practice, current impulses generated by discharging a large capacitor bank were used to achieve the required garter spring displacement.

The new method was successfully developed and implemented to reposition the displaced garter springs in five new CANDU reactors in Ontario. The savings in the reactor repair cost, interest charges and replacement energy costs were in the order of hundreds of millions of dollars. Equally large benefits and savings will be realized if the need to use this technique in commissioned reactors becomes mandatory. The practical aspects of the work including the design of pulse power cables and a coil sufficiently compact to fit in the pressure tube, but strong enough to withstand

the stress, were developed by the author at the Ontario Hydro laboratories. The Thesis describes not only this aspect but also develops a model for analysis of the operation and design of the device.

There are a number of other applications of the electromagnetic technique which may also benefit from the analysis, especially for electromagnetic metal forming and fusion technologies.

ACKNOWLEDGEMENTS

Dr. Ray Findlay has not only served as supervisory for this work and for this thesis, he has also been mentor, friend, counsellor, and "in loco parentis" my constant inspiration. I acknowledge his help, the many weekends, and evenings he gave freely to help guide me, with heartfelt thanks. Dr. Gary Ford has supervised this work at Ontario Hydro and served on the University Supervisory Committee. His encouragement, guidance and persistent effort over many months ensured the successful development and implementation of this work. I gratefully acknowledge his contribution. Special thanks are directed to Dr. Mohamed El-Kady for serving on the Supervisory Committee and for his invaluable guidance, help and advice.

The author is also grateful to the officers of Ontario Hydro for making provision for me to do the project and also to the many people in the various divisions of Ontario Hydro who contributed most significantly to its successful completion. There are several people in associated industries who have also assisted me particularly in the experimental portion of the work. As well, the

author acknowledges with thanks the support of the Natural Science and Engineering Research Council for its support. The author is also most grateful to McMaster University for admitting him as the first part-time Ph.D. candidate to the Electrical and Computer Engineering Department.

Najat, the author's wife, for her many sacrifices in enabling the author to work, for her deep understanding and undying patience, I dedicate the work. Without her support, both in terms of moral encouragement and untiring effort, the work and this thesis could not even have been attempted.

TABLE OF CONTENTS

Page

Page

Page

Page

LIST OF FIGURES

Figure		Page

Figure		Page

Figure		Page

LIST OF TABLES

CHAPTER 1

INTRODUCTION

1.1 Thesis Objectives

A novel electromagnetic technique to reposition the coolant tube spacers in the fuel channels of CANDU nuclear reactors was successfully developed in the fall of 1983 at Ontario Hydro Research Division. The need to reposition dislocated spacers in non-commissioned reactors was discovered subsequent to the rupture of a pressure tube in one reactor at the Pickering Nuclear Generating Station. A contributing factor to the failure of the tube was the fact that the annular spacers (garter springs), used to maintain the coaxial configuration between the pressure tube and its surrounding calandria tube, had been displaced longitudinally for a number of years. Subsequent to this finding, it was discovered that a number of garter springs in non-commissioned reactors were displaced due to vibration induced by various sources, during the construction

stage. Because the garter springs are not directly accessible by mechanical means, extensive dismantling of the fuel channels would have been necessary to repositon the springs in their designated locations.

The primary objectives of this thesis are to present the new concept of the electromagnetic repositioning method and to describe the experimental and theoretical milestones achieved during the development, simulation and implementation of this method. A secondary objective is to provide a comprehensive documentation for the theoretical and experimental development of the technique, the difficulties encountered during the implementation of the technique and the corrective measures developed, and to highlight such other developments arising out of the research that have particular advantages not only for this application but for pulse power technologies in general.

1.2 Historical Background

On August 1, 1983, a sudden pressure tube rupture was experienced in reactor number two at the Pickering 'A' Nuclear Generating Station (NGS). A contributing factor to the rupture of the tube was the fact that the annular spacers, known as garter springs (G/S), used to maintain the coaxial configuration between the pressure tube (P/T) and

its surrounding calandria tube (C/T), had been displaced longitudinally for a number of years. The displacement of the G/S allowed the P/T to come in contact with the C/T when the uranium fuel bundles were loaded into the P/T: such contacts were enhanced further after the P/T started to sag due to longitudinal growth caused by Neutron bombardment. The annular space between the P/T and C/T is filled with an inert gas (Nitrogen or CO_2) which can be circulated and monitored to detect any heavy-water leak. The primary heat transport fluid is heavy water with an outlet temperature of about 295°C. The P/T is insulated from the cool heavy-water moderator by the C/T and the annular space. Local contact between the P/T and C/T over the period of many years was thought to have contributed to conditions which led to the P/T rupture in unit 2 at the Pickering 'A' NGS [1]. Apparently, the local contact was thought to have caused hydride blistering and helped to accelerate the propagation of hydride layers through the wall of the P/T.

Inspection of the fuel channels in non-commissioned reactors indicated that the G/S had shifted from their design positions during the construction stage and thereafter during hot conditioning of the primary heat transport system. The probable cause of G/S displacement has been attributed to vibrations created by various sources. Vibration induced motion of the spacers was possible due to the

fact that they are loose with respect to the P/T: they conform to the inner radius of the C/T and come in contact with the P/T only when the latter is loaded with the uranium fuel bundles, or if the spacer tilts to an inclined plane from the original vertical position. This arrangement was designed to allow small relative axial movement between the P/T and C/T without causing any metallurgical damage to the outer surface of the P/T and to minimize heat losses from the P/T to the moderator [2].

Sufficient evidence has been gathered to confirm that the movement of the spacers is minimal after a reactor is loaded with fuel bundles, effectively pinching them between the P/T and C/T. All of the findings mentioned above were established just prior to the scheduled start-up of unit 6 at Bruce 'B' NGS. This unit could not be brought into service because it was deemed mandatory to reposition the displaced garter springs in new reactors in order to avoid potential P/T failures similar to that of August 1, 1983.

Since there is no direct mechanical access to the spacers after assembly of the reactor fuel channels, the most obvious method and the only available option at that time to reposition the G/S would have involved major dismantling of the fuel channel and replacement of the P/T and

associated end fittings. The cost of such a reactor repair and the cost of energy replacement during the repair was prohibitive. The novel electromagnetic technique presented in this thesis is an alternative method for repositioning these spacers [3,4]: it does not require direct mechanical access. The fuel channel need not be disassembled and the required repair time is minimal.

The electromagnetic technique was conceived and proposed on October 13, 1983. Because of the excessively high costs of shutdown of operating reactors, and delays in commissioning reactors, it was necessary to establish a solution technique in as short a time as conceivable. In spite of several technical difficulties, the feasibility of the technique was demonstrated experimentally within one week. The extreme urgency imposed by the in-service schedule of two reactors at Bruce 'B' NGS necessitated the establishment of an extensive development program to carry the technique from the conceptual stage to the application stage within a time frame of eight weeks. Further development and optimization of the technique, with a strong emphasis on experimental work, were carried out from January to August, 1984. Before the end of 1984, garter springs repositioning programs in five CANDU reactors at Bruce and Pickering NGS were completed. Because it was not possible to carry out any theoretical analysis in support of the

technique during the crash development program, a detailed theoretical analysis program was initiated in September 1984 to simulate the electromagnetic repositioning process and to establish theoretical models that could be used for future development of the concept.

1.3 Description of the Problem

A simplified illustration of a fuel channel in CANDU nuclear reactors is shown in Figure 1.1. In each reactor there are either 390 or 480 channels depending on reactor size. In each channel there are four spacers. The P/T is approximately 6.1 m long, 4.2 mm thick, and has an inner diameter of 104 mm. All of the P/T, G/S and C/T are made of non-magnetic zirconium alloy which has an electrical conductivity of 1.246×10^6 S/m (approximately 47 times less than the conductivity of copper). The C/T is only 1.5 mm thick: its ends are flared to fit the bore of the tube sheet into which it is mechanically rolled. In some fuel channels, one or more of the G/S were shifted to the end sections of the fuel channel. This created an additional difficulty for the repositioning process since the G/S would have to be squeezed slightly as it is pushed back into the annular section.

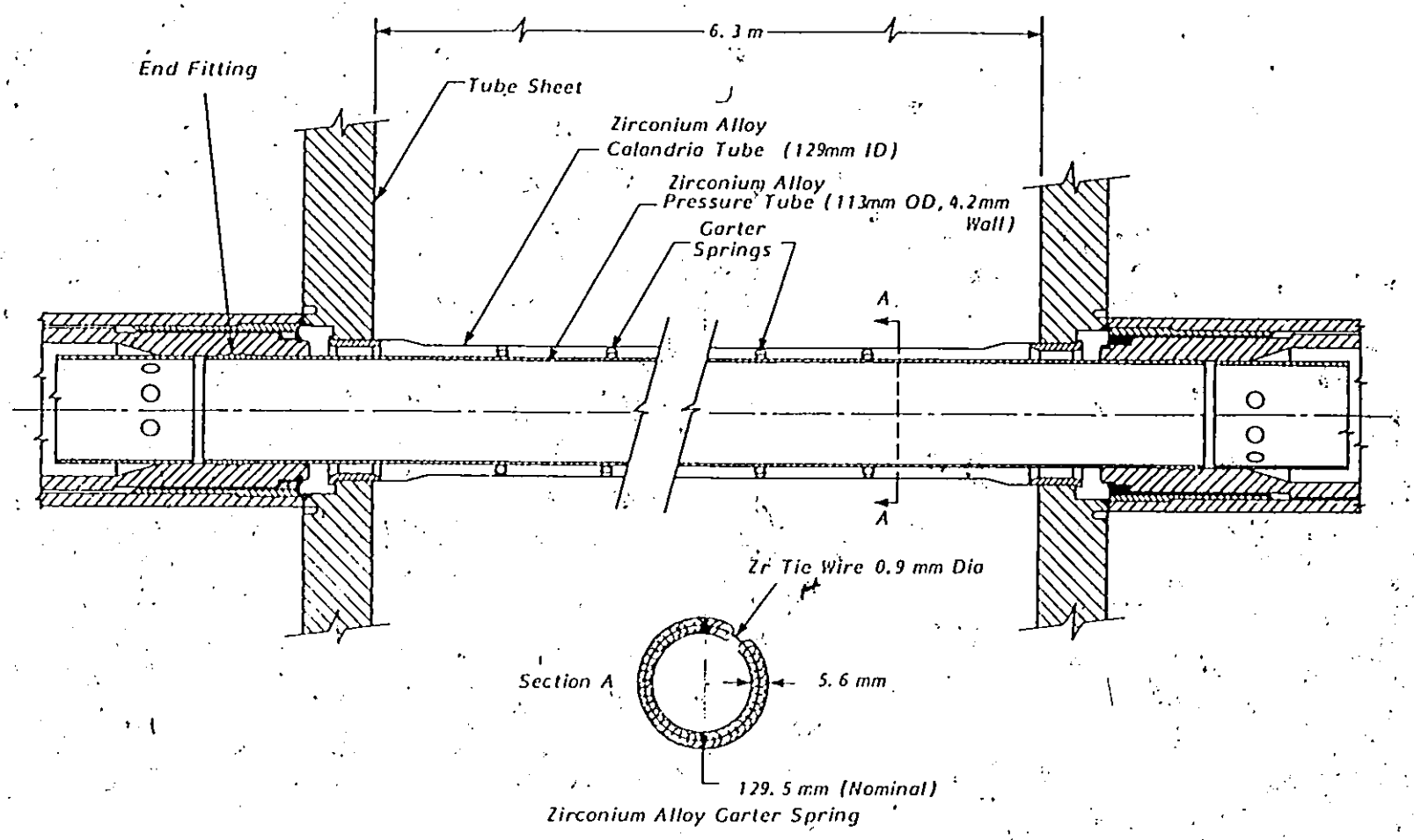

Figure 1.1

Simplified illustration of a fuel channel in CANDU nuclear reactors.

A survey of the G/S location in the fuel channels of units 5 and 6 at Bruce 'B' NGS was made using radiographic or eddy-current-probe locating methods. The survey indicated that one or more G/S in eighty percent of the channels needed to be repositioned. The amount of G/S displacement in each fuel channel varied from a few centimeters to several meters. In some extreme cases all four G/S were shifted to one end of the fuel channel. The total amount of G/S displacement in each unit was approximately 580 meters. In total, there were five reactors to be repaired: units 5, 6 and 7 at Bruce 'B' NGS and units 7 and 8 at Pickering 'B' NGS. The reactors at Bruce NGS are 800 MW units having 480 channels each, while the reactors at Pickering NGS are 540 MW units having 390 channels each.

In general, the main difficulty in repositioning the G/S was the lack of direct access to the annular space between the P/T and C/T. Other investigators recommended various vibratory methods including sonic vibration. These methods encountered one or more of the following problems:

1. Movement of the spacers away from the designated locations because of their initial orientation. Displaced spacers were tilted toward the right or the left with respect to the vertical plane in which they were

initially installed. When the P/T is subjected to vertical modes of vibration, spacers would move in the same direction as their tilted planes.

2. Simultaneous movement of all four spacers unless special arrangements were made to fix those that did not have to be moved. Development of the necessary measures to fix some of the spacers required several months.

3. Repositioning of two or more G/S that were located close to each other presented a severe problem for most of the vibratory repositioning methods.

4. Repositioning of spacers that were located in or near the flared section of the C/T proved to be impossible with the available methods at that time. Sonic vibration methods may have succeeded to overcome this problem in late 1984 but still suffered from another set of problems that prevented its deployment.

5. The response of G/S to various modes of vibration varied significantly in different channels, because the inlet and outlet pipes attached to the P/T end fittings

were connected at different distances away from the tube sheets and presented different loading depending on the location of the fuel channel in the calandria vessel. Also, the location of the G/S in the fuel channel caused a large variance in its response to any particular mode of vibration.

The above list of problems illustrates the magnitude of the difficulties involved in some of the possible repositioning schemes. The method described in this thesis, and adopted for development, overcame all of these limitations. One vibratory scheme was developed coincidentally such that after the completion of the repositioning program at Bruce B, unit 6, using the electromagnetic method alone, it was able to move individual spacers provided that the spacers were oriented in the proper direction and some distance away from the ends of the fuel channel. This method was then used jointly with the electromagnetic method as outlined in Chapter 3 of this thesis.

The main conceptual difficulties for application of the electromagnetic technique can be summarized as follows:

1. The lack of direct access to the G/S and the presence of the P/T which acts as an electromagnetic shield for

any source electromagnetic field generated within it. Note that the interior of the P/T is the only accessible region of the fuel channel.

2. The fact that both the P/T and G/S are made out of the same material.

3. The poor electrical properties of the G/S (relatively low electrical conductivity and high resistance). Note that the spring itself is open ended and the only secure closed conductive loop is the tie wire, as shown in Figures 1.1 and 1.2.

4. The relatively large thickness of the P/T as compared to the size of the spacer tie wire.

5. The need to create a reasonably large amount of electromagnetic energy in a very small volume, and to transport this amount of energy without any significant distortion over a relatively significant distance.

Initially, the above difficulties along with several other restrictions seemed to be insurmountable from both theoretical and practical points of view. The technical

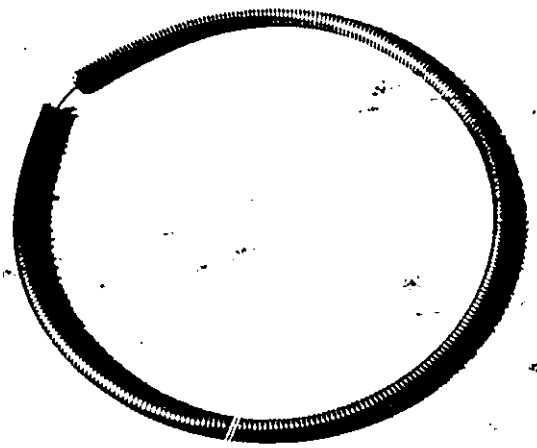

Figure 1.2

Photograph of the G/S.

significance and complexity of these difficulties, as well as the innovative measures designed to overcome them are discussed in detail in subsequent sections and chapters.

1.4 A Proposed Solution Technique

The concept of the electromagnetic technique for G/S repositioning is based on the induction phenomena. The G/S are made of zirconium-niobium 2.5% (weight), a non-magnetic alloy having a relative permeability of approximately unity. The only conceivable way of interacting electromagnetically with the G/S is to induce in them an electrical current. This can be easily achieved if the G/S were to be subjected to a time-varying magnetic field [5, 6 and 7], regardless of how the time variation of this field were to be achieved. However, since the only available access is through the interior of the P/T, subjecting the G/S to a varying magnetic field becomes a complex issue.

The concept consists of inserting an electromagnetic coil into the P/T adjacent to a G/S, as shown in Figure 1.3, and passing a transient electrical current of particular magnitude and waveshape through this coil, so that the generated magnetic field penetrates the wall of the P/T without suffering severe attenuation. The amount of

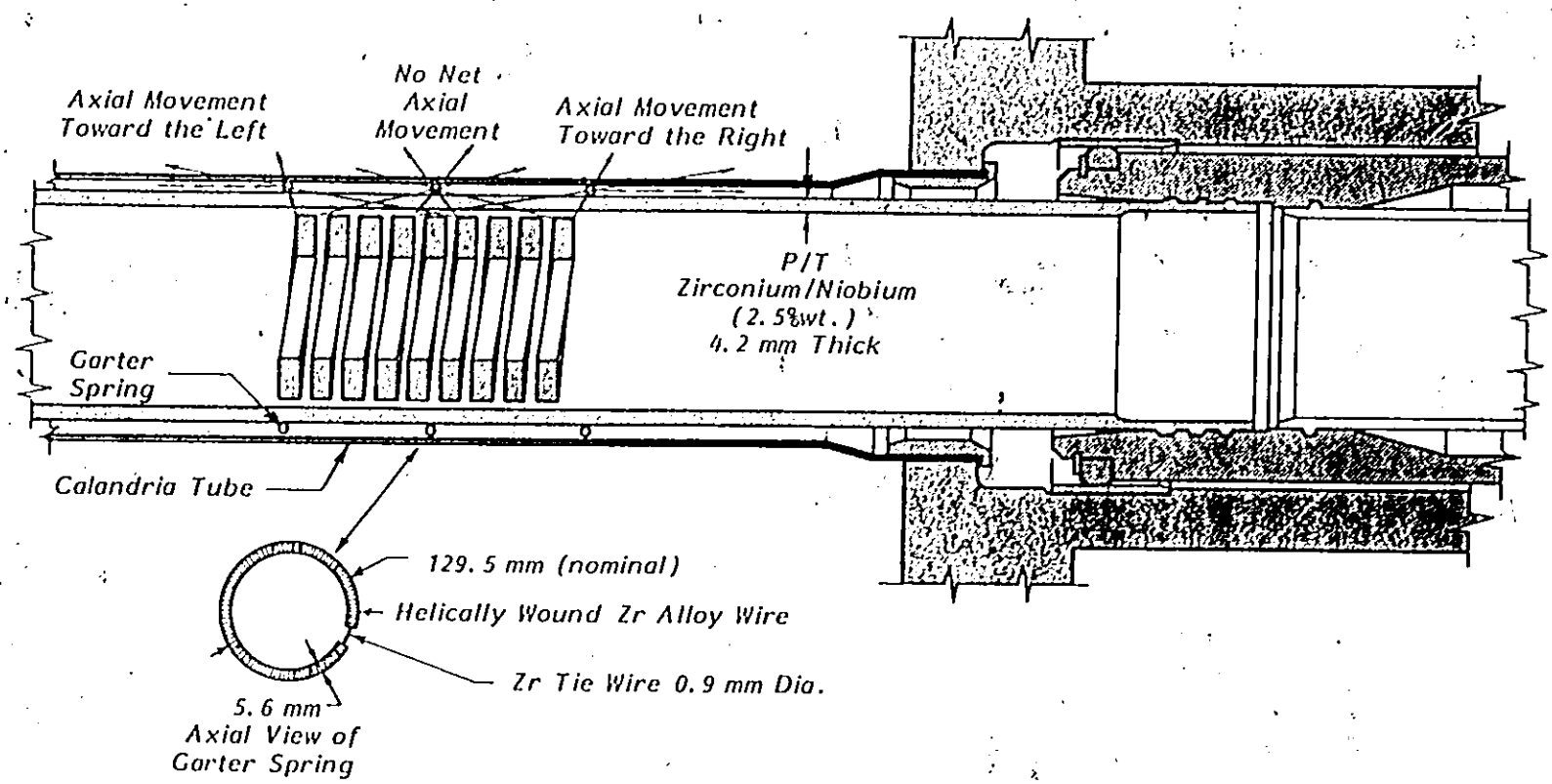

Figure 1.3

Simplified illustration of the fuel channel geometry and the electromagnetic technique for G/S repositioning.

magnetic flux linking the G/S, and its rate of change with respect to time (di/dt), have to be sufficiently high to induce sufficiently high voltage in the G/S. Consequently, induced eddy currents circulate in any closed path in the G/S. The interaction between the induced currents and the magnetic field that created them gives rise to an electromagnetic force, known as Lorentz force [5, 6], which acts on the G/S. If the axial component of this force is large enough to overcome static friction, the G/S can be shifted in the axial direction.

The axial component of the Lorentz force can be maximized by appropriate selection of the coil position with respect to the location of the G/S, as illustrated in Figure 1.4. Placing one end of a solenoidal coil under the G/S is the optimal position as far as the direction of the force is concerned. However, the magnitude of the magnetic flux density in the outer region of the solenoid ends is much smaller than the flux density in the central interior of the solenoid. It is therefore important to note that while the magnetic field effects at the ends of the coil are neglected in most conventional applications, this particular application capitalizes on them very heavily: the magnetic field in those regions is an important factor in creating the required axial force to move the springs remotely.

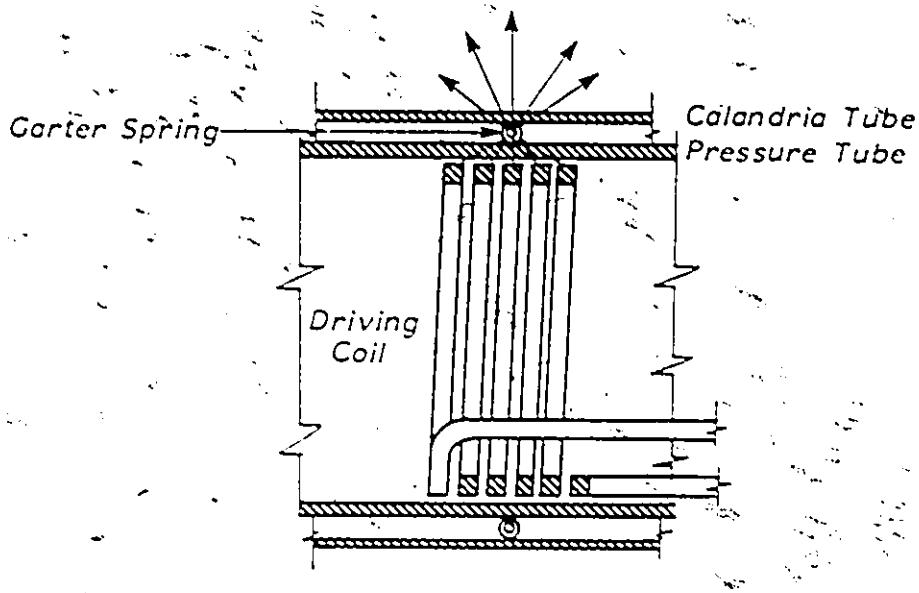

Lateral components of the forces are balanced and so cancel, leaving only the outward-thrusting components. Since the garter spring is restrained in that direction, it does not move at all.

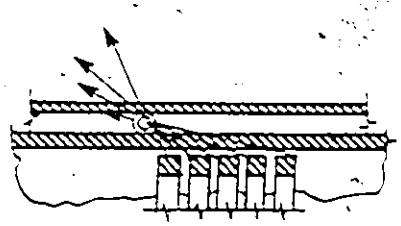

When the lateral components are all on one side, they are additive, and the garter spring is moved to the right or left, accordingly.

Figure 1.4

Forces exerted on the garter spring for various positions with respect to the driving coil position.

So far, two main difficulties have been stated:

1. The attenuation of the magnetic field as it penetrates the wall of the P/T.

2. The need to rely on the magnetic field in regions outside of the coil, where the magnetic field is relatively small.

In addition to the above, the G/S is highly resistive. This emphasizes the need for inducing as high a voltage as possible if a useful induced current and consequently an electromagnetic force are to be generated in the G/S. To increase the induced voltage in the G/S there are two options, each having a penalty associated with it:

1. Increase the rate of change of the magnetic flux with respect to time by increasing the frequency of the source current in the driving coil. This increases the attenuation of the magnetic field across the wall of the P/T.

2. Use an intense source field to increase the flux linkages with the G/S. This increases the secondary interaction between the induced eddy currents in the P/T, C/T and G/S. Moreover, this increases the

mechanical and thermal stresses not only on the coil but also on the P/T.

Having established the need for as strong a source magnetic field as possible, some important questions had to be answered. Can such a field be generated within the confined geometry of the P/T? Can this field be shaped to interact with a thin wire after penetrating a thick tube, made of the same material, without causing any metallurgical damage to this tube and without destroying the drive coil? Can the energy required to generate such a field be transported into the long fuel channel remote from an external source?

The following section outlines the technique for demonstrating the feasibility of the method.

1.5 Feasibility of the Technique

The first set of experiments were performed at the Dobson Laboratories of Ontario Hydro. They were effected using the most readily available source of time-varying current which is supplied by the power utility at 60 Hz. The objective of these initial experiments was to demonstrate that the magnetic field at the ends of a solenoid of

small enough radius to fit inside the P/T could induce the necessary current to move the G/S in the axial direction. Unfortunately, the 110 volts (V) supply circuit used to conduct these experiments was limited by a supply breaker with an upper limit of sixty amperes (A). Also, the number of turns in the solenoid had to be kept below approximately 30 in order to be able to draw 50 to 60 A from that supply. The solenoids used in these experiments were simple single or double-layer coils wound by hand on non-conductive tubes using flexible wires of appropriate sizes.

Using the solenoids described above at a current level below 60 A failed to produce any G/S displacements. Similar results were obtained when a 100 A direct current supply was switched "on" and "off" very quickly to produce an exponentially varying current in the solenoids. However, it was realized from these experiments that a more substantial current was needed. It was also realized that a faster time variation of the magnetic flux is preferable and short single-layer coils with exaggerated spacing between turns to enhance the end effects, were desirable. The above experiments were completed rapidly, setting the stage for the next set of experiments using a modified power supply.

A capacitor bank system used in metal forming experiments was available in the laboratory. Its primary

advantage was that it could provide current pulses ranging in magnitude from a few amperes to several hundred kilo-amperes with a ringing frequency in the range from approximately 100 Hz to several kHz. Figure 1.5 shows a simplified block diagram of the first capacitor bank system used in the second day of the experimental program. This capacitor bank had a capacity of 60 kilojoules (kJ) when charged to 10 kV.

The solenoids used in this set of experiments were made of flexible insulated grounding cable. They have a copper diameter of about 1.0 cm, and were wound by hand on plastic tubes. The number of turns varied from 6 to 12 turns (single layer) and were reinforced with a few layers of electrical insulating tape only. The capacitor bank system was operated in the oscillatory mode by appropriate selection of the circuit resistance (R), inductance (L) and capacitance (C). Typical voltage and current discharge waveforms achieved in this mode of operation are illustrated in Figure 1.6 below.

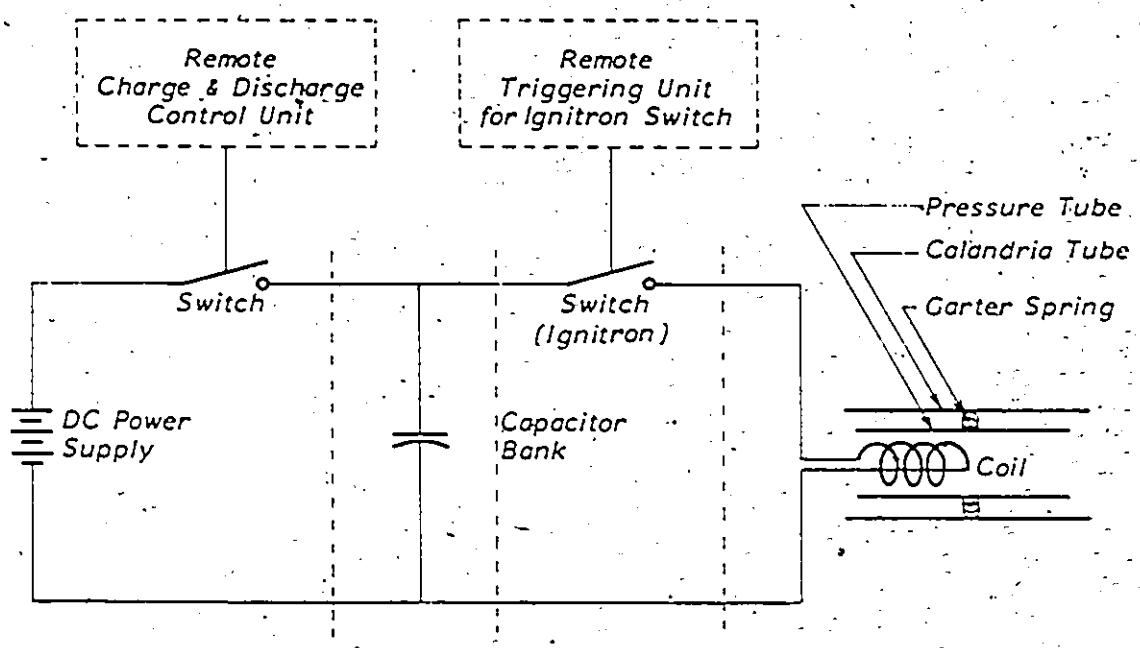

Figure 1.5

Circuit block diagram of the system used to prove the feasibility of the G/S repositioning technique.

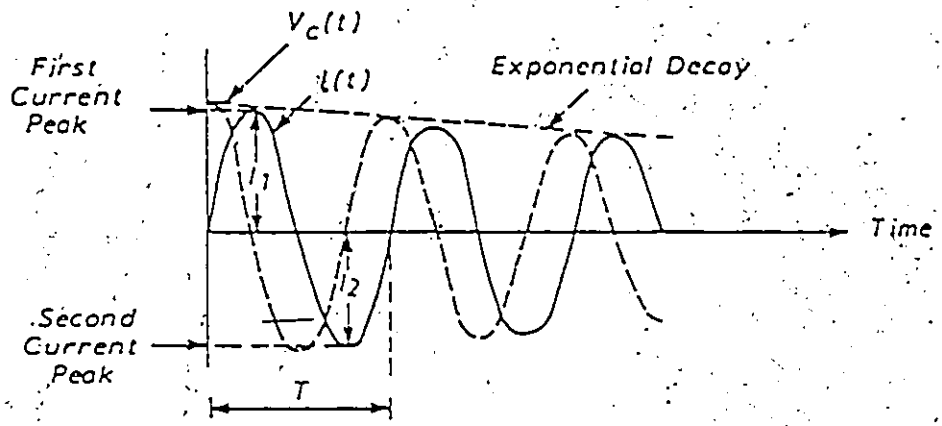

Figure 1.6

Voltage and current waveforms of a capacitor bank discharged in an oscillatory mode ($R \ll 2\sqrt{L/C}$). Oscillations diminish to zero as a function of total circuit resistance

In the first few experiments using the 60 kJ capacitor bank system, the solenoid was inserted inside a plexiglas tube with an actual G/S placed over the first turn on the outside of tube. The magnitude of the first peak of the current pulse was increased gradually by increasing the charging voltage of the capacitor bank. The first positive signs were signalled when minute G/S displacements in the order of 1.0 to 5.0 mm were observed as the first current peak was increased from 2000 to 5000 A. More significant G/S displacements were observed as the current level was increased further.

The next set of experiments were performed in a similar fashion, but with the solenoids inserted into a 50 cm long section of an actual P/T. The first signs of G/S displacement started to appear at about the 12 kA level. Excellent displacements up to 5 cm were observed at current levels of about 80 kA.

However, close examination of the video tapes used to record the actual movements, clearly showed that the P/T and driving coil also moved when the capacitor bank was discharged, since one end only of the P/T specimen was held between two sand bags. This P/T movement made accurate measurement of G/S movement as a function of the current somewhat difficult. There was no doubt left that the G/S could be made to move even when the P/T was completely fixed. The difficulty was to estimate how much of the total G/S movement should be attributed to the movement of the P/T itself.

The above experiments were repeated using various wire loops, including a close replica of the G/S made out of copper. The purpose of replacing the zirconium G/S by a more conductive loop was to allow higher induced currents to flow for the same level of induced voltages. Consequently the resultant axial force would be much higher and the G/S

displacement would increase significantly. Indeed, displacements of the copper replicas of the G/S were observed at the 2 kA level even when the P/T specimen was used. At current levels exceeding 20 kA, displacements of these copper specimens exceeded 50 cm, and eventually these specimens started to bounce off the room wall at least 1.5 m away from their initial position. This gave strong evidence that the higher the current induced in the spring the greater the displacement.

Even though, the amount of G/S displacement was rather small, there was no doubt that the concept of the technique had been reasonably demonstrated. The small G/S displacement observed using the actual springs was a most important milestone. It provided the impetus to develop the technique as a practical and economical solution to reposition the G/S in non-commissioned reactors.

1.6 General Criteria for Development of the Technique

The experimental results described in the previous section were conveyed quickly to upper levels of management at Ontario Hydro. Videotape records of the experiments were seen by these authorities including the Chairman of a task force that had been formed to manage the G/S problem in

non-commissioned reactors. After a detailed discussion of the various issues related to the development and implementation of this technique, the Chairman of the task force outlined the following criteria and conditions for the acceptance of the technique as a base-line repair method:

1. A G/S movement of about five cm should be demonstrated using a fuel channel "mock-up" with both the P/T and C/T present. The mock-up should be about 2 m long and should be prevented from moving during the capacitor bank discharge. A deadline of one week was outlined for this phase.

2. The technique should be sufficiently developed and ready for use at Bruce 'B' NGS within four weeks (for unit 6), or a maximum of eight weeks (for unit 5).

3. The equipment used to generate the necessary current and to implement the technique safely should be readily available or can be acquired within the time frame mentioned above.

4. The integrity of the fuel channels and other reactor components should be preserved, and the implementation of the technique should not cause any electromagnetic

interference with other equipment used in the reactor. Also, all safety regulations, requirements of the National Electric Code and other standards, and the requirements of the Atomic Energy Control Board should be satisfied.

In order to meet the above challenges, an extensive developmental program was outlined. A first priority was assigned to this program for all the needed facilities and resources at the Ontario Hydro Research Division.

1.7 Development and Implementation of the Technique

The first objective of the development program was to demonstrate a G/S displacement of 5 cm, in a fuel channel mock-up having both the P/T and C/T. This objective was met on October 26, 1983: a G/S displacement of 55 mm was achieved using a 91 kJ capacitor bank system, charged to 7 kV (ie, 49% of its rated energy storage capacity) and yielding an oscillatory current having a first peak of 89 kA. At this stage, the technique was assessed by the task force on G/S as the most promising method that Ontario Hydro had for repositioning the dislocated G/S. It was adopted as the base-line technique for repositioning the G/S in the new

reactors. Arrangements to specify and acquire the necessary equipment for "field" use were started immediately.

One of the laboratory capacitor bank systems was sent to Bruce 'B' NGS for the purpose of training operating crews. Work at Ontario Hydro Research Division was continued using a 200 kJ capacitor bank system. Numerous engineering problems related to improvement of the technique, development of durable coils and ensuring the fuel channel integrity were resolved. The capability of the technique to move G/S regardless of their location was fully demonstrated.

Initial tests of the field systems indicated that specifications related to the oscillation of the discharge current were not met because of excessive resistance in the transmission lines. However, there was no choice but to accept these systems, assess what this shortcoming meant in terms of G/S displacement and provide corrective measures as these systems were commissioned and used. It should be remembered that each unit at Bruce NGS produces approximately a million dollars worth of electricity per day and would cost Ontario Hydro about $395,000.00 per day for replacing this energy. Hence time was of the utmost importance in solving the problem.

Part of the solution for the transmission problem was to increase the current level. This, in combination with increased requirements on the discharge duty cycle, had the undesirable effect of shortening the life of the driving coils. Therefore, new programs were outlined to address these and other new issues encountered during the implementation of the technique in units 6 and 5 at Bruce NGS. These programs resulted in the development of superior pulse power coils and coaxial cables and established some major modifications in the design of the capacitor bank systems.

As a result, G/S repositioning programs in the reactors repaired subsequent to the completion of the repositioning program in unit 6 progressed at a much faster rate and with many fewer coils.

During the summer of 1984, experimental work was conducted to demonstrate that the electromagnetic technique can be applied in operating reactors during a shut-down period, but without having to defuel the reactor. Also, experiments were conducted using the high current laboratory at Ontario Hydro to supply 60 Hz alternating current to the driving coil. These experiments proved that the use of 60 Hz ac is a viable alternative. At that stage, the need for

strong theoretical models to carry out an effective and economical optimization of the technique was addressed, since the repositioning work in all five new reactors was nearly completed.

Development of the theoretical models involved the use of advanced numerical methods to calculate the electromagnetic fields generated by the impulse current input. This permitted accurate calculation of the impulse forces, mechanical stresses on the coil and fuel channel components and various other related parameters of interest. The models and computer programs developed in this project can be utilized for a variety of other applications involving complex transient electromagnetic field problems. The development of these models and the methods devised to check validity of the results are described in Chapters four and five of this manuscript.

1.8 Status of the Prior Art

To date there is essentially no record of a prior art to use electromagnetic techniques through a shield to effect movement as described. In the preliminary search report, received from the European patent court [3], the examiner did not cite any patent that contradicts the above

statement. A further detailed computer survey of the literature, conducted in the fall of 1984, did not produce any reference that describes or even recommends such a concept.

However, there is a great body of literature on direct electromagnetic drive mechanisms. From the dawn of electricity generation history, electromagnetic forces have been utilized in a direct fashion in a very wide range of applications, ranging from applications in electrical machines and various electromagnetic actuators to modern electromagnetic levitation and propulsion systems. However, due to the unique requirements of the G/S repositioning application, useful literature related to practical aspects of indirect methods was very limited [8-11].

Another area of interest, which is well covered in the literature, is electromagnetic shielding. Researchers working in this area attempt to minimize the penetration of the electromagnetic fields across the walls of enclosures housing electrical equipment. In some cases, the objective is to confine the electromagnetic fields within the enclosures [12-14], for example large transformer tanks, while in other cases the objective is to prevent external fields from penetrating into the enclosures [15-17], for

example shielded rooms, electronic systems cabinets and rockets. For G/S repositioning, the case was different. The main objective was to maximize the penetration of the electromagnetic fields across the P/T wall, while maintaining a high rate of change of magnetic flux.

The literature on the subject of theoretical modelling and analysis of pulse power applications is limited [18-27]. However, the literature on numerical methods that can be employed effectively to perform such an analysis is very extensive, as will be detailed in chapter four. In general, the following statements describe the state of the art for the theoretical analysis:

1. To reduce the number of variables involved, the problem is posed in terms of the magnetic vector potential. This technique occupies much of the current literature.

2. Most published studies address electromagnetic field problems involving either static distribution or quasi steady state problems in one or two space dimensions.

3. Studies involving impulse or transient excitations are found mostly in the literature on thermal, structural and applied mechanics problems.

Review of the literature led to the conclusion that finite element and variational solution techniques are the most appropriate tools for analyzing the G/S application.

1.9 Thesis Structure

The structure of this thesis is organized to present the vast amount of technical information, related to theoretical and practical development of the electromagnetic concept for G/S repositioning, according to the chronological order of developing or processing this information. Under normal conditions, development of a project such as this would proceed by performing a detailed theoretical analysis first, then the validity of the established models and results would be verified experimentally. However, in view of the strict deadlines imposed by the in-service schedules of the reactors at Bruce 'B' and Pickering 'B' NGS, heavy emphasis was placed on the experimental program first until the repair procedure was brought to a

sufficiently satisfactory pace. The availability of the necessary equipment made this approach logically practical.

Chapter 1 has presented the historical background, general description of the technique and the criteria for its application, an overview of the technique development and implementation, and status of the prior art. Chapter two describes the electromagnetic technique and the conclusions drawn from the preliminary experiments on the applicability of the technique. The most influential parameters affecting G/S displacement are identified and specifications for the equipment to achieve appropriate current parameters are summarized. Preservation of fuel channel integrity and other safety measures are also discussed in this chapter. The experimental program and results, the implementation of the technique, the performance and operational problems of the capacitor bank systems and the corrective measures devised to rectify these problems, the design of a special pulse power cable, the development of compact durable pulse power coils, and the technical benefits of developing this technique are presented in chapter three. The development of the special cable and coils was a critical factor in the subsequent successful application of the G/S repositioning program.

The theoretical simulation and development of the numerical solution algorithm for the electromagnetic technique are presented in Chapter 4. The finite element technique, with a special transformation of variables to correlate the axisymmetric vector field problem to the two-dimensional cartesian coordinates case, was adopted for determining the magnetic vector potential distribution in the space domain, while a finite difference representation was used to accommodate variation in the time domain. Chapter 5 describes the computerized solution, the method used to verify the validity of this solution and some of the most important results. A comparison between some numerical and experimental results, and an assessment of the numerical technique with suggestions for improvement are also included in this chapter. General conclusions are summarized in Chapter 6.

CHAPTER 2

PROBLEM FORMULATION AND PRELIMINARY EXPERIMENTAL STUDY

2.1 Introduction

The concept of the electromagnetic technique and the main difficulties involved in creating a sufficiently large force to move the G/S in the axial direction have been presented in Chapter 1. The experimental set-up, the preliminary experiments and the conclusions drawn from the results on the applicability of the technique are described in the two subsequent sections of this Chapter. This portion of the work was carried out at the Dobson Laboratories at Ontario Hydro.

Since the time was at a premium in the development of the project, the questions related to acquiring the necessary equipment, the implementation procedures and the operating limits imposed by safety considerations had to be addressed as soon as was logically possible. Therefore, the most influential parameters on the amount of G/S displacement achieved during each discharge "shot" of the capacitor bank were investigated first. Some experiments were

designed to establish a sufficient data base to be used for projecting some of the important results with reasonable certainty, and for ranking the involved parameters according to their benefits and associated costs and penalties. This approach made the task of specifying the equipment designated for use in the reactors at an early stage of the program possible. Investigation of the above parameters, the specifications of the production equipment and the preliminary operating limits are presented in this chapter.

2.2 General Description

The magnitude, frequency and duration of the electrical current required to effect G/S displacement varied over a wide range of respective values. A large variety of equipment ranging from 60 Hz ac supplies to homopolar generators could have been utilized to develop the electromagnetic technique. The capacitor bank systems available at the Ontario Hydro (OH) Research Laboratory were used because these systems offered several advantages from technical and operational points of view. A simplified circuit diagram of the laboratory capacitor bank systems is shown in Figure 2.1.

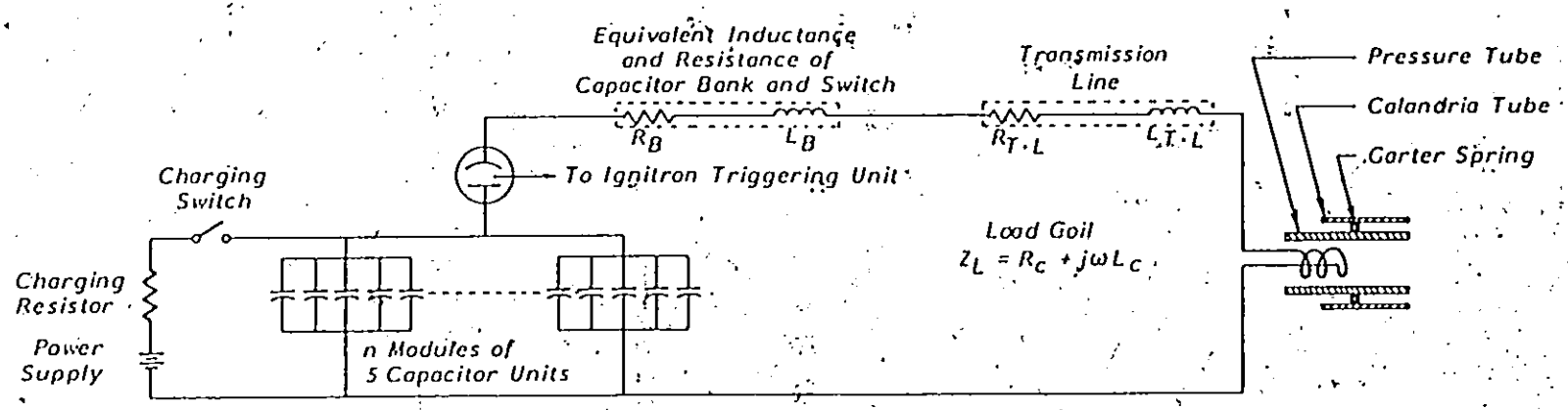

Figure 2.1

Simplified circuit diagram of the laboratory capacitor bank systems.

The capacitor bank itself consisted of at least twenty capacitor units connected in parallel and arranged in modules consisting of five units each. The ignitron switch used to discharge the capacitor bank was rated for a maximum current peak of 630 kA: it had a special triggering unit that accepted a five volt signal transmitted from a remote control room via a fibre-optic link which was used to isolate the operator completely from the system. The unit amplified the control signal to result in a 2000 V pulse. The output of this triggering unit was connected to the ignitor pin and caused the ignitron to conduct if its anode was at a positive potential with respect to its cathode (with a difference of at least 400 V). When the energy stored in the capacitor bank was completely dissipated the ignitron switch stopped conducting and returned to the open or "off" state. The maximum charging voltage of all the capacitor banks used was 10 kV maximum.

The capacitance, inductance and resistance of the discharge circuit were selected to operate these systems in the under-damped [28] or oscillatory mode ($R \ll 2\sqrt{L/C}$). As can be seen from Figure 1.6, the current or voltage reversal of the discharge waveform was as high as 92%. Note that this reversal is defined as the ratio of the second current or voltage peak over the first one: it is a measure of the amount of damping caused by the circuit resistance. The

total resistance in the discharge circuit of these systems was kept very small by using large bus bars to connect the capacitors and bundles of flexible conductors to connect the ignitron to the bank and work coil, and by making the work coil from copper conductors.

The frequency of the discharge current impulse is given by:

$$f = \frac{1}{2\pi} \sqrt{\frac{1}{LC} - \frac{R^2}{4L^2}} \qquad (2.1)$$

Variation of this frequency over a narrow range, using the same capacitor bank system, was achieved by changing the inductance of the system. This was accomplished by changing the distance between the conductors of the transmission line (TL) and the distance between the copper bus bars connecting the positive terminals of the capacitors and those connecting their cases (ground terminals). Large variations in the frequency were accomplished by changing both the inductance and capacitance of the system. Larger capacitances were naturally needed for delivering current pulses having larger magnitudes to the same loads.

The first phase of the experimental program, carried out prior to the delivery of the production capacitor bank systems, used the following laboratory systems:

1. 60 kJ system (1200 μF, 10 kV) consisting of 20 capacitors 60 μF each.

2. 91 kJ system (1818 μF, 10 kV) also made of 20 capacitors 90.9 μF each.

3. 151 kJ system (the above two banks connected in parallel). A single power supply and a single ignitron were used to charge and discharge this bank, respectively.

4. 200 kJ system (4000 μF, 10 kV). This bank was arranged in six modules with four high energy storage capacitors in each. Each module had its own ignitron switch (rated for 100 kA peak current). All six modules were charged and discharged simultaneously.

The most important results obtained with each of the above pulse power systems are presented in Chapter 3 and Appendix A. Initially, the last three systems were not charged to full capacity because the first-generation coils were not capable of withstanding many current impulses

exceeding 100 kA. The preliminary feasibility experiments were performed using coils made of grounding cables and wound by hand around hard plastic pipes. Following encouraging results, the first generation coils were made from rectangular copper rods wound around pre-machined forms made out of teflon or various other materials (as illustrated in Figures 2.2 and 2.3). The problem of building durable coils, capable of withstanding a large number of current impulses in the 150 to the 200 kA range, was resolved as outlined in Chapter 3.

All of the experiments performed at the OH Research Laboratory were conducted as follows:

- The capacitor bank was short-circuited to ground at all times, except during a charge and discharge cycle, via two separate paths: one was connected and disconnected remotely from a separate control room, the other manually by a human operator to fully ensure that there was no residual charge on the capacitors. Note also that the capacitor bank system and test mock-up were located in a separate room that was made inaccessible during the charge and discharge cycle. A video camera was used to monitor the experimental set-up and record some of the results. The storage oscilloscope used to

Figure 2.2

First-generation coils wound on a teflon form (tapered coil is designed for varying the direction of the forces).

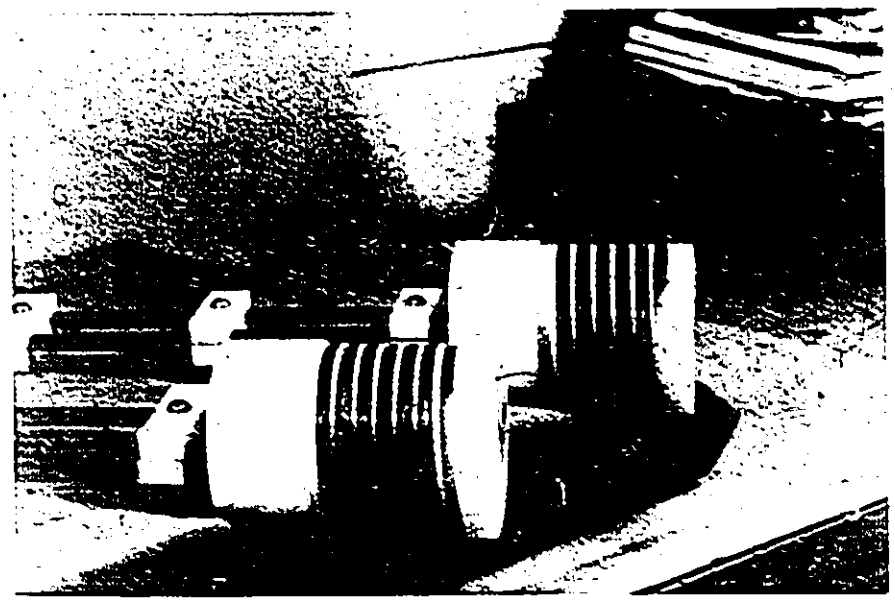

Figure 2.3

First-generation coils wound on polyethelene form (Jaytrex).

record the current pulse waveform was located in a shielded room.

- One (or more) G/S was placed over the P/T, or between the P/T and C/T, at a specific location with respect to the load coil inserted into the P/T. After the application of one capacitor discharge the amount of G/S displacement was measured and recorded, and the load coil was visually inspected.

- The charging voltage of the capacitor bank required to generate a specific first current peak, for any particular circuit loading conditions, was quickly determined by extrapolating the results obtained from one or two capacitor discharges performed at very low charging voltage levels.

The minimum amount of information collected in every experiment consisted of the charging voltage and circuit parameters, the current waveform characteristics (first peak, frequency and current reversal), load coil parameters and resultant G/S displacements. Many experiments were conducted using simple coils, of the first-generation class, at current levels below 120 kA. The main objectives of these experiments were to confirm suppositions related to

the applicability of the technique and the required equipment, and to assess the role of the several system parameters. These considerations are outlined in the subsequent sections of this chapter.

2.3 Experimental Conclusions on Applicability of the Technique

Prior to the specification of the production equipment the greatest displacement noted was 11.5 cm with both the P/T and C/T present in the mock-up [8]. The current impulse used to achieve this result had a first peak of 110 kA, a frequency of 1,425 Hz and a current reversal of approximately 90%. A G/S placed on the P/T (with no C/T present) was moved by 15.0 cm at a current level (first peak) of 91 kA. The charging voltage of the 150 kJ capacitor bank system, used to deliver the above current impulses, did not exceed 8.0 kV. Therefore the maximum initial amount of energy stored in the capacitor bank did not exceed 96 kJ. These results confirmed the following conclusions:

1. The electromagnetic technique represents a practical method to reposition the dislocated G/S in the new reactors.

2. Capacitor banks with at least 150 kJ capacity were required for field use in order to deliver the necessary current impulses, with a much longer TL than the one used in the laboratory.

3. Once the static friction of the G/S is overcome, the amount of displacement achieved can be increased significantly by moderately increasing the current magnitude. Clearly the limiting factor was the current carrying capability of the coil. The service life of the load coil was also of economic significance.

4. The G/S can be moved in either the positive or negative axial direction by adjusting the relative position of the drive coil. Also, G/S located close to each other can be readily separated.

5. The load coils showed visible signs of deformation as well as growth in the radial direction before they failed. The life of the coil decreased rapidly as the magnitude of the current increased.

6. The pressure tube can be plastically deformed as illustrated in Figure 2.4 if the load coil fails during a discharge cycle. This deformation is caused by two main factors:

Figure 2.4

Photograph of a deformed pressure tube.

i) The shock wave created by the impulsive growth of the coil in the radial direction. This is substantiated by the fact that the coil could not be removed from the deformed tube without destruction of the tube.

ii) The electromagnetic stresses created by the large short circuit current impulse and the interaction of the resultant magnetic field with the eddy currents induced in the P/T. Even though this finding represents one major limitation on the maximum G/S displacement in this

application, it has important advantageous implications for some metal forming applications [10,19,21,29].

Some other important observations that were still (at that stage) subject to further investigations can be summarized as follows:

A. When the magnitude of the first current peak exceeded approximately 90 kA, a small spark was observed across the gap between the ends of the spring. This indicated that the voltage induced in the open-circuit spring is sufficient to cause conduction across the gap even though there is a loose contact through the tie wire of the G/S. This additional current aids the establishment of the reaction field of the tie wire. Hence there is an increased axial displacement force on the G/S. However, the potential side effects of the spark included damage to the integrity of the G/S and pitting of the surfaces of the P/T and C/T. Hence, the matter demanded further investigation.

B. The temperature of the P/T section surrounding the drive coil was a function of the current impulse characteristic. However, even under maximum operating conditions this temperature was still far below the

normal operating temperature. In addition, the thermal and electromagnetic stresses which were generated showed their effects on the drive coil at much lower current level than that imposed by the safety of the P/T.

C. The magnetic field that penetrated the C/T as well was attenuated sufficiently to prevent noticeable effects on neighbouring metallic parts. This alleviated the concern about a possible influence on the control rods located between the fuel channels of the reactors (outside the C/T).

2.4 Projected Influential Parameters on G/S Displacement

The amount of G/S displacement achieved by exerting an electromagnetic force on it depends on a large number of parameters related to various aspects of the overall repositioning process. Most of these parameters are interdependent and are functions of a secondary set of parameters related to specific components in the capacitor bank systems and to the position of the G/S. The primary factors that have significant influence on the amount of G/S movement achieved in each capacitor discharge are:

1. Magnitude, duration and shape of the impulse current waveform.

2. Type of electromagnetic coil and its design.

3. Proximity of the G/S to the optimum force position with respect to the electromagnetic coil.

4. Orientation of the G/S, ie, degree of tilting, and the amount of pinching exerted on the G/S by the P/T and C/T.

Some of the above parameters are design parameters since they can be selected and optimized, while others are beyond the control of system design. The impulse current waveform is determined by the parameters of the capacitor bank system, the TL and the electromagnetic coil. The control parameters that can be adjusted to produce the desired waveform are discussed in the next section of this chapter. Also, the influence of the coil parameters as they relate to the current waveform on one hand and to the shaping of the magnetic field profile on the other, will be discussed in Section 2.6.

The proximity of the G/S to the optimum force position at either end of the coil is determined by the

method used to locate the G/S and the accuracy of positioning the electromagnetic coil with respect to the G/S. As will be shown in the theoretical development, a close proximity between the G/S and the first or last full turn of the coil is needed to maximize the current induced in the G/S and consequently to maximize the force exerted on it. The need for this close proximity is accentuated by the presence of the P/T which acts as a physical barrier that limits the coil diameter, and as an electromagnetic shield that limits the frequency and magnitude of the current waveform. The amount of G/S displacement decreases rapidly as the distance between the G/S and the optimal force position on the coil increases. Experimental results demonstrating this relationship are presented in Figure 2.5, for a typical nine-turn coil and a current impulse having a first peak of 150 kA, current reversal of 85% and a frequency of 1250 Hz. This current impulse was achieved by charging the 150 kJ capacitor bank to 8.8 kV. The cross-section of the coil conductor was 7 x 11 mm and its outer diameter was 9.27 cm.

The position and orientation of the G/S play an important role in the repositioning process. They dictate the amount of static and dynamic friction to be overcome, as well as the electromagnetic coupling between coil and G/S. Experiments performed using a short P/T - C/T "mock-up"

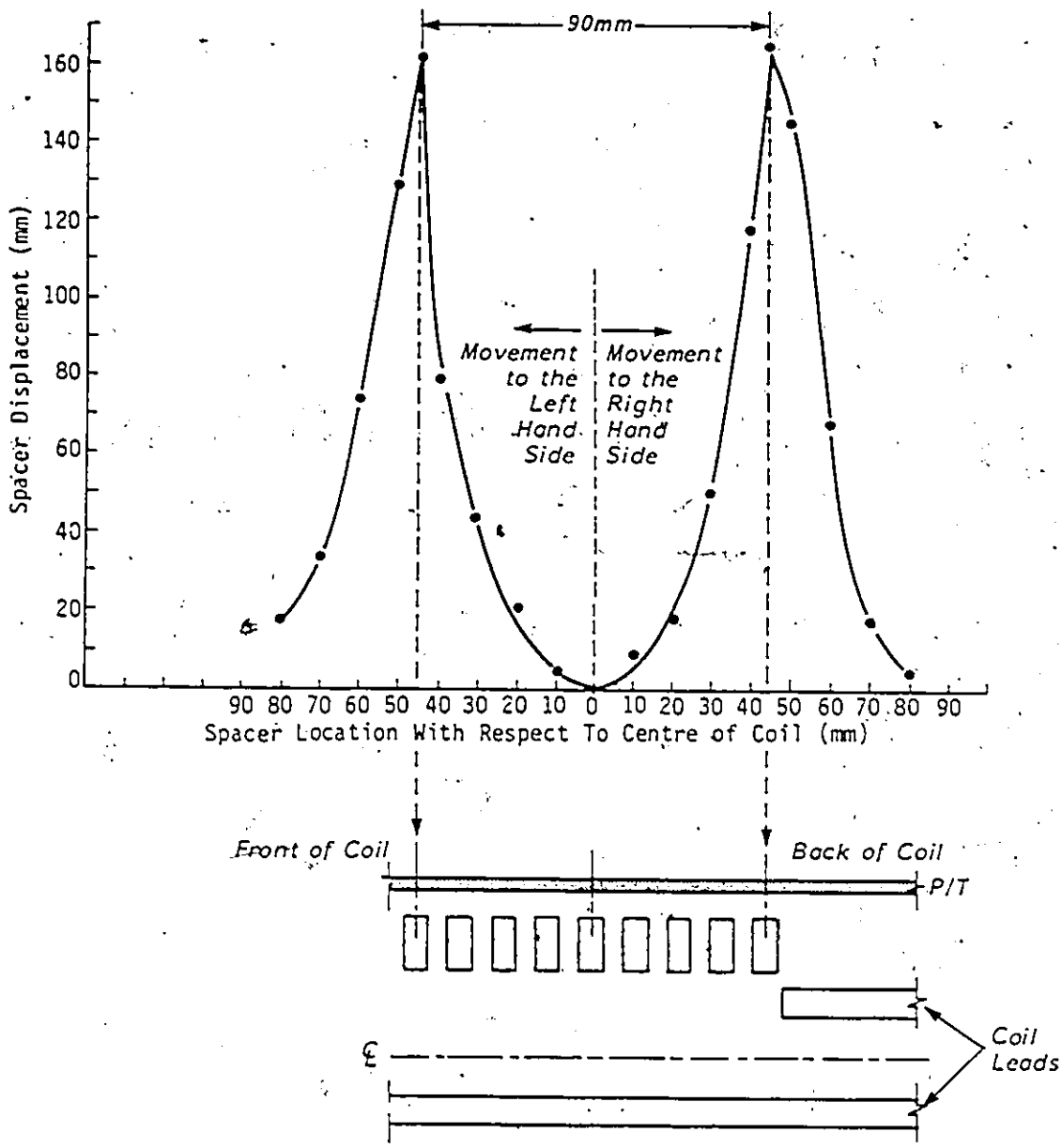

Figure 2.5

Spacer displacement vs spacer location with respect to center of coil.
(1st current peak ≈150kA, current reversal ≈85%)

showed that maximum G/S displacement is accomplished when the G/S is in a vertical orientation. As the degree of G/S tilt increases, the G/S displacement decreases. Displacements as low as 40% of the maximum displacement were obtained when the G/S was placed in a maximum tilt position. However, if the G/S is oriented away from the vertical plane, the electromagnetic force exerted on the section of the G/S closest to the coil is higher than the force exerted on the remaining section of the spring. The reason for this is the presence of local eddy currents in the spring turns that are short-circuited via their contact with the P/T or the C/T. The presence of these local conduction loops was confirmed by observing the occurrence, size and intensity of the spark across the spring ends as a function of its location in the circumferential direction around the P/T. Therefore, the described force profile causes the G/S to "flip" or to change the direction of tilt with respect to the vertical plane passing through its center of mass. This action has been successfully demonstrated experimentally on several occasions using various capacitor banks. At lower current levels or with inferior current waveforms two or three "shots" may be required to completely flip the G/S. In such cases mechanical vibrators may be used in conjunction with the electromagnetic technique (chapter 3).

The positioning of the electromagnetic coil with respect to the G/S was determined by the procedure followed to bring the G/S into final position. The eddy-current probe (ECP) used to locate the G/S indicated the location of the center of mass of the G/S with an accuracy of ± 1.0 cm (or at best ± 0.5 cm) but did not provide any information about the degree or direction of G/S tilt. In the absence of such information, a statistical average of G/S tilt had to be determined.

2.5 Role of the Impulse Current Waveform

The time-varying electromagnetic field created by the coil current is one of the most important parameters in the G/S repositioning process. The voltage it induces in neighbouring metallic objects causes a current to circulate in any closed path. The direction of this induced current is such that the magnetic field associated with it tends to oppose the variation of the source field that created it, hence, it circulates in the opposite direction to that of the source current (Lenz's law) [30]. Parallel conductor elements carrying currents in opposite senses repel each other. The magnitude of the repelling force is proportional to the product of the two conductor currents and inversely proportional to the distance separating them.

Therefore, the magnitude of the source current is clearly of primary importance with respect to the amount of G/S displacement, since the force exerted on the G/S is a function of a power of the value of instantaneous current. The rate of change of the magnetic field, determined by the frequency of the source current, is also of importance because it influences the current induced in the G/S. This is one of the product parameters in the force equation: upper limits on the current magnitude and frequency are imposed by the presence of the P/T between the load coil and the G/S. The physical and geometrical requirements of this application impose specific limits on the current characteristics that can be achieved with practical capacitor bank systems.

The third important parameter is the duration of the current impulse. The amount of G/S displacement is proportional to the force exerted on it and to the duration of this force. The duration of the current impulse is determined by the resistive damping of the waveform. The current or voltage reversal is a convenient measure to represent this damping of the capacitor bank circuit. Therefore, the ideal way to move the G/S from one point "A" to a point "B", is to pass through the drive coil a current having sufficiently large magnitude and frequency to move

the G/S, and to sustain this current for the duration needed to advance the coil, and consequently the G/S, to the final position. However, from a practical point of view, the high static and dynamic friction on the G/S, the electromagnetic shielding effect of the P/T, the poor electrical conductivity of the G/S material and the small cross-section of the G/S tie wire increase the need for high current magnitude. Sustaining a high current for any reasonable length of time would necessitate cooling of the coil and possibly the equipment used to deliver this current. Since such systems were not readily available, the G/S had to be moved in discrete steps, ie, applying the necessary current in short high-current pulses.

Having identified the desired characteristics of the current pulse as they relate to the G/S displacement, their dependence on the circuit parameters of the capacitor bank systems should now be examined. Figures 1.5 and 2.1 show simplified representation of the equivalent circuit diagram for a typical capacitor bank system. As mentioned earlier in order to maximize the duration of the current pulse, the laboratory capacitor banks were operated in the "oscillatory" or under-damped mode. This was effected by keeping $R \ll 2\sqrt{L/C}$. Figure 1.6 presents typical voltage and current waveforms for this mode of operation. The frequency of

these oscillatory waveforms is given in equation 2.1 (of Section 2.2). When the resistance of the circuit is very small the frequency can be approximated by:

$$f = \frac{1}{2\pi} \sqrt{\frac{1}{LC}} = \frac{1}{T} \qquad (2.2)$$

where T is the period of one complete cycle.

The damping in the circuit for this mode of operation may be represented by the ratio of the second current peak to the first current peak (Figure 1.6), and is given by:

$$\frac{I_2}{I_1} = e^{(-\frac{R}{2L})\frac{T}{2}} \qquad (2.3)$$

The instantaneous current at any time (t) is given by:

$$I(t) = \frac{V}{\omega L} e^{-\frac{R}{2L} t} \sin(\omega t) \qquad (2.4)$$

where $\omega = 2\pi f$ (angular frequency) and V is the charging voltage of the capacitor bank. From equation 2.4 it can be seen that the first current peak can be approximated by:

$$I_1 = \frac{V}{\omega L} = \frac{V}{\sqrt{L/C}} \qquad (2.5)$$

Equation 2.2 clearly indicates that the frequency is mainly determined by the inductance and capacitance of the system. These two parameters have to be selected to obtain a frequency range such that the penetration depth (p) of the magnetic field through the P/T is sufficiently large to minimize the shielding effects of the P/T; p is given by:

$$p = \left(\frac{2}{\omega \mu \sigma}\right)^{1/2} \qquad (2.6)$$

where μ is the magnetic permeability and σ is the electrical conductivity of the metallic medium. To achieve the above objective, ω should be reduced by increasing (C) and/or (L) while maintaining the size of capacitor bank within practical limits. Note that increasing (L) alone would limit the maximum current that can be delivered by the system, as indicated by equation (2.5). The inductance of the load coil is of particular importance in the selection of the above parameters, since it is related to the design of the coil which should provide a specific magnetic field distribution to maximize the axial component of the force exerted on the G/S. This illustrates part of the interdependance of the current characteristic, the coil design

and the circuit parameters, and the problem of optimizing these parameters to achieve maximum force.

The frequency range of 1000 to 1500 Hz was selected as a practical compromise after analysis of G/S displacements achieved in the frequency range of 700 to 3000 Hz, taking account of the various capacitor bank systems with an approximate calculation of the shielding effects. For a frequency of 1000 Hz, it was estimated that the magnetic field at the outer surface of the P/T is approximately 76% of the field at its inner surface. Hence this particular frequency was chosen as a preferable compromise between the desired rate of change of the magnetic field, its penetration depth into the P/T and the size of the system that can deliver the required current magnitude with some spare capacity.

The other major influential parameter in the capacitor bank system is the total resistance. This resistance not only limits the magnitude of the current that can be drawn from the system, it determines the mode of operation and the shape of the discharge current waveform. In the laboratory it was quite easy to minimize the total resistance and achieve current reversals as high as 92%. However, when a TL 21 m long, made of coaxial cables, was

incorporated into the production systems the total resistance presented a major problem. Solution of this problem necessitated the development of a special pulse power cable as outlined in Chapter 3. From the experimental results it can be concluded that the current reversal is a more dominant factor than the frequency of the current pulse. In terms of G/S displacement it can be ranked as the second most important parameter after the current magnitude, since it determines the magnitude of the second current peak as well as the duration of the pulse.

2.6 Role of the Electromagnetic Coil Design

The electromagnetic coil plays a very crucial role in the G/S repositioning process, since it determines the spatial distribution of the electromagnetic field created by the discharge current on one hand, and affects the characteristic of this current on the other. The main control parameters that influence the final coil design from the electromagnetic field distribution point of view as determined by experiments include the following:

(a) outer and inner diameters of the coil
(b) coil length
(c) number of turns

(d) spacing between turns

(e) geometry of the coil conductor

(f) size and shape of the coil leads and connections

Selection of the above parameters had to take into consideration several requirements that were consistently opposite to the requirements of higher G/S displacement; these requirements were:

1. Strength of the coil and other mechanical considerations
2. Available space
3. Electrical insulation
4. Thermal considerations
5. Life of the coil

Also, selection of the coil material was restricted to metals with high electrical conductivity. Normally such materials have poor mechanical properties. However, for the reasons described in the previous section a low resistance is required in the capacitor discharge circuit. Typical coils made of copper had a dc resistance of about 3.0 mΩ, while coils made of stainless steel or zirconium had dc resistances exceeding 22 mΩ. In terms of damping, the latter type of coil reduced the current reversal from 90%

(for copper coils) to approximately 20%. This proved unacceptable.

Single layer solenoids were considered the most convenient type to satisfy the electrical and mechanical requirements. Also, in view of the need to move the G/S in either the positive or negative axial direction and the limited information about the position of the G/S, it was necessary to provide sufficient margin on the coil length to accommodate all possible location errors while still providing the drive to move the G/S in the desired direction. This function was easily fulfilled using solenoidal-type coils. Coils with multiple layers and flat or "pancake" type coils were avoided initially in order to avoid complicating the coil construction. But they were considered as viable alternatives to the single-layer solenoids, since more turns can be packed in closer vicinity to the G/S.

In addition to experiments performed using several coils of the type shown in Figures 2.2 and 2.3, many experiments were conducted using much stronger coils to quantitatively assess the influence of each design parameter on the amount of G/S displacement. Figure 2.6 shows one coil prototype (Bitter type coil) machined out of a solid

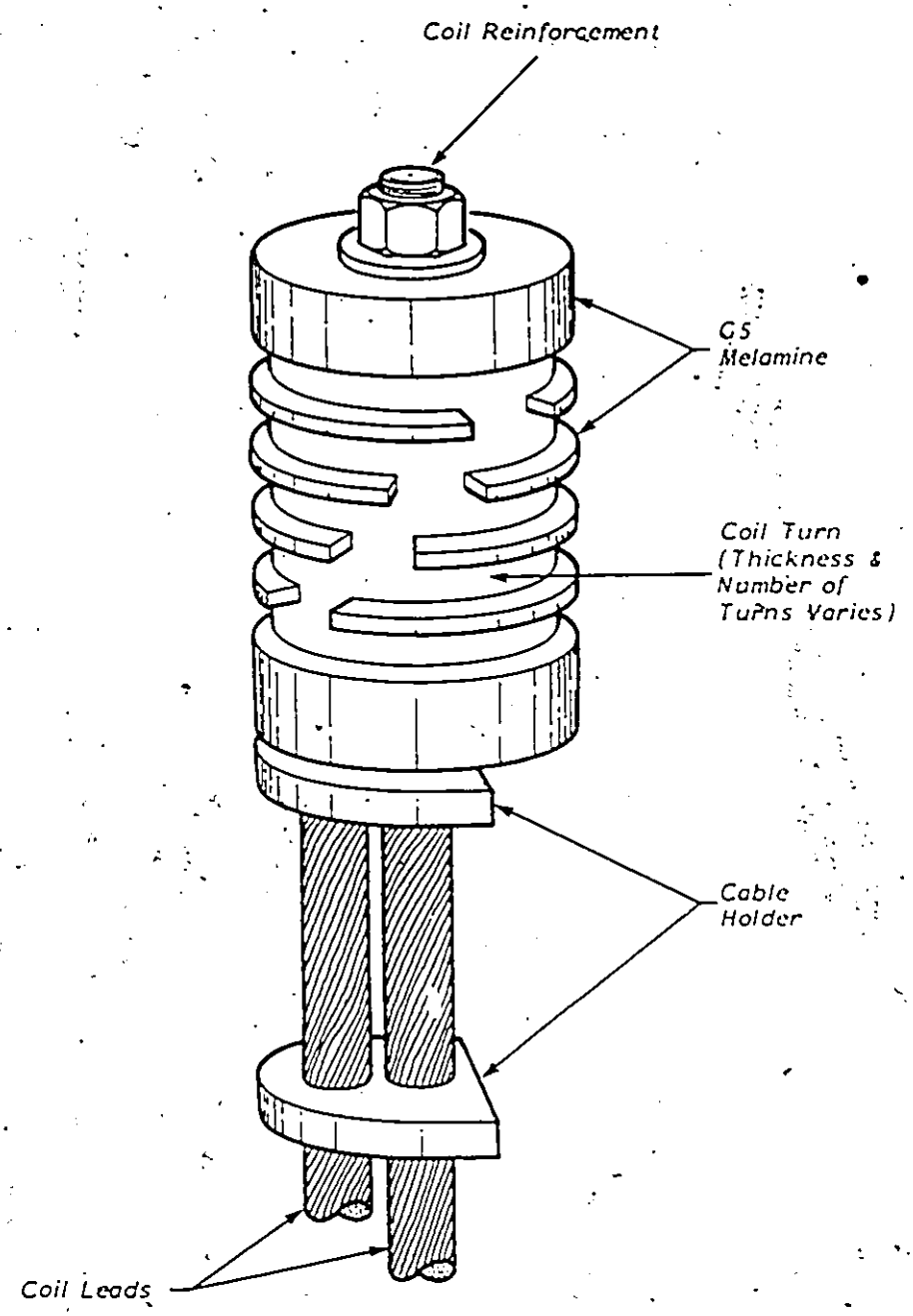

Figure 2.6

Prototype of a strong "Bitter" type coil.

copper rod and equipped with parallel leads, the cross-section of this coil turns was 12 x 16 mm. This coil demonstrated excellent mechanical capability: it withstood current impulses as high as 250 kA without suffering any visible deformation. Unfortunately, the price for this mechanical strength was a severe and unacceptable reduction in the efficiency from the G/S repositioning point of view.

Figure 2.7 shows another coil prototype designed to combine to a great degree the desired electrical characteristics and mechanical strength. This coil was also machined out of a solid copper rod, its helical windings resembled those of the first-generation coil (Figure 2.2). The cross-section of copper in the coil turns was approximately 7 x 13 mm. Coaxial leads were used to connect this coil into the circuit. This coil served its design purpose very well and revealed that the connection between the outer coaxial lead and the turn at the back of the coil played a very important role. Comparison of G/S displacements at the front end and back end of this coil indicated that the connection to the outer coaxial lead reduced the current density in the adjacent turn and presented additional shielding which caused a significant reduction in the G/S displacement.

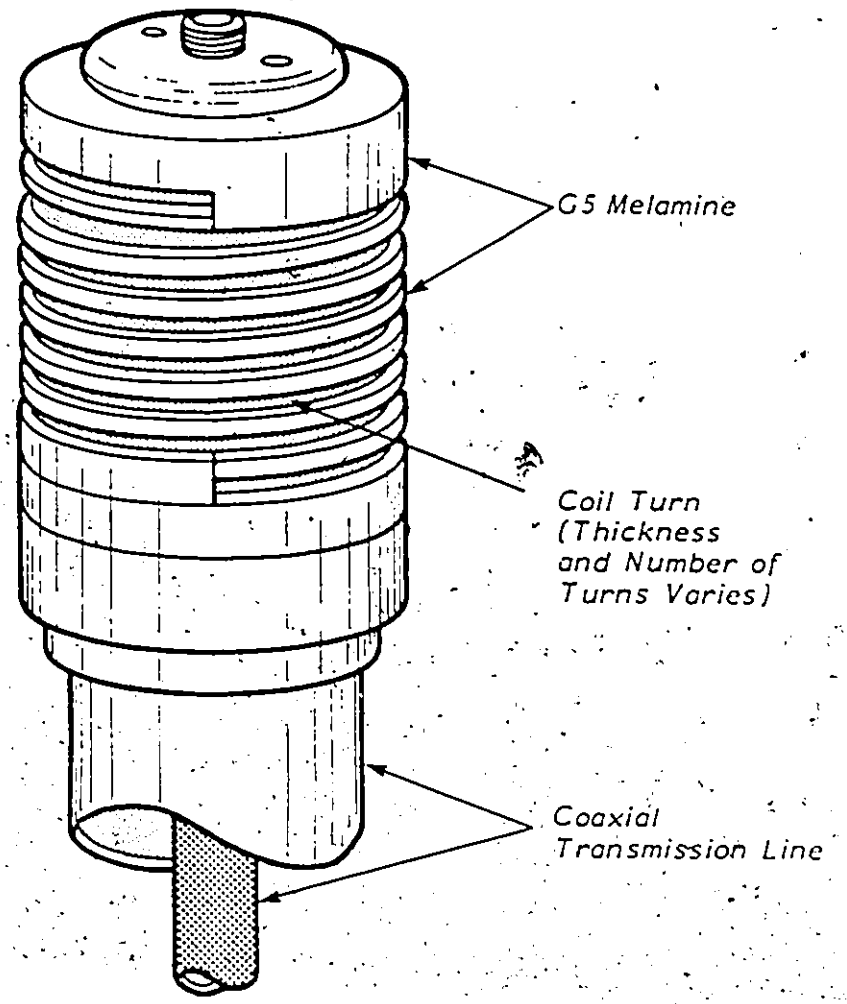

Figure 2.7

Prototype of a coil machined out of a solid copper rod.

Analysis of the experimental results combined with approximate calculations indicated that the amount of G/S displacement, for this particular coil design, tended towards a saturation level as the number of turns in the coil exceeded nine turns. Also, the following empirical observations were made:

1. The cross-sectional area of the copper strip used to wind a coil was relatively more dominant than other dimensional coil parameters. The spacer displacement increased rapidly as this cross-section was decreased, because higher current density was achieved. However, a minimum cross-section of 6 x 11 mm had to be maintained initially to ensure mechanical integrity of the coil.

2. G/S displacement decreased as the outer diameter of the coil was reduced, due to the increase in the distance between the coil turns and the G/S.

3. Smaller spacing between the turns of the coil was preferred to reduce the coil length, and consequently increase the magnetic flux density. However, the electrical insulation requirement and mechanical integrity of the spacers imposed a minimum limit of about 3 mm.

4. Coil leads that were an extension of the coil windings were the most efficient electrically, and the most preferred mechanically, because welding was not needed. The interface connecting the coil parallel leads to a TL, made of three or four coaxial cables connected in parallel, had to be located at least 5 cm away from the last turn of the coil, so that the electromagnetic field distribution at the back end of the coil was not affected.

Chapter 3 describes the specifications and development of durable and efficient pulse power coils that incorporated the above observations and met severe mechanical, thermal and service life requirements.

2.7 Specifications of the Equipment:

When the feasibility of moving the G/S with both the P/T and C/T present had been demonstrated, procedures to acquire the necessary equipment for field use were initiated immediately. Every effort was concentrated to identify the characteristic of the required current impulse and the load coils as soon as possible, to define the specifications of the capacitor bank system. In order to meet a delivery date of mid-December, 1983, an order for the equipment had to be

placed almost immediately. Before visiting two companies in California to provide technical specifications of the required systems the following parameters and requirements were established:

1. The inductance of the load coil was specified to be 2.5 ± 0.5 μH and its dc resistance was specified to be approximately 3.0 mΩ.

2. The maximum first current peak, for the above coil, was specified to be in the range of 190 to 200 kA under normal conditions. This current was not to exceed 300 kA under short circuit conditions at the load coil.

3. The preferred frequency of the current pulse was 1000 Hz.

4. The minimum current reversal was specified to be 65%. Higher reversals were preferable.

5. A TL approximately 18 m long was required to allow the placement of the capacitor bank on the floor of the reactor with access to all G/S.

The above requirements formed basically the output specifications of the system. The details of the system

design to produce the described current pulse were the responsibility of the manufacturer.

Discussions with the manufacturer resulted in the agreement to expand the design of standard capacitor bank systems used for magnetic metal forming applications [31] to meet the above listed requirements. Four complete capacitor bank systems were to be produced and delivered to Ontario Hydro according to an accelerated schedule, and the purchase of four additional systems was to be confirmed later. The technical specifications for each of these systems can be summarized as follows:

1. Operating voltage: 10 kV (maximum)
2. Total bank capacitance (20 units): 4000 μF
3. Maximum energy stored: 200 kJ
4. Bank inductance: Less than 0.1 μH
5. Ringing frequency (under normal operating conditions with a 2 to 4 μH load coil): 1000 to 1500 Hz
6. Ringing frequency (under short circuit conditions at the load coil): 2500 Hz (maximum)
7. Peak current (under normal operating conditions): 200 kA
8. Peak current (under short circuit conditions at the load coil): 300 kA (maximum)

9. Tuning coil (variable inductance): 0-5.0 μH
10. TL made of two sections with an interface block and a terminal block for connecting the load coil: 18 m long
11. Life of the bank with 80% voltage reversal: over 10,000 discharges
12. Minimum voltage reversal: 65%

In addition to the tuning inductor, TL and interface connections, each system included the following components:

1. 20 ignitron switches (one switch for each capacitor unit)
2. Adequate power supply to charge the capacitor bank
3. Triggering unit to fire all ignitrons simultaneously
4. Ignitron "misfiring" detection system
5. Control box for remote operation of the system
6. Capacitor "dump" system (to discharge the energy of the bank into a set of resistors connected to ground, in case of failing to discharge the capacitor bank into the load coil)
7. Extra grounding system (to place a dead short across the capacitors when they are not in operation)
8. Current monitoring probe
9. Heavy duty enclosure to house the complete system

A simplified schematic of the capacitor bank system configuration is shown in Figure 2.8.

Although capacitor banks as small as 140 kJ could have been acquired to deliver the required current pulses, the 200 kJ systems were selected for the following reasons:

1. The ensure that the systems have sufficient flexibility to allow changes in the impedance of the load coil and the characteristics of the generated current pulse waveforms.

2. To extend the life of the high-energy density capacitor units by operating them below their maximum charging voltage and current ratings. This was important since the equipment was intended for an extensive usage. By operating at 7 kV, for example, the capacitor would survive over 100,000 discharges.

3. To accommodate the use of long TL and avoid extended work stoppage even if one or more capacitor units failed.

4. The price of the 200 kJ system was only about 10% higher than the price of the 140 kJ system (a very small price for all the additional advantages).

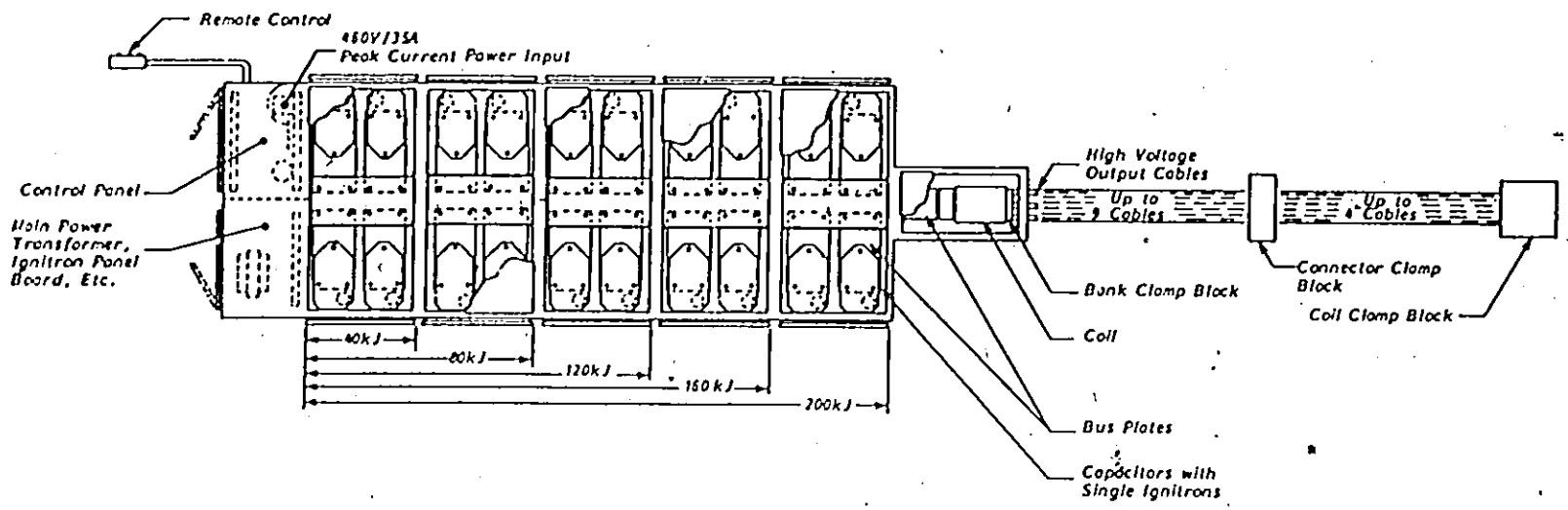

Figure 2.8

200 kJ Capacitor bank system.

Figure 2.9 illustrates the circuit diagrams for the main components of the 200 kJ Capacitor Bank system.

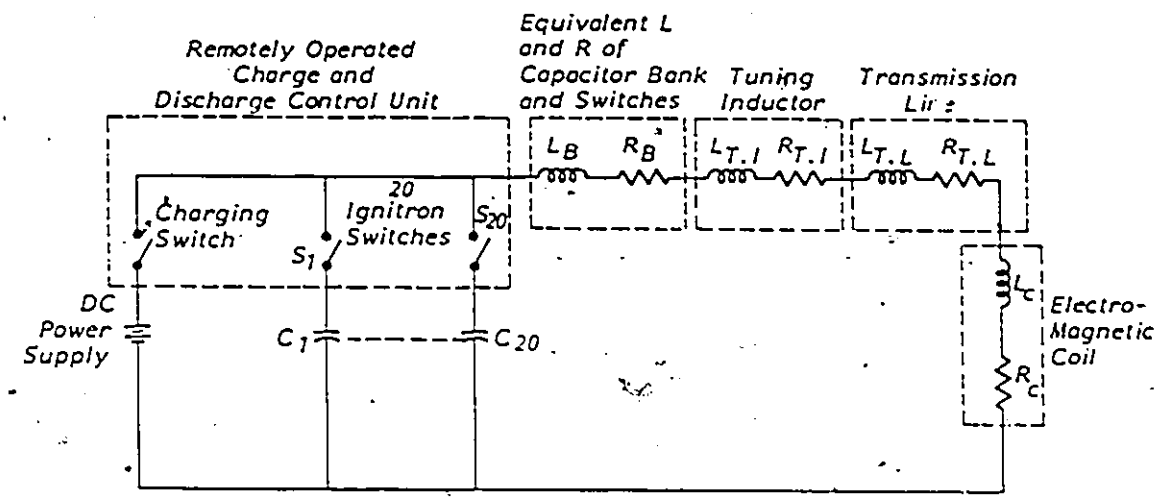

Figure 2.9

Circuit diagram showing the main components of the 200 kJ capacitor bank system.

2.7.1 Specifications of the Tuning Coil, TL and Connections

The main functions of the tuning inductor was to limit the short circuit current and ringing frequency in the event of a coil failure and to provide the flexibility of changing the impulse under normal operating conditions. The

maximum current and frequency specified for short circuit conditions were deduced from the data of the current impulse during the coil failure that caused a P/T deformation. Therefore the requirements that had to be accommodated by the tuning coil were:

1. The tuning coil had to survive at least as long as the capacitor bank. It had to be placed in a separate compartment in the enclosure of the capacitor bank to avoid any damage to personnel or equipment in case of its failure, and to confine its magnetic field within that compartment under normal operating conditions.

2. Five connection points (taps) along with the necessary connector plates had to be provided to allow insertion of the desired fraction of the total inductance.

Two sections of TL consisting of sets of coaxial cables, connected in parallel to reduce the resistance of the TL, were required to connect the driving coil to the capacitor bank. The main restriction on the section that had to be inserted with the coil into the P/T was imposed by the inner diameter of the P/T. This restriction was also valid for the interface block connecting the coil to the TL. Initially, the manufacturer produced an interface block

that could accommodate 3 coaxial cables with an outer diameter of 2.54 cm each. Figure 2.10 shows the construction and termination of these cables. The cable termination was standardized to fit all of the interface blocks. Note that the copper ferrules used to connect the braided conductors of the cable to the brass ferrule which are connected to the interface blocks were assembled using a magnetic metal forming machine [31].

Selection of the size and number of cables in each section as well as the design of the connection blocks were assigned to the manufacturer since it was necessary to coordinate the parameters of these components with the parameters of the capacitor bank and tuning coil in order to meet the specified current characteristics.

2.8 Consideration of Potential Side Effects

The main concerns associated with applying an electromagnetic force on the G/S from within the P/T, using any type of current waveform included mechanical effects, thermal effects and metallurgical effects.

Mechanical considerations included the following:

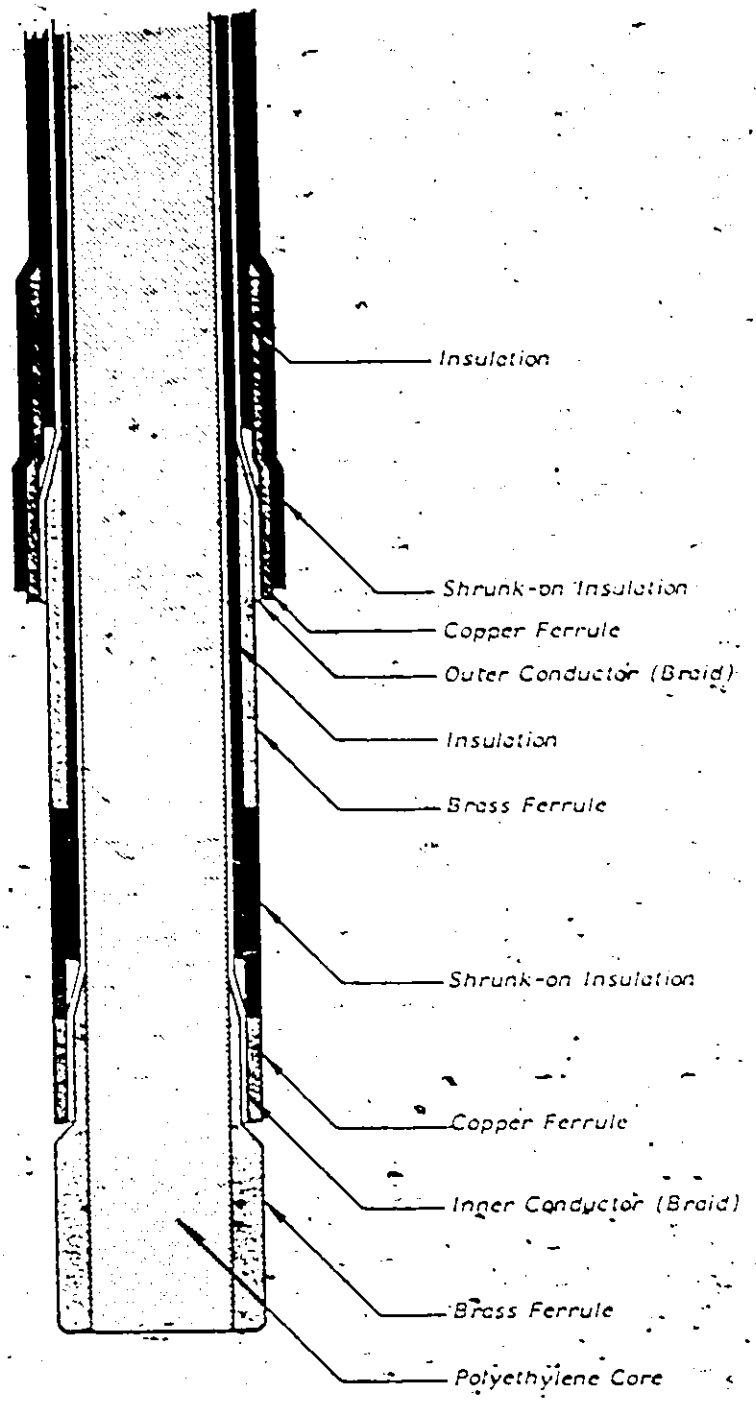

Figure 2.10

Termination of the coaxial cable used initially in the transmission line.

1. Can a sufficient force be applied on a G/S to move it in the axial direction without over-stressing or deforming the P/T?

2. The tie wire is tac-welded. Can its integrity be preserved?

3. Can the P/T and C/T provide sufficient shielding for the resultant magnetic field to prevent any noticeable interaction with other reactor components such as the control rods?

4. Can the failure of load coils be prevented or minimized, to avoid damaging the inner surface of the P/T or depositing copper molecules on it from the failing coil?

From the thermal point of view, the concerns were related to the temperature of the P/T, G/S, and the load coil. As for the metallurgical effects, the following issues, which are direct results of the mechanical and thermal effect, were raised and investigated:

1. Preservation of the crystalline structure and other mechanical and metallurgical properties of the P/T.

2. Preservation of the quality of the P/T and C/T surfaces.

3. Possible erosion of the G/S tie wire and the inner surface of the C/T due to the spark across the ends of the G/S.

Most of these concerns were alleviated in the early stage of the program. However, because of the seriousness of concern, an extensive investigation program was carried out by the electrical, mechanical and metallurgical Departments at Ontario Hydro. The objectives of this program were to ensure that no damage is caused in any way to the reactor components and to establish maximum operating limits that are well within safety margins.

2.8.1 Operating Limits to Ensure Fuel Channel Integrity

Advanced metallurgical and mechanical techniques, including holography methods, were used at Ontario Hydro Research Division to examine various P/T, C/T and G/S test specimens subjected to several strong electromagnetic pulses at current levels as high as 200 kA. As a result of these investigations, the electromagnetic technique was approved by the Atomic Energy Control Board for use in the new CANDU reactors.

In order to maintain a large margin of safety, the maximum allowable operating current for a nine-turn single-layer solenoid was set at 189 kA for a pulse frequency of 1000 Hz and 200 kA at 750 Hz, on the basis of calculation of the electromagnetic stress imposed on the P/T. The actual operating current for reactor repair ranged from 140 to 160 kA (first current peak) at a frequency of 950 to 1050 Hz. Improvement of the coil construction to extend their life and minimize the potential number of failures was a major consideration, as described in Chapter 3.

2.9 Summary

The preliminary development and demonstration of the practicability of the impulse electromagnetic technique have been presented in this chapter. The conceptual difficulties, practical limitations and most influential parameters affecting the amount of G/S displacement have been identified. The equipment used to establish a quantitative data base has been described. Experiments performed with the equipment have served as practical reference to rank the influence of the design parameters, assess the potential of implementing the technique and establish the specifications of the production equipment. Also, the issues related to preserving the fuel channel integrity and the establishment of maximum operating limits have been outlined.

CHAPTER 3

EXPERIMENTAL TESTING PROGRAM AND IMPLEMENTATION OF THE ELECTROMAGNETIC TECHNIQUE

3.1 Introduction

The analytical tools needed to accurately compute the impulse electromagnetic forces on the G/S and other fuel channel components were not readily available. Analytical formulae derived for simple cases with harmonic time variations had to be carefully interpreted to establish some rough approximations. In view of the urgency and magnitude of the application, the above deficiency was compensated by an extensive experimental testing program aimed at verifying and quantifying the necessary theories and information. This approach provided an adequate degree of confidence and certainty necessary to formulate important decisions upon which hinged many significant and costly consequences.

During the early stage of implementing the electromagnetic technique in Unit 6 at Bruce 'B' NGS, the magnitude

of the first current peak had to be increased to a level of 140 to 160 kA in order to compensate for significant reduction in the G/S displacement, caused by the poor characteristics of current impulses delivered by the production capacitor bank systems. Also the number of capacitor discharges and the frequency of their application had to be increased to cope with the consequences of poor accuracy in locating the G/S and to accelerate the repair process. These new operating requirements caused a significant reduction in the life of the first-generation "field" coils and necessitated the development of a special pulse power cable and durable coils that are capable of withstanding current pulses as high as 200 kA.

This chapter presents the scope and major results of the experimental program which was carried out at Ontario Hydro Laboratories. It also describes the implementation of the electromagnetic technique and the testing program to address the performance and operational problems of the capacitor bank systems. The development of a special pulse power cable and the design, construction and testing of various coil prototypes are also described. The technical benefits of developing the impulse electromagnetic technique are outlined.

3.2 Scope of the Experimental Program

Subsequent to the completion of the work phases that demonstrated the practicability of the technique and provided the basic information needed to specify the production equipment, particular emphasis was placed on fulfilling the following objectives:

1. Optimize the design of the electromagnetic coil with the objective of producing an efficient and strong coil within the dimensional constraints. Produce specifications for the coil construction method and one or two coil prototypes for "field" use.

2. Maximize the amount of G/S displacement that can be achieved with every capacitive discharge subject to the coil current capability and system parameters.

3. Establish optimum operating parameters and procedures for actual reactor repair.

4. Perform experiments at the maximum allowable operating levels to prepare samples of fuel channel components for metallurgical examination.

5. Test samples of the TL, interface connections and "field" coil prototype to qualify them for reactor use and specify safe service life for the coils.

The next subsection along with Appendix A present typical results of the experiments performed to achieve the above objectives.

3.2.1 Main Experimental Results

The approach followed to study quantitatively the effect of each important parameter on the amount of G/S displacement was to vary one parameter over an appropriate range, while keeping all other parameters constant (whenever possible). In most cases two or more parameters had to be changed simultaneously, for example, when the number of turns in the coil was varied, not only the coil length (or the spacing between turns and/or cross-section of the turns) had to be varied, but also the coil resistance and inductance and consequently the damping and frequency of the current impulse waveform had to vary as well. Therefore, the influence of parameters that can be varied alone, such as the current magnitude, or with minimum number of other parameters were investigated first. This facilitated the assessment of the influence of other simultaneously

changing variables, and allowed their ranking in terms of benefit factors related to G/S displacements, and penalty factors related to reducing the life of the coil and necessitating larger equipment.

In addition to the experimental results and observations presented in the previous chapter, important representative results are summarized in this section in condensed graphical form. Additional results are presented in a more detailed tabular form in Appendix A. Displacement of G/S were measured with the P/T only present to achieve higher accuracy and save experimental set-up time.

Figure 3.1 shows the influence of the magnitude of the first current peak on the G/S displacement, for two sets of current impulses having different waveform characteristics. The impulses used to obtain the results represented by curve A had a frequency of 1300 Hz and current reversal of approximately 92%; whereas those yielding curve B had a frequency of 950 Hz and current reversal of 72%. The coils used to perform the two sets of experiments were similar but had different outer diameters. For curve A the coil outer diameter was 97 mm as compared to 92.7 mm for the other one. The main observation that should be made from this

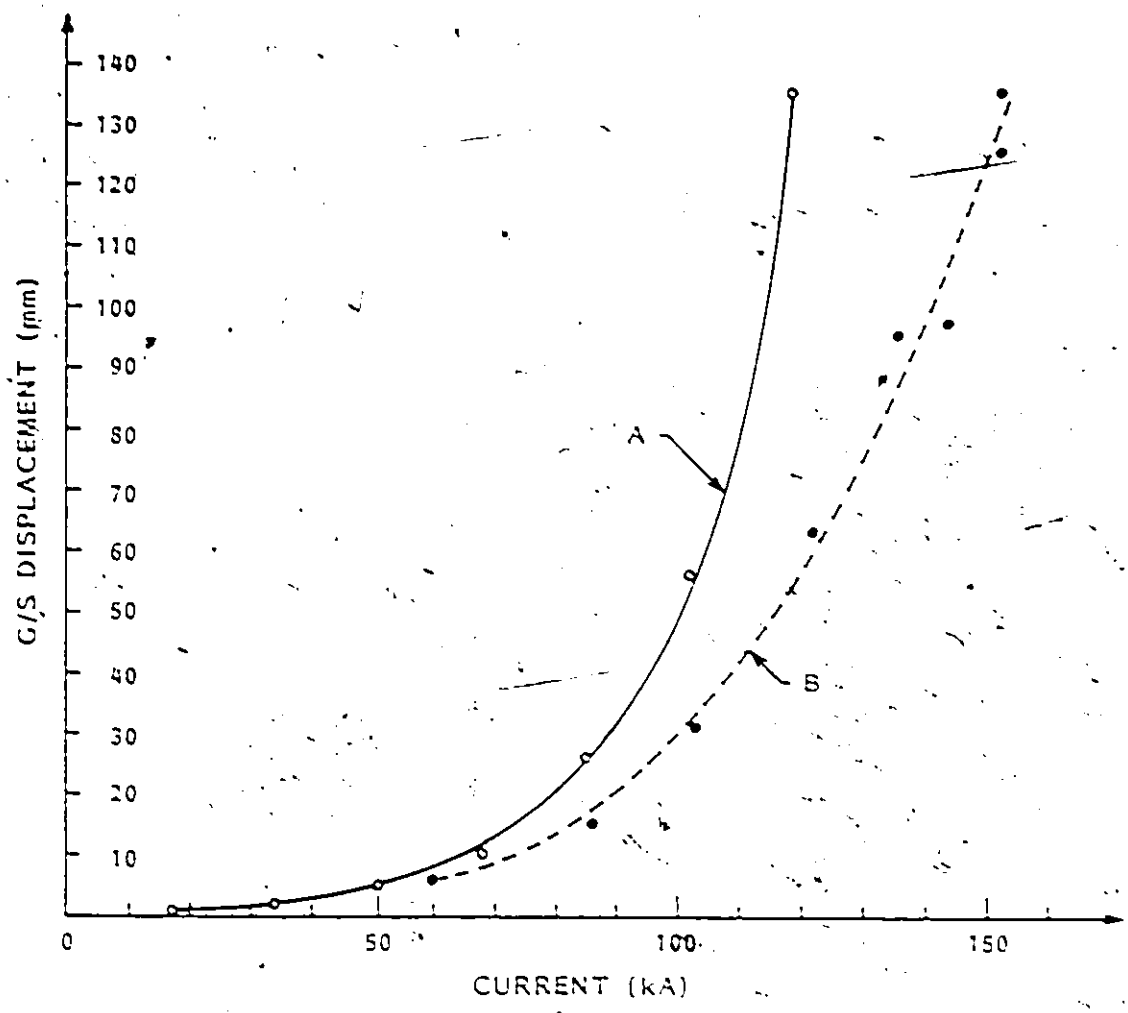

Figure 3.1

G/S displacement vs the first current peak of impulses having different wave form characteristics.

figure is the rapid increase in G/S displacement at current levels higher than 70 kA. This type of profile, but with a different slope, (Figure 3.2) was observed in every case that was studied regardless of the coil design and impulse current characteristics. This illustrates why the current magnitude ranked very highly on the parameter list. Even though the penalty paid in terms of coil life when this magnitude increased was very high, it proved to be the single most efficient and easy way to compensate for other deficiencies in the coil design and other current characteristics.

Figure 3.2 presents the results of five sets of experiments all of them performed with identical coils using the various laboratory and production capacitor bank systems. This figure illustrates the combined influence of the current reversal and frequency of the current impulse. Close examination of Figure 3.2 clearly indicates that the current reversal has a greater effect on G/S displacement than the frequency. Comparison of the curve for 85% reversal with those for 59% and 46% reversals clearly substantiates this observation: G/S displacements for the first curve are at least three times higher than those for the latter curves, in spite of the higher frequency

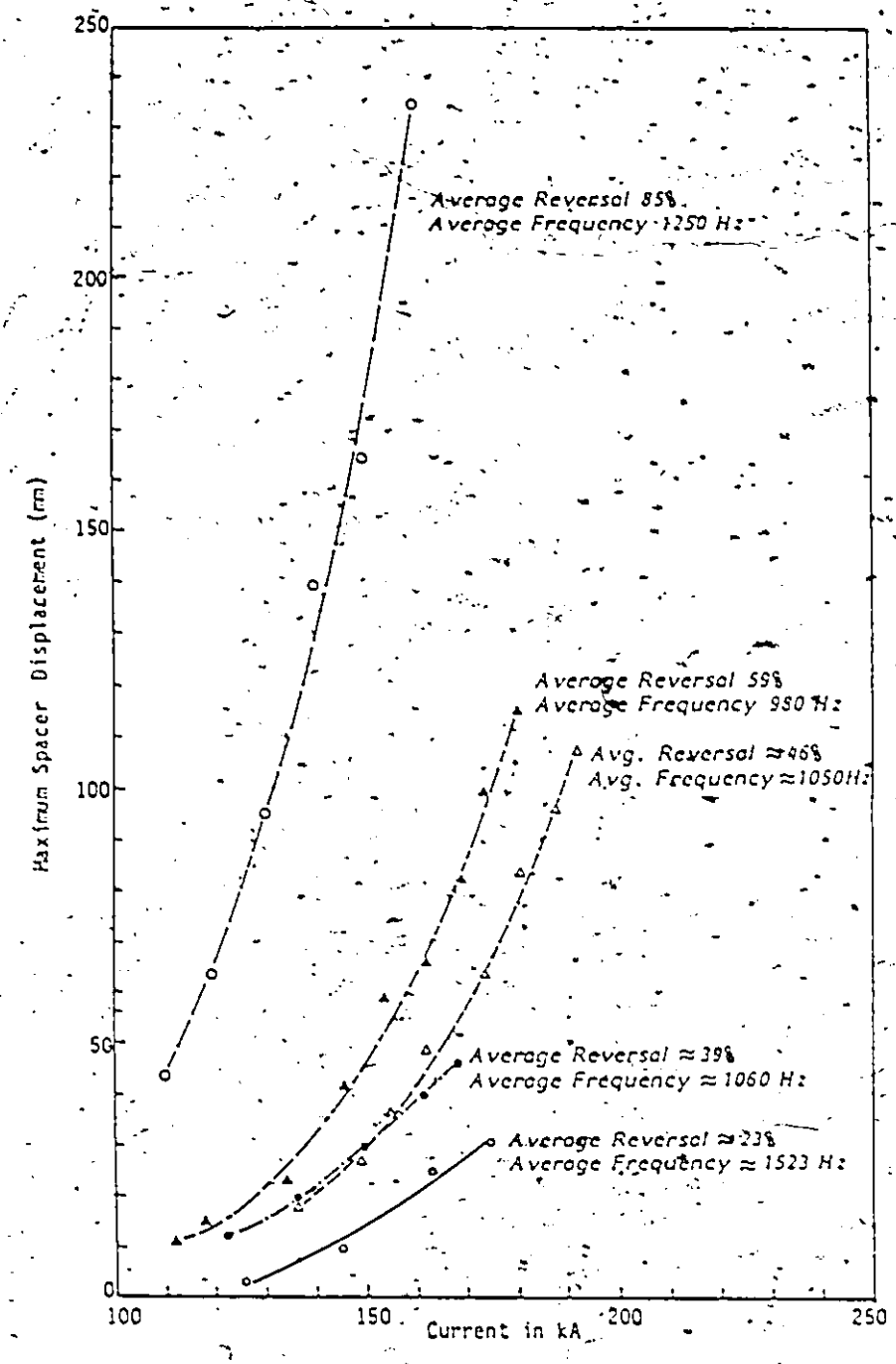

Figure 3.2

Spacer displacement vs current magnitude for various frequencies and per cent current reversal

differential. Figure 3.3 illustrates the influence of the current (or voltage) reversal more explicitly. All of the data points were selected from experiments utilizing identical coils for a first current peak of 175 kA.

The increase in G/S displacement due to lower frequency can be assessed by comparing curves number 1 and 2 of Figure 3.4. These two curves represent results of experiments performed using the same capacitor bank and identical five-turn coils. The 1250 Hz frequency was obtained by adding a dummy inductor in the circuit; the resistance of this inductor helped to maintain the current reversal about 5% higher than it was for the experiments at 1780 Hz. The contribution of this increase towards the higher G/S displacement of curve number 2 should be subtracted from the total increase to determine the net gain due to the frequency differential. Figure 3.4 also provides for similar comparison to assess the influence of the number of turns in the coil (curve number 3 versus curve number 2).

The important influence of locating the first or the last turn of the coil under the G/S is displayed in Figure 2.5. The results shown can be interpreted to further

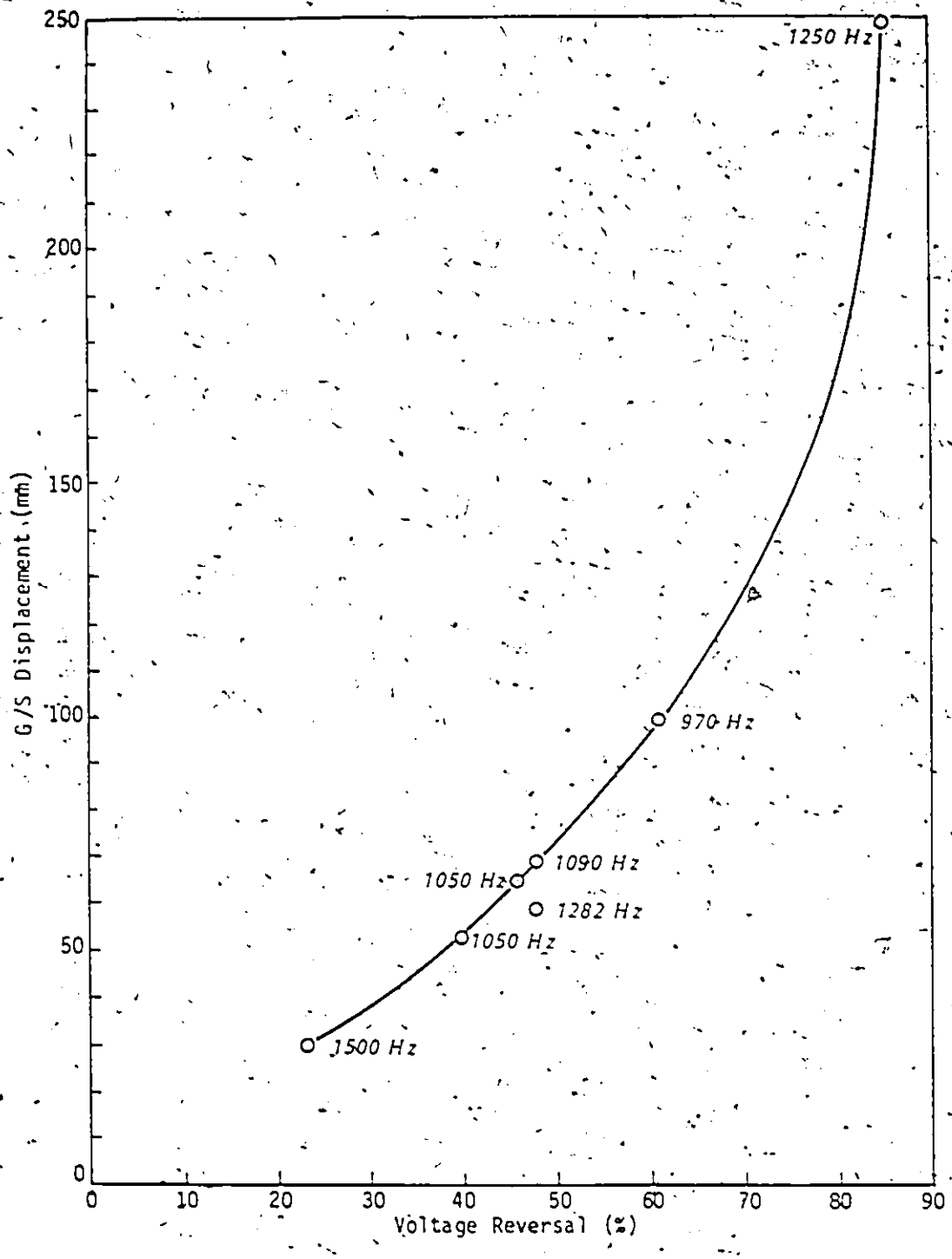

Figure 3.3

G/S displacement vs voltage reversal and frequency at a current level of 175 kA.

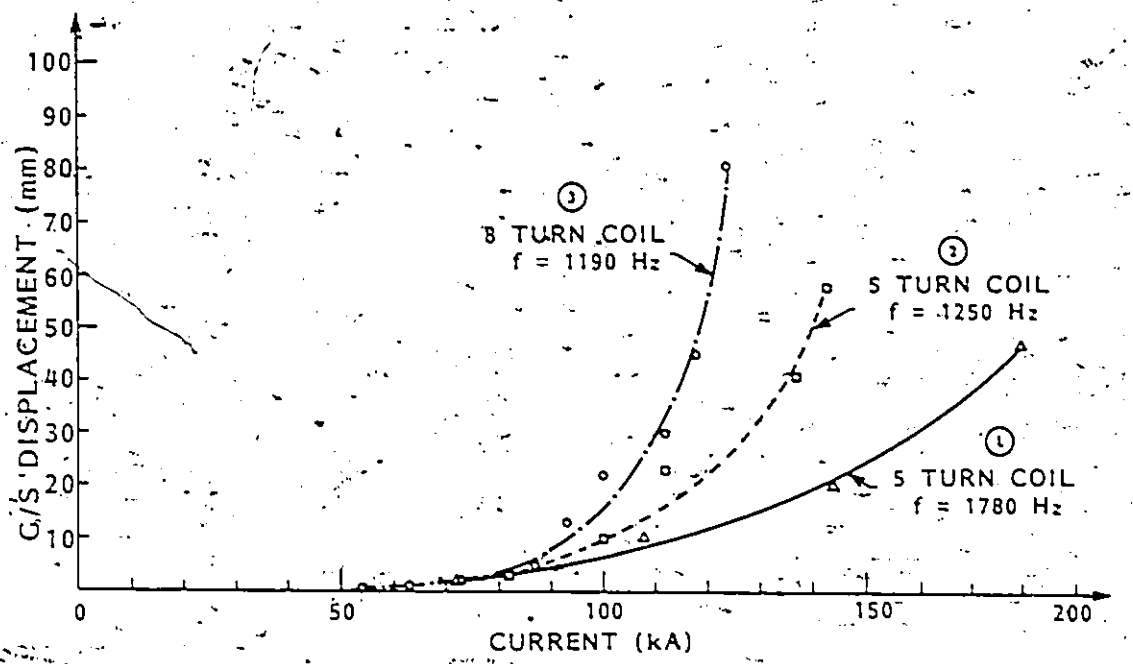

Figure 3.4

G/S displacement vs current magnitude for coils with different number of turns and for different frequencies.

confirm that G/S displacement decreases if the coil outer diameter is reduced. As mentioned in the previous chapter, G/S displacement increases as the spacing between coil turns and the cross-section of the coil conductor decrease. However, minimum dimensions for these parameters were imposed by the requirements of electrical insulation, mechanical integrity and durability of the coil. Analysis of the results presented so far, along with the results of a large number of experiments performed to determine the capability and life of several coil prototypes provided the basic information for selecting the final coil design and parameters of the current waveform.

The question of applying the electromagnetic technique for repositioning the G/S in commissioned reactors had also to be addressed. The answer to this question would have been straightforward if the reactors were to be defuelled and dried. However, the objective was to avoid the defuelling operation to minimize the outage period. In such cases, the fuel bundles would have to be removed from very few channels; after repositioning of the G/S in these channels, fuel bundles from other channels would be loaded, the repositioning being carried out sequentially. The implication here is that the primary coolant system has to be kept

on to maintain the temperature of the fuel bundles under control. Therefore, the technique had to be applied with the P/T filled with heavy-water.

The presence of the heavy-water in the P/T does not affect the G/S displacement in any way. However, it would facilitate the deformation of the P/T in the event of a short circuit inside the P/T, since it presents a good energy transfer medium for the shock wave generated by the energy discharge in the short circuit [32-35]. In view of the advances achieved in building strong durable coils the risk of coil failure was reduced significantly. Therefore, the work related to G/S repositioning in commissioned reactors concentrated on demonstrating the applicability of the technique using capacitor discharges and the feasibility of using 60 Hz alternating currents.

Since this work does not fall within the scope of this thesis, it suffices to indicate that the feasibility of both approaches was demonstrated. The need for developing the required analytical tools and models to accurately simulate the electromagnetic interaction with the G/S was then addressed, since stringent deadlines did no longer exist.

3.3 Implementation of the Electromagnetic Technique

The electrical resistances of the 21.0 m long TL, of commercial coaxial cables were found to be excessively high. Severe damping of the discharge current occurred. The current reversal was limited to approximately 20%: consequently the amount of G/S displacement achieved with such a current pulse was reduced significantly (Figure 3.2). As an immediate but temporary solution, the length of the TL was reduced to 11.0 m. This necessitated the placement of the capacitor bank on a platform built in front of the calandria structure. As a result, the current reversal was increased to approximately 40%. The long-term solution involved the development of a low-resistance pulse power cable which was custom designed and built (Section 3.4). Introduction of the new cable resulted in increasing the current reversal from 40% to 60%.

In addition to the above problem, the mechanical vibration method mentioned previously could not be implemented due to time limitations on design. Therefore, repositioning of the G/S in units 6 and 5 at Bruce 'B' NGS was initiated using the electromagnetic technique alone. In order to speed up the repositioning process, the operating

current level was increased from 120 kA to 140 kA. Also the charging and discharging duty cycle of the capacitor banks had to be maximized. These new operating requirements caused a significant reduction in the life of the electromagnetic coil. Therefore, a major effort was launched to produce stronger and more durable coils.

During implementation of the electromagnetic technique in units 6 and 5, serious operating problems with the ignitron switches on the four capacitor banks systems were encountered. Diagnosis of these problems and the corrective measures introduced to alleviate them are described in reference 36. Rearrangement of the ignitron switches as shown in Figure 3.5 resulted in increasing the current reversal from 60% to 72%, which was basically the initial expected level. This arrangement necessitated minor modifications of the bus work and the use of blocking diodes and limiting resistors in the ignitor circuits of the ignitrons that are triggered directly by the capacitor bank. Figure 3.6 shows a photograph of the modified capacitor bank system. In view of these successful developments four more capacitor bank systems were acquired for use at Pickering 'B' NGS. These systems, as well as the original systems, were modified to incorporate all of the devised corrective

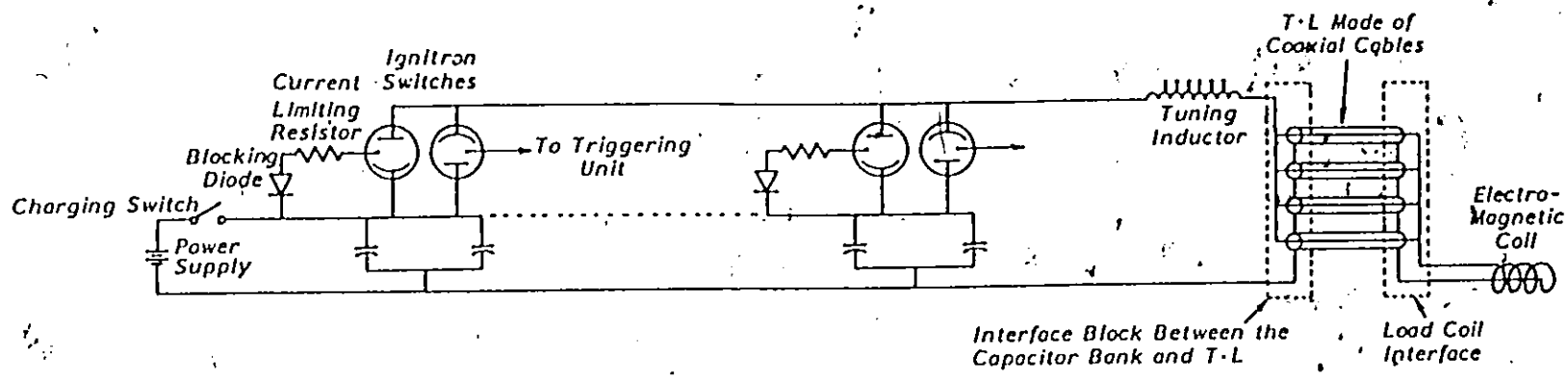

Figure 3.5

New arrangement of the ignitron switches in the 200 kJ capacitor bank systems.

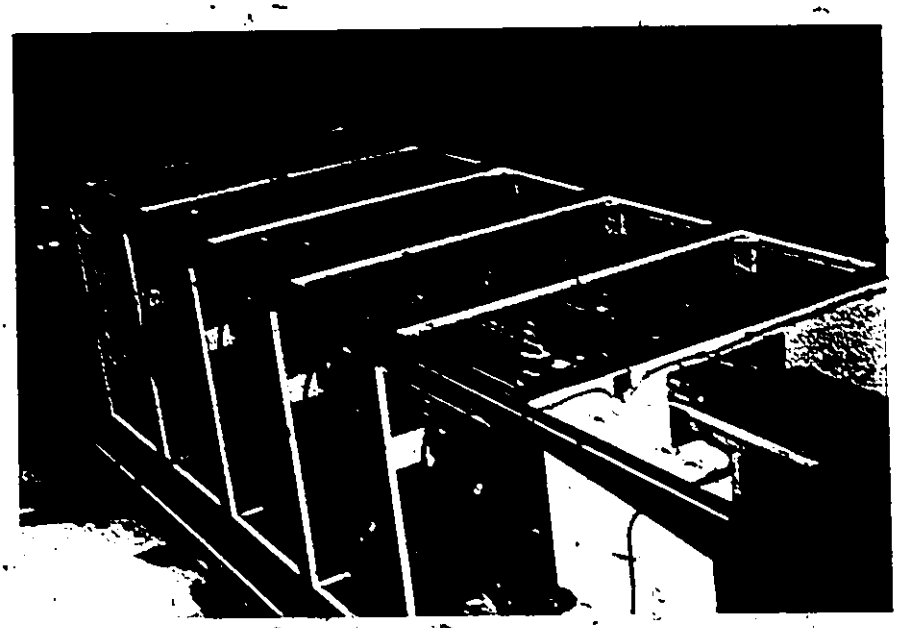

Figure 3.6

Photograph of the modified capacitor bank system (with the covering panels removed)

measures [36]. On the other hand, the problems encountered by the vibration method were also alleviated. The electromagnetic and vibration methods were coordinated together during the repositioning program at Bruce Unit 5 and thereafter for Bruce Unit 7 and Pickering Units 7 and 8. All of the repositioning work in the five reactors was completed before the end of 1984.

3.4 Design of a Special Pulse Power Cable

The basic function of the TL in the G/S repositioning process was to transmit a large amount of energy from the capacitor bank to the coil without causing significant distortion of the impulse current characteristics. The dc resistance of the commercial cable was measured and found to be 3.5 mΩ/m and its inductance to be 33 nH/m. Therefore, the objective was to reduce the dc resistance of the custom built cable to less than 1.0 mΩ/m and to maximize its inductance to provide more favourable conditions for the capacitor bank to operate in the oscillatory mode, subject to keeping the outer diameter of the cable within a maximum of 3.3 cm.

Each cable in the TL was expected to carry 50 kA pulses applied as frequently as one pulse every two minutes

and to survive short-circuit current pulses as high as 100 kA (first peak). In view of the extremely large forces associated with these high current pulses, the outer conductor was to be made of "braided" copper strand to prevent distortion of the outer conductor [37]. The operating voltage of the capacitor bank was 10 kV maximum: as much as 95% voltage reversal was expected under short-circuit conditions. Hence, the cable insulation had to be capable of withstanding an equivalent stress of 20 kV under impulse conditions.

The repetition rate of the high-current pulses causes a cumulative temperature build-up. However, since the duration of the pulse is short, and since the resistance of the cable was to be reduced by at least a factor of three, the maximum temperature of the cable insulation was not expected to exceed 90°C.

A cable design which satisfies all of the above dimensional, electrical, mechanical and thermal requirements was developed (Table 3.1). Figure 3.7 shows a cross-sectional view of this cable and Figure 3.8 shows a longitudinal cross-section of the cable termination. Reference 37 presents a detailed description of the cable design, construction and testing.

TABLE 3.1

Original Cable Design

CONSTRUCTION	
Inner Conductor	- 4/0 AWG (107 mm^2) (18 wire) compact copper (to ASTM B496)
	- nominal diameter 13.0 mm
Insulation	- Natural low-density polyethylene (to ASTM D1248 Type 1A-E5)
	- nominal thickness 3.5 mm
	- nominal diameter 20.0 mm
Outer Conductor	- 24 x 30 x 0.25 mm soft bare copper wire braid
(First layer)	- braid lay (approx) 113 mm
	- total cross-section 36.5 mm^2
	- diameter (approx) 24.0 mm
(Second layer)	- 24 x 30 x 0.25 soft bare copper wire braid
	- total cross-section 13 mm^2
	- diameter (approx) 25.6 mm
Outer Jacket	- black low-density polyethylene (ASTM D1248) Type 1A-E5 with 0.5% carbon black added)
	- thickness 2.2 mm
	- diameter approx 30.0 mm
ELECTRICAL CHARACTERISTICS	
Loop Resistance (with one layer of copper braid)	- 0.922 mΩ/m (0.167 + 0.755) at 20°C
Loop Resistance (with two layers of copper braid)	- 0.545 mΩ/m (0.167 + 0.378) at 20°C
Rated Voltage	- 15 kV dc between conductors
Loop Inductance (calculated)	- 384 nH/m

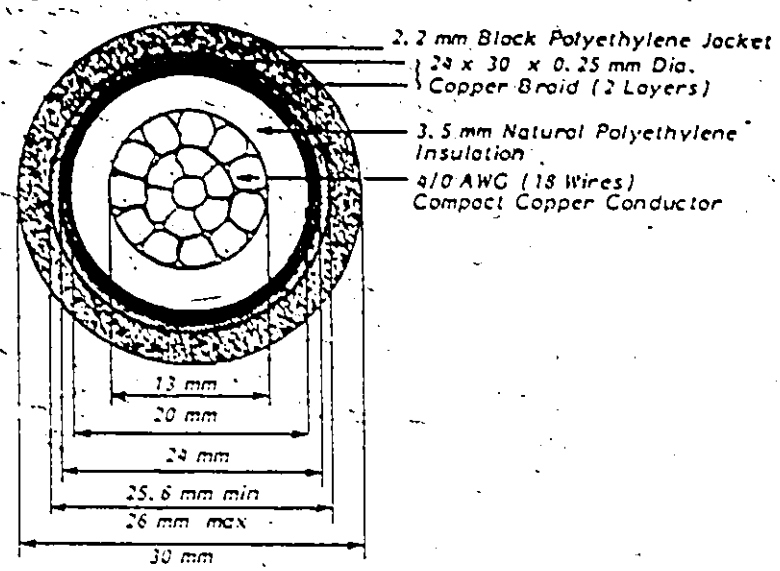

Figure 3.7

Cross-sectional view of the low-resistance cable.

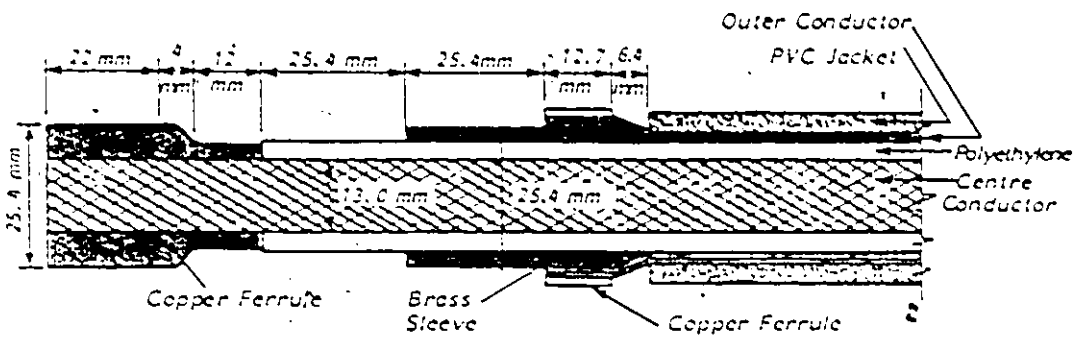

Figure 3.8

Longitudinal cross-section of the cable termination.

3.4.1 Performance Of The Cable

The first TL made of the test cable consisted of an 11 m long bundle having four cables connected in parallel. The performance of this TL was very satisfactory from both an electrical and practical point of view. The electrical resistance of the TL was low enough to allow proper operation of the capacitor bank in the oscillatory mode: including the contribution of other modifications in the system, a current reversal of 72% was achieved and a first current peak of 140 kA was attained at 100 kJ energy level, in comparison to 124 kJ which was needed when the 11 m TL made of commercially available cable was used. The ratio of the ac resistance at 1000 Hz over the dc resistance of the cable was determined empirically and found to be approximately 1.3:1. The ac resistance of the TL, was determined from the current waveforms delivered by the capacitor bank into a short circuit with and without the TL included in the circuit. A small error was unavoidable due to the fact that the frequency of the discharge current waveform was increased slightly when the TL was excluded from the test circuit.

The TL described above and a similar TL made of three cables connected in parallel, have been used to discharge capacitor banks several thousand times, with a

first current peak in the range of 140 to 160 kA. Another TL 21 m long, consisting of two cables connected in parallel, has been used to carry the same current pulses. A satisfactory current reversal of 68% was achieved with this TL. After several hundred capacitor discharges, the two cables were still in excellent condition. These results indicated that each cable can operate at a first-peak current level of 70 kA, with a repetition rate described previously for a significant number of high current pulses. A limited number of short-circuit tests indicated that the cable can survive current pulses exceeding 100 kA, at a pulse frequency of 1500 Hz and current reversal exceeding 80%.

The most interesting results were obtained using a TL 30.5 m long, made of a single cable and the 150 kJ capacitor bank system. The cable was subjected to several impulses having a first current peak in the 100 to 150 kA range: subsequent to these tests the cable did not display any sign of damage. Moreover, the current reversal achieved in this configuration was approximately 68% which indicated the good balance between the cable resistance and inductance achieved with this cable design. This had the implication that the capacitor bank systems could have been placed outside the reactor vault and a TL made of two cables

connected in parallel could in such a case be used to transmit the current impulse with acceptable distortion.

3.5 Design and Development of the Electromagnetic Coils

Analysis of the large amount of data generated by the experimental program to assess the influence of coil design parameters, as outlined in chapter 2 and Section 3.2, and consideration of the various criteria involved resulted in establishing the following coil design specifications:

1. The outer diameter of the coil windings was chosen to be 96.52 mm (this was later reduced to 92.71 mm to accommodate a fibreglass reinforcing sleeve). The finished outside diameter of the coil was restricted to 101.6 mm maximum in order to ensure adequate clearance inside the P/T.

2. The number of turns was restricted to a minimum of eight turns and a maximum of nine turns.

3. The cross-section of the coil turn was chosen as 6.35 x 12.7 mm. Although smaller cross-sections would increase the G/S displacement they compromised the high mechanical integrity required of the coils.

4. The spacing between turns was chosen as 3 mm. Smaller spacings would reduce the coil length but the electric insulation level and mechanical integrity of the spacers would have been jeopardized.

5. The coil length was determined by the three previous parameters and was restricted to a maximum of 9.0 cm.

6. The coil inductance and resistance were determined by the dimensions and material of the coil. The inductance was in the 2.0 to 2.5 μH range and the dc resistance of the coil was less than 2.5 mΩ. Tough pitch, hard drawn copper was used to minimize the electrical resistance in the capacitor bank circuit. Coils made of stainless steel or zirconium were much stronger than those made of copper; however, their high electrical resistance caused a severe damping on the oscillation of the capacitor discharge current. This deterioration in the current waveform had to be compensated by operating at higher current levels eliminating the mechanical advantage.

7. Coil leads that were integral parts of the coil with the same dimensions as the coil turns were the most efficient electrically (since the same current density distribution was maintained near the ends of the coil). They were also the most preferred mechanically since no welding was needed. The interface connecting the coil to the coaxial cables of the TL was located a minimum of 10 cm away from the coil not to disturb the electromagnetic field distribution at the back end of the coil.

The experience gained in building numerous experimental coils (Figures 2.2, 2.3, 2.6 and 2.7) and the observations made in analyzing the various failure modes of these coils led to the following conclusions [38]:

1. A compromise between the mechanical strength of the coil windings and the electromagnetic performance of the coil had to be made. For example, "bitter" type coils that were machined out of a solid 10.0 cm copper rod were capable of withstanding current pulses exceeding 200 kA. However, because of the large cross-section of the windings (12.5 x 19.0 mm) and the shape of the lead connections, they were highly inefficient in achieving good G/S displacements.

2. Unlike traditional applications where the end effects of the coil are not of particular importance, in this application the first and last turn of the coil played a crucial role in determining the generated force profile and net G/S displacement. Hence, a great deal of attention had to be given to the design of the lead connections if the leads were not integral and contiguous parts of the coil windings.

3. The insulation material used to support the coils and space their turns had to be selected very carefully. Materials having good electrical and thermal properties, such as teflon, did not withstand the mechanical stresses. Formers made of polyethylene (Jaytrex) rods displayed better mechanical behaviour than teflon but their thermal properties for repetitive operation were disqualifying factors. Other strong materials such as nylon and various epoxy resins, were found to be too brittle and often cracked or shattered after one shot. Fortunately, sheets of laminated fibreglass reinforced resin (G-5 and G-10 melamine) met the mechanical, electrical and thermal criteria and provided an appropriate solution.

Figure 3.9 shows a typical coil prototype machined out of solid copper rod. Melamine G-5 was used as spacer material both inside the coil and in between turns. Two end plates made of melamine were used to squeeze the coil in the axial direction via the center conductor as could be seen in the photograph of a dissected coil in Figure 3.10. Polyurethane 70D was used as a potting material to fill any void at the interface of the coil spacers and provide a covering layer that insulated the coil and restrained it somewhat in the radial direction.

This generation of coils was tested in the laboratory at a current level of 125 kA. The tested coil successfully survived over 50 shots without displaying any sign of deformation. However, at a current level of 142 kA signs of outward growth in the diameter became visible after about 30 shots and unacceptable after 50 to 60 shots. Figure 3.10 shows a typical deformation near the end region of a coil that was used for over 60 shots at a current level of 140 kA.

3.5.1 Analysis Of The Failure Modes

The incentives to improve the coil construction with the objective of achieving longer coil life were very

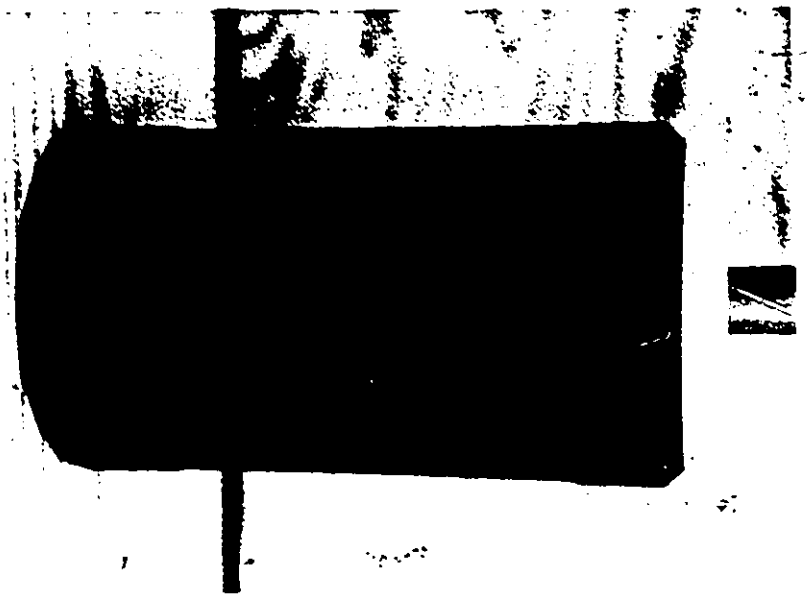

Figure 3.9

Photograph of the preliminary "field" coil prototype.

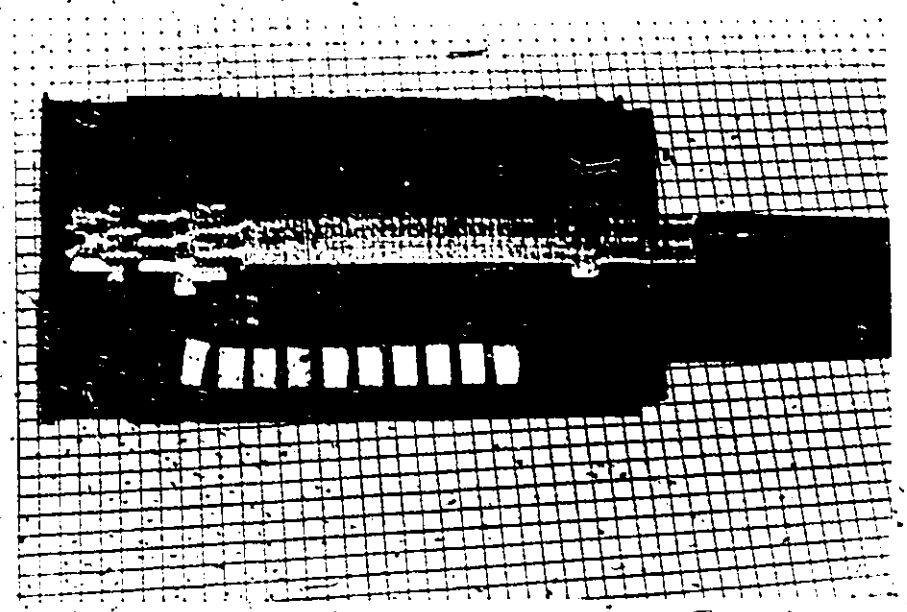

Figure 3.10

Photograph of a preliminary "field" coil disected after it was used for over 60 shots at 140 kA current level.

great. In addition to minimizing or eliminating the number of coil failures inside the fuel channels, application of one capacitor discharge every two to three minutes, in a sequence of three to six shots before an eddy current probe inspection is made to determine the new location of the G/S, reduces the time required to complete the repositioning program. Hence, a major effort was concentrated on analyzing the failure modes of the coil, estimating the mechanical stresses and seeking better coil construction techniques.

Examination of several coils used for a number of shots, or until they had a major failure, revealed that deformation in both the radial and axial directions were present near the ends of the coils as well as in the central plane of the coil. These deformations grew at an accelerated rate when the surface temperature of the coils exceeded 90°C as a result of high repetition rates on the current pulses.

The location of the deformation was a function of spacer material between the coil turns. Some coils that were fully cast in polyurethane 70D showed more deformation near the midplane of the coils, as can be seen in Figure 3.11, while coils constructed using hard melamine spacers

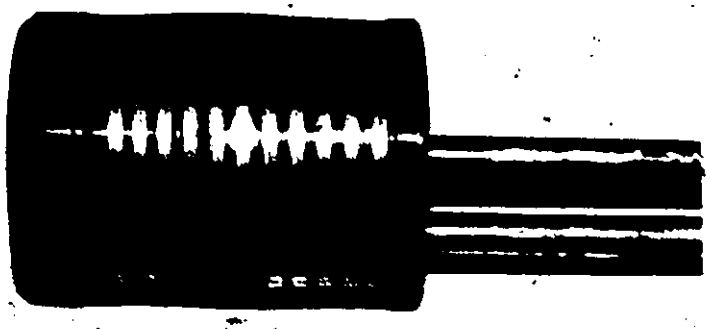

Figure 3.11

Photograph of a coil prototype fully cast in polyurethane 70D (midplane deformation)

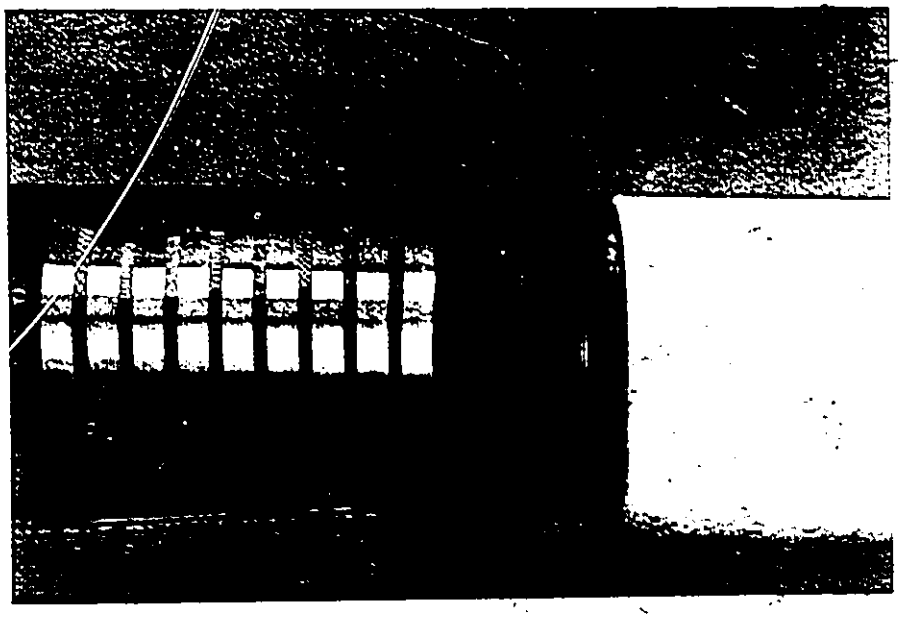

Figure 3.12

Photograph of a coil exhibiting deformation near its ends.

displayed more deformation near their ends as illustrated in Figures 3.10 and 3.12. This was indicative of the important role played by the insulation and spacer materials in shaping the profile of the stress experienced by the coil.

The main difficulties in accurately calculating the mechanical stresses exerted on the coil can be summarized as follows:

1. The electromagnetic coils used for this application had to be placed inside the thick pressure tube with a high degree of inductive coupling. This was required for efficient G/S displacement. Therefore, a strong interaction exists between the source current in the coil and the induced eddy currents in the P/T. The resultant force tends to push the P/T radially outward while crushing the coil radially inward.

2. A secondary component of force is that generated by the interaction between the coil current and its magnetic field, resulting in stress within the coil. This force tends to burst the coil radially outward and compresses it in the axial direction.

3. The radial component of the field gives rise to an axial compressive stress. This effect is strongest near the ends; however, unless the turns of the coil are separated from each other by solid spacers, the compressive stress is cumulative, achieving a maximum at the midplane [8]. There exists also a circumferential tension and a force that arises from the difference in forces on the inner and outer surface of the coil.

4. The strength of the coil structure (coil windings, support, spacers and end caps) could not easily be determined. Unless this strength is known to an order of magnitude, it is meaningless to calculate the stresses accurately [8].

5. The change in the coil temperature as a function of the operating duty cycle, introduces a large margin of variation in the material properties. These variations are not easily determined, especially for the insulation materials.

6. The impulse nature of the current input creates a dynamic loading situation which is more complex to analyze than steady state or static loading situations. The repetition nature of the application of

current impulse raises the possibility of failure due to fatigue.

Although exact solutions to the stress calculations are difficult to perform, useful approximations can be made in an effort to corroborate the stress distributions. The assumption is that all the field was actually generated by a current sheet at the inside diameter of the coil, while the remainder of the coil merely supports that current sheet [8], thus eliminating the need for calculations of distributed body forces. This is the equivalent of a thick-walled cylinder supporting an internal pressure. Reference 6 shows that a magnetic field with its associated stored energy is equivalent to a gas under pressure. The argument is based on the work required to move the boundary and thereby alter the stored energy [6,8].

In pursuing the concept of the magnetic pressure, the interaction between the coils and the P/T was ignored. The forces exerted on each coil turn due to only the source current (200 kA) were calculated. These forces were expressed as the vector sum of the individual forces between any particular turn and all other turns in the coil. Here, the assumption of uniform current density distribution in the coil turns and the replacement of the turns by thin

current elements located at the mean geometric radii of the turns were adopted in order to use standard force calculation formulae [6,39]. The pressures or stresses in the radial and axial directions were obtained by dividing the corresponding force component by the area of winding side normal to this force component.

Figure 3.13 shows the maximum calculated axial and radial stresses as functions of the total number of turns in the coil. Although the stresses can be reduced by reducing the number of turns in the coil, a minimum of eight turns was required to satisfy other criteria for efficient G/S displacement. The radial pressure as related to individual copper turns for a nine-turn coil is shown in Figure 3.14 [38]. This distribution is confirmed by the deformation of several coils, particularly those that were not strongly restrained.

3.5.2 Construction and Performance of the "Field" Coils

The necessity of introducing radial and axial restraining measures to minimize the amount of coil deformation was recognized. As an intermediate step, an epoxy resin fibreglass sleeve was used to replace the polyurethane

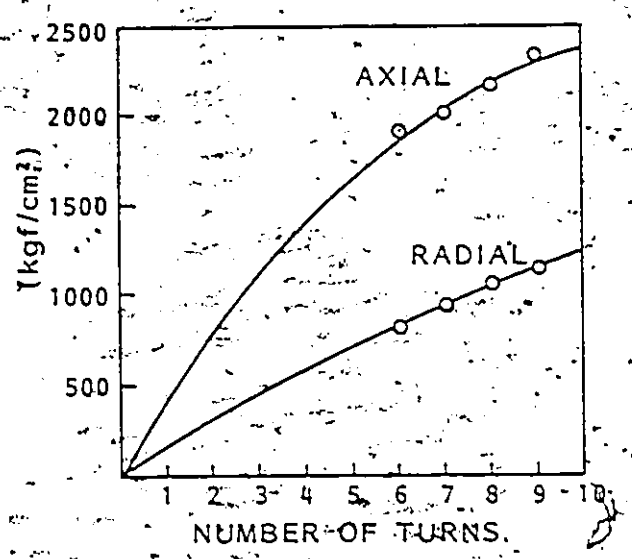

Figure 3.13

Axial and radial electromagnetic pressures as functions of number of turns.

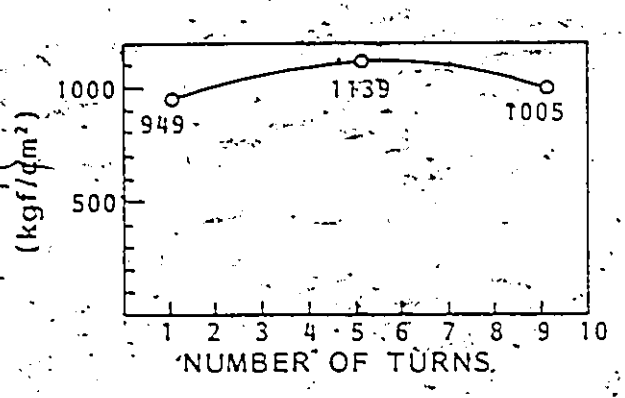

Figure 3.14

Radial electromagnetic pressure distribution on a 9-turn coil.

cover, as illustrated in Figure 3.15. Experimental results indicated that the sleeved coil could withstand several shots at current levels as high as 190 kA. Also, from a thermal point of view, the fibreglass performance was superior to that of polyurethane. Therefore, all coils for field service were equipped with immediately available sleeves, while an effort was made to optimize the design and dimensions of custom-built fibreglass sleeves.

Several custom-built fibreglass sleeves with thicknesses varying from 2.0 to 4.5 mm and different fibreglass weaving angles were tested in the laboratory. Many of these sleeves cracked after a limited number of shots at current levels of 140 - 160 kA (an example is shown in Figure 3.16). The best results were achieved with sleeves that had a weaving angle of approximately 67°. From theoretical considerations this particular angle was also judged to be optimum or near optimum if the sleeve is treated as a pressure vessel. A wall thickness of 3.0 to 4.0 mm was found to be satisfactory. Using such a sleeve, the life of the "field" coils was increased significantly; some coils survived over 600 shots at the 140 kA current level with the sleeve replaced once or twice before the coils were taken out of service.

Figure 3.15

Photograph of a coil prototype covered by an epoxy resin fibreglass sleeve.

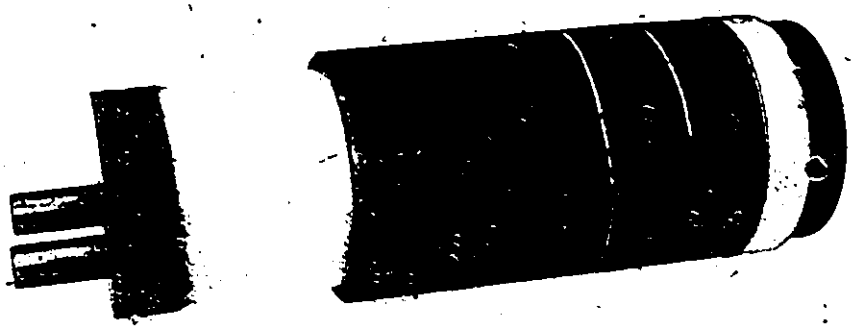

Figure 3.16

Photograph of a coil prototype showing typical signs of sleeve failure.

As well, personnel at the Bruce 'B' station experimented in the early phases with sleeves made of Kevlar, carbon fiber and composite sleeves made of an inner layer of fibreglass and an outer layer of carbon fiber. The composite sleeves performed extremely well mechanically, but caused about 25% reduction in the G/S displacement. This was attributed to the additional shielding caused by the carbon sleeve.

No insulating rods were found to have the required strength to improve prestressing in the axial direction of the coils. Instead, two or three stainless steel bolts, housed in teflon tubes or wrapped with sheets of mica, were used through the inside of the coil in conjunction with washers and nuts that were located about 4.0 cm away from the edges of the coil and torqued against the melamine end caps. Both the optimum fibreglass sleeve and the composite sleeve were accepted and were used depending on their availability. The operating current level ranged between 140 and 160 kA. "Field" reports indicated that these coils prototypes were surviving as many as 1600 shots before they were taken out of service; a marked improvement from the first "field coil prototypes.

Radial growth of the intermediate coil prototypes was not fully controlled by the fibreglass sleeve,

particularly when the temperature of the coil was raised due to a sequence of shots. The sleeve was a close fit but did not exert any force on the copper prior to operation. Therefore, it was decided to preload the coil in the radial direction to account for the excess stress above the copper yield strength (especially if the current was raised near 200 kA).

To achieve the above objective, B-stage epoxy loaded fibreglass bands were applied directly on the coil windings under high tension. During the curing process, the bands would shrink and consolidate to create the necessary preload. Canadian General Electric has a banding facility which is largely used for motor windings but also applicable to these coils. Coils preloaded according to the above method were capable of operating successfully at 200 kA in the laboratory.

Canadian General Electric also developed an insulating potting compound with a compressive strength of 2813 kgf/cm^2 (higher than that of melamine). They were able to embed two bolts with a 12.7 mm diameter, insulated with a mica sleeve, into the potting compound in order to restrain the axial reaction forces. Coils built according to this procedure were considered the final "field" coil

prototypes. Figure 3.17 shows photographs of such a coil, as well as the interface used to connect it to a transmission line consisting of four coaxial cables.

The final coil prototype was subjected to a set of severe laboratory tests to determine its pulse current carrying capacity. First a set of shots at current levels of 100 to 200 kA were applied. (200 kA was the maximum current obtainable from the 200 kJ capacitor bank for the particular transmission line and coil used). Then, 12 shots were applied at a current level of 192 kA, but with reasonable cooling time allowed between shots. There were no visible signs of any deformation. Hence, another series of 150 shots at a current level of 168 kA was applied with a duty cycle similar to the one required in the actual reactor application. Figure 3.18 shows a photograph of that coil after it was subjected to the above tests. Most of the cracks were developed after the temperature of the coil was relatively high. To eliminate the limitation imposed by the temperature of the coil and to provide an "operator-proof" coil that can survive the maximum duty cycle that can be achieved in the reactor (about one shot every two minutes), the interface of the coil was modified to accommodate an air hose for cooling purposes.

Figure 3.17

Photograph of the final "field" coil prototype and its interface connection to a TL made of four coaxial cables.

Figure 3.18

Photograph of the final "field" coil prototype after severe laboratory testing.

Field reports from Pickering 'B' NGS Units 7 and 8 indicated that with cool air blown constantly over the coil in operation, there were no visible signs of any cracking or deformation. The coils were used for 5000 shots at a current level of 140 to 160 kA and they were taken out of service only to avoid the risk of coil failure inside the fuel channel. After 5000 shots the coils were still in excellent condition. Their ultimate life span still remains to be determined.

It should be noted that the above coil construction techniques were applied to build a coil consisting of two single coils joined together in series with a 4 cm spacing between them. The objective of this double coil was to consistently flip the G/S in one shot. Figure 3.19 shows a double coil with a fibreglass sleeve, and Figure 3.20 shows a banded double coil.

3.6 Technical Benefits Of Developing The Technique

In addition to the extensive monetary benefits that were realized as a result of developing the impulse electromagnetic technique to reposition the dislocated G/S in new CANDU reactors, significant technological benefits related

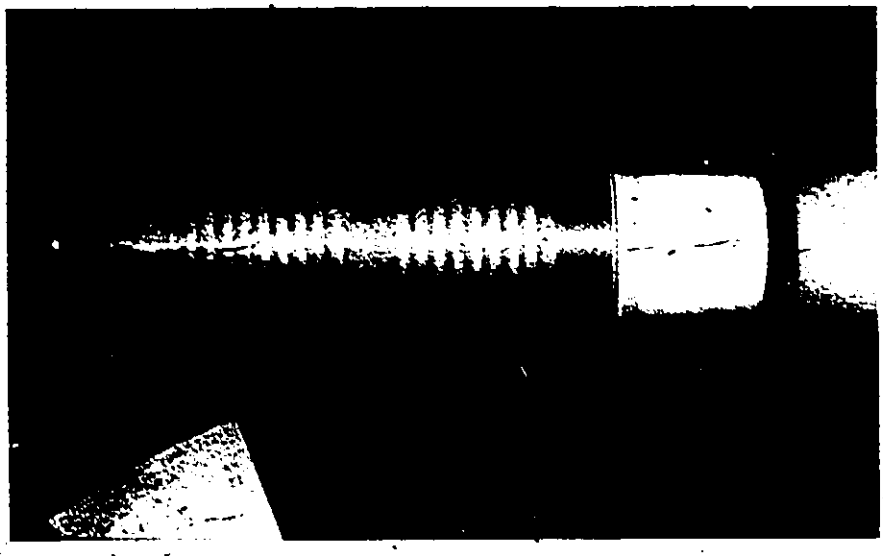

Figure 3.19.

Typical double-coil with a fibreglass sleeve.

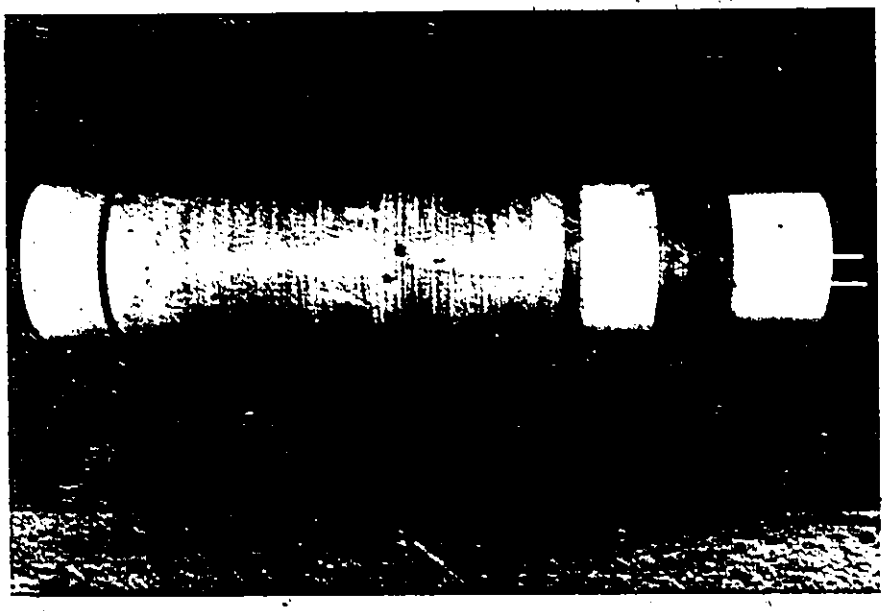

Figure 3.20

Typical "banded" double-coil after several current discharges at 140 and 160 kA.

to potential future G/S repositioning in commissioned reactors and to the pulse power industries at large were created. The capability of the electromagnetic technique to relocate the G/S regardless of their initial position or location in the fuel channel, and the high degree of controllability of the process gave this method unchallenged, and up to date unmatched advantages over all other G/S repositioning methods that have been extensively investigated.

Ever since the feasibility of the electromagnetic repositioning concept was experimentally demonstrated, a large number of practical approaches, centered on this idea, were foreseen as possible candidates for development as a reactor repair method. The potential variations in the coil design and the current characteristics, or the combination of several coils and combinations of time and space variation of their magnetic field are hardly limited; the main restriction is the designer's imagination, since the requirements of the fuel channel integrity can be easily met. Therefore, one of the main technical advantages attributed to development of the impulse current approach is that it laid the necessary foundations required for the development of any other electromagnetic approach.

Intelligent use of the extensive data base established during the development and implementation of the impulse technique can save a substantial amount of time and effort in selecting and optimizing other variations of the electromagnetic approach. The use of the developed theoretical model, described in chapters 4 and 5, in conjunction with the established experimental data base provides an excellent opportunity to advance the G/S repositioning methodology much further than what would have been considered a "wild dream" when the project was initiated.

The technical benefits of the above developments are not restricted to only potential G/S repositioning in commissioned CANDU reactors, they have far reaching implications to several applications in the pulse power industries. Sufficient to say that the advances achieved in both creating a large energy density in a relatively small volume (coil and surrounding portion of the P/T) and in transporting this energy economically over a relatively long distance without causing severe losses and distortion would provide important links to achieve higher objectives or add to the efficiency and flexibility of several technologies.

3.7 Summary

Development and implementation of the electromagnetic technique within the imposed time limits presented a significant engineering challenge. In the absence of strong analytical tools to accurately model the process, a large emphasis had to be placed on the empirical approach. This chapter presented the objectives of the experimental program established to acquire the necessary information, and the main results obtained throughout this program. The problems encountered during the implementation of this technique as well as the corrective measures adopted to rectify them, have been discussed. The development of a pulse-power cable and durable pulse-power coils has been described. The technical advantages of developing this particular technique have also been briefly discussed.

CHAPTER 4

THEORETICAL SIMULATION AND DEVELOPMENT OF THE NUMERICAL SOLUTION FOR THE ELECTROMAGNETIC TECHNIQUE

4.1 INTRODUCTION

The main objective of the theoretical program was to establish a general method to solve axisymmetric electromagnetic field problems in cylindrical structures involving an impulse or transient current input. Such a solution enables the determination of various electromagnetic, thermal and mechanical quantities of interest as functions of both space and time. The solution technique provides the necessary mechanism to optimize the G/S repositioning process by optimizing the coil design and the characteristics of the time-varying current, in a highly efficient and economical fashion.

The theoretical study was subdivided into three main phases as follows:

1. Literature study: the objective of this phase was to determine the state of art for solving similar problems from both the analytical and numerical points of view.

2. Selection of the solution method and formulation of the problem: this phase consisted of establishing the most suitable method to handle the transient nature of the current input, the shielding effect of the P/T, and the overall interaction between the source and induced currents. Formulation of the problem from the electromagnetic point of view as well as the numerical formulation of the selected technique were also included in this phase.

3. Actual solution of the problem and assessment of the results: this phase included the development of the necessary computer programs to provide the final numerical solution and the assessment of these results.

This chapter presents the work carried out to complete the first and second phase of the above program. The work related to the third phase along with some numerical results are described in the next chapter.

4.2 Literature Study

A computer search of the literature on pulse power analysis and applications produced a very extensive list of publications reflecting the rapidly growing trend, particularly in the past two decades, of using pulse power in a multitude of applications, ranging from high energy-density physics and fusion technology to metal forming and mass acceleration [40-51]. However, most of these publications dealt with the physical realization of the required energy densities and addressed the practical problems from a system point of view rather than from their analytical aspects. Also, it is important to note that the highest interest in the emergent pulse power technologies originated from military applications and the development of fusion reactors. A great deal of this information is classified or subject to proprietary rights. This imposes restrictions on the transfer and availability of recent information. Therefore, it is difficult to describe with certainty the actual state of the art of some of these technologies. However, the immense number of publications on this area is indicative of the substantial progress that has been achieved in recent years.

Particular attention has been given to publications dealing with the solution of transient electromagnetic field problems and the numerical methods to solve them. The references listed are restricted to those of direct relevance to theoretical analyses covered in this thesis. They are not intended as a complete list of the available literature. However, the documents cited form a sufficiently complete representation for a full understanding of the subject.

4.2.1 Solution of Transient Electromagnetic Field Problems

As indicated in chapter one, the number of publications dealing with the theoretical analysis and solution of transient electromagnetic field problems has been relatively limited. Most of the pulse power studies relied very heavily on empirical results [10,11,18-21,29,45-51]. For researchers having the necessary equipment, the empirical approach has provided a convenient method to correlate input and output parameters of interest without the necessity to accurately analyse the very complicated equations describing the problem. The complexity of the problem for nearly all practical applications, involving pulsed or transient electromagnetic fields, has precluded exact solution so far. The same is true in many applications involving

electromagnetic fields created by sinusoidal time-varying currents [52]. The finite element technique has proven to be a viable method for solving electromagnetic problems of this class [22-25,53-63].

The finite difference technique has also been used to solve electromagnetic problems involving diffusion process. This technique has fallen out of favour [64-67]. Researchers now are shifting their attention more towards the finite element technique.

The main difference between the finite difference and finite element techniques is that the former approximates the partial differential equations, written for every node in a mesh subdividing the region of interest, while the latter approximates the solution for the partial differential equation by a set of interpolating functions, written for every element that constitutes a small portion of the total region of interest. The finite element technique has the added advantage in its flexibility to handle complex geometries with general regions and materials and the way it handles the boundary and continuity conditions [68,70].

Another numerical approach is the integral formulation for solving Maxwell's equations. This particular solution method offers certain advantages for a particular class of problems involving open regions: however it seems to be applied mostly to steady state electrostatic and magnetostatic field problems in straightforward configurations [71-73] and very seldom to transient field problems [74] with complex geometries. In a few applications it is combined with the finite element method to minimize the size of the mesh representing the region while providing accurate representation for the boundary of this mesh [75-77]. This is particularly advantageous for exterior or unbounded field problems [78,81].

A numerical method based on circuit models has also been reported in the literature [82;83]. This method involves the subdivision of the conductive components in the particular configuration into a number of square or rectangular filaments, and the formulation of the impedance or admittance matrix to relate the input voltage to the current in each filament. This method can be employed for solving eddy-current problems in simple cases. However, it is inferior to the other numerical methods mentioned above because it lacks the capability to determine the electromagnetic fields in non-conducting media and suffers from several computational disadvantages.

Solenoids and electromagnetic actuators have received much attention from the automobile industry, due to their applications in engine controls and fuel-metering systems. These devices have also been used in non-destructive testing techniques for instruments using eddy-current probes [84-88]. Although most actuator and solenoid studies deal with steady state harmonic time-variation, some deal with mechanical motion and transient electromagnetic phenomena [84-89].

Two approaches can be used for the arbitrary time-variation associated with the transient electromagnetic field problem:

1. Discretization of the current pulse input in the time domain: in this method, the finite element or some other numerical technique is used to solve the magnetic vector potential distribution in the regions of interest at each time step, at which the current pulse is discretized. The solution at each time step is used to establish the initial and boundary conditions for the subsequent solution at the next time step [90,91].

2. Decomposition of the current pulse into its Fourier components: in this approach the Fourier analysis

technique is used to express the current pulse as a sum of sinusoidal waveforms. Numerical techniques are then used to solve for each of these waveforms and the principle of superposition is used to obtain the general solution [92,93]. This technique offers significant advantages for linear cases involving pulses that can be represented by a small number of harmonic components. Its main disadvantage is that it can not handle nonlinearities and variations in the system parameters unless the problem is subdivided into a set of piecewise linear problems. This would negate the main benefits of the technique.

4.2.2 Selected Solution Method

Assessment of the available formulation and solution methods and the particular needs of the G/S repositioning process has led to the selection of the following general solution approach:

1. The electromagnetic field problem was formulated in terms of the magnetic vector potential ($\bar{A}$), in order to minimize the number of unknown variables involved in the solution process. This particular formulation is used extensively to solve both transient and

steady state (static and time-varying) electromagnetic field problems involving eddy-currents [22-25,56,58,62-66,94-103]. The magnetic field components can be calculated from the spatial distribution of $\bar{A}$, while the electric field components can be determined from the variation of $\bar{A}$ in time. Other parameters of interest can then be easily determined.

2. The finite element technique was selected to solve for the magnetic vector potential in the space domain. First order triangular elements were used for their simplicity, flexibility and suitability for the fuel channel geometry [104-108].

3. Discretization of the current impulse in the time domain was chosen to represent the variation of the magnetic vector potential and current density in the time domain. This selection was made as a means to leave unrestricted the rate of change of the current input and its shape and to facilitate the verification of the numerical results as outlined in chapter 5 of this thesis.

4. The Crank-Nicolson recurrence scheme was used to represent the variation in the time domain. An

alternative approach is to use the Galerkin method. This treats the time variable as a new dimension (ie. similar to the space dimension). However, the Crank-Nicolson scheme has advantages in respect of the stability of the numerical solution [68,90,91].

The detailed development of this solution approach, together with the computer algorithms and programs are presented in the subsequent sections of this chapter and in chapter five.

4.3 Formulation of the Electromagnetic Field Problem

The behaviour of the electric field vector ($\bar{E}$) and the magnetic field vector ($\bar{H}$) is governed by Maxwell's equations. The classical differential form of Maxwell's equations for time-varying fields may be written as:

$$\text{Curl } \bar{E} = -\frac{\partial \bar{B}}{\partial t} \tag{4.1}$$

$$\text{Curl } \bar{H} = \bar{J} + \frac{\partial \vec{D}}{\partial t} \tag{4.2}$$

$$\text{div } \bar{D} = \rho \tag{4.3}$$

$$\text{div}\,\bar{B} = 0 \tag{4.4}$$

where $\bar{D}$ is the electric flux density, $\bar{B}$ is the magnetic flux density, $\bar{J}$ is electric current density and ρ is the electric charge density. Note that an equivalent set of four equations in integral form may be derived from these through the application of Gauss' and Stokes' theorems.

Equations (4.1) - (4.4) apply only at space points where the required partial derivatives exist, ie. at any point in a continuous medium but not at medium interfaces where discontinuities in material properties may give rise to discontinuities in the vectors themselves [105]. Therefore at the interface of two media, with different magnetic permeability (μ), electrical permittivity (ε) and electrical conductivity (σ), the following continuity conditions should be satisfied:

$$\bar{n} \times (\bar{E}_1 - \bar{E}_2) = 0 \tag{4.5}$$

$$\bar{n} \times (\bar{H}_1 - \bar{H}_2) = \bar{J}_s \tag{4.6}$$

$$\bar{n} \cdot (\bar{D}_1 - \bar{D}_2) = \sigma_s \tag{4.7}$$

$$\bar{n} \cdot (\bar{B}_1 - \bar{B}_2) = 0 \qquad (4.8)$$

The above equations state that the tangential components of the field vectors must be continuous at any material interface, except if a surface current exists (in such a case, the magnetic field vector may possess a discontinuity equal to the surface current density $\bar{J}_s$), and that the normal components of both flux densities must be continuous, except if a surface charge resides at the interface (in that case, the electric flux density vector may possess a discontinuity equal to the surface charge density σ_s).

Equations (4.1) - (4.8) are applicable regardless of the nature of the materials involved. However, they are computationally intractable because the system of equations remains indeterminate; there are four equations but five distinct vectors. Since equations (4.1) and (4.2) are vector equations, the implied total number of (scalar) differential equations is in fact eight,—the number of independent vector components is fifteen. Since no other boundary or interface conditions can be deduced from Maxwell's equations, additional equations are obtained by relating the flux densities to the fields through the constitutive relations:

$$\bar{D} = \epsilon\bar{E} \tag{4.9}$$

$$\bar{B} = \mu\bar{H} \tag{4.10}$$

The permittivity and the permeability may be nonlinear tensor quantities. Fortunately, in most practical cases they are nearly constants, and for many materials they may be nonlinear but scalar. A similar classification of materials is possible with respect to the conductivity (σ), which relates the current density to the electric field through Ohm's law:

$$\bar{J} = \sigma\bar{E} \tag{4.11}$$

Now the number of equations is sufficient to determine the field vectors. However, from a computational point of view direct solution of Maxwell's equations is the least efficient and a more economical representation is usually sought.

From the finite element analysis point of view, two desirable properties would render the representation of the electromagnetic field ideal. First, every field describable by a linear combination of the finite element basis

functions should be physically realizable. Second, the equations describing the field should lend themselves to a variational or projective formulation such as to encompass within it as natural boundary conditions all the electromagnetic phenomena actually occurring at source-free surfaces or material interfaces [105]. In addition, the ideal representation would involve the minimum possible number of variables at each space point to maximize the computational efficiency. For analysis of the G/S repositioning problem, the field representation in terms of the magnetic vector potential permits special simplifications and yields substantial computational savings because only a single variable at each node in the finite element mesh has to be used. Since the source current can be assumed to flow in the circumferential direction, the magnetic vector potential has only one component in the same direction while the magnetic field has two components: one in the radial the other in the axial direction.

4.3.1 Transient Field Problems - Diffusion Equation

The Maxwell magnetic divergence equation (4.4) can conceivably be satisfied if one defines a vector $\bar{A}$, commonly known as the magnetic vector potential, such that

$$\bar{B} = \nabla \times \bar{A} \tag{4.12}$$

From vector analysis, it is well known that the divergence of the curl of any twice differentiable vector vanishes identically, thus

$$\nabla \cdot \nabla \times \bar{A} = 0 \tag{4.13}$$

Equation (4.12) does not define $\bar{A}$ fully, because a vector is uniquely defined if and only if both its curl and divergence are known, as well as its value at some one space point (Helmholtz theorem). However, the divergence of $\bar{A}$ can be chosen arbitrarily to satisfy certain conditions. If $\bar{A}$ is defined in any manner which satisfies equation (4.12), the first Maxwell equation (4.1) may be written in the form

$$\nabla \times (\bar{E} + \frac{\partial \bar{A}}{\partial t}) = 0 \tag{4.14}$$

From vector analysis, the curl of any gradient vanishes, analogous to equation (4.14), so that for any twice differentiable scalar function V,

$$\nabla \times \nabla V = 0 \tag{4.15}$$

Thus equation (4.14) indicates that $\bar{E}$ differs from the rate of change of $\bar{A}$ with respect to time by some irrotational vector ∇V (grad V),

$$\bar{E} = -\frac{\partial \bar{A}}{\partial t} - \nabla V \tag{4.16}$$

V is the electric scalar potential, since in the static case when no time variations are present $\bar{E}$ becomes:

$$\bar{E}_{static} = -\nabla V \tag{4.17}$$

Note that nearly all electric field analyses reported in the literature to date are carried out in terms of the electric scalar potential. In time-varying situations, the magnetic and electric potentials are also used to minimize the number of variables associated with every point in space. A wave equation in $\bar{A}$ can be derived [105] by taking curls of both sides of equation (4.12), yielding

$$\nabla \times \nabla \times \bar{A} = \nabla \times \bar{B} \tag{4.19}$$

substitution of equations (4.2), (4.9), (4.10) and (4.17) yields in the case of homogeneous and isotropic materials

$$\nabla \times \nabla \times \bar{A} = \mu\bar{J} + \mu\varepsilon \frac{\partial^2 \bar{A}}{\partial t} - \nabla(\mu\varepsilon \frac{\partial V}{\partial t}) \tag{4.20}$$

Using the well known vector indentity

$$\nabla \times \nabla \times \bar{A} = \nabla(\nabla \cdot \bar{A}) - \nabla^2 \bar{A} \tag{4.21}$$

equation (4.20) can be then written as:

$$\nabla^2 \bar{A} = \nabla(\nabla \cdot \bar{A} + \mu\varepsilon \frac{\partial V}{\partial t}) + \mu\varepsilon \frac{\partial^2 \bar{A}}{\partial t^2} - \mu\bar{J} \tag{4.22}$$

Equation (4.22) can be simplified very considerably by choosing the divergence of $\bar{A}$ as

$$\nabla \cdot \bar{A} = - \mu\varepsilon \frac{\partial V}{\partial t} \tag{4.23}$$

Equation (4.23) is called the Lorentz condition [105]. Thus, the inhomogenous wave equation is obtained:

$$\nabla^2 \bar{A} - \mu\varepsilon \frac{\partial^2 \bar{A}}{\partial t^2} = -\mu\bar{J} \tag{4.24}$$

In the case of magnetostatic fields, the wave equation in $\bar{A}$ assumes the form of a vector Poisson equation,

$$\nabla^2 \bar{A} = -\mu \bar{J} \tag{4.25}$$

Equation (4.25) can be solved analytically for axisymmetric field problems. It has been presented here because its analytical solution was used to check the validity of the computerized solution (for steady state cases) as outlined in the next chapter.

In most time-varying cases the current density distribution is not known unless A is known. The total current in the conductors used to carry a source current may be determined by measurements but, in this case, not the current distribution. Therefore an alternative definition of the divergence of A may prove to be more desirable for the time-varying cases than the Lorentz choice. Returning to equation (4.19), the terms on the right hand side may be eliminated by substituting equations (4.9) and (4.11), then inserting equation (4.16) to obtain:

$$\nabla^2 \bar{A} = \nabla(\nabla \cdot \bar{A}) + \nabla(\mu\sigma V + \mu\epsilon \frac{\partial V}{\partial t}) + \mu\sigma \frac{\partial \bar{A}}{\partial t} + \mu\epsilon \frac{\partial^2 \bar{A}}{\partial t^2} \tag{4.26}$$

Examination of Equation (4.26) indicates that it can be reduced to a very simple form by choosing the divergence of $\bar{A}$ as:

$$\nabla \cdot \bar{A} = -\mu\sigma V - \mu\varepsilon \frac{\partial V}{\partial t} \tag{4.27}$$

This choice yields the homogeneous wave equation [105]

$$\nabla^2 \bar{A} - \mu\sigma \frac{\partial \bar{A}}{\partial t} - \mu\varepsilon \frac{\partial^2 \bar{A}}{\partial t^2} = 0 \tag{4.28}$$

Equation (4.28) is particularly convenient for low frequency applications in which the second time derivative term may be neglected. This is valid for the G/S repositioning problem since the frequency has to be maintained at low levels. For frequencies below 10 kHz, for example, the term $\mu\sigma\partial\bar{A}/\partial t$ is much larger than the last term in equation (4.28) for material having good electrical conductivity. Thus equation (4.28) assumes the form

$$\nabla^2 \bar{A} - \mu\sigma \frac{\partial \bar{A}}{\partial t} = 0 \tag{4.29}$$

Equation (4.29) is more appropriate for the analysis of the G/S repositioning problem than equation (4.24) because it represents the diffusion phenomena and accounts for the induced eddy currents that play a more dominant role in this application than the propagation phenomenon represented by the expression $\mu\varepsilon\partial^2 A/\partial t^2$. To correlate $\bar{A}$ in

equation (4.29) to the input current and render this equation computationally useful, let $\bar{A}$ be written as the sum of two components $\bar{A}_0$ and $\bar{A}_e$

$$\bar{A} = \bar{A}_0 + \bar{A}_e \tag{4.30}$$

where $\bar{A}_0$ may be taken to represent the magnetic vector potential distribution that would exist were the frequency of the current variations to be very low. Therefore, $\bar{A}_0$ may be considered known, since the static problem as formulated above (equation (4.25) and appropriate boundary conditions) is readily solvable. Substituting equation (4.30) into equation (4.29) yields:

$$\nabla^2\bar{A}_e - \mu\sigma \frac{\partial \bar{A}_e}{\partial t} = -\nabla^2\bar{A}_0 + \mu\sigma \frac{\partial A_0}{\partial t} \tag{4.31}$$

Using equation (4.25) and noting that the second term on the right hand side of equation (4.31) can be neglected, the problem may be reformulated as:

$$\nabla^2\bar{A}_e - \mu\sigma\frac{\partial \bar{A}_e}{\partial t} = \mu\bar{J}_0 \tag{4.32}$$

where $\bar{J}_0$ is the current distribution that would exist in the absence of time variation. There is an alternative derivation which leads to the same results [56,95,103]. The diffusion equation for nonlinear field problems is written as:

$$\nabla \times \frac{1}{\mu} \nabla \times \bar{A} = - \sigma \frac{\partial \bar{A}}{\partial t} + \bar{J}_0 \tag{4.33}$$

In the case of linear field problems, the diffusion equation becomes (using the vector identity (4.21)):

$$\nabla^2 \bar{A} = \mu\sigma \frac{\partial \bar{A}}{\partial t} - \mu \bar{J}_0 \tag{4.34}$$

4.3.2 Boundary Conditions

The diffusion equation derived above together with the interface continuity conditions (equations (4.5) - (4.8)) describe an infinitely-extending field. This is not convenient from a computational viewpoint. The magnetic vector potential and the associated variables obviously vanish at infinity. However, appropriate selection of boundary conditions allows reduction of the solution region to a manageable size without causing any significant deterioration in the accuracy of the solution, particularly

at points remote from the established boundaries. Conventional proof of the conditions satisfied at a boundary by normal and tangential components of the field vectors, and proof of the uniqueness of the solution within a bounded region are given in reference 6.

It should be noted that both the Dirichlet and homogeneous Neumann boundary conditions are fulfilled by the variational method (finite element) used to obtain a numerical solution, unless another boundary condition is explicitly specified. These boundary conditions are used almost universally to solve various classes of electromagnetic field problem, hence they have received substantial attention in the literature [5,6,30,88-105]. The continuity conditions at the interface between two different materials are implicitly satisfied by the finite element formulation. To effect solution, the following boundary conditions were adopted:

1. The magnetic vector potential at the axis of the coil is specified. This also satisfies the requirement of defining this vector in at least one point in space to render the problem determinant. In the G/S repositioning problem, axial symmetry is assumed. In this case, it is easy to see from the

definition of $\bar{A}$ and from Ampere's law that the value of the magnetic vector potential along the coil axis is equal to zero [30,109].

2. On the other three sides bounding the region of interest, the natural or homogeneous Neumann boundary conditions are adopted. These conditions are represented by:

$$\frac{\partial \bar{A}}{\partial \bar{n}} = 0 \qquad (4.35)$$

where $\bar{n}$ is a directional vector normal to the side under consideration.

The reasons for using these boundary conditions are:

i. In order to reduce the size of the finite element mesh subdividing the region of interest, only one quarter of the longitudinal cross-section of the coil and fuel channel configuration is considered. That is, advantage is taken of the symmetry about the coil axis and the plane normal to it. The plane divides the coil through the middle. At both sides of the symmetry line (located at z=0) the value of the magnetic vector

potential is the same at any distance from the center. This means ($\partial\bar{A}/\partial\bar{n} = 0$). Here $\bar{n}$ is normal to the r-axis.

ii. For the remaining two sides, using the Neumann boundary condition allows the placement of these boundary lines much closer to the coil peripheries than if the Dirichlet boundary conditions ($\bar{A}=0$) were used.

The study presented in reference 109, provides numerical results for an infinitely long coreless coil in free space, with the outer boundary placed at various distances outside the coil. It also compares the results obtained when the Neumann boundary condition was used to those obtained with the Dirichlet boundary condition. The conclusion drawn from this work was that placing the boundary line (parallel to the coil axis) at a distance from the center equal to five times the coil radius, is sufficient to reduce the error to less than 4% at the points near the boundary. In the work presented in reference 110, the boundary line was only one coil radius away from the outer coil radius and about one coil length away from the edge of the coil in the axial direction.

In the case of the G/S problem, the boundary line parallel to the coil axis does not have to be placed much further from the outer surface of the C/T, since the magnetic field is attenuated by both the the P/T and C/T. However, for good accuracy, (probably less than 1% error) the boundary was placed about one coil radius away from the C/T. The fourth side was placed at a distance twice the coil length away from the edge of the coil. This is considered more fully in the next chapter.

4.3.3 Representation of The Source Current Impulse

The magnetic vector potential has to be expressed in terms of a known source quantity in order to make the formulation computationally useful. The only measurable source variables for this class of electromagnetic field problems are the total current and the applied voltage. For particular cases involving time-varying excitations and, solenoidal coils, a problem arises from the fact that the current is not distributed uniformly in the cross-section of the coil turns and the applied voltage is not shared equally among the coil turns. The formulation approach illustrated in subsection (4.3.1) of this chapter represents an efficient method to circumvent this difficulty, particularly for transient problems.

An important reason for avoiding the alternative formulation in term of the voltage input is that the voltage drop in the windings near the center of the coil is normally higher than the voltage drop in the turns at the ends of the coil. Reference 111 shows that this uneven distribution is more prominent when the number of turns in the coil is small. As the number of turns increases, the difference in voltage drop decreases since the coil approaches what can be considered an infinitely long solenoid. The length of the coils used for G/S repositioning was approximately equal to their diameter. Hence the difference in voltage drop per turn is near maximum and any simplifying assumption would compromise the accuracy of the model.

To overcome the difficulty associated with representing the source voltage, other researchers [110] expressed the voltage drop in each coil turn in terms of the total current in the coil. The reported method was developed for harmonic time-varying currents where the total current density in the conductor was given by:

$$\bar{J} = \bar{J}_0 + j\omega\sigma\bar{A} \qquad (4.36)$$

For a coil having N turns, the N-unknown voltages [$\dot{U}$] are expressed in terms of the N-known total currents

I_k (k=1,2----N) by means of a symmetric admittance-coefficient matrix [Y] as shown below:

$$[Y][U] = [I] \tag{4.37}$$

In order to obtain the coefficient of [Y], a set of linear equations, produced by a finite element formulation, must be solved N times. Each time an arbitrary voltage is assumed to be applied to one turn only; the voltages being applied to each successive turn for N solutions. After each solution, a set of the coefficients of [U] is calculated and the principle of superposition is used to assemble [U]. Subsequent to these steps the final solution of the magnetic vector potential is carried out. A similar approach was used by Weiss and Csendes [112]. Another approach to achieve the same objective consists of solving a coupled system of differential and algebraic equations [113]. Implementation of these approaches for transient situations would increase the cost of solution considerably, particularly if the number of turns is increased to optimize the G/S repositioning process nor would it improve the accuracy of the results in comparison to modelling the current density. On the contrary if a good accuracy is to be achieved via this approach, the current impulse would need to be represented by a Fourier series. An admittance-

coefficient matrix must also be calculated for each harmonic component, a lengthy and tedious procedure. Hence the representation of equaton (4.34) is chosen over other approaches for solution of the G/S repositioning problem.

4.3.4 Summary of Simplifying Assumptions

In the axisymmetric transient electromagnetic field analysis presented in this chapter, the following assumptions were made in deriving the associated partial differential equation.

1. Displacement currents are neglected for the operating frequencies (below 2000 Hz) of interest for this application. Note that at this frequency level the displacement currents are several orders of magnitude smaller than the source conduction and induced eddy-currents.

2. The materials of the coil and the fuel channel components are homogeneous and isotropic. This assumption is valid since all of the involved materials are non-magnetic (copper or zirconium-niobium alloys).

3. The conductivities of the media are assumed constant: temperature effects are neglected. After approximately 500 μs, a half cycle of the current pulse, the G/S would be at a distance far enough from the coil end not to be affected by temperature variation. The largest temperature rise which would result from fast repetition rate is in the coil. To minimize the error associated with variation in the temperature of the coil, the conductivity of the coil material at the average operating temperature can be used in the numerical calculation.

4. Local variation of the magnetic vector potential distribution due to the G/S movement is neglected. The G/S is modelled by its tie wire only, hence the volume occupied by it as compared to the volume of the P/T wall exposed to the magnetic field, is negligible.

Other assumptions related to the geometry of the coil are:

1. The pitch of the coil is neglected and the current in the winding is assumed to be in the circumferential direction. Consequently, the magnetic vector

potential has only one component in the same direction. This allows the treatment of the problem as an axisymmetric field problem (one component for $\bar{A}$ ($A\phi$) and two components for the magnetic field $\bar{H}$ (H_r and H_z)). This obviates the necessity of solving a three dimensional field problem.

2. The coil leads are assumed to be contiguous to the coil. They have the same cross-section as the coil windings. It is also assumed that there is an integral number of turns such that at each end of the coil there is a complete turn. The presence of the central coil lead as well as the bolts used to prestress the coil in the axial direction is neglected. Experimental results did not show any measurable changes in the G/S displacement when the bolts were incorporated into the coils. Neglecting the coil leads is justified because of their direction with respect to the G/S: the current in the leads causes an induced current in the P/T in the axial direction which does not affect movement of the G/S.

3. The interface block connecting the coil leads to the coaxial cables (TL) is assumed to be far enough from

the coil end not to affect the distribution of the magnetic vector potential. Physically this interface was located at least 10 cm away from the edge of the coil.

4.4 Finite Element Technique - General Description

The finite element method is a powerful numerical procedure for solving mathematical or physical problems which are usually defined in a continuous domain either by local differential equations or by equivalent global statements. The method was born in the aerospace industry in the early 1950's [91]. A report on the first practical application was published by Turner, Clough, Martin, and Topp in 1956 [114]. Several technical articles dealing with the application of the method to structural and solid mechanic problems followed. But a major theoretical contribution was made by Melosh in 1963 when he showed that this method was really a variation of the well known Raleigh-Ritz procedure. In structural problems the method produces a set of linear equilibrium equations by minimizing the potential energy of the system.

The connection of the finite element method with a minimization procedure quickly led to its use on other

engineering topics. The use of this method was enlarged further when other investigators [115,116] showed that the element equations can be derived using a weighted residual approach such as the Galerkin's, collocation or least square methods. This knowledge allowed the finite element method to be applied to solve almost any differential equation. In electrical engineering the finite element method did not make its first appearance until about 1968. Since then it has been used for a wide range of applications [68,90,91,104-108].

The fundamental concept of the finite element method is that any continuous quantity in a domain (Ω) can be approximated by a discrete model composed of a set of piecewise continuous functions defined over a finite number of sub-domains which divide Ω without overlap or exclusion. This effectively replaces the infinite number of degrees of freedom, normally associated with a continuous quantity, by a finite number of unknown parameters. Piecewise continuous functions are defined using values of the continuous quantity at a finite number of points in its domain. The basic steps for describing a finite element solution procedure can be summarized as:

1. Sub-division of the continuum into finite elements (mesh discretization).

2. Formulation of the finite element equations for the chosen alternative solution method. This step involves the establishment of a set of linear algebraic equations to represent the problem, via the minimization of an energy-related expression, called a functional.

3. Construction of an equation-solving algorithm.

4. Evaluation of subsidiary element quantities.

Some of the advantageous properties of the finite element method which contributed to its extensive use are:

1. The material properties in adjacent elements need not be the same. This characteristic of the method permits its application to systems composed of several materials.

2. The method is not limited to systems with regular shapes and easily defined boundaries since elements with straight or curved sides can be used to match irregularly shaped boundaries and contour lines.

3. Various types of boundary conditions can be handled easily.

4. The size of the elements can be varied within a region. This allows the element grid to be refined as desired.

5. The above properties can be incorporated into a general computer program for a particular class of problems. For example a general computer program for axisymmetric vector field problems can be used for solving any problem of this type that may arise.

The application of the finite element method requires computer programs and computer facilities because the computations involved are too numerous for hand calculations.

4.4.1 Mesh Discretization

The discretization of the domain into subregions is more of an art than a science [91]. Good engineering judgement is crucial to avoid producing inaccurate results because of poor discretization, even if all other steps are correctly executed. The discretization process involves decisions as to the number, size and shape of subregions used to model the entire domain, including boundaries. This process can be divided into two general parts; the division

of the region into elements and the labelling of the elements and nodes. The latter part seems quite simple but is complicated by the necessity of ensuring computational efficiency. An important practical point of the finite element procedure is that the contributions of the elements to the global matrix are highly localized and only a few nonzero terms are contributed by each element. This results in very large systems of sparse equations. Techniques are required to reduce computer requirements. Proper labeling of the nodes can effect great savings to minimize the computer storage requirement: a highly desirable feature particularly for transient field problems.

As in other engineering problems, one is faced with the delicate balance of making the elements small enough to achieve high accuracy and yet large enough to reduce the computational effort. As a general rule the element size should be decreased in the areas where the desired results vary rapidly (high gradient values). To model a two-dimensional domain there are two general element families: the triangle and the quadrilateral. The linear elements in each family have straight sides, but higher order elements can have either straight or curved sides or both. The use of first-order simplex triangular element is analytically the simplest of the two types of elements. Higher order

finite elements entail a considerably more complicated methodology than the first order counter-part. However higher order finite elements have the advantage of increasing the accuracy or decreasing the cost of the solution [105]. The economical advantages of higher order finite elements are offset to a large extent by the cost of performing the necessary numerical integrations [91].

Consideration of the various criteria associated with modelling the G/S repositioning problem, and the development of a flexible computer algorithm that can be used for other pulse power applications, led to the selection of first order triangular element for the following reasons:

1. To establish a solution method to optimize and improve the repositioning technique.

2. Simplicity of formulation and programming.

3. The dimensions of the coil and thickness of the P/T, G/S and C/T are inherently small. To obtain reasonably detailed profiles of the current density and force density distributions, a large number of very small elements is required regardless of the order

selected. Hence, to reduce the cost of the solution, higher order elements requiring numerical integration had to be avoided.

4. The use of very small elements in conjunction with small time steps minimizes the probability of having numerical oscillation that may exist when the Crank-Nicolson central difference procedure is used [90,91].

5. The use of small elements minimizes the error that results from correlating the axisymmetric field problems to rectangular two-dimensional problems as outlined in the next section.

Particular attention was given in the development of the procedure to labeling of the nodes in order to minimize the bandwidth of the global stiffness matrix. A listing of the equations generated by the finite element process shows that all nonzero values and some zero values fall between two lines parallel to the main diagonal of the stiffness matrix as shown in Figure 4.1. The bandwidth is defined as the number of columns between the main diagonal and the line above it [91]. Efficient computer programming uses only the coefficients within the bandwidth, which is calculated using:

$$BW = (D + 1)\ NDOF \tag{4.38}$$

where D is the largest difference between the node numbers in a single element (with all elements in the mesh being considered in its determination) and NDOF is the number of degrees of freedom at each node. Labeling the nodes across the dimension of the body with the least number of nodes in it minimizes D which in turn minimizes BW.

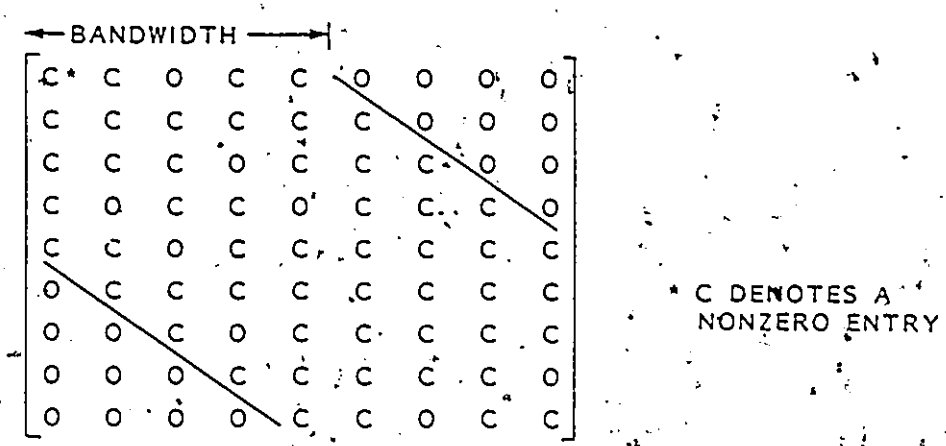

Figure 4.1

The bandwidth of a matrix.

4.4.2 Formulation of The Finite Element Equations

The most widely used finite element solution methods are the variational and Galerkin techniques. The former is employed whenever a minimizable functional expression can be conveniently written. Failing this, the Galerkin approach

is utilized. In this approach a non-minimizable functional is constructed directly from the elliptic governing partial differential equation. The result is then equated to zero in order that a stationary point, rather than a true minimum, may be sought. A detailed description of these techniques is given in practically any recent book on the subject [90,91].

The variational approach was adopted for the study presented in this thesis because a minimizable functional can be readily written and a numerical procedure that is unconditionally stable can be used to solve the transient problem. However, note that the time variation must be treated in a special manner. Basically, the parabolic differential equation (equation 4.34) must be converted to an equivalent elliptic differential equation.

This objective can only be realized by the implementation of an appropriate finite difference time progression representation. In this technique, the solution in the time domain is discretized into equal time intervals of suitable width, while the time derivative in the governing partial differential equation is replaced by its finite difference model [81,90,91]. Then assuming known boundary values, the ensuing spatial elliptic boundary value problem

is solved at each time step using the magnetic vector potential values computed during the previous time interval as intitial conditions. For initiation of the first iteration a zero initial condition is assumed as a solution for time ($t=0^-$) is obtained. This step is also necessary from the programming point of view, particularly if the source impulse is a step function.

The main steps involved in deriving the finite element equations that represent the problem governed by the partial differential equation and boundary conditions for transient problems can be summarized as follows:

1. The partial differential equation and associated boundary conditions are formulated in variational terms by an energy-related expression (the energy functional).

2. In each element of the finite element mesh an approximate solution to the field problem is defined in terms of the potentials at the nodes.

3. The functional is extremized by setting its first variation with respect to the nodal potential to zero.

4. The time-stepping is carried out by an implicit forward difference scheme or the well known Crank-Nicolson recurrence method.

The above process is well documented in the literature for both scalar and vector field problems that can be solved using two-dimensional (2-D) cartesian coordinates. The same is true for axisymmetric scalar field problems. For these classes of problems final finite element matrices that can be used for programming of the solution are readily available [90,91,102-106]. However, for axisymmetric vector field problems the situation is different and is not so well documented. The functional minimization process is complicated by the fact that the functional for axisymmetric vector fields contains a singular term (1/r) which does not allow a polynomial expansion. To overcome this difficulty other investigators have resorted to various methods to eliminate this singularity [104,113,117,118]. The resulting derivations are tedious and lengthy. The implementations are, in general, costly.

In this study a simple alternative formulation was developed and employed to solve the axisymmetric vector field problem deriving from the G/S repositioning project. The method consisted of demonstrating that a change in

variables can be used not only to remove the singularity but to make the functional for the axisymmetric vector field identical to the functional used in 2-D vector or scalar field problems. Consequently, the well-developed finite element matrices for 2-D fields can be used with minor modifications to solve axisymmetric vector field problems. The advantages of such a formulation are not limited to eliminating the tedious derivations of the finite element matrices, they also include the benefits of allowing the developed computer program to handle electromagnetic field problems in any one of the above mentioned classes without expending too much effort.

To illustrate the finite element formulation process, the two-dimensional case is presented in the next subsection, and the correlation between the axisymmetric case and the two-dimentional case is presented in the next sections.

4.4.3 Formulation For the Two-Dimensional Planar Case

In a two-dimensional cartesian coordinate system, the partial differential equation describing the behaviour of the magnetic vector potential (equation 4.34) along with the Dirichlet and Neumann boundary conditions can be written in the general form

$$\frac{\partial^2 \bar{A}}{\partial x^2} + \frac{\partial^2 \bar{A}}{\partial y^2} = -Q(x,y,t), \quad 0<x,y<1 \tag{4.39}$$

where

$$Q(x,y,t) = -\mu\sigma \frac{\partial \bar{A}^*}{\partial t} + \mu \bar{J}_0 \tag{4.40}$$

(*Note that this term is discretized to reduce the diffusion equation to Poisson's equation at each time step)
with the boundary conditions

$$\bar{A} = \hat{A}_1 \text{ on } y = 0 \text{ (coil axis)}$$

$$\frac{\partial \bar{A}}{\partial \bar{n}_y} = \hat{g}_1(x) \text{ on } y = 1 \text{ (unit length)} \tag{4.41}$$

$$\frac{\partial \bar{A}}{\partial \bar{n}_x} = \hat{g}_2 \text{ on } x = 0 \text{ and } x = 1 \text{ (unit length)}$$

where $\hat{A}_1$, $\hat{g}_1(x)$ and $\hat{y}_1(y)$ are specified values

Reference 68 contains a detailed treatment of functional analysis and presents a three step procedure for developing an appropriate functional for Poisson's equation. The functional shown in equation 4.42 is readily available from the literature [68,90,91,104-107]

$$F(\bar{A}) = \frac{1}{2}\int_0^1\int_0^1 [(\frac{\partial\bar{A}}{\partial x})^2 + (\frac{\partial\bar{A}}{\partial y})^2 - 2Q\bar{A}]dxdy + \tag{4.42}$$

$$\int_0^1 \hat{q}_1(x)\hat{A}_1(x,0)dx + \int_0^1 \hat{q}_2(y)dy$$

Note that for the Neumann boundary conditions (and for $\hat{A}_1(x,0) = 0$), the two right most integrals vanish invariably. This illustrates why the Neumann boundary conditions are automatically satisfied by the finite element process, unless other specific boundary conditions are explicitly stated. Hence the functional shown in equation (4.42) reduces to

$$F(\bar{A}) = \frac{1}{2}\int_0^1\int_0^1 [(\frac{\partial\bar{A}}{\partial x})^2 + (\frac{\partial\bar{A}}{\partial y})^2 - 2Q\bar{A}]dxdy \tag{4.43}$$

With Q written explicitly and the integration limits dropped equation (4.43) takes the form

$$F(\bar{A}) = \frac{1}{2}\iint[(\frac{\partial A}{\partial x})^2 + (\frac{\partial\bar{A}}{\partial y})^2 - 2Q\bar{A}]dxdy + \mu\sigma\iint(\frac{\partial\bar{A}}{\partial t})\bar{A}dxdy \tag{4.44}$$

$$-\mu\iint\bar{J}_0\bar{A}dxdy$$

Minimization of the above functional yields the solution to the partial differential equation, and associated boundary conditions, provided the Euler equation of the functional is identical to the original differential equation [68,90,104,107]. The minimization of the above functional for first order triangular elements leads to a matrix equation of the form

$$[S]\,\{A\} + [C]\,\{\frac{dA}{dt}\} = \{F\} \tag{4.45}$$

where $[S]$ is known as the stiffness matrix and $[C]$ as the capacitance matrix, $\{A\}$ is a column vector of the unknown magnetic vector potential at each node, $\{\frac{dA}{dt}\}$ is a column vector of the time derivative of (A) at each node and $\{F\}$ is a forcing vector representing the source terms. Derivation and assembly of the above matrices is well documented in the literature. However, for the sake of completeness Appendix B of this thesis shows the main steps of this process; the above known matrices for each triangular element with nodes i, j and k are shown to have the following forms [56,90,91,104-107]:

$$[S] = \frac{1}{4\mu\Delta}\begin{bmatrix} (b_i b_i + c_i c_i), & (b_i b_j + c_i c_j), & (b_i b_k + c_i c_k) \\ (b_i b_j + c_i c_j), & (b_j b_j + c_j c_j), & (b_j b_k + c_j c_k) \\ (b_i b_k + c_i c_k), & (b_j b_k + c_j c_k), & (b_k b_k + c_k c_k) \end{bmatrix} \tag{4.46}$$

$$[C] = \frac{\Delta\sigma}{12} \begin{bmatrix} 2 & 1 & 1 \\ 1 & 2 & 1 \\ 1 & 1 & 2 \end{bmatrix} \tag{4.47}$$

$$\{F\} = \frac{\Delta J_0}{3} \begin{bmatrix} 1 \\ 1 \\ 1 \end{bmatrix} \tag{4.48}$$

where the constants used in the above equation are defined in appendix B.

4.5 The Axisymmetric Vector Field Problem

In cylindrical coordinates the Laplacian of a vector $\bar{A}$ can be expanded as follows:

$$\nabla^2\bar{A} = \nabla(\nabla \cdot \bar{A}) - \nabla \times \nabla \times \bar{A}$$

$$\nabla^2\bar{A} = \nabla\left[\frac{1}{r}\frac{\partial}{\partial r}(rA_r) + \frac{1}{r}\frac{\partial A_\phi}{\partial \phi} + \frac{\partial A_z}{\partial z} \right] -$$

$$\nabla \times \begin{vmatrix} \frac{i_r}{r} & i_\phi & \frac{i_z}{r} \\ \frac{\partial}{\partial r} & \frac{\partial}{\partial \phi} & \frac{\partial}{\partial r} \\ A_r & rA_\phi & A_z \end{vmatrix}$$

Where i_r, i_ϕ, and i_z are unit vectors in the radial, circumferential and axial directions respectively. In the case of axisymmetry $A_r = 0$, $A_z = 0$ and $\partial/\partial\phi = 0$. Therefore the above equation reduces to

$$\nabla^2 \bar{A} = -\nabla \times \left[\frac{1}{r} \frac{\partial}{\partial r} (rA_\phi)\, i_z - \frac{1}{r} \frac{\partial}{\partial z} (rA_\phi)\, i_r \right]$$

Taking the curl and dropping the vector notation since there is only one component (A_ϕ), the above equation becomes

$$\nabla^2 A_\phi = -\frac{\partial^2 A_\phi}{\partial z^2} - \frac{\partial^2 A_\phi}{\partial r^2} - \frac{1}{r}\frac{\partial A_\phi}{\partial r} + \frac{A_\phi}{r^2} \qquad (4.49)$$

substituting the above equation in the diffusion equation (equation (4.34)) yields:

$$\frac{\partial^2 A_\phi}{\partial z^2} + \frac{\partial^2 A_\phi}{\partial r^2} + \frac{1}{r}\frac{\partial A_\phi}{\partial r} - \frac{A_\phi}{r^2} = \mu J_0 - \mu\sigma \frac{\partial A_\phi}{\partial t} \qquad (4.50)$$

Note that the above equation for a vector field is different from the diffusion equation for a scalar field since the Lapacian for the two fields is different. The

functional for the above equation and associated boundary conditions has the form [56,90,104,105].

$$F(A_\phi) = \int_\Omega [\frac{1}{2\mu}[\frac{\partial A_\phi}{\partial z})^2 + \frac{1}{r^2}(A_\phi + r\frac{\partial A_\phi}{\partial r})^2] + (\frac{1}{2}\sigma\frac{\partial A^*_\phi}{\partial t} - J_0)A_\phi]2\pi r dr dz$$

which can be written as

$$F(A_\phi) \cong 2\pi\int_\Omega r[(\frac{\partial A_\phi}{\partial z})^2 + (\frac{\partial A_\phi}{\partial r})^2 + \sigma\mu\frac{\partial A^*_\phi}{\partial t}A_\phi - 2\mu J_0 A_\phi]$$

$$+ 2A_\phi\frac{\partial A_\phi}{\partial r} + \frac{A_\phi^2}{r}]drdz \qquad (4.51)$$

The above functional is different from its scalar counterpart; it is particularly inconvenient because it contains the term A_ϕ^2/r which does not allow a polynomial expansion. Silvester and Ferrari [104] brought this expression into the general finite-element framework by a change in variable which consisted of setting

$$A'_\phi = \frac{A_\phi}{\sqrt{r}} \qquad (4.52)$$

$$J'_\phi = \frac{J_\phi}{\sqrt{r}} \tag{4.53}$$

To complete the development of the finite element solution for the new variable, the usual polynomial expansion for the trial function,

$$A'_\phi = \sum_j A'_j \, \alpha_j \, (\zeta_1, \zeta_2, \zeta_3) \tag{4.54}$$

must be substituted. The functional is then minimized. This expansion is lengthy because of the many terms in the functional: it is seldom performed. An alternative method is presented in reference 118 where two steps are taken to circumvent this difficulty. First, the triangular elements are made to be sufficiently small to allow the vector potential at the nodes of the triangle to be replaced by a fixed approximation (A_c/r_c) without introducing a significant error. A_c and r_c are the values of these variables at the centroid of the triangle and are given in terms of the true nodal values by:

$$A_c = \frac{1}{3} \sum_{k=1}^{3} A_k \text{ and } r_c = \frac{1}{3} \sum_{k=1}^{3} r_k \tag{4.55}$$

Secondly, the elements of the stiffness matrix are moved by a distance equal to $2\Delta/3r_c$ (Δ=the area of the triangular element) yielding a new element of this matrix. A similar approach that replaces A_ϕ by its value at the centroid of the element is reported by Andersen [113]. In this study, the singularity was removed by reformulating the problem in terms of a new variable: instead of solving for the vector originally desired, one solves for [119,120]

$$A'_\phi = A_\phi r \tag{4.56}$$

Correspondingly, it is convenient to write the source term as

$$J'_0 = J_0 r \tag{4.57}$$

Substituting equation (4.56) and (4.57) in the functional equation (4.51) yields

$$F(A'_\phi) = 2\pi\int_\Omega \{r[\frac{k}{r^2}(\frac{\partial A'_\phi}{\partial z})^2+(\frac{1}{r}\frac{\partial A'_\phi}{\partial r}-\frac{A'_\phi}{r^2})^2+\sigma\mu\frac{A'_\phi}{r^2}\frac{\partial A'_\phi}{\partial t}-2\mu J'_0\frac{A'_\phi}{r^2}]+$$

$$2\frac{A'_\phi}{r}[\frac{1}{r}\frac{\partial A'_\phi}{\partial r}-\frac{A'_\phi}{r^2}]+\frac{A'^2_\phi}{r^3}\}drdz$$

which after some simplification becomes

$$F(A'_\phi) = 2\pi \int_\Omega \frac{1}{\mu r}\left[\left(\frac{\partial A'_\phi}{\partial z}\right)^2 + \left(\frac{\partial A'_\phi}{\partial r}\right)^2 + \sigma \frac{\partial A'_\phi}{\partial t} A'_\phi - 2J'_0 A'_\phi\right] dr dz \quad (4.58)$$

Comparison of the above functional with equation (4.44) shows that the expression inside the brackets is of the same form as the functional for planar two-dimensional fields. Using the usual polynomial expansion for the trial function

$$A'_\phi = \sum_k A_{k\phi} c_k \quad (4.59)$$

and the standard procedure outlined in Appendix B one can easily obtain the matrix equation of the form shown in equation (4.45)

$$[S'][A'_\phi] + [C'][\frac{dA'_\phi}{dt}] = [F'] \quad (4.60)$$

where the matrices are given by

$$[S'] = \frac{1}{4\Delta\mu r_c}\begin{bmatrix} (b_i b_i + c_i c_i), & (b_i b_j + c_i c_j), & (b_i b_k + c_i c_k) \\ (b_i b_j + c_i c_j), & (b_j b_j + c_j c_j), & (b_j b_k + c_j c_k) \\ (b_i b_k + c_i c_k), & (b_j b_k + c_j c_k), & (b_k b_k + c_k c_k) \end{bmatrix} \quad (4.61)$$

$$[C'] = \frac{\Delta\sigma}{12r_c}\begin{bmatrix} 2 & 1 & 1 \\ 1 & 2 & 1 \\ 1 & 1 & 2 \end{bmatrix} \tag{4.62}$$

$$\{F'\} = \frac{\Delta J_0'}{3r_c}\begin{bmatrix} 1 \\ 1 \\ 1 \end{bmatrix} = \frac{\Delta J_0}{3}\begin{bmatrix} 1 \\ 1 \\ 1 \end{bmatrix} \tag{4.63}$$

r_c denotes the radius from the axis of symmetry to the centroid of the triangular element. This approximation gives sufficiently accurate results if the elements are small. Remember that this was one of the reasons for selecting first order and small elements instead of higher order and large elements. The combinations of a large radius and a large element can be a source of error, but it is questionable whether this error is significant [91]. An alternative would be to write the radial distance r in terms of area coordinates as outlined in reference 91.

Subsequent to the calculation of the new variable A'_ϕ one can easily compute the original magnetic vector potential

$$A_{\phi j} = \frac{A'_{\phi j}}{r_j} \tag{4.64}$$

where r_j is the distance of the node (j) from the axis of symmetry. Hence, demonstrating the similarity between the functionals for axisymmetric and planar field problems makes the solution for the axisymmetric case quite straightforward.

4.6 Representation Of The Time-Dependent Variables

One of the most popular time-stepping procedures is based on the numerically stable Crank-Nicolson method. The adaptation of this procedure to the finite element method is presented in this section [55,91].

In general, the first derivative of the nodal values between two points in time at the midpoint of the time increment (Figure 4.2) can be approximated by

$$\frac{d\{A\}}{dt} = \frac{1}{\Delta t}\left(\{A\}_1 - \{A\}_0\right) \tag{4.65}$$

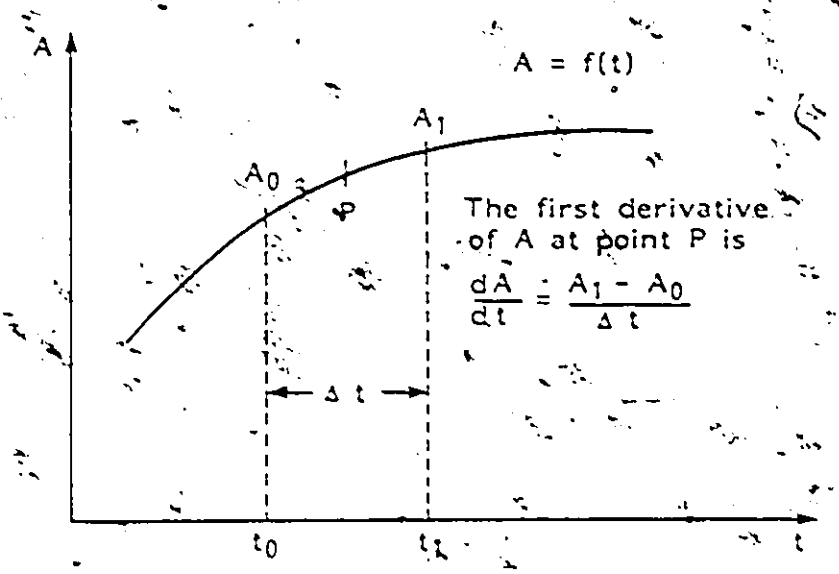

Figure 4.2

Numerical representation of the time derivative.

Since $d\{A\}/dt$ is evaluated at the midpoint of the time interval, the variable itself and the forcing vector of equation (4.60) must also be evaluated at this point. These variables become

$$\{A\}^* = \frac{1}{2}\left(\{A\}_1 + \{A\}_0\right) \tag{4.66}$$

and

$$\{F\}^* = \frac{1}{2}\left(\{F\}_1 + \{F\}_0\right) \tag{4.67}$$

Substitution of equations (4.65), (4.66) and (4.67) into equation (4.60) and dropping the prime (') notation give

$$\frac{1}{\Delta t}[C]\{A\}_1 - \frac{1}{\Delta t}[C]\{A\}_0 + \frac{1}{2}[S]\{A\}_1 + \frac{1}{2}[S]\{A\}_0 + \{F\}^* = 0 \tag{4.68}$$

which can be rewritten as

$$\left([S] + \frac{2}{\Delta t}[C]\right)\{A\}_1 = \left(\frac{2}{\Delta t}[C] - [S]\right)\{A\}_0 - 2\{F\}^* \tag{4.69}$$

Solution of equation (4.69) yields the nodal values of A_ϕ at the time $(t+\Delta t)$ provided the nodal values at time (t) are known. The column vector $\{F\}^*$ is composed of known parameters and can be computed at (t) and $(t+\Delta t)$ before equation (4.69) is solved. If the values of A_ϕ at the midpoint of the time interval are required, they can be calculated by substituting the results obtained from solving (4.69) along with $\{A\}_0$ into equation (4.66). Another approach is to eliminate the $\{A\}_1$ terms from equation (4.68) using (4.66). This procedure yields the recursive equation

$$\left([S] + \frac{2}{\Delta t}[C]\right)\{A\}^* = \frac{2}{\Delta t}[C]\{A\}_0 - \{F\}^* \tag{4.70}$$

Regardless of whether the nodal values are calculated at the end of the time interval or at its midpoint via equations (4.69) and (4.70) respectively, the final system of equations have the general form:

$$[S_p]\{A\}_{New} = [C_p]\{A\}_{Old} - \{F\} \qquad (4.71)$$

where the matrix $[S_p]$ is a combination of the stiffness and capacitance matrix and is dependent on the time step Δt. If the same time step is used throughout the total excitation time and if the material parameters are independent of the time and $\{A\}$, then the matrices $[S_p]$ and $[C_p]$ are the same for all time points. If either Δt or the material parameters do change during the solution process, these matrices must be re-evaluated and $[S_p]$ must be triangularized. This process rapidly increases the cost of the solution.

As mentioned earlier, the above form of the Crank-Nicolson central difference procedure was used in this study because it is unconditionally stable [90,91]. "Unconditional stability means that if the magnetic vector potential distribution at time t is transformed to the frequency domain using a Fourier transform, the amplification factor for every frequency component decays

with time". Although the method itself is stable, an oscillation in the calculated values can occur. The amplitude of the oscillation is dependent on the size of the element and the time step, the material properties and the Fourier components at the beginning of the time step. Therefore, reduction of the element size and time step together are the most effective way to decrease the seriousness of the oscillations. This was another reason first-order triangular elements with very small areas were chosen in this study.

4.7 General Algorithm For The Numerical Solution

The third major step in the finite element process is the construction of the equation-solving algorithm. The computer program developed in this study for this purpose is presented in the next chapter. One of the subroutines in this program is dedicated to the evaluation of subsidiary element quantities that can be derived from the distribution of the magnetic vector potential in space and its variation in time. The general algorithm for the finite element solution of the magnetic vector potential and the determination of other variables of interest are briefly described in this section.

The complete computerized solution for calculating the electromagnetic forces on the G/S and other involved components at each time step of the input current impulse is subdivided into five major segments as follows:

1. The main program.

2. Generation of the data necessary to describe the finite element mesh and discretization of current impulse.

3. Pre-processing of the finite element equations.

4. Solution of the finite element equations.

5. Post-processing of the information produced by the solution.

The main program is designed to serve as a central command center to invoke all of the necessary subroutines in the proper sequence to execute the desired numerical solution. This modular structure provides excellent flexibility to modify or expand the program quickly and efficiently. The second segment consists of two subroutines: in the first one, data to define the geometry of the configuration

including the coordinates of the nodes, connectivity of the elements, boundary values and material properties is either read or generated. The second subroutine handles the generation and discretization of the current impulse. The third segment includes three subroutines that assemble the global stiffness matrix $[S_p]$ and the constant parts of the forcing vector, introduce the specified boundary values to $[S_p]$ and perform the necessary modifications, and decompose the modified stiffness matrix. Descriptions of these operations are given in Appendix B and the next chapter. In the fourth segment, complete assembly and updating of the forcing vector, its modification to account for the specified boundary conditions, its decomposition and the final steps in solving for the nodal values at the particular time step are performed. The calculation of the magnetic flux density (B), the induced current density and the force densities is carried out in the final segment using the relations outlined below [5,6,30].

The radial and axial components of the magnetic flux density (B_r and B_z) are determined from the basic definition of the magnetic vector potential ($B = \nabla x A$) which is written in cylindrical coordinates as

$$\bar{B} = \left(\frac{1}{r}\frac{\partial A_z}{\partial \phi} - \frac{\partial A_\phi}{\partial z}\right) i_r + \left(\frac{\partial A_r}{\partial r} - \frac{\partial A_z}{\partial r}\right) i_\phi + \frac{1}{r}\left(\frac{\partial (rA_\phi)}{\partial r} - \frac{\partial A_r}{\partial \phi}\right) i_z \quad (4.72)$$

For the axisymmetric case, equation (4.72) reduces to

$$(B)_r + (B)_z = (-\frac{\partial A_\phi}{\partial z})ir + \frac{1}{r}(\frac{\partial(rA_\phi)}{\partial r})iz \qquad (4.73)$$

The above vector equation can be rewritten as

$$B_r = -\frac{\partial A_\phi}{\partial z} \qquad (4.74)$$

and

$$B_z = \frac{A_\phi}{r} + \frac{\partial A_\phi}{\partial r} \qquad (4.75)$$

From finite element analysis, at any point in the region A_ϕ can be expressed in terms of the shape functions and the nodal values of the corresponding element ijk (Appendix B) as:

$$A_\phi - N_i A_{\phi i} + N_j A_{\phi j} + N_k A_{\phi k} \qquad (4.76)$$

where the shape functions are given by

$$N_i = \frac{1}{2\Delta}(a_j + b_i r + C_i z)$$

$$N_j = \frac{1}{2\Delta}(a_j + b_j r + c_j z) \qquad (4.77)$$

$$N_k = \frac{1}{2\Delta}(a_k + b_k r + c_k z)$$

In the above functions, Δ denotes the area of the triangular element, the a's b's and c's are constants representing geometrical coefficients; they are given in terms of the node coordinates (r,z) by:

$$\Delta = \frac{1}{2}(r_i z_k - r_k z_j + r_k z_i - r_i z_k + r_i z_j - r_j z_i) \qquad (4.78)$$

and

$$a_i = r_j z_k - r_k z_j \;;\; b_i = z_j - z_k \;;\; c_i = r_k - r_j$$

$$a_j = r_k z_i - z_k r_i \;;\; b_j = z_k - z_i \;;\; c_j = r_i - r_k \qquad (4.79)$$

$$a_k = r_i z_j - r_j z_i \;;\; b_k = z_i - z_j \;;\; c_k = r_j - r_i$$

Substituting equations (4.76) and (4.77) into equation (4.74) and (4.75) and performing the differentiation yield the following expressions for B_r and B_z:

$$B_r = -\frac{1}{2\Delta}(c_i A_{\phi i} + c_j A_{\phi j} + c_k A_{\phi k}) \tag{4.80}$$

$$B_z = \frac{1}{2\Delta r}[(a_i + b_i r + c_i z) A_{\phi i} + (a_j + b_j r + c_j z) A_{\phi j} +$$

$$(a_k + b_k r + c_k z) A_{\phi k}] + \frac{1}{2\Delta}[b_i A_{\phi i} + b_j A_{\phi j} + b_k A_{\phi k}] \tag{4.81}$$

Note that B_r is constant within an element while B_z depends on the coordinates. The values of these components at the centroids of the triangular elements

$$(r_c = \frac{1}{3}(r_i + r_j + r_k) \text{ and } z_i = \frac{1}{3}(z_i + z_j + z_k)$$

were computed for all the elements at each time step.

The electric field intensity ($\bar{E}$) has only one component in the circumferential direction (E_ϕ). It is given by the time derivative of $\bar{A}_\phi$ ($E = -\partial A/\partial t$). The induced current density can be computed from the constitutive relationship ($J_\phi = \sigma E_\phi$). Hence, using a finite difference approximation for the time derivative of $\bar{A}$ [64], the induced eddy current density can be written as:

$$J_e = -\sigma \left(\frac{A_{r,z,t} - A_{r,z,t-1}}{\Delta t}\right) \tag{4.82}$$

Once the magnetic and electric fields are known the electromagnetic forces in any conductor which may be present in the region can be calculated. The force exerted by an electromagnetic field on a unit volume of isotropic matter is given by [6]

$$\bar{F} = \rho\bar{E} + \bar{J}\times\bar{B} - \frac{1}{2}\bar{E}^2\nabla\varepsilon - \frac{1}{2}\bar{H}^2\nabla\mu + \frac{K_m K_e - 1}{c^2}\frac{\partial\bar{S}}{\partial t} \qquad (4.83)$$

where ρ is charge density, K_m and K_e are magnetization and polarization constants, c is the speed of light and S is the energy given by Poynting's theorem. The above expression does not include the forces associated with the deformation. Neglecting these forces does not introduce any error in calculating the G/S displacement since they do not produce a net force that causes displacement. The first term in equation (4.83) vanishes when the charge density is summed over the electrons and ions. The third and fourth terms are also taken to be zero for the interior of a nonmagnetic metal. The last term is due to the light pressure and is negligibly small. Thus the force density reduces to:

$$\bar{F} = \bar{J}\times\bar{B} = -\sigma\left(\frac{\partial\bar{A}}{\partial t}\right)\times\nabla\times\bar{A} \qquad (4.84)$$

For the axisymmetric case in cylindrical coordinates, equations (4.80), (4.86) and (4.82) can be substituted to derive the radial and axial components of the force density and write them in the form:

$$F_r = J_e B_z \tag{4.85}$$

$$F_z = J_e B_r \tag{4.86}$$

Since B_r and B_z were calculated at the centroids of the elements, J_e, F_r and F_z were calculated at the same locations but only for the conductive elements in coil and fuel channel components. At selected locations in the P/T, C/T and G/S the impulse force densities, defined as the sum of all the instantaneous force densities calculated at each time step, were also calculated by the post-processing subroutine. Results of these calculations and others are presented in chapter 5.

4.8 Summary

In this chapter, the state of the art methods for solving transient electromagnetic field problems have been outlined. The formulation of the G/S repositioning problem in terms of the magnetic vector potential and the impulse

current input, the reasons for selecting the finite element method in conjunction with the Crank-Nicolson recurrence scheme and a comprehensive description of the numerical procedures have been presented. In order to avoid tedious derivation of the stiffness and capacitance matrices for the axisymmetric vector field problem, a technique was developed involving a change of variables to correlate the energy functional for this class of problems to its counterpart in two-dimensional cartesian coordinates. This procedure not only allows the use of the well-known matrices for two-dimensional scalar and vector field problem with minor modification, it also provides the opportunity of using the same computer program, with a small additional effort, to solve problems belonging to both of these classes. The general algorithm for the numerical solution and all of the necessary equations for computing the particular parameters of interest in this application have also been presented.

CHAPTER 5

COMPUTERIZED SOLUTION AND ASSESSMENT OF THE NUMERICAL RESULTS

5.1 Introduction

This chapter develops the basis for a computer program to implement the finite-element/finite difference solution presented in the previous chapter. The validity of the model and numerical solution is also assessed. In view of the absence of any published results for geometrical configurations and pulse current inputs similar to those used in this study, alternative methods to check the validity and accuracy of the numerical solution are developed. The obvious method to achieve this objective is to compare the numerical results to the experimental results. However, in this study, such a comparison was not considered to be sufficient to assess the accuracy of the solution. The numerical results provided the instantaneous and impulse forces exerted on the G/S while the experimental results provided validation for the expected displacements

of the G/S. Measurement of the G/S displacements was adopted because of the extreme difficulty in measurement of any other variable with a reasonable degree of accuracy. Although, computation of the G/S displacements can only be achieved via a simplified model, the only comparison that can be performed is between the measured G/S displacements and those that can be predicted from the computed impulse forces. This approach can only be expected to produce approximate correlation unless a major study to establish accurate mechanical models is undertaken. Moreover, the accuracy of the experimental results is limited because of several sources of error that exist in measuring the various parameters involved.

To circumvent the above difficulty, a second method to validate the accuracy of the numerical solution was established. This method consisted of developing the computer program with the capability to solve the electromagnetic field problem of an infinitely long solenoid for which analytical formulae are available. This was accomplished by making minor modifications in one of the data files used to study the G/S problem, while leaving the actual computer program intact. This approach not only provided an efficient and accurate scheme to debug the computer program and verify the validity of the numerical

results, it also increased the usefulness of the developed program and expanded its range of possible applications.

A general description of the computer program developed to implement the numerical solution is presented in Appendix C. This chapter presents the main cases used to develop this program and verify the numerical results. Some typical numerical results for the G/S repositioning problem and a simplified mechanical model used to determine the G/S displacement as a function of the computed forces are also presented. A general assessment of the technique with suggestions for improvement is included as well. Note that in view of the extensive amount of information produced by the computer program, only the most important parameters are presented in this chapter. Discussion is restricted to the most influential parameters and the most relevant issues in the G/S repositioning process.

5.2 Verification of the Numerical Results

The computer program was developed and tested using case studies for which analytical formulae to calculate the magnetic vector potential and the magnetic field are available. A finite element mesh was designed during the development and preliminary checking of the computer program

to be small enough to facilitate the process of checking the results while keeping the computer cost down. Figure 5.1 shows this mesh. It consists of 170 nodes and 288 elements: it represents a six turn coil inserted inside two coaxial tubes representing the P/T and C/T (the actual dimensions are marginally different from those of the actual P/T and C/T due to the finite element grid size). The G/S is represented by one conductive element (element #216). Note that the boundary parallel to the r-axis (central line of symmetry) was located only 2.2 cm away from the end of coil, and the boundary parallel to the z-axis was located only 1.6 cm outside the C/T to investigate the accuracy of the solution when these boundaries are placed at minimal distances from the coil.

The input data describing the materials properties (permeability and conductivity) of each region in the configuration includes one flag that indicates the location of the source current. The configuration shown in Figure 5.1 has five distinct regions consisting of: (1) all non-conductive elements, (2) coil elements, (3) P/T elements, (4) G/S element, (5) C/T elements. To indicate that the source current originates in the C/T, for example, the flag indicating the current type for region (5) is set to one and zero for all other regions. If the case of a

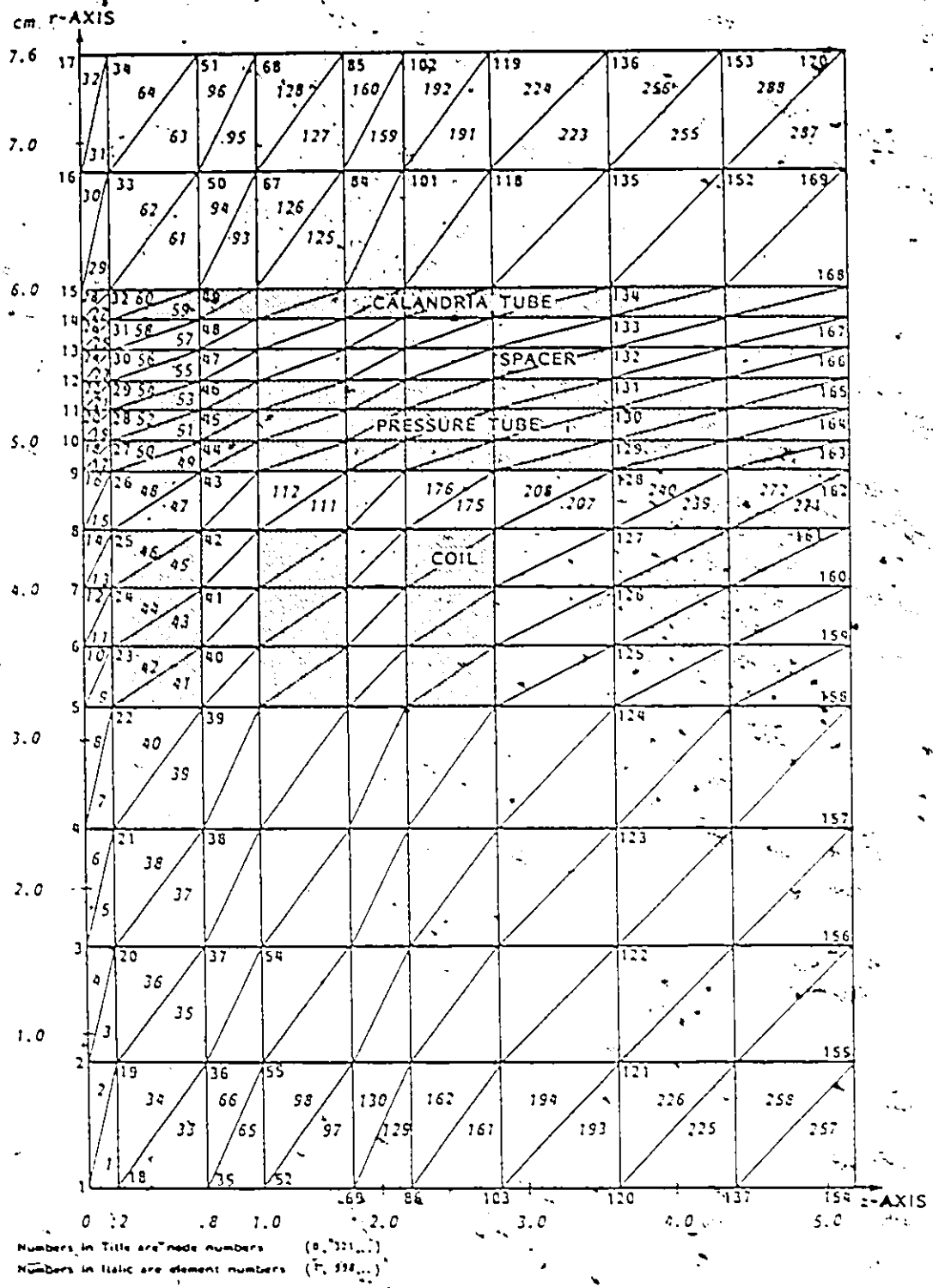

Figure 5.1

Preliminary finite element mesh used for development and testing purposes.

solenoid in free space is to be studied, the current-type flag for region (2) is set to 1 (and zero elsewhere) and the conductivity of regions (3), (4) and (5) is also set to zero. Similarly, assuming a current sheet of finite thickness is to be investigated, either the P/T or C/T can be used by indicating that the source current originates in the selected tube and by setting the conductivity of all other regions equal to zero. Furthermore, to investigate the case of a constant direct current input, the conductivity of all the regions is set to zero. This reduces the capacitance matrix to zero (equation 4.62). In other words instead of solving the time-dependent diffusion equation (equation 4.34), the vector Poisson equation (equation 4.25) is solved. Note that all of the above mentioned cases can be analysed without any alteration in the computer program: only the input data files need be adjusted to represent the desired case.

5.2.1 The Magnetostatic Case

The magnetostatic case was the first test case considered in order to verify the finite element formulation for the axisymmetric vector field problem and to ensure that the program was free from programming errors. The case was modelled by simulating a direct current in the calandria

tube representing a thin current sheet in free space. Since the C/T in Figure 5.1 extends to the outer boundary ($z = 5.2$ cm) where the Neumann boundary condition is enforced, the effect of the tube is represented as an infinitely long solenoid (or solenoidal current sheet). This case was selected because the analytical solution expressing the magnetic vector potential and the magnetic flux density (at least inside the current sheet) are readily available [5-7,30] or can be easily derived. In the region inside the current sheet the magnetic flux density is given by:

$$\bar{B} = B_z = \frac{\mu_o NI}{\ell} = \mu_o J(r_1 - r_2) \qquad (5.1)$$

where N is the number of turns, I is the current, ℓ is the length, J is the current density, r_1 and r_2 are the inner and outer radii of the sheet respectively. The following expression for A_ϕ can be written

$$A_\phi = \frac{1}{2} B_z r \qquad (5.2)$$

where r is the radius ($0 \leq r < r_1$).

Figure 5.2 shows the numerical solution for A_ϕ produced by the computer program. Also shown is the analytical solution given by equation (5.2) for a constant current input of 11.0 kA (or a current density of 0.10577×10^9 A/m^2) in the C/T. The C/T is modelled with an inner and outer radius of 5.8 and 6.0 cm respectively. Figure 5.3 presents the error between the numerical and analytical solutions as an error function defined by:

$$\delta A_\phi(r) = \frac{A_{\phi n}(r) - A_{\phi a}(r)}{A_{\phi a}(r)} \tag{5.3}$$

As can be seen from Figure 5.3, the numerical solution differs from the analytical solution by less than one percent for most of the points. For points that are in the immediate vicinity of the axis, the error is larger than 1% but is still quite acceptable considering the size of the elements in that part of the mesh and remembering that the axis (r = 0) is basically a singularity point when equation (4.64) is used to compute A_ϕ. Similar agreement is observed when the numerical values of B_z are compared to the analytical value computed using equation (5.1), as illustrated in Table 5.1 below.

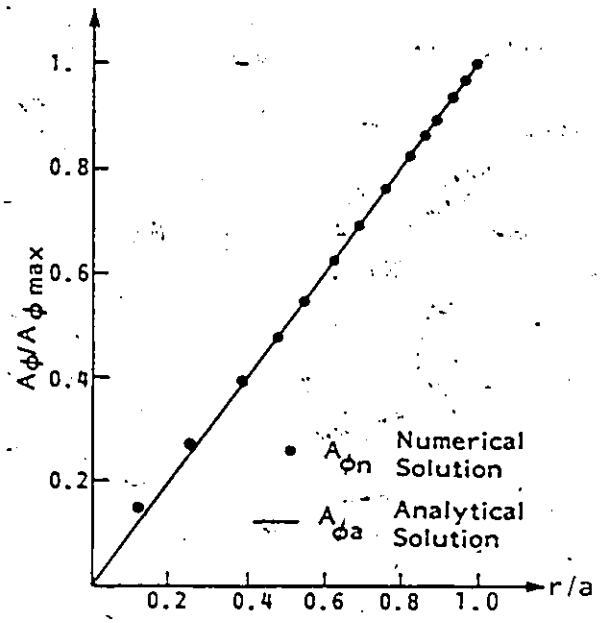

Figure 5.2

Numerical and analytical solution for $A\phi$ at different radial distances (dc case).

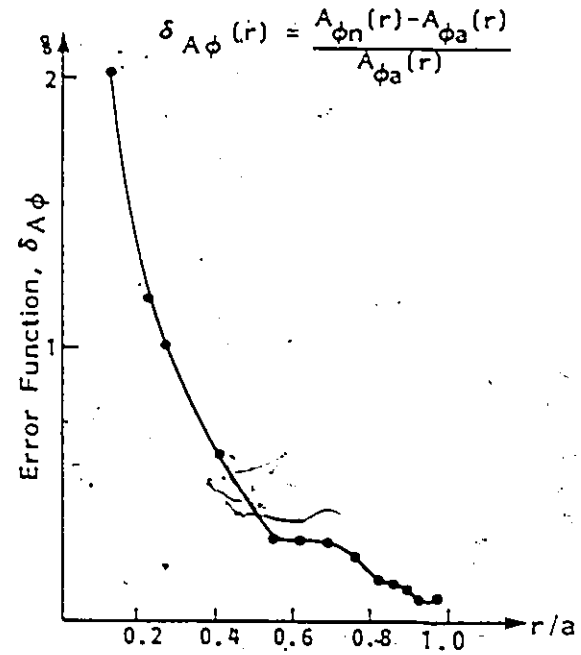

Figure 5.3

Error function showing the percentage difference between the numerical and anlytical solutions for $A\phi$.

TABLE 5.1

Comparison of Analytical and Computer Solutions for B_z (dc case)

Element Number	Radius (in cm)	Magnetic Flux Density (B_z) in Tesla		% Difference
		Analytical	Numerical	
2	0.4	0.2658	0.2596	2.40
4	1.33	0.2658	0.2640	0.68
6	2.13	0.2658	0.2653	0.20
8	2.93	0.2658	0.2662	0.17
10	3.47	0.2658	0.2646	0.47
12	3.87	0.2658	0.2654	0.16
14	4.27	0.2658	0.2659	0.03
16	4.67	0.2658	0.2665	0.25
18	4.93	0.2658	0.2658	0.0
20	5.13	0.2658	0.2665	0.25
22	5.33	0.2658	0.2672	0.53
24	5.53	0.2658	0.2686	1.04

Several other computational tests using various levels of direct current input, or a sequence of levels in the same run, were performed: in each case excellent agreements, similar to the one presented above, were obtained.

5.2.2 The Time-Dependent Case

Investigation of the dc cases provides sufficient assurance that the formulation of the problem with the associated computer program, with the possible exception of

the capacitance matrix, are correct. Analysis of the time-dependent case involves the use of the capacitance matrix, therefore it can be used to validate the complete formulation and computer solution. A detailed analytical analysis for the time dependent case is not practicable. Instead a current impulse represented by a step function or sequence of step functions was used to establish validity for the capacitance matrix. The duration of the step function was selected large enough, depending on the material used for the current sheet, to allow the magnetic field to reach its maximum value. This maximum value is taken to be identical to the value obtained with a direct current, having the same magnitude as the step function used.

First a step function of 11.0 kA and a width of 3 ms was used in conjunction with the C/T. The conductivity of the C/T was assumed to be 1.246×10^6 S/m (zirconium-niobium alloy). The step function was discretized using a time step $\Delta t = 100$ μs. After approximately 0.6 ms the distributions of A_ϕ and B_z become identical to those obtained in the dc case (11.0 kA level) which are partially presented in Figure 5.2 and Table 5.1. The conductivity of the C/T was changed to 5.7×10^7 S/m (copper) and a step function having the same magnitude as above but a width of 30 ms was used.

It took approximately 22 ms for the distributions of A_ϕ and B_z to reach their steady state values as outlined above.

To illustrate the time variation of the magnetic flux density in response to step changes in the current input and to check the computer solution further, the current-impulse shown in Figure 5.4 was used in conjunction with the C/T current sheet (σ = 1.246 × 10^6 S/m). Figure 5.5 presents a plot of B_z at the centroid of element number 6 versus time. At the end of each step function the computer results were within 1% of the analytical results.

The distribution of B_z in space at one instant of time (t = 0.625 ms) for the case discussed above (Figure 5.4) is presented in Figure 5.6. The analytical solution for B_z inside the C/T is 0.2658 T while outside the C/T it is zero. Note that the largest deviation from the analytical solution is in the elements closest to the axis: the conclusions made in the previous subsection with respect to the accuracy of the solution are also valid for this case.

The forces on the conductive elements as computed were compared with those obtained using equations (4.82),

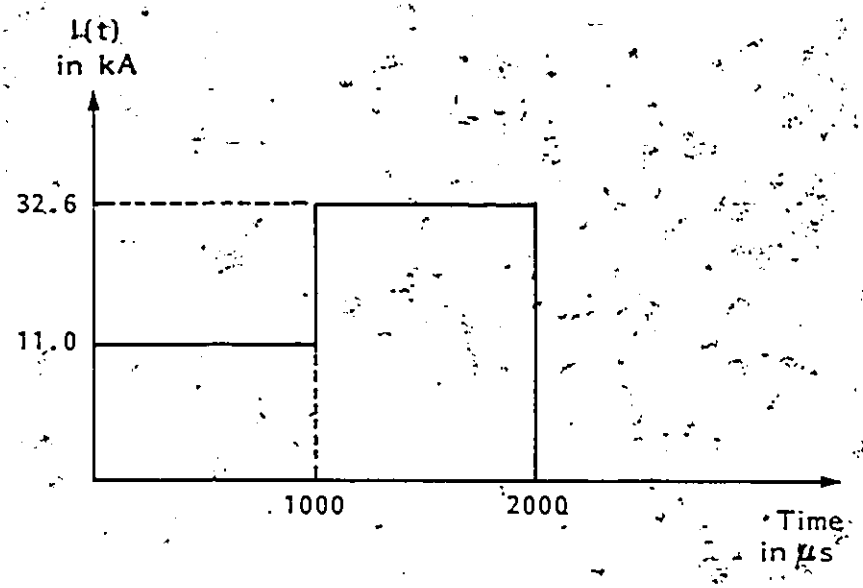

Figure 5.4

Current impulse used for testing the time dependent case.

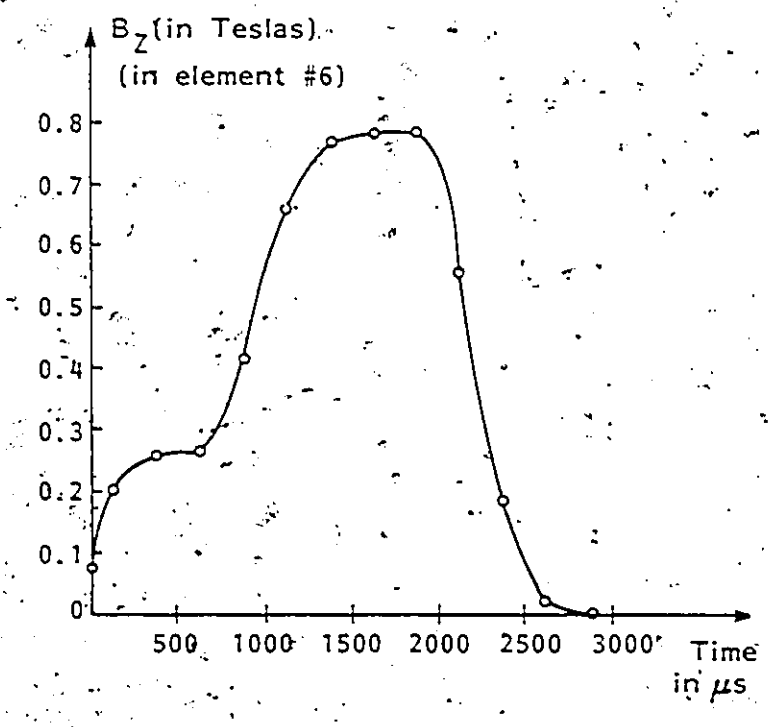

Figure 5.5

Time variation of B_Z in response to step changes in the current input (zirconium C/T)

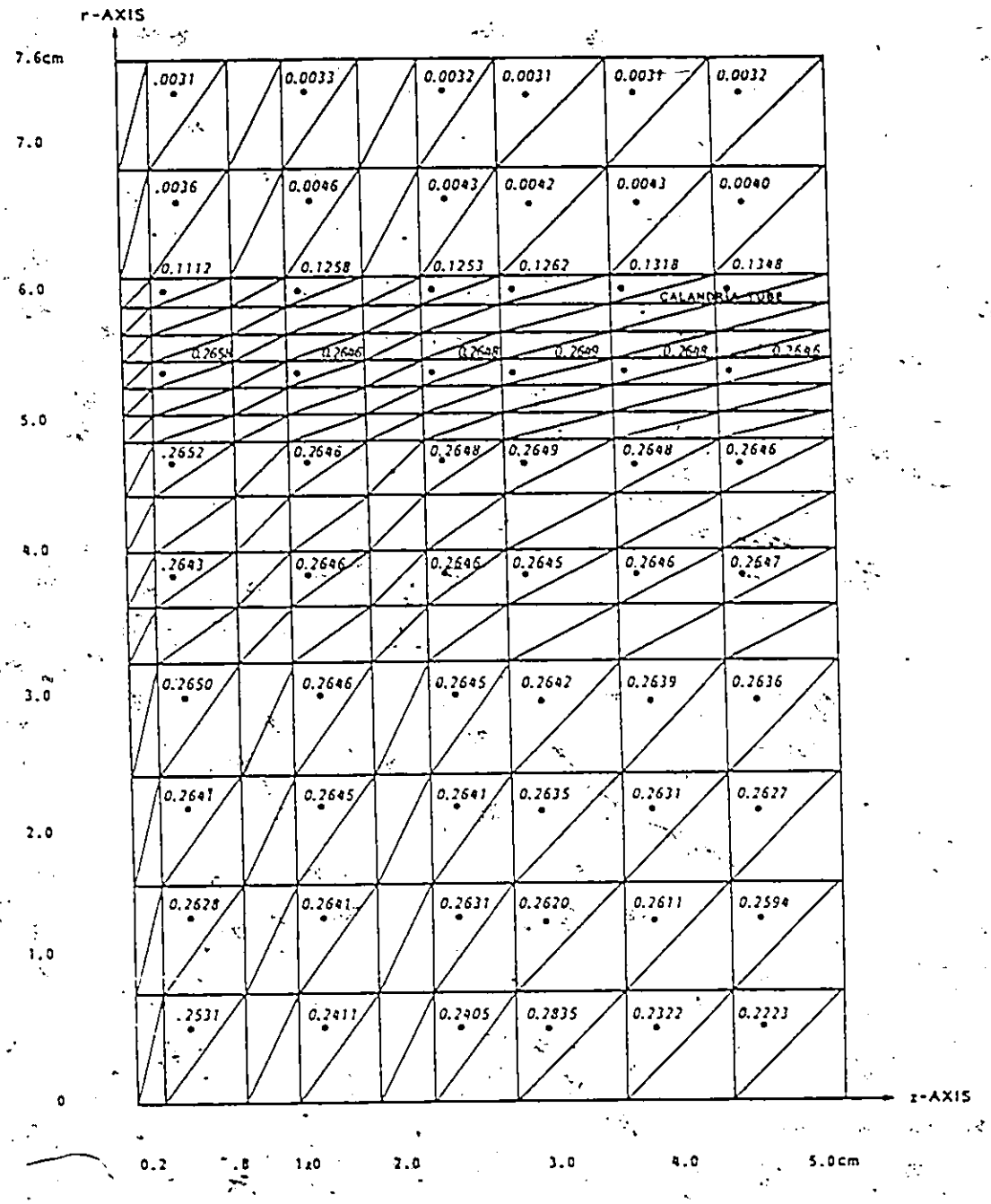

Figure 5.6

Distribution of B_Z (in Teslas) at time $t = 0.625$ ms (zirconium C/T)

(4.88) and (4.89) and the values of A_ϕ, B_r and B_z that have already been validated. The calculations were in excellent agreement (less than 1% error) with the computer results. Figure 5.7 shows the instantaneous radial force density exerted on one element in the C/T; the profile shown is for the current impulse depicted in Figure 5.4 and a zirconium C/T.

Computational tests were then performed as described above but with the P/T considered as an infinitely long tube in free space (the conductivity of all the regions except the P/T was zero). Again, different materials were considered for the P/T. In every case examined the results were in excellent agreement with the analytical solutions.

Subsequent to the tests mentioned above, the case of a solenoid of finite length in free space was investigated using similar current impulses to those used in previous cases. For comparison purposes Montgomery and Wegel [10] examined the magnetic flux density produced by a single-layer coil in free space, although their coil had somewhat different geometry from that considered here. Nevertheless, their results provided a typical profile inside the coil: this profile agreed very well with that produced in this test case. A typical profile along with various other

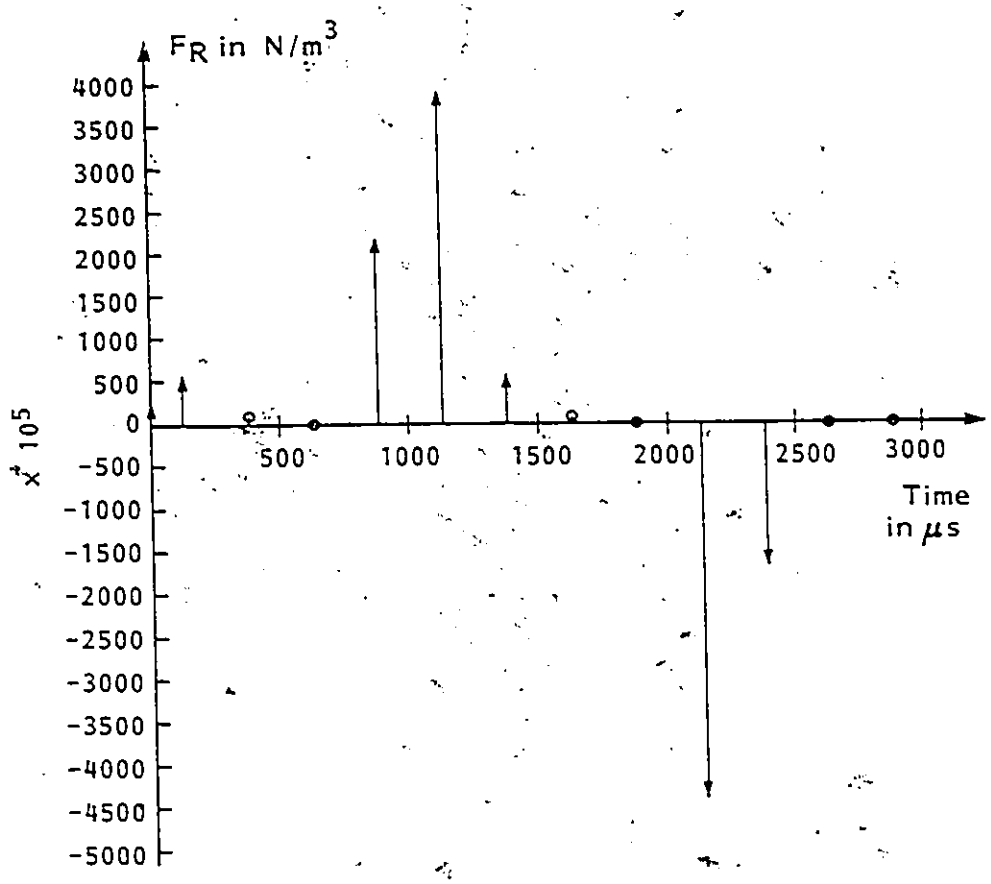

Figure 5.7

Instantaneous radial force density exerted on element #155 in the C/T.

results for the actual fuel channel configuration are presented in the subsequent sections of this chapter. The results of the various computer runs for this coil in both free space and inside the fuel channel, indicate a substantial degree of confidence in the method without showing any irregularity.

5.3 Representation of the Coil and Fuel Channel Components

Results of the computational tests performed using the finite element mesh described in the previous section indicated that the size of the elements used was satisfactory. However, it was decided to use smaller elements in the coil region and the section of the P/T and C/T directly around it, in order to obtain more detailed information about the distribution of various parameters of interest. Coincidentally, using smaller elements further enhances the accuracy of the finite element solution in regions of high gradients.

The accuracy of the results for the elements near the outer boundaries of the mesh depends on how far these boundaries are from the source of excitation: remember that

the gradient of A_ϕ is assumed constant at these boundaries. In order to determine an optimum location for these boundaries, particularly the side that is parallel to the r-axis, the finite element mesh used previously was expanded as shown in Figure 5.8.

The boundary line that is parallel to the z-axis was not shifted because the magnetic flux density there was found to be near 1% of its maximum value. The other boundary line was moved to a distance of 30 cm from the origin (five times the coil length) to investigate the influence of this boundary on the accuracy of the solution. The expanded finite element mesh consisted of 269 nodes and 472 elements.

Several computational tests were performed using the above mesh. As expected, in the case of an infinitely long current sheet, the distributions of A_ϕ and B were not affected by the shift of boundary since the boundary condition at the relocated side represents the physical system exactly, regardless of location. In the case of a coil of finite length, significant changes in the elements near the original boundary line (elements 257 to 288) were observed for the same current input in the original and expanded mesh. The maximum difference in the values of B was found for these elements. This difference was in the

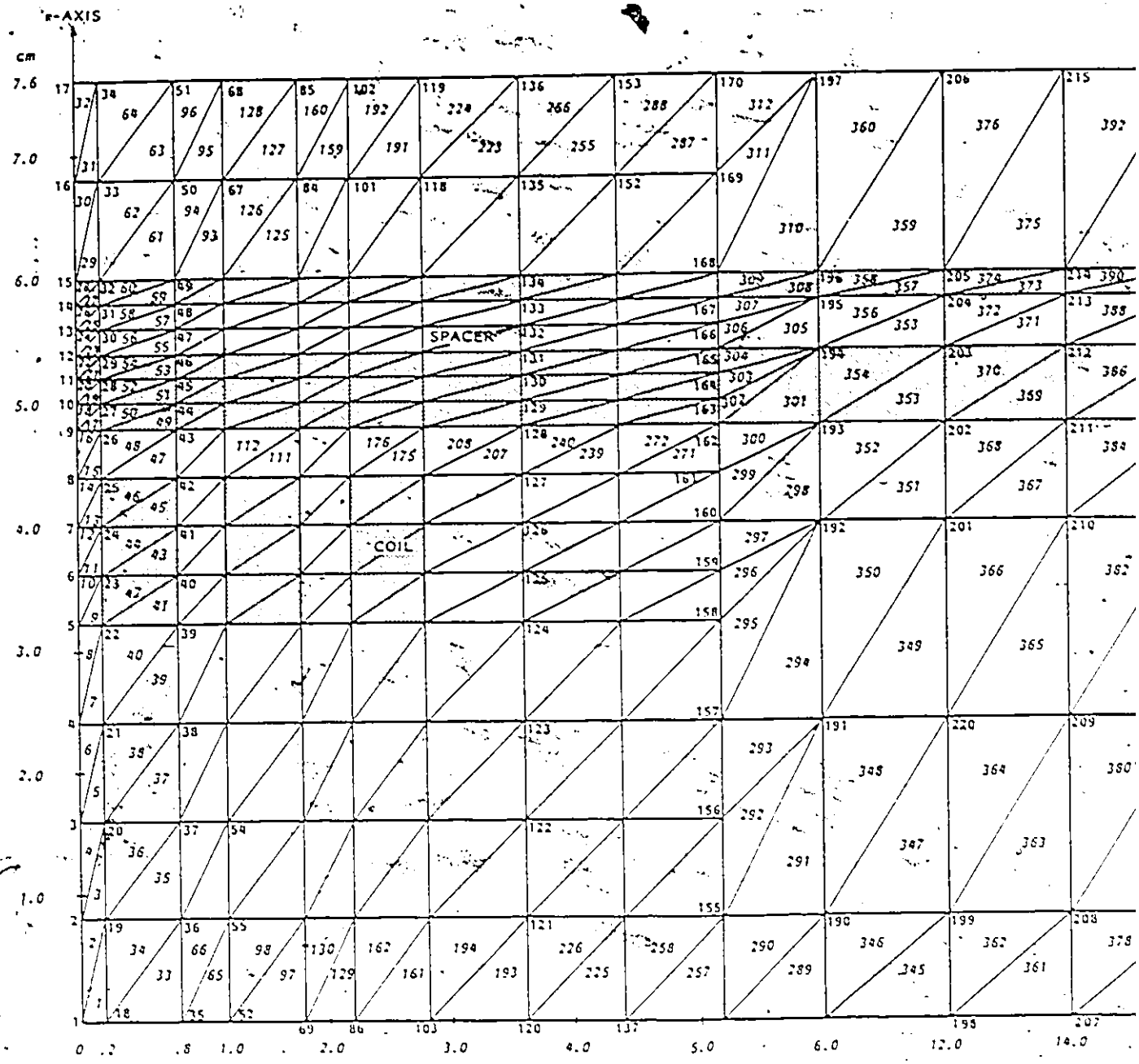

Numbers in Title are node numbers (0, 221...)
Numbers in Italic are element numbers (1, 994...)

Figure 5.8

Expanded finite element mesh used for testi

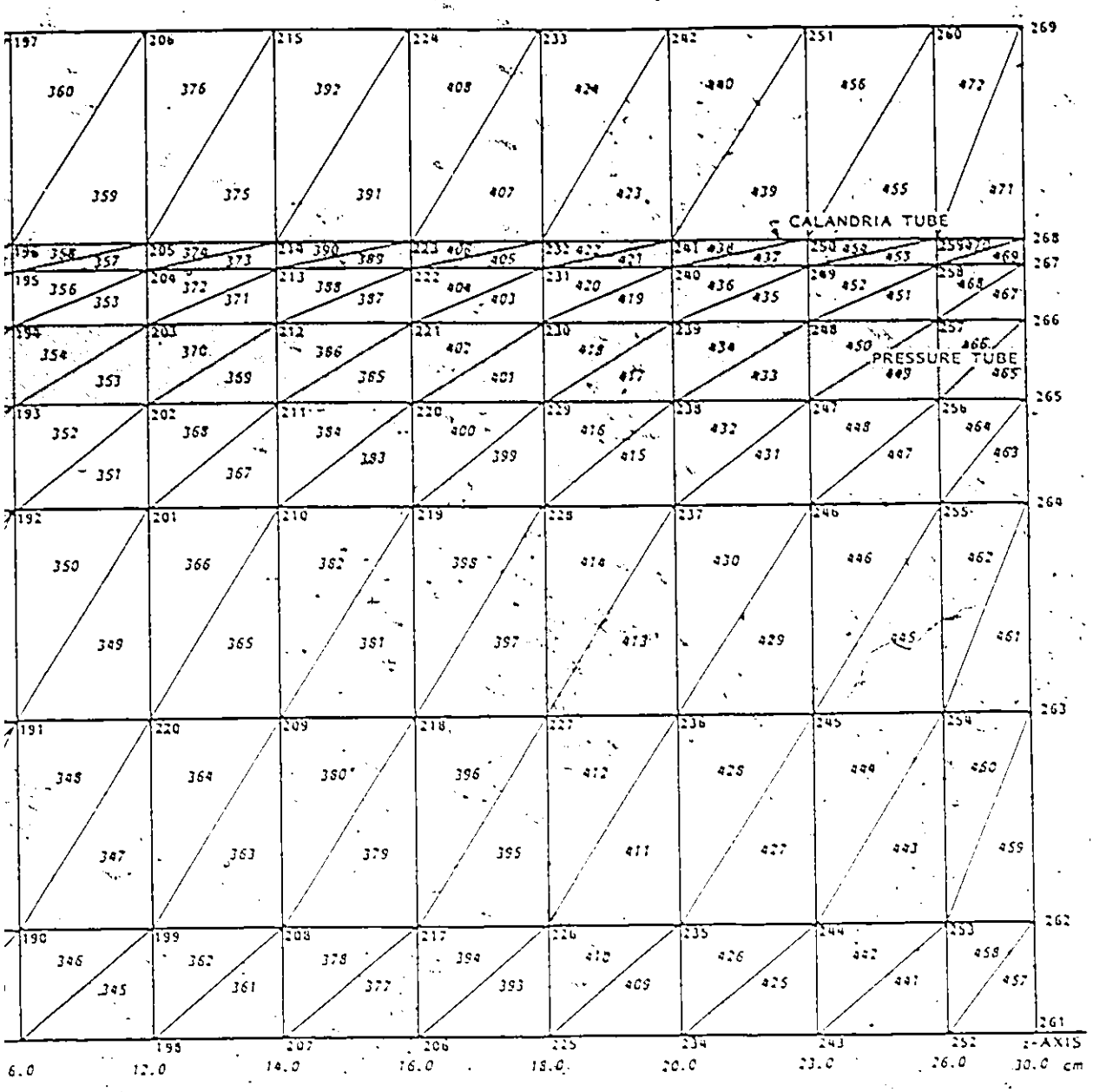

Figure 5.8

ement mesh used for testing purposes.

order of 15%, decreasing to less than 5% in the elements near the r-axis. Figure 5.9 shows typical normalized distribution of B_z for the case of a coil with G/S only (P/T and C/T are not present) at one instant of time, during the first quarter of a current pulse taken as the first period of a capacitor discharge. Examination of the flux density distribution provided sufficient insight to select an optimum location for the boundary line parallel to the r-axis. The objective was to locate this line in a region where the magnetic field has decayed to a level below 1% of its maximum value. This would assure a high degree of accuracy in the interior regions of the mesh while keeping the size of the mesh within practicable bounds.

Analysis of the above results, and consideration of the various criteria involved, led to the subdivision of the actual fuel channel configuration into a mesh as shown in Figure 5.10. This finite element mesh consisted of 940 nodes and 1766 elements. A typical "field" coil prototype consisting of 9 turns was represented in this mesh. The G/S was represented by a single element (element number 1100) that has an area equal to the cross-section of the tie wire in the G/S. No attempt was made to represent the helical windings of the G/S since it is not known how many of these turns would be short-circuited by the tie wire itself or by

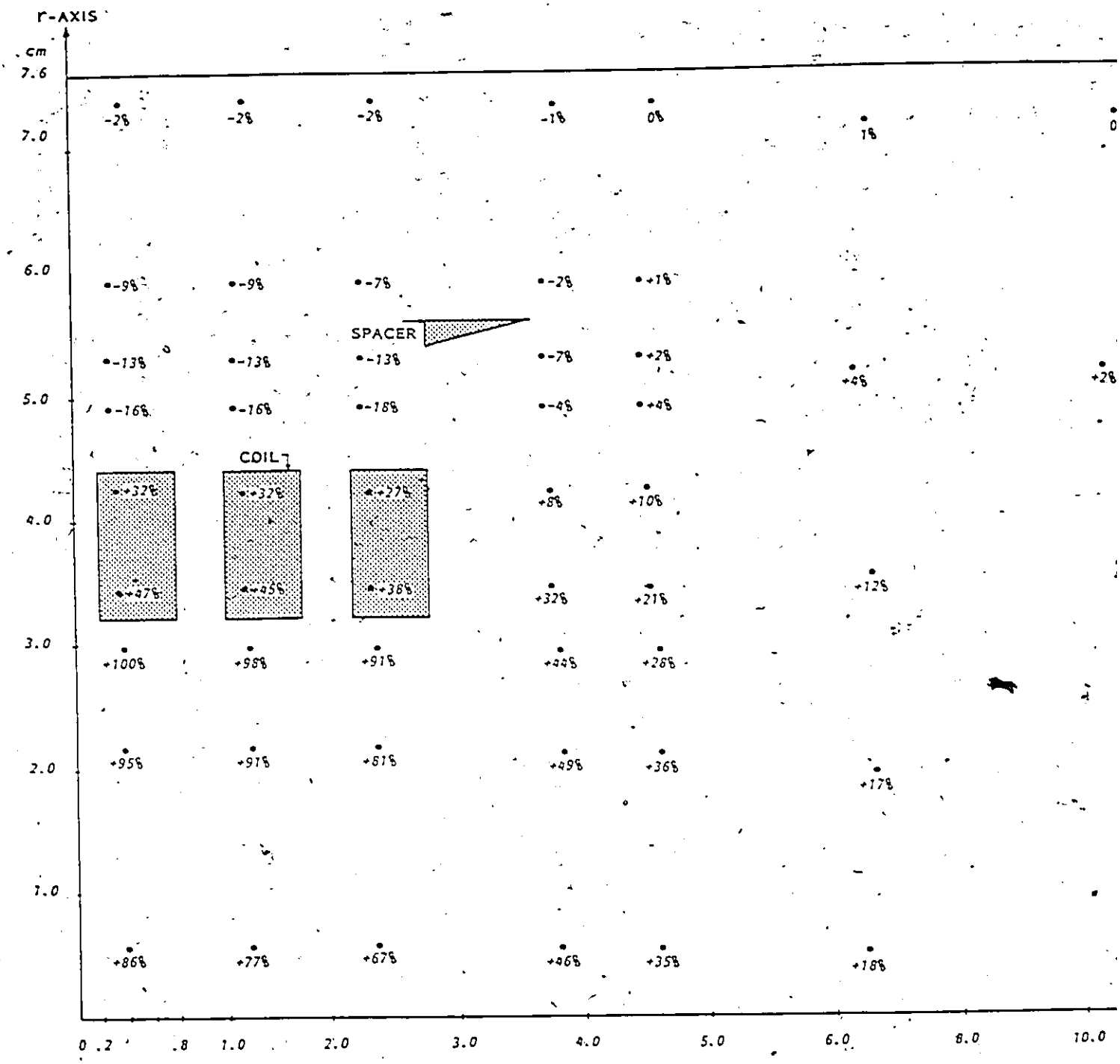

Figure

Normalized distribution B_z/B_{zmax} in

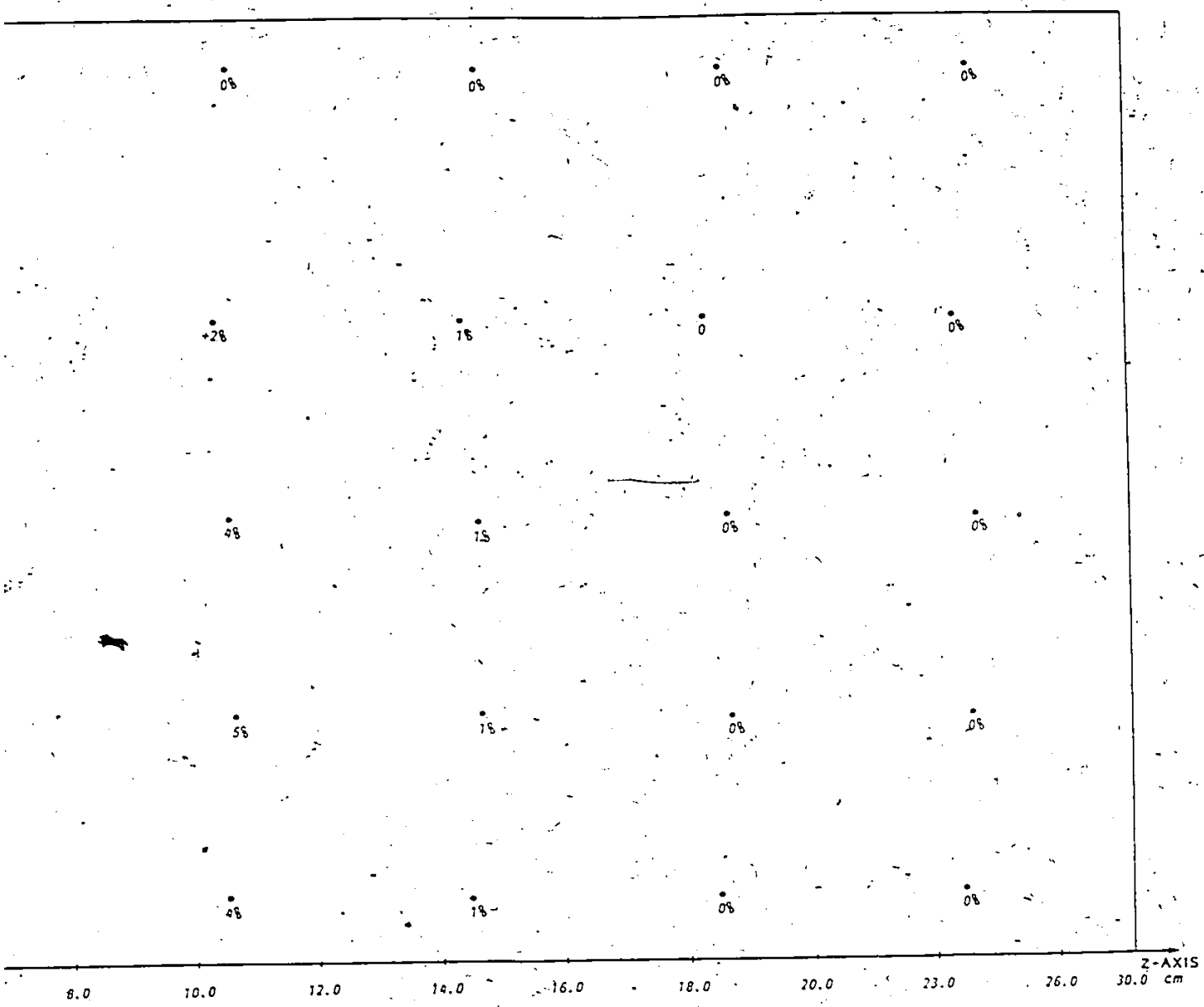

Figure 5.9

ɔution B_z/B_{zmax} in the expanded finite element mesh.

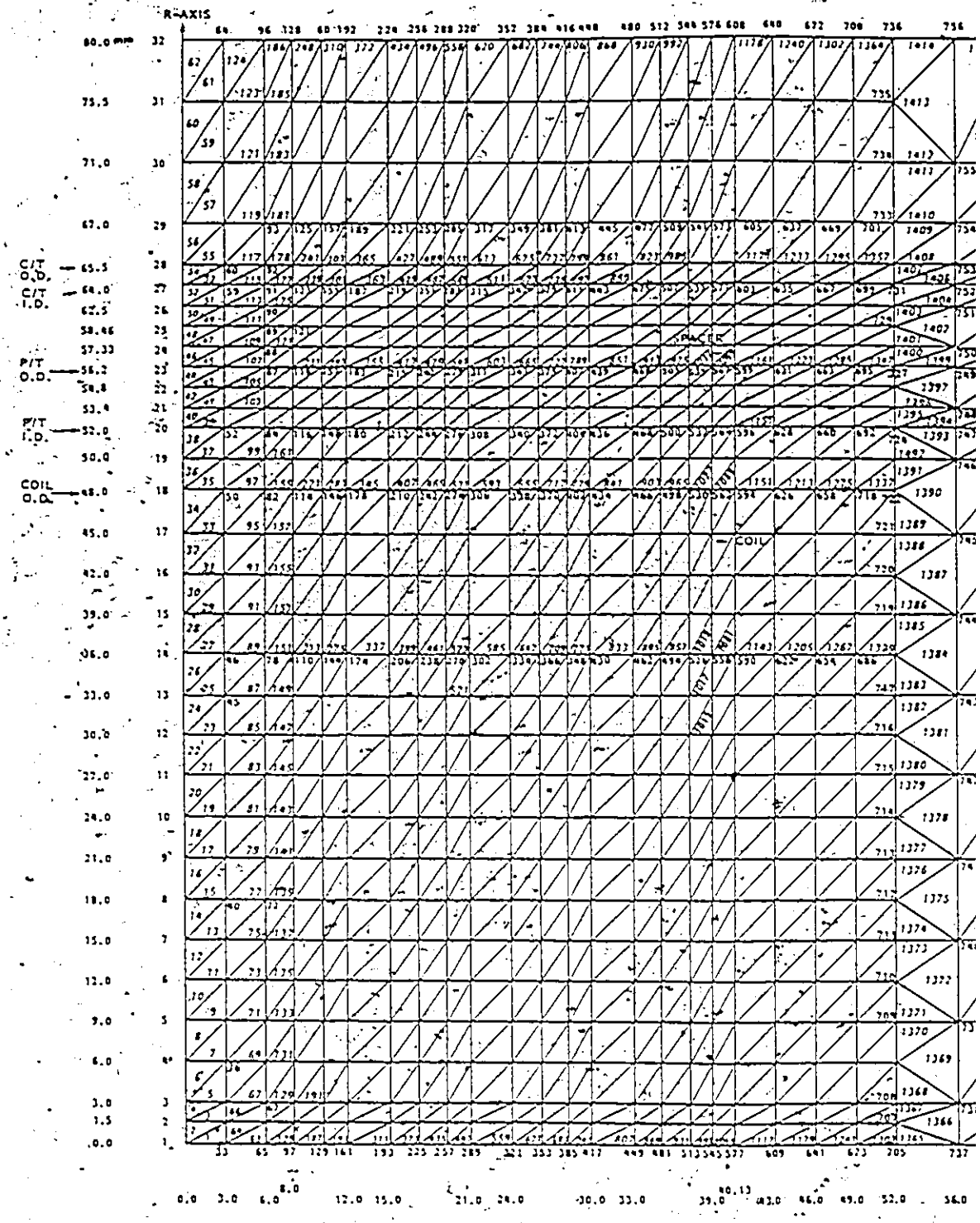

Numbers in Title are node numbers (0, 321,...)
Numbers in Italic are element numbers (1, 356,...)

Figure

Finite element mesh used to analys

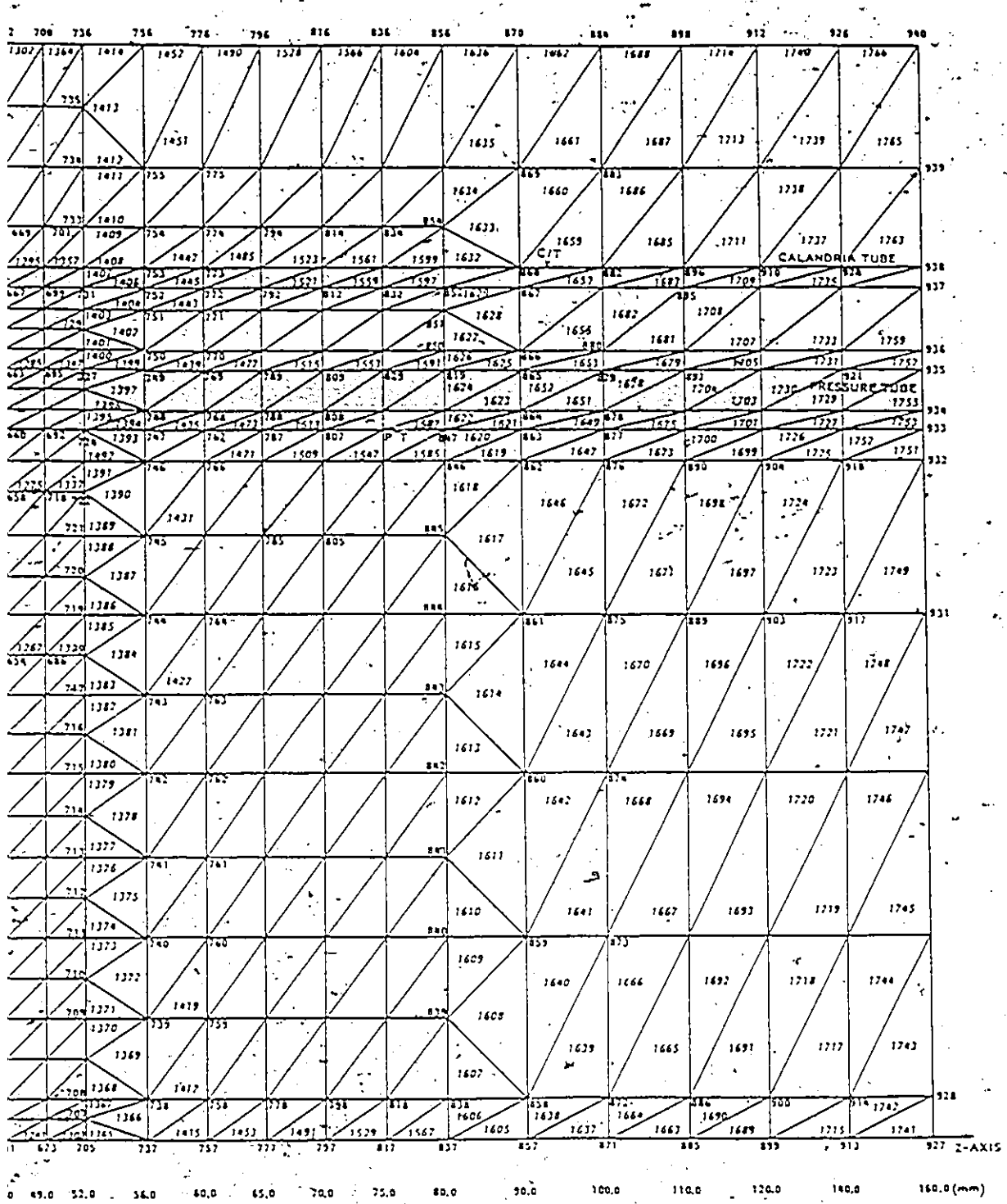

Figure 5.10

ed to analyse the G/S repositioning problem.

the P/T and C/T (Figures 1.1 and 1.2). Hence the calculated forces on the G/S would be on the conservative side. Note that the main objectives are to demonstrate the presence of an axial force that is capable of moving the G/S then to establish a calculation method to serve as an optimization tool.

Several computational tests were performed replacing the C/T and P/T with current sheets as described in the previous section to establish validity of the method. Also the case of a solenoid of finite length and current impulse represented by an exponentially decaying sinusoidal wave was examined thoroughly: All checks indicated that everything was in order and free from error.

5.4 Presentation of Typical Numerical Results

Several computer runs were made using the finite element mesh shown in Figure 5.10 to analyze the general electromagnetic field problem of the G/S application and to investigate the influence of some of the most important parameters involved in the process. Each of the computer runs produced an extensive amount of selected output data that provided a full description of spatial and time variations for the variables of interest. For each time step,

the magnetic vector potential (A_ϕ), B_z, $|B|$, and angle of B at each node and at the centroid of each element in the mesh were available: also the induced eddy current, radial and axial force densities for all the conductive elements in the mesh were calculated. The impulse radial and axial force densities for the G/S and specified elements in the P/T and C/T were calculated and printed at each time step.

A typical current impulse having a first current peak of 140 kA, a current reversal of 50% and a frequency of 1000 Hz (Figure 5.11) was used as the basis for reference purposes. This impulse was discretized using time steps ranging from 5 to 100 μs to determine a suitable step size. As a result, it was found that a time step of 25 μs represents a practical compromise between the accuracy of the results and size of computer output. Hence it was used for all subsequent computer runs.

The second set of computer runs was aimed at determining the optimum location of the G/S with respect to the coil. Elements number 914, 976, 1038, 1100, 1162 and 1224 (see Figure 5.10) were considered (one at a time) to represent the G/S. The coordinates of the element under consideration were adjusted to make the area of the element

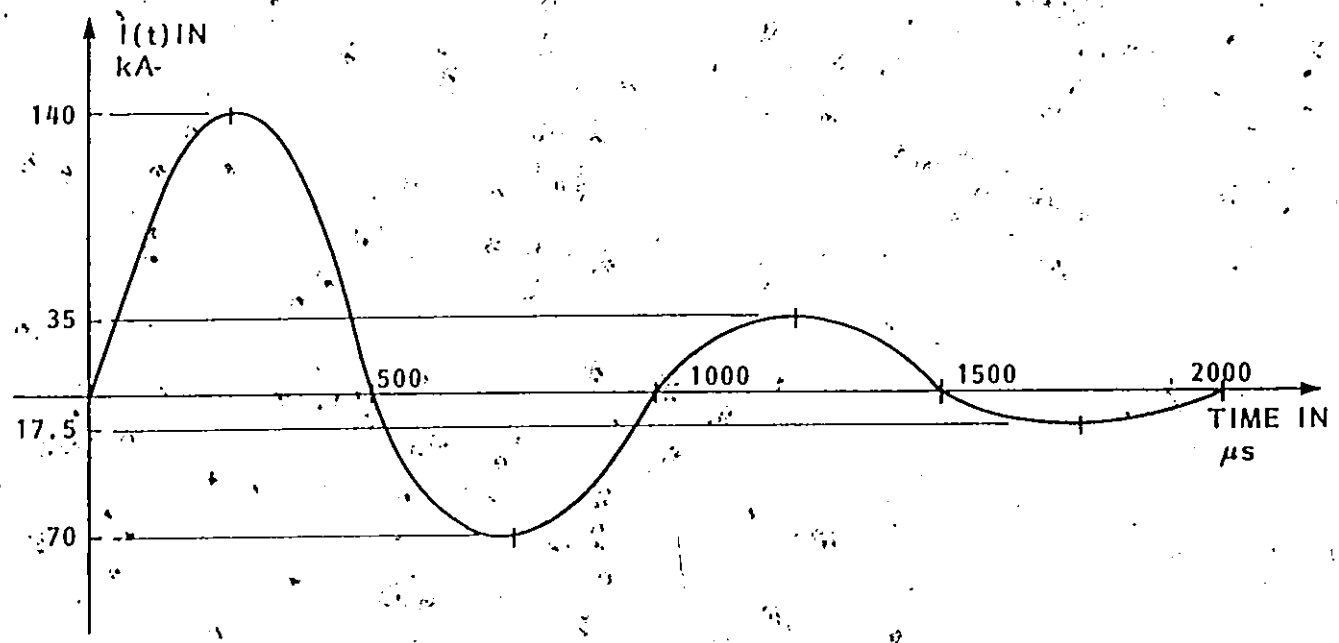

Figure 5.11

Typical impulse current used for computational purposes.

equal to the cross-section of the tie wire in the G/S. Only the first five time steps of the impulse shown in Figure 5.11 had to be examined in each run. The results clearly indicated that the maximum instantaneous axial force exerted on the G/S was obtained when element number 1100 was used to represent the G/S. This result agreed with and confirmed the experimental finding (Figure 1.4) that the maximum G/S displacement was achieved when the G/S was located over the edge of the first or last turn in the coil.

Figures 5.12 and 5.13 show the normalized distribution of the magnetic field density, in a graphical and numerical form respectively, at time t = 262.5 μs (ie, 12.5 μs past the first current peak) using the impulse waveshape of Figure 5.11. Note that in the central zone of the coil the magnitude of B is reasonably constant but starts to decay rapidly near the coil end and beyond. These figures illustrate that the value of B near the boundary is below 1% of its maximum value. We may conclude from this that the boundary is sufficiently far from the axis to effect reasonably accurate solution. Another interesting observation is the large attenuation of B as it penetrates the P/T. Figure 5.14 shows the time variation of B at one point (element number 6). Note that B increases steadily during the first half cycle of the current pulse. In view

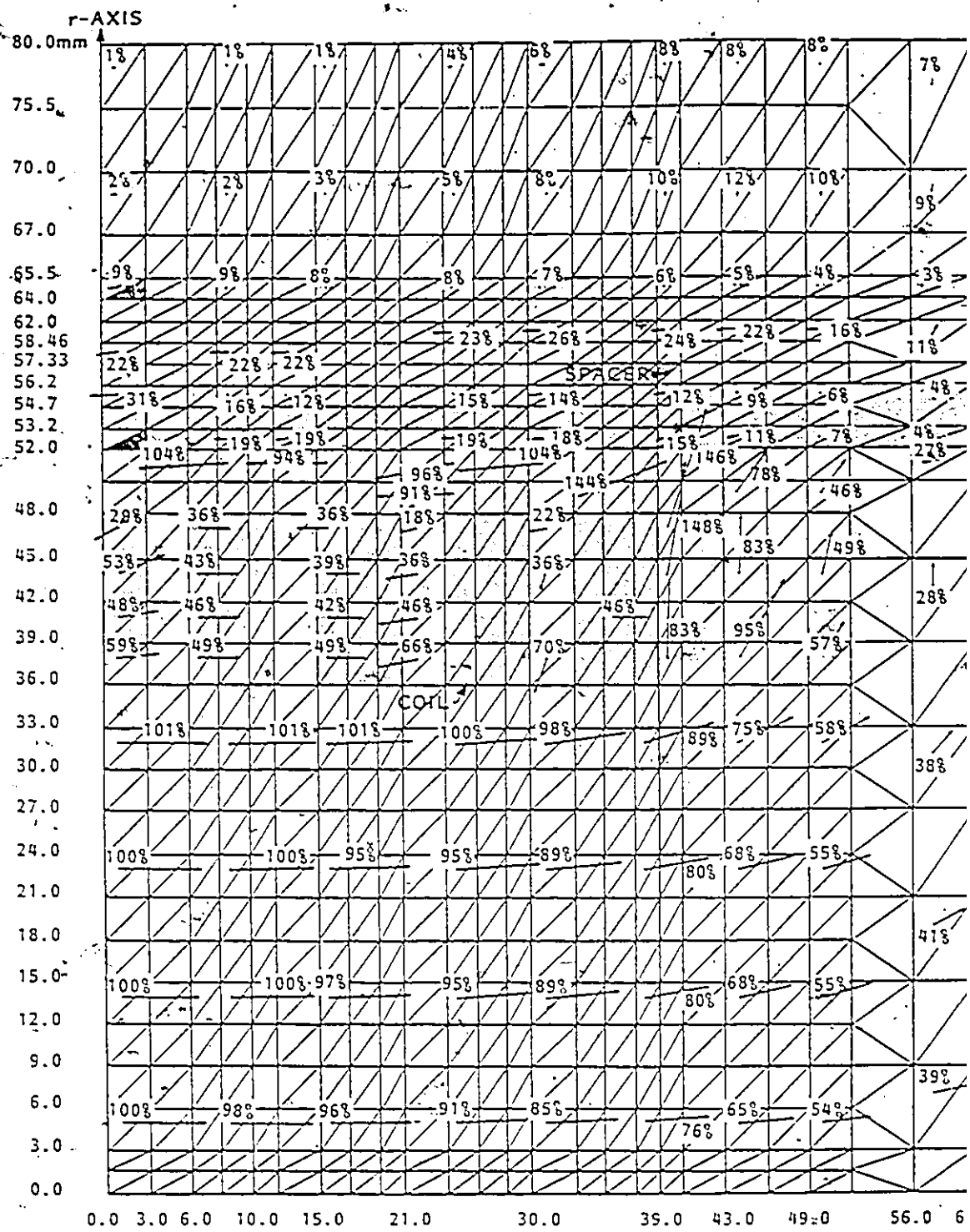

Figure 5.1

Normalized magnetic field density (B/B_{center}) at t

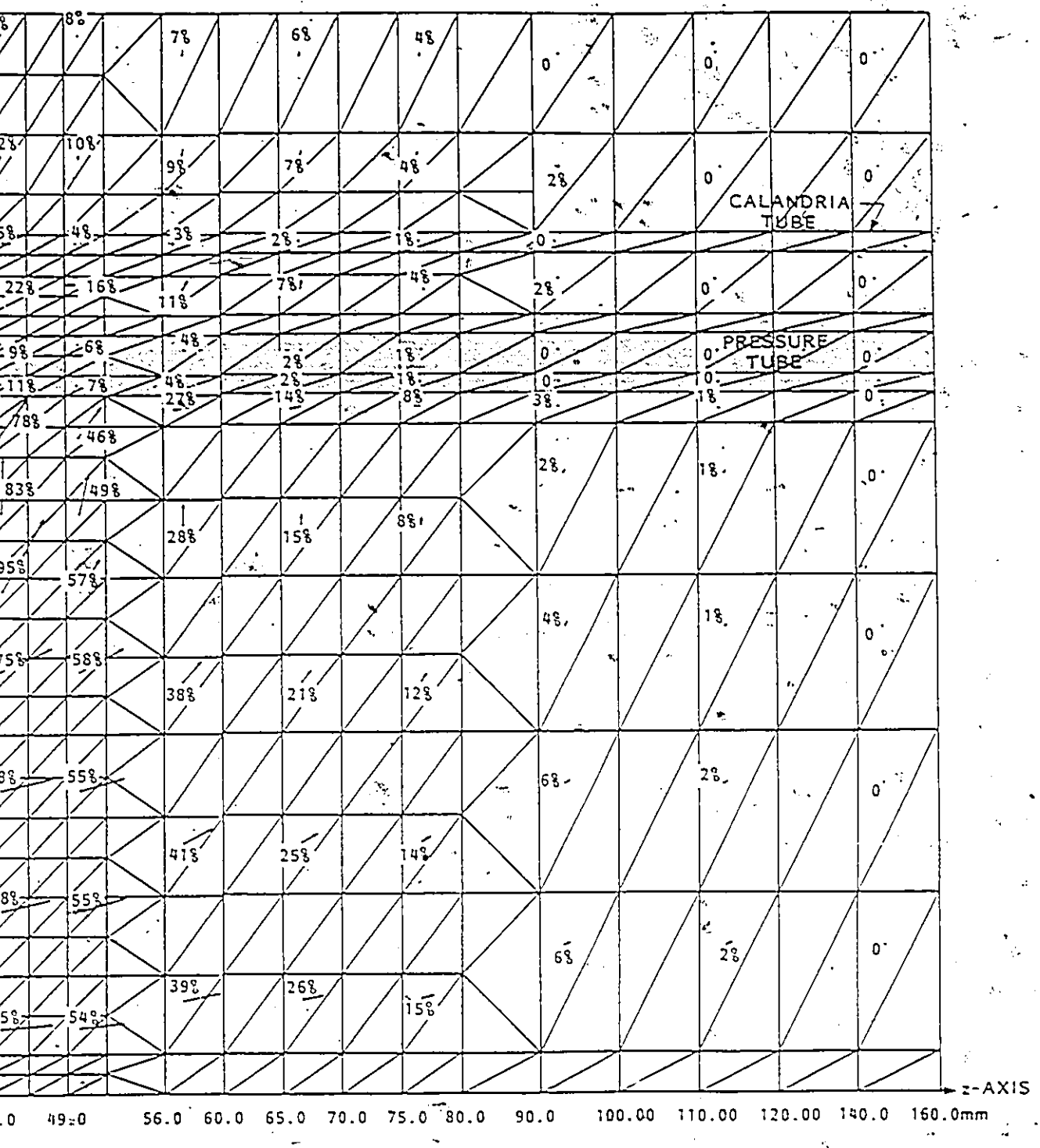

Figure 5.12

B/B center) at time t = 262.5 μs (graphical representation).

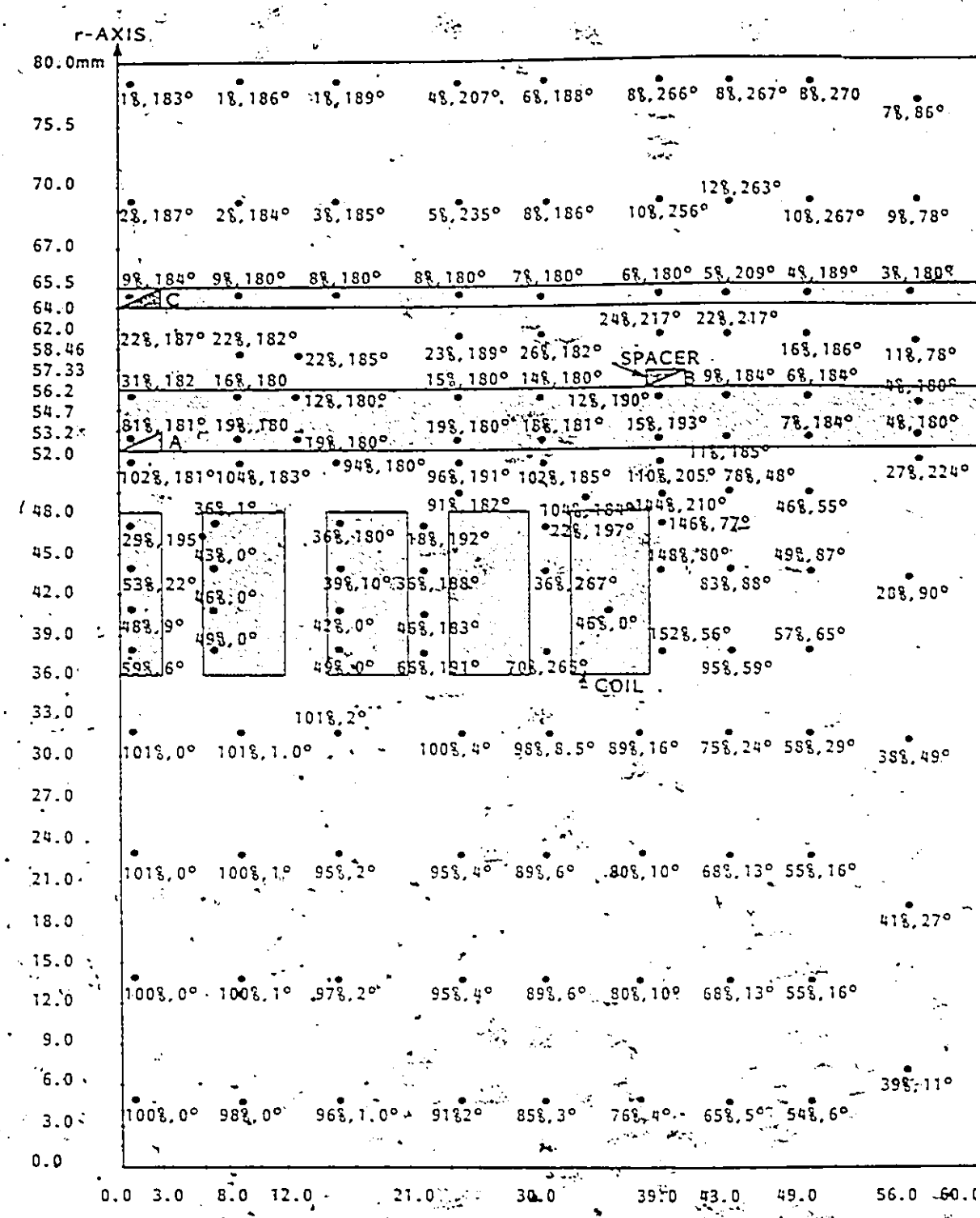

Figure 5.13

Normalized magnetic field density (B/B_{center}) at

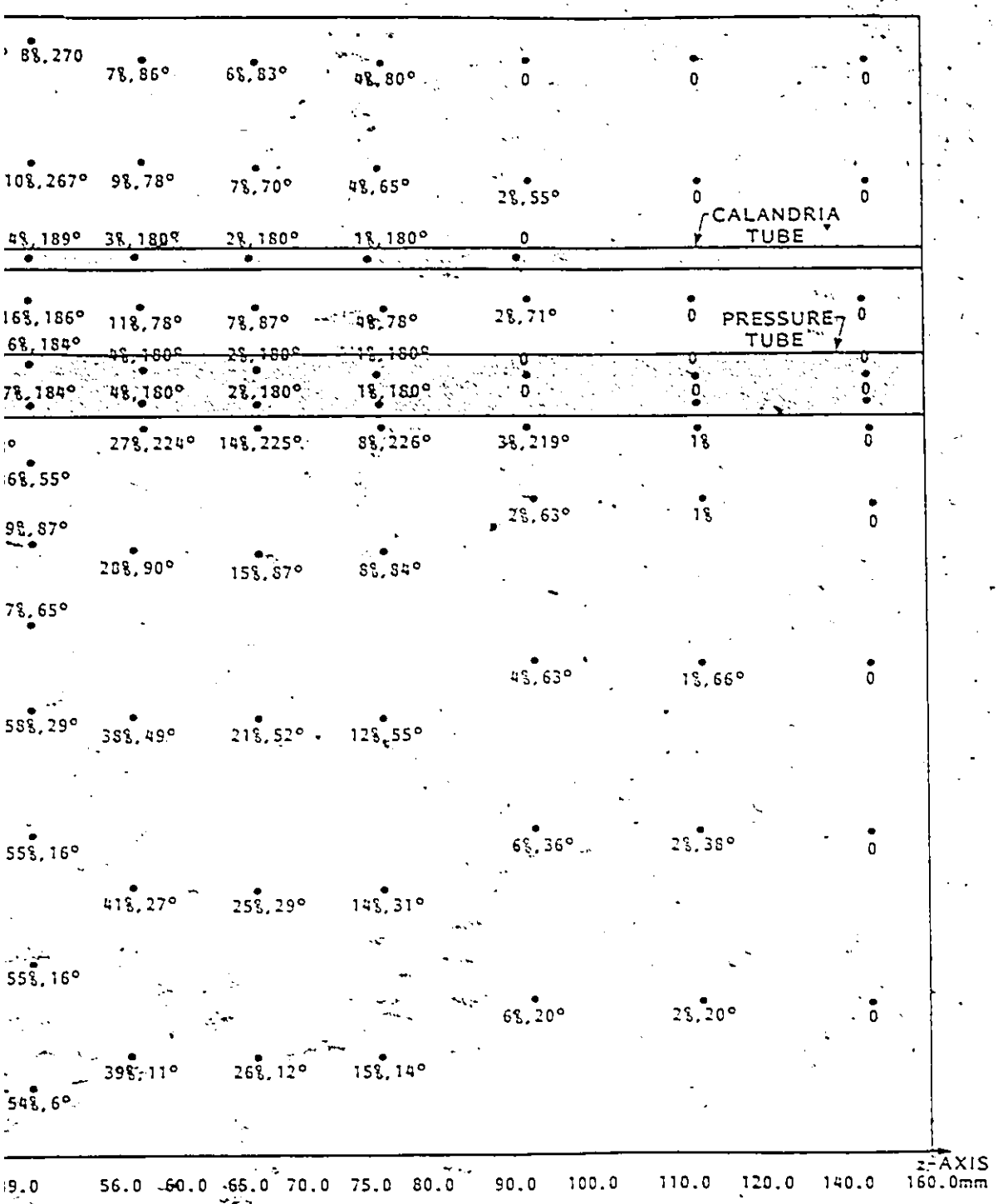

Figure 5.13

/B center) at time t = 262.5 μs (numerical representation).

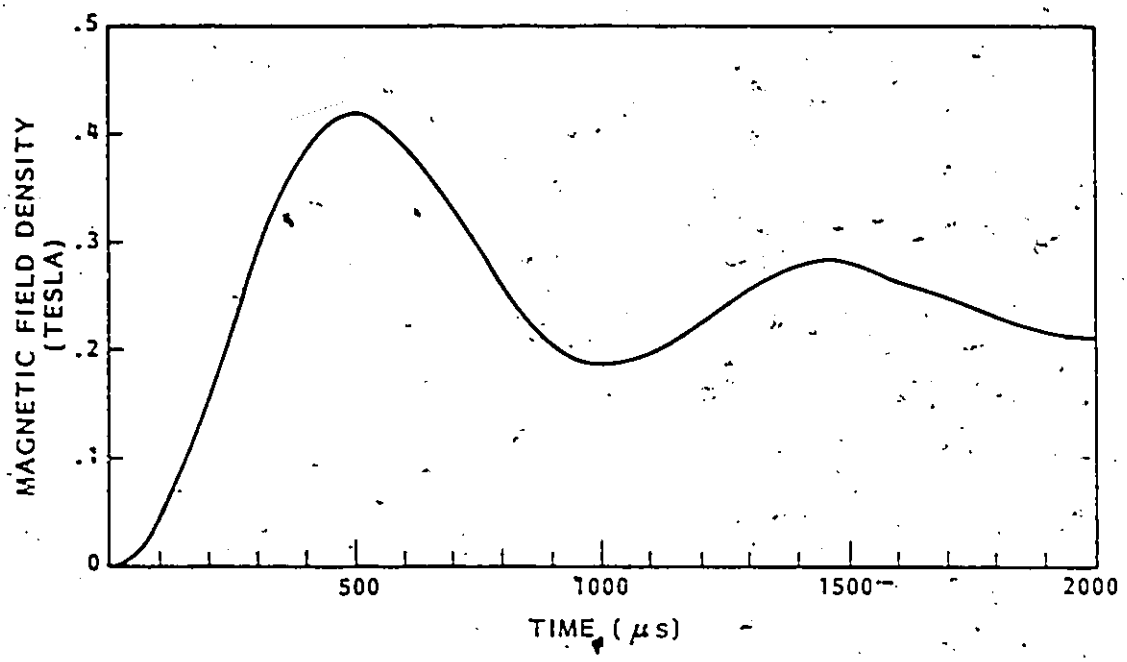

Figure 5.14

Time variation of |B| in element number 6 near the center of the coil.

of the 50% reversal in the current pulse and the relatively long diffusion time associated with the copper coil, B does not reach the zero level in the second half cycle. In other words the amount of inductive energy stored in the coil and surrounding tubes during the first half cycle (with a current peak of 140 kA did not have sufficient time to be transferred out or to be dissipated completely during the negative half cycle (with a current peak of 70 kA). Also due to the finite diffusion time, B does not go immediately to zero at the end of the input current pulse.

In this application, the axial force exerted on the G/S is of prime interest. Figure 5.15 presents the instantaneous axial force density (in N/m^3) in response to the impulse current of Figure 5.11. Each arrow represents the magnitude and sign of this variable. The axial component of force (length of the arrow) is plotted every 50 μs to avoid overcrowding of the lines. It is calculated every 25 μs. The largest peak was 0.899×10^6 N/m^3 and was reached at time t = 387.5 μs (ie, 137.5 μs after the first current peak). Also, the first sign reversal occurred at approximately 612.5 μs: this gives a clear indication of the phase shift in the time domain.

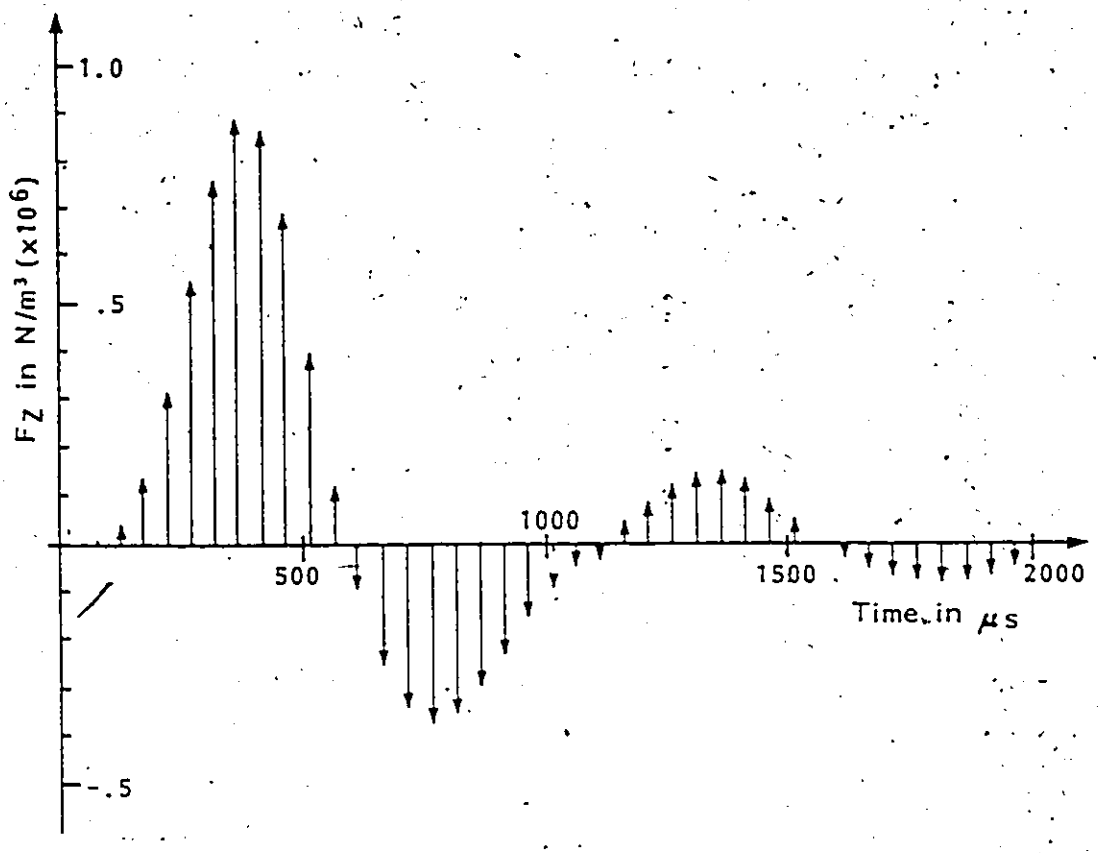

Figure 5.15

Instantaneous axial force density exerted on the G/S (Element #1100)

In order to calculate the G/S displacement produced by the above force profile, the impulse energy transfered to the G/S has to be determined. This can be accomplished if the impulse axial force density exerted on the G/S is known. Figure 5.16 shows this impulse force obtained by summing the instantaneous force density over the time domain [85].

Figures 5.17 and 5.18 present the distribution of induced eddy-current density in the coil and the fuel channel assembly respectively, at time t=262.5 μs. Several interesting observations can be made:

1. In any turn of the coil the induced current density is at a maximum in the central zone of the cross-section instead of the outer zone, as would be expected if the P/T and C/T were not present. In other words, the proximity effect between the coil and the P/T may be partially responsible for the distribution shown. However, the main contributing factors toward the establishment of this profile are:

   a) The assumption that the source current was distributed uniformly in the cross-section of the coil turns.

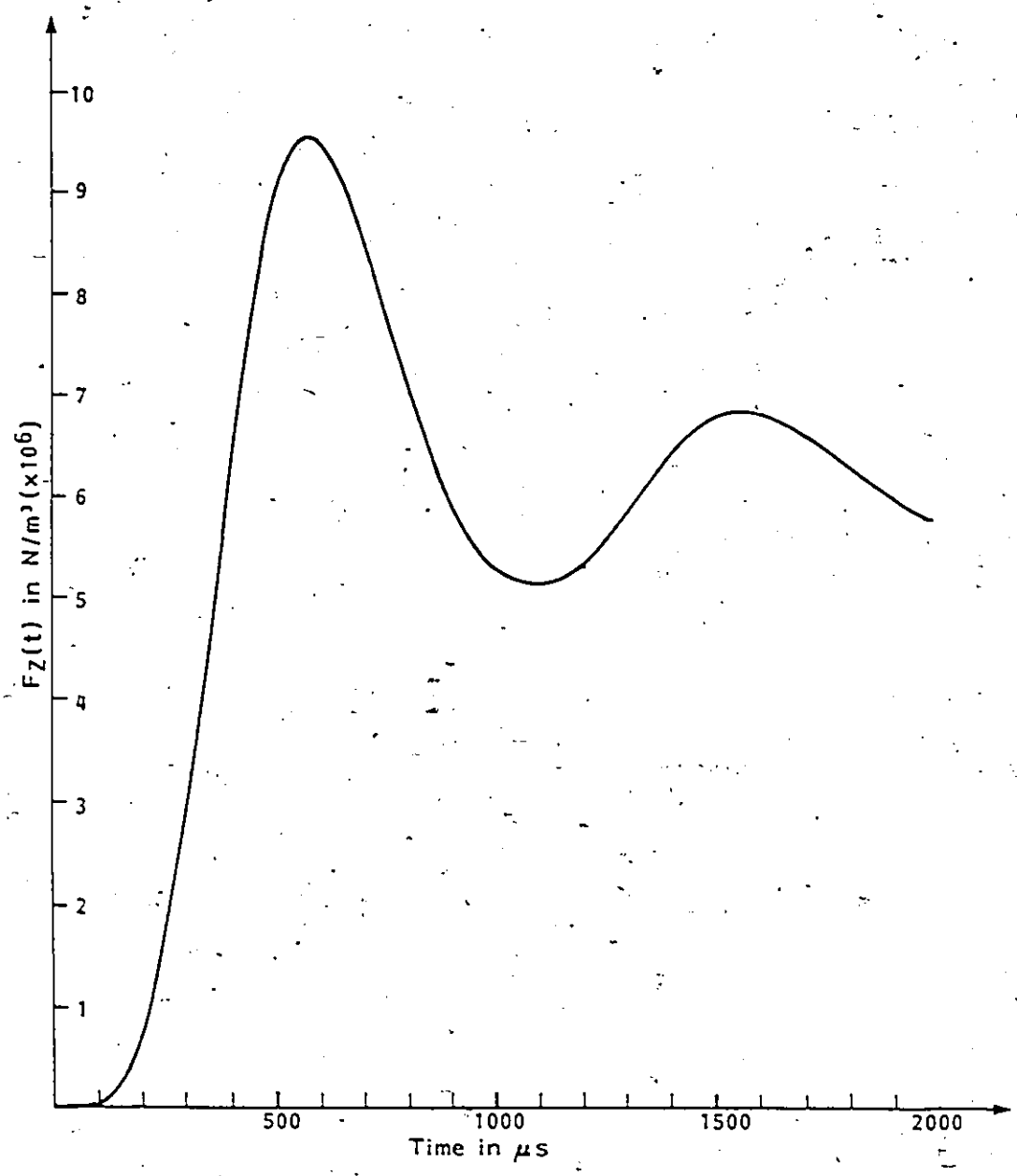

Figure 5.16

Impulse axial force density on the G/S
(Element #1100)

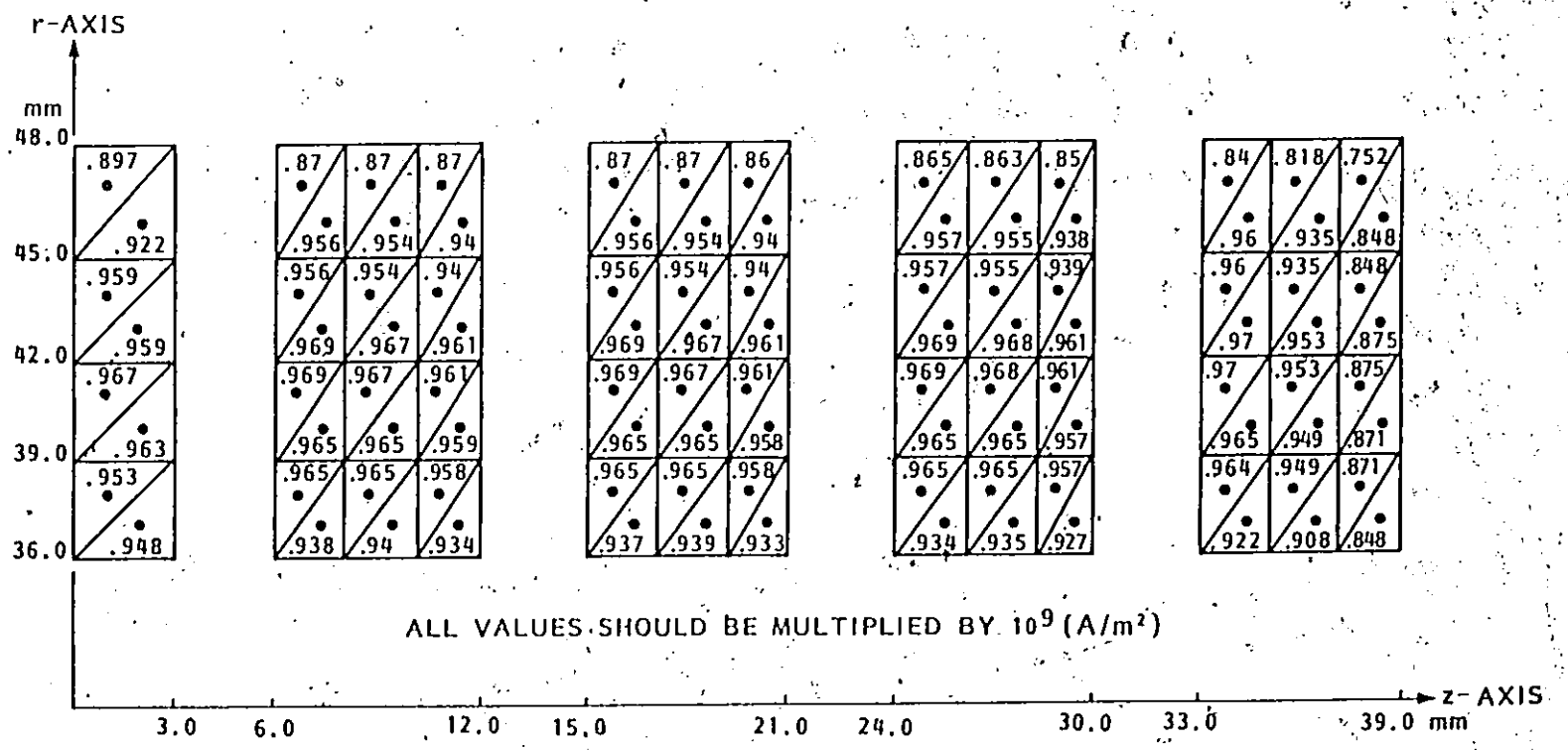

Figure 5.17

Distribution of induced eddy current density in the coil at time t = 262.5 μs (with the P/T, G/S and C/T present)

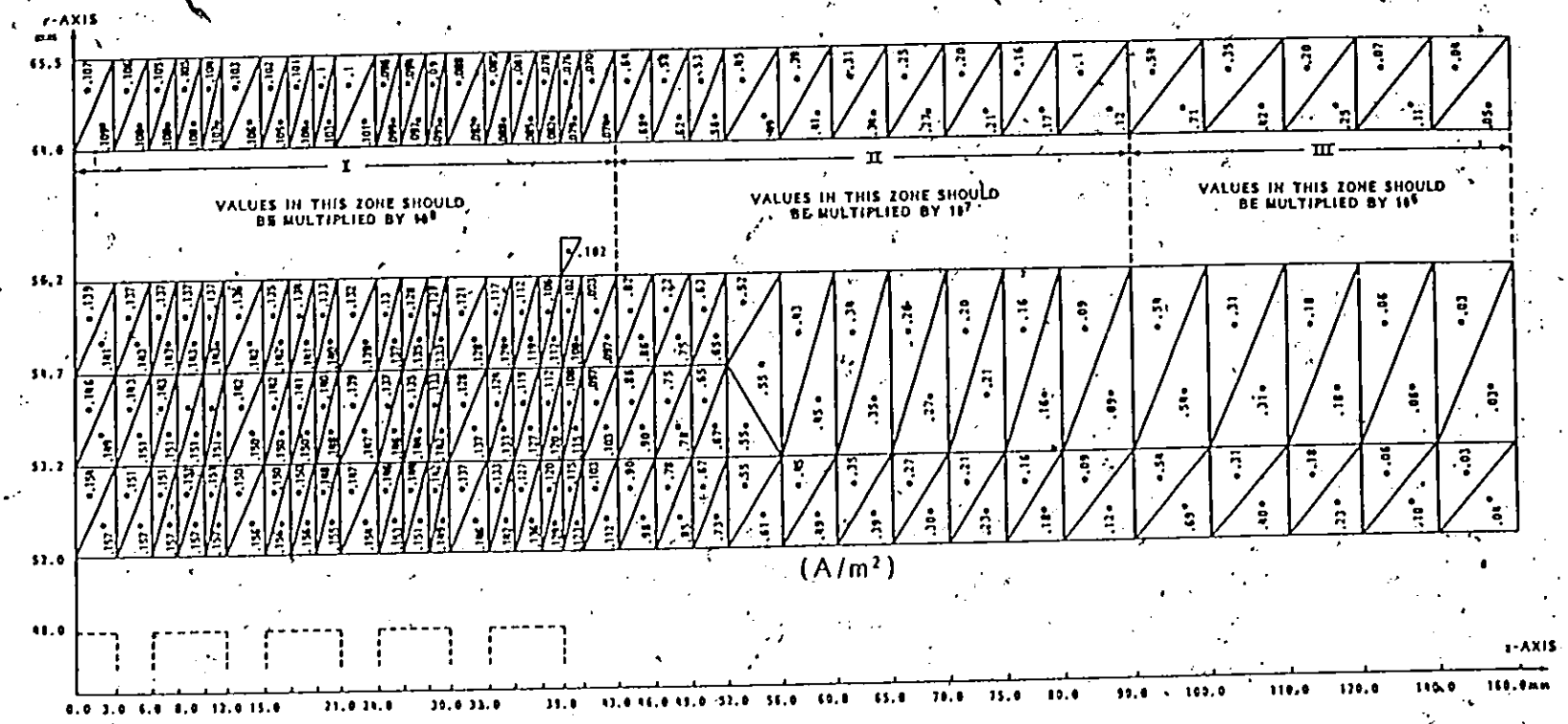

Figure 5.18

Distribution of induced eddy current density in the P/T, G/S and C/T at time t = 262.5 μs.

b) The diffusion time for the magnetic field (and consequently the duration of induced currents in the copper) is relatively long when compared to the same quantity in metals with lower electrical conductivity. Thus 262.5 μs is too short for the induced current to reach the final distribution that is attained if the source current were sustained for a longer period of time.

2. The induced current density in the last coil turn has larger gradient in the axial direction than the gradient shown in the other turns. This is clearly due to the proximity effect of the coil turns on each other and to the fact that the magnetic flux lines are more densely packed in the central region of the coil than near the end.

3. The magnitude of the induced current in the coil is more than an order of magnitude larger than it is in the P/T because the coil has higher electrical conductivity. The distance between the P/T and the coil is also a contributing factor to this difference.

4. The profile of the induced current density in the P/T and C/T in both the radial and axial directions is as expected. The diffusion time in zirconium-niobium

alloys is much smaller than the diffusion time in copper; hence the induced current density reaches its normal distribution much faster than it would in the copper coil.

Figure 5.19 presents the time variation of the induced eddy-current density in one representative element in each of the coil, P/T, C/T and G/S. To facilitate the comparison of this variable in the subject elements the same scale was used for all of the curves. However, since the current density in the P/T, G/S and C/T is much smaller than the current density in the coil, a smaller scale was used to clearly show the distributions with lower magnitudes.

Figures 5.20 and 5.21 show the profiles of the radial force density on the coil, P/T, G/S and C/T at time t = 262.5 μs. Figure 5.22 shows the instantaneous radial force density (as a function of time) in one element of the coil, in the G/S and one element in the P/T. Similar representations for the axial force density are shown in Figures 5.23, 5.24 and 5.25. The radial and axial force densities in the coil reach their maxima in element 1019 which is located in the lower right hand side corner of the last turn. This observation substantiates the coil

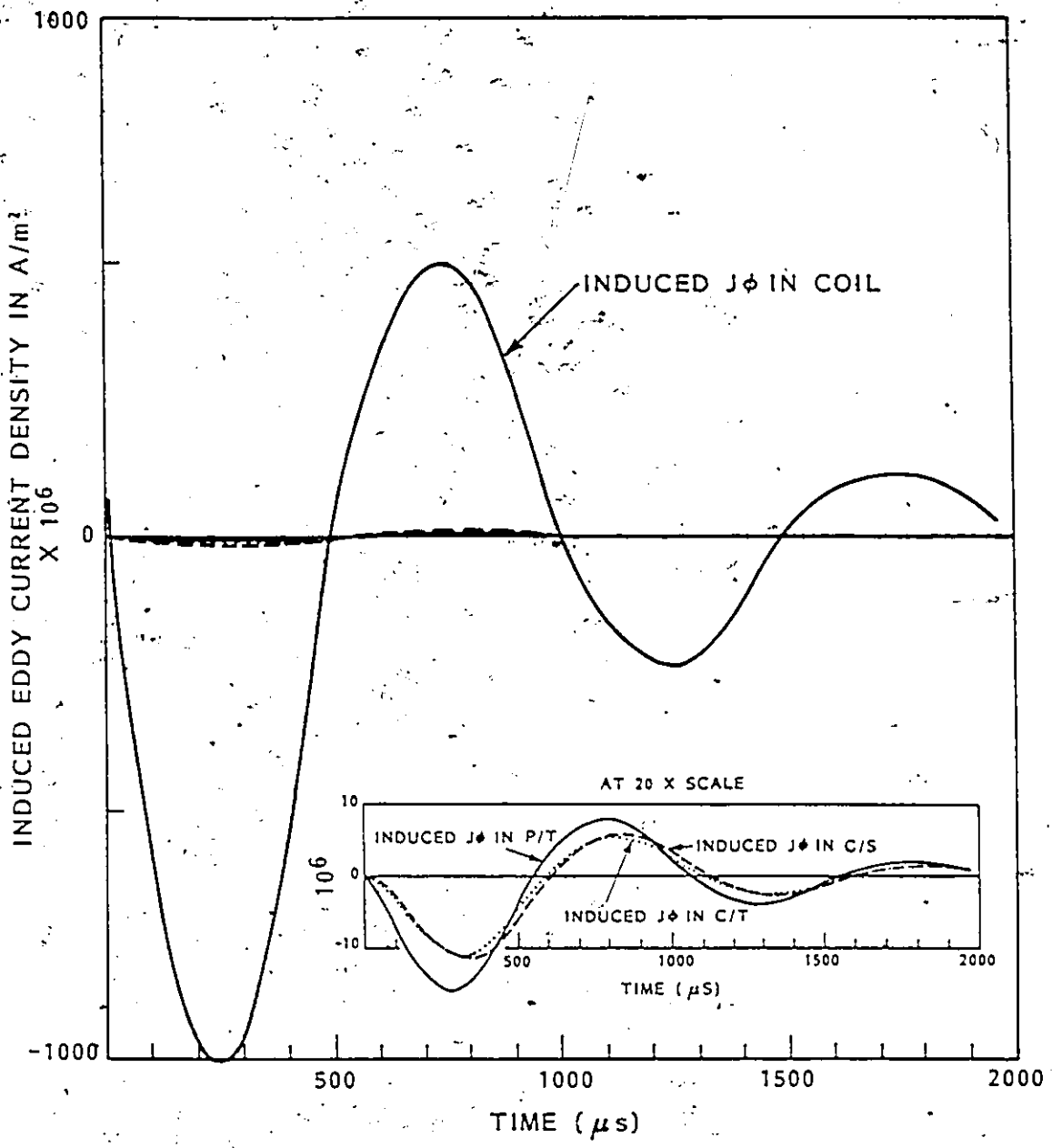

Figure 5.19

Induced eddy current density in elements #466, 473, 487 and 1100 in the coil, P/T, C/T and G/S respectively.

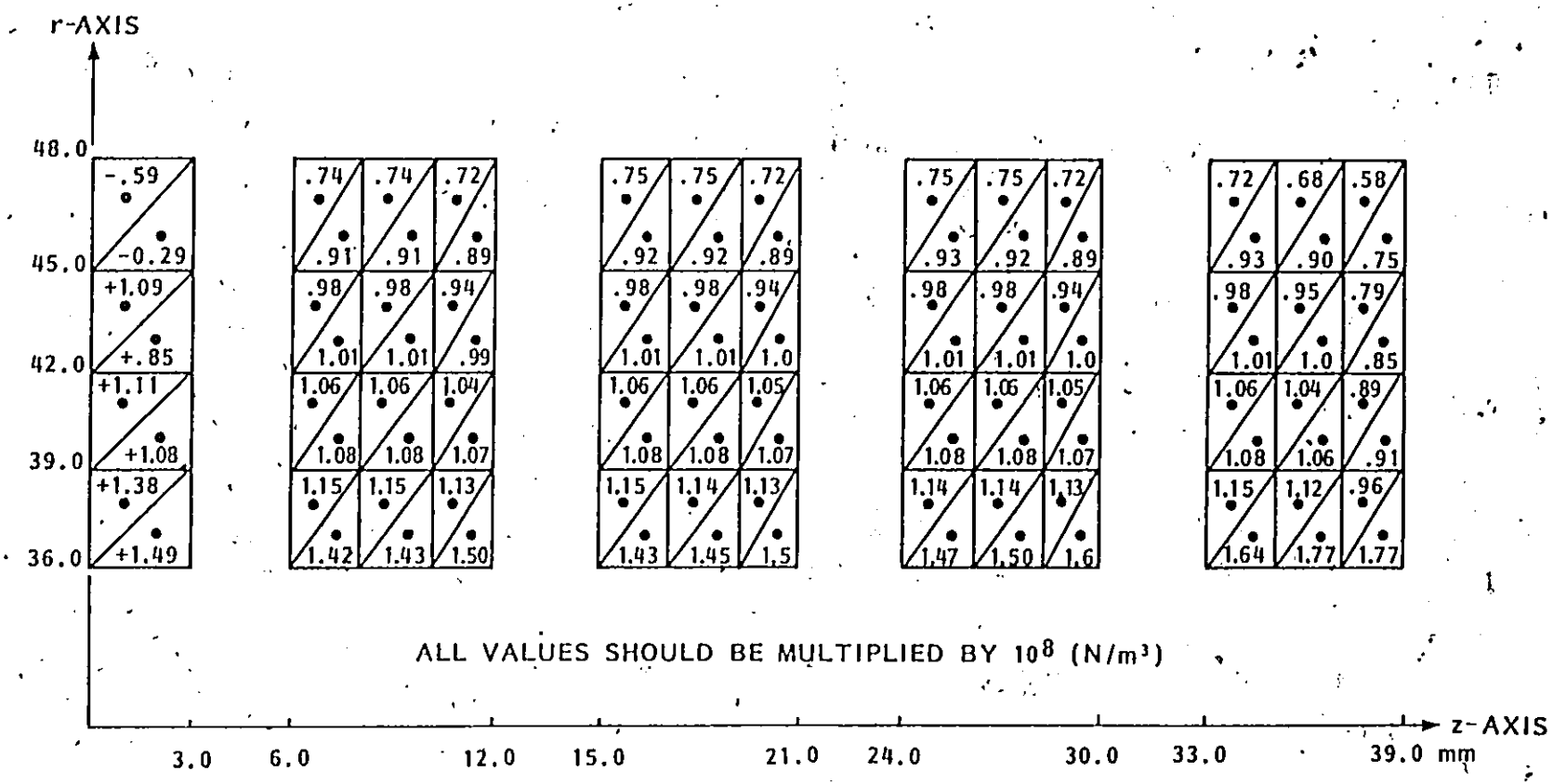

Figure 5.20

Distribution of radial force density on the coil at time $t = 262.5\ \mu s$ (with the P/T, C/T and G/S present)

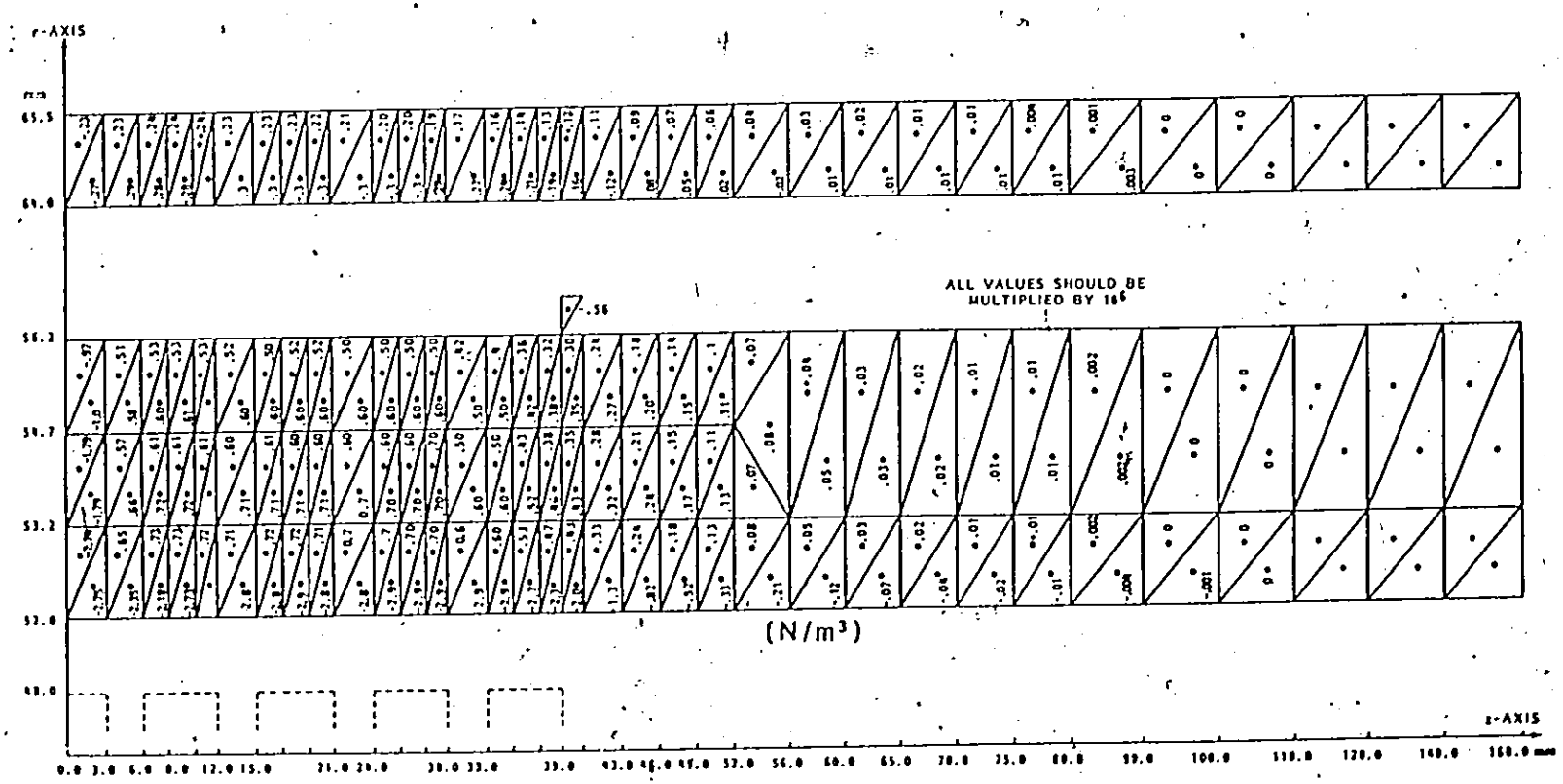

Figure 5.21

Distribution of radial force density on the P/T, G/S and C/T at time t = 262.5 μs.

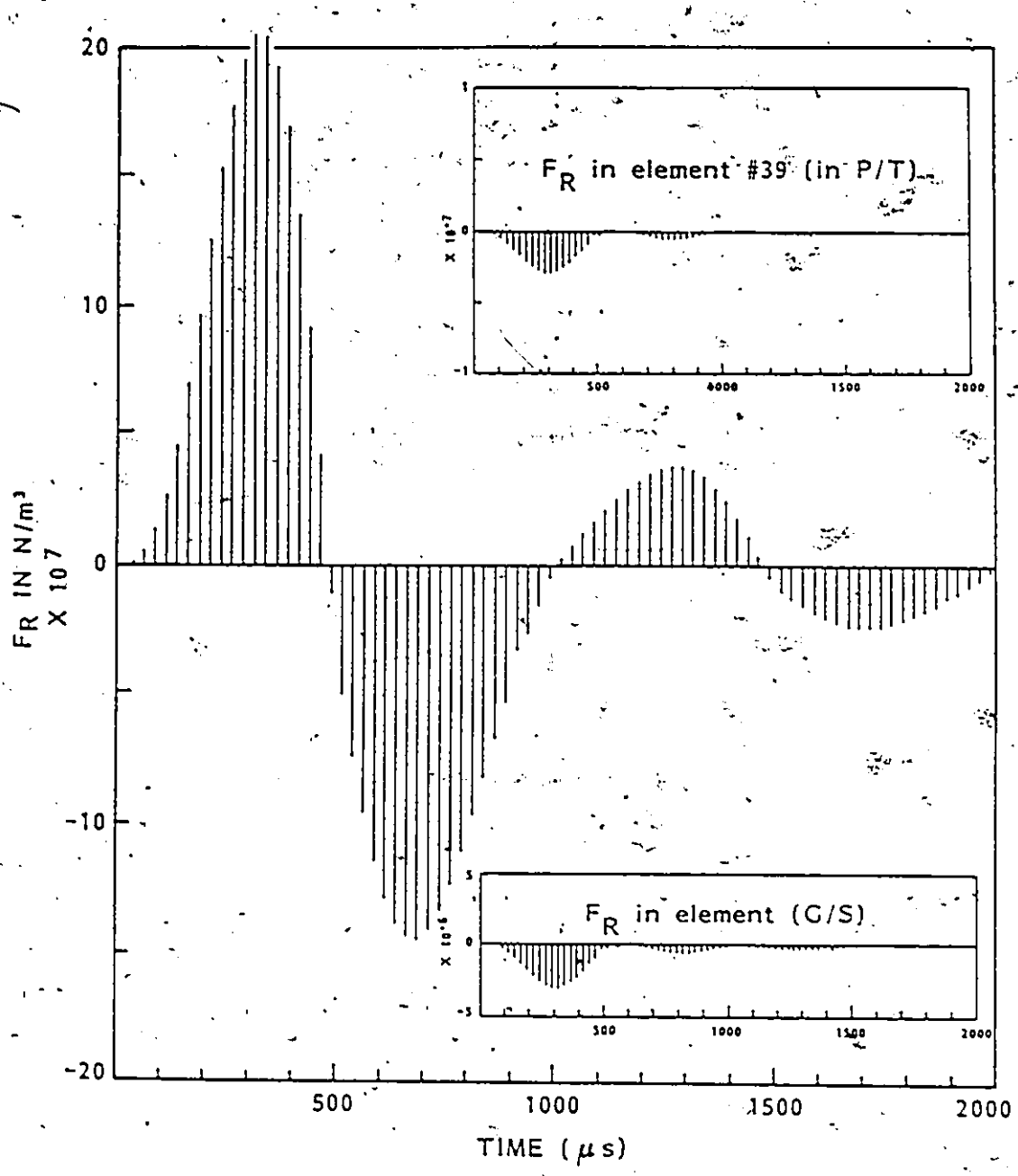

Figure 5.22

Instantaneous radial force density on elements #1019, 39 and 1100 in the electromagnetic coil, P/T and G/S respectively.

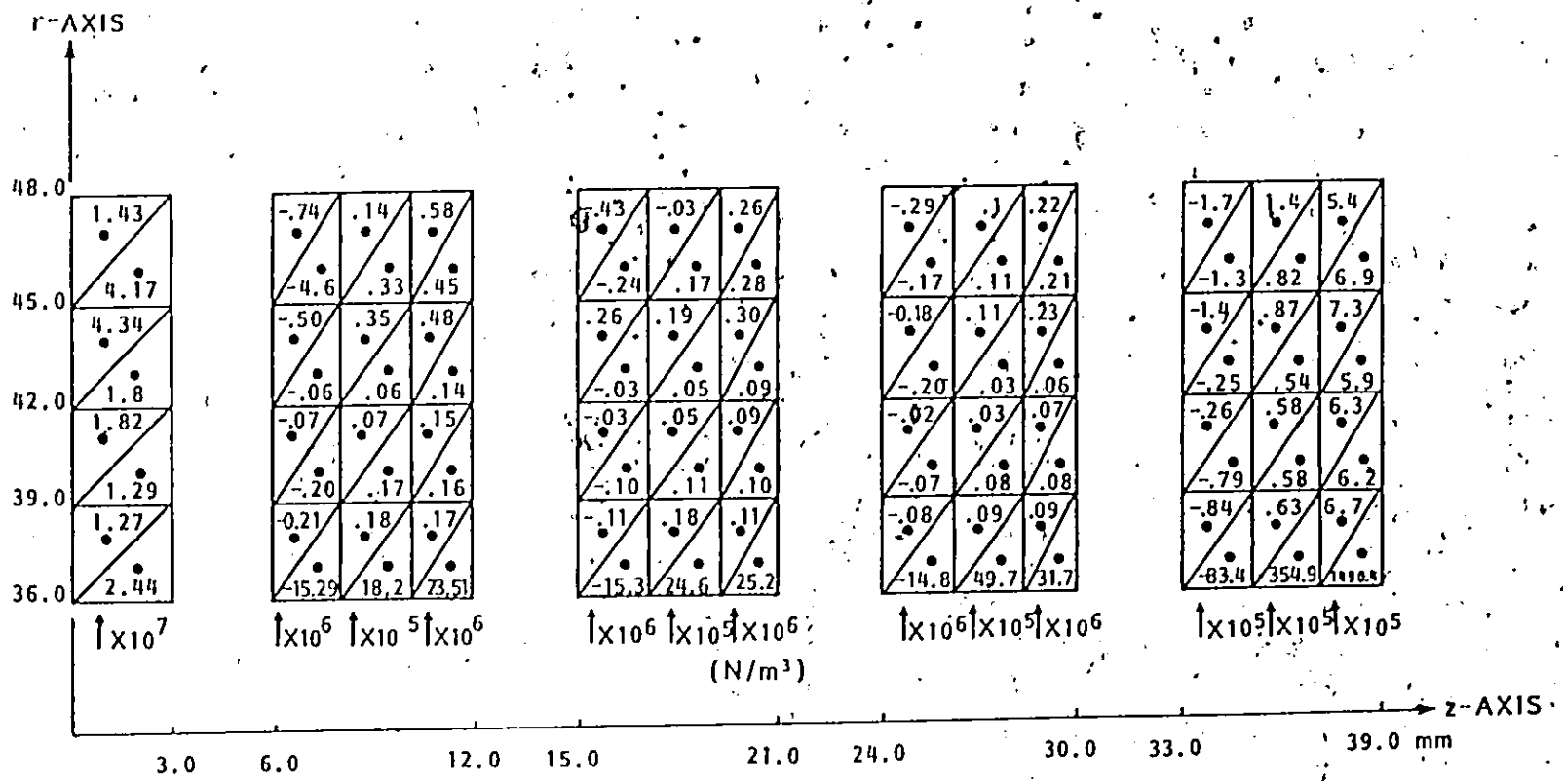

Figure 5.23

Distribution of axial force density on the coil at time $t = 262.5\ \mu s$ (with the P/T, G/S and C/T present)

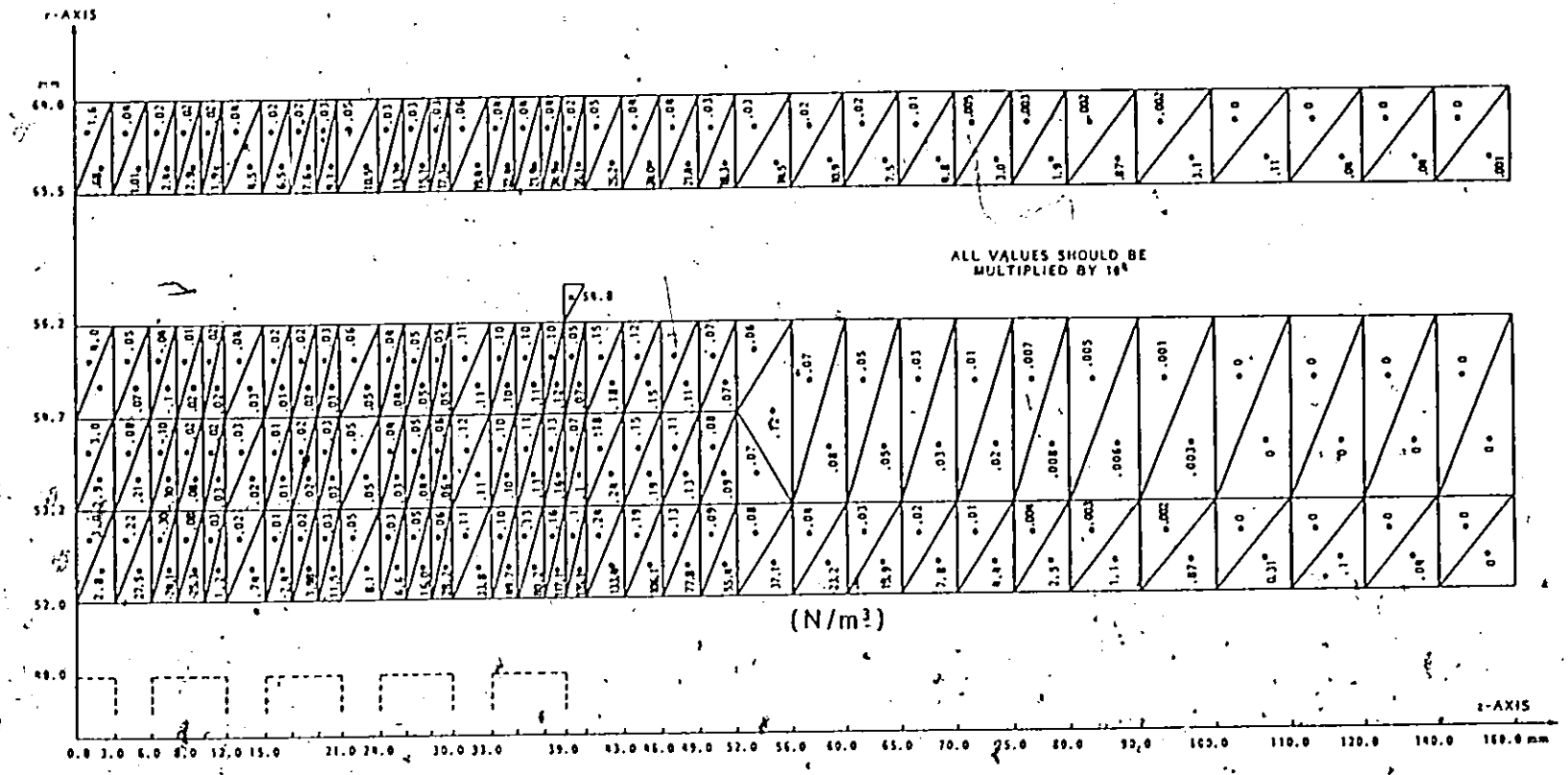

Figure 5.24

Distribution of axial force density on the P/T, G/S and C/T at time t = 262.5 μs.

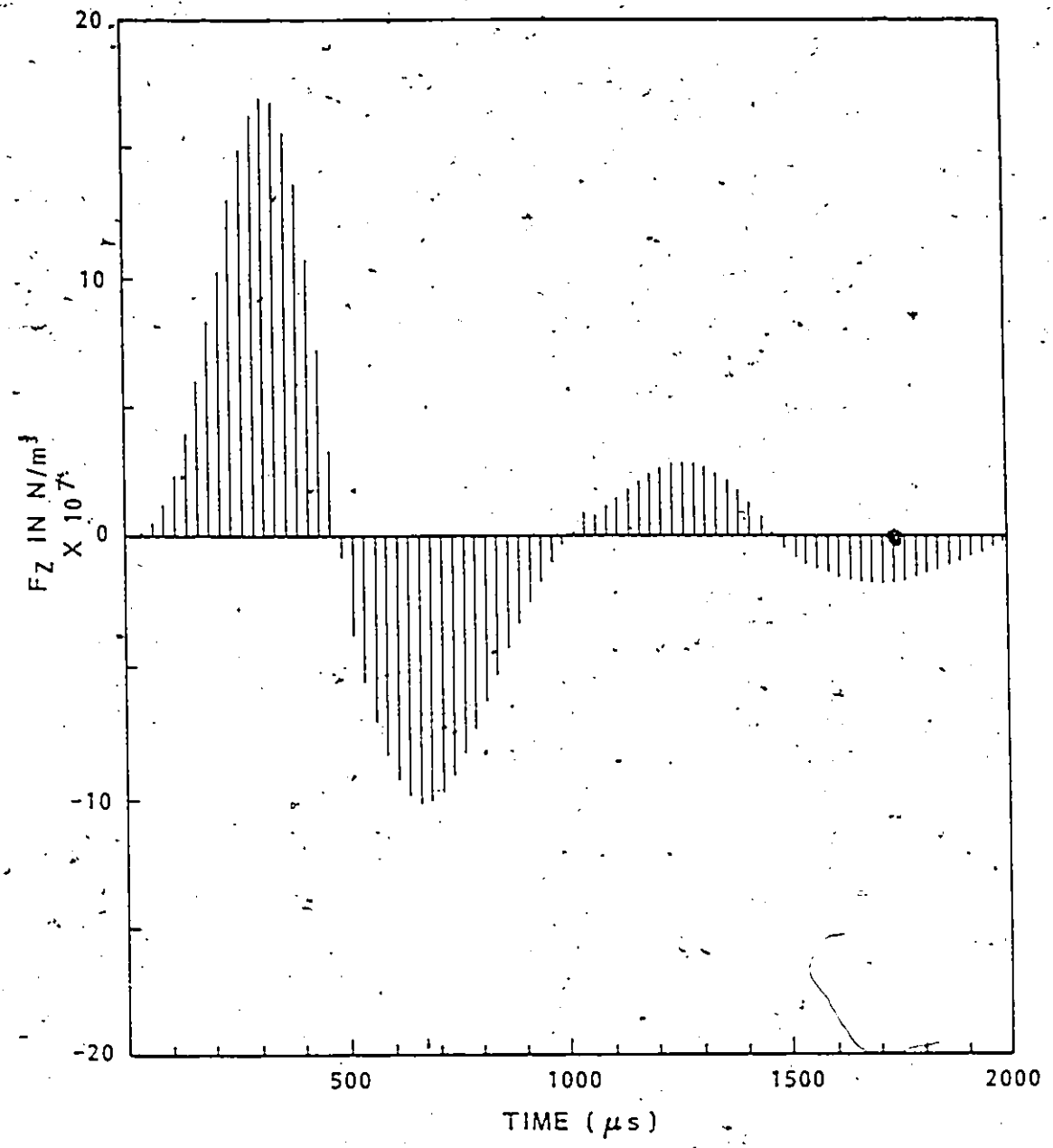

Figure 5.25

Instantaneous axial force density on element #1019 in the electromagnetic coil.

deformations observed during the experimental program (Figures 3.10 and 3.12). The outward growth and twisting of the first and last turns of the coil were greater than for any other turn. Deformation in these turns led to coil failure in most cases. The profile of the axial force density clearly illustrates the torsional type of forces exerted on the coil turns.

5.5 Comparison of Simulation with Experimental Results

As indicated earlier, the experimental results expressed the G/S displacements in terms of various control and design parameters, while the theoretical simulation produced, among other things, the axial instantaneous and impulse force densities exerted on the G/S. Although the validity of the numerical solution has been verified by examining cases for which analytical solutions exist, an additional comparison between numerical and experimental results has been carried out to further substantiate the validity of the simulation and to demonstrate that the computed forces are large enough to displace the G/S. This comparison was made possible by establishing a simplified mechanical model to correlate the G/S displacement to the computed instantaneous axial force density exerted on the G/S as described below.

The impulse applied to the G/S via the electromagnetic induction process can be defined as:

$$I.E. = \int_0^{t_1} F(t)\, dt = \frac{w}{g}(v_1 - v_0) \qquad (5.4)$$

where F(t) is the instantaneous axial force in newtons, t_1 is the duration over which the force is exerted in seconds, w is the weight in newtons, g is the gravitational constant ($g = 9.81\ m/s^2$) and v_1 is the velocity in m/s [121]. Noting that the initial velocity v_0 is zero since the G/S is initially at rest and that the integral expression represents the area under the curve F(t) in the time interval 0 to t_1, equation (5.4) can be used to determine the velocity v_1 of the G/S during its displacement. Once v_1 is known, the energy balance equation

$$E_1 = E_2 + \text{losses} \qquad (5.5)$$

which states that the energy of the G/S at its initial position is equal to its energy at the new position plus the losses incurred during its movement, can be used to calculate the G/S displacement. Equation (5.5) can be rewritten in the form

$$\frac{1}{2}\frac{w}{g} v_L^2 = F_r d \qquad (5.6)$$

where F_r is the friction force exerted on the G/S and d is the amount of G/S displacement. Note that E_2 is equal to zero since the G/S does not possess any Kinetic energy at its final position.

The mass of the G/S is 33 g. The friction force encountered by the G/S when it is moved in the axial direction with only the P/T present was measured and found to be 19.6 mN. The volume of the G/S is 10.06 mm^3. The impulse energy defined in equation (5.4) was computed by summing the product of the instantaneous force (calculated at each time step) by the size of time step (25 μs). The instantaneous force was obtained by multiplying the computed axial force density in the G/S by the volume of the G/S. Calculation was performed for the case presented in Figure 5.15, ie, an impulse current having 140 kA for its first peak, a frequency of 1000 Hz, 50% current reversal and a duration of 2.0 ms.

The impulse energy for the case considered, that is the area under the curve joining the tips of the arrows in

Figure 5.15, was found to be 4.35 mJ. Thus, using equations (5.4) and (5.6) yields a G/S displacement d = 15 mm. The measured value of G/S displacement, for the same conditions, is approximately 18 mm (see Figure 3.2). Therefore, the computed G/S displacement is approximately 17% lower than the measured value. This is quite satisfactory considering the simplicity of the mechanical model and the several sources of error involved in the various measurements.

In addition to the above comparison, which can be performed for any specified case, there are other important indicators which illustrate that the experimental and simulation findings are in agreement. For example, the influence of the current magnitude on the G/S displacement was found to play a primary role during the experimental program: this finding was confirmed by the numerical results. To illustrate this agreement refer to Figures 3.2 and 5.15. Figure 3.2 shows that the G/S displacement increases very rapidly as the current magnitude increases, while Figure 5.15 shows that the axial force density also increases very rapidly as the current magnitude (in the first quarter of a cycle) increases. Clearly, if the first current peak is increased, the impulse energy as defined above will increase and yield higher G/S displacement.

The other two major parameters of interest with respect to the current impulse were the current reversal and the frequency. Several computer runs were executed for various current reversal (maintaining the first peak at 140 kA and the frequency at 1000 Hz) and for various frequencies (maintaining the first peak at 140 kA with a reversal of 50%). In the case of varying the current reversal, the area under the curve (Figure 5.15) in the second, third and fourth halves of the current pulse increased when the current reversal was increased. According to the mechanical model presented above, the G/S displacement clearly increases as the impulse energy transferred to it is increased. A quantitative comparison between the experimental and numerical G/S displacements for the various computed cases was not attempted for two main reasons:

1. For very high current reversal, the impulse energy transferred to the G/S during the first cycle is sufficient to move it more than 2.0 cm. Thus, it is uncertain how much energy is transferred to the G/S during the remaining portion of the current impulse, since it would be more remote from the electromagnetic coil. In other words the simplified model would fail to produce accurate results if the time t_1 is not selected accurately.

2. At lower current reversals, the amount of G/S displacement is very small and there are not sufficient experimental measurements to make additional useful comparisons.

In the case of varying the frequency, the width or duration of each cycle in the current pulse is varied. Clearly, with lower frequencies the duration of the cycles is increased, yielding larger impulse energy and consequently larger G/S displacement. Also, at lower frequencies the shielding effects of the P/T are reduced and a larger fraction of the magnetic field interacts with the G/S exerting a higher force on it. The influence of the frequency on the axial force and consequently on the displacement of the G/S, is illustrated in Table 5.2 below. In this table the maximum instantaneous axial force density reached in the first half cycle of the corresponding current pulse, as well as, the instant of time at which this maximum is reached for various practical frequencies are summarized. The time at which F_{zmax} is reached corresponds to about one quarter of the period of the instantaneous axial force density. The difference between this time and one quarter of the period for the current impulse represents the time delay or phase shift of the axial force on the G/S with respect to the current impulse. This time delay is also summarized in Table 5.2.

TABLE 5.2

Maximum Instantaneous Axial Force Density Exterted on the G/S as a Function of Frequency of the Current Impulse

Frequency (Hz)	Maximum F_z on G/S (N/m^3)	Time at which F_{zmax} is reached (μs)	Time delay with Respect to Current Impulse (μs)
100	0.5881×10^7	3125.0	625
500	0.1737×10^7	712.5	212.5
1000	0.8986×10^6	387.5	137.5
1667	0.5106×10^6	247.5	97.5

The information presented in Table 5.2 indicates that in this frequency range. The impulse energy transferred to the G/S to move it in the axial direction would increase significantly as the frequency of the current impulse decreases. This is in full agreement with the experimental results summarized in Figure 3.4. Close examination of the impulse energy exerted on the G/S during one cycle, for any particular frequency, helps to determine an optimum duration of the current input which maximizes the G/S displacement and minimizes the heating of the coil.

The influence of the presence of the P/T on G/S displacement has also been investigated. One computer run was executed with the P/T and C/T omitted from the finite

element mesh. This was easily achieved by setting the conductivity of these two regions as zero. For the test current impulse shown in Figure 5.11, the maximum instantaneous axial force density on the G/S was found to be 0.2712×10^9 N/m^3. This is higher than the same force density when the P/T and C/T are present (F_z = 0.8986×10^6 N/m^3) by a factor of 302. This clearly confirms the screening effect and the experimental findings that the G/S moved much further when the P/T was replaced by a non-conductive tube. The case where the P/T was present but the C/T was omitted yielded a maximum instantaneous axial force density on the G/S equal to 0.9364×10^6 N/m^3. This is only 4% higher than the case with the C/T present. The experimental results indicated that the G/S movement is reduced by about 20% when the C/T was introduced. This was attributed to the additional friction encountered by the G/S. The numerical results provided specific insight to the electromagnetic contribution in reducing the G/S displacement due to the presence of the C/T.

5.6. Assessment of the Numerical Technique

The numerical solution technique presented in Chapters 4 and 5 to analyze the electromagnetic field

problem associated with the method for repositioning the G/S has been successfully developed and used to achieve the objectives of the theoretical study undertaken in this project. The validity of this technique and the accuracy of the numerical results have been demonstrated by investigating several theoretical and experimental cases. Computational experience with the computerized solution has indicated that the technique is highly flexible. The performance of the technique in addressing axisymmetric field problems* under transient and steady state conditions has been highly satisfactory.

The development of this technique and the necessary computer program to implement it has provided a unique tool that can be used to optimize aspects of the G/S repositioning process. The availability of such a simulation mechanism at the beginning of this project would have saved an enormous amount of effort involved in experimental assessment of the influence of various design and control parameters. The numerical model will be useful for future investigations. The number of alternative variations that can be used to move the G/S electromagnetically is only limited by the imagination of the designer. The developed numerical solution can be used to asses and optimize a wide variety of electromagnetic approaches.

* Due to axisymmetric nature of the problem the leads of the coils were not considered in the numerical analysis of the problem.

The usefulness of the technique presented is not limited to applications involving electromagnetic forces and stresses: other induction heating or direct impulse heating applications can benefit substantially from this development. Also, since the axisymmetric vector field problem has been correlated to the two-dimensional vector or scalar field problem, any problem falling in any of these categories can be analysed using this technique. The only necessary change in the computer program is to modify the common multiplier of the stiffness and capacitance matrices (exclusion of the parameter r_c) to suit the application considered.

The modular construction of the computer program has proven to be an advantageous feature during the development of the program. It also provided the required flexibility to expand this program and generalize it to handle other two-dimensional vector and scalar field problems. The organization of the two main data files that define the geometry of the finite element mesh and characteristic of current input made the investigation of various cases quite straightforward. The mode of storing the stiffness and capacitance matrix as well as the algorithm used to repeatedly solve the set of linear algebraic equations made the solution of transient cases very economical.

To further improve the numerical technique, with respect to the G/S repositioning application, a better mechanical model to determine the displacement of the G/S should be developed. The most accurate approach to achieve this objective would be to solve the coupled transient electromagnetic and mechanical problem. The movement of the G/S can be represented by a partial differential equation that can be solved at various instants in time. The finite element mesh should then be modified to update and specify the new position of the G/S, so that the exact amount of impulse energy transferred to it can be specified as new input for the mechanical equation. Similarly, the coupled thermal and electromagnetic field problem should be analysed if the technique is to be used for induction and direct heating applications.

By solving in three dimensions the number of applications for the technique could be expanded significantly. This would enable the analysis of applications where axial or other symmetries do not exist. However, such an undertaking for transient source vectors requires a major effort and unless the application and end results warrant such an effort alternative options should be considered. The rapid advances in three-dimensional modelling, computer technology and numerical methods will make this task easier in the future.

From a programming point of view, a fully automatic mesh generator could be employed to minimize the amount of effort required for the preparation of input data related to the geometry of the finite element mesh. Also, plotting packages should be incorporated to facilitate the presentation and interpretation of the final results.

CHAPTER 6

CONCLUSIONS

5.1 Introduction

The novel electromagnetic technique for G/S repositioning in the fuel channels of CANDU nuclear reactors has been successfully developed and implemented in five new reactors in Ontario. Theoretical modelling of the electromagnetic field problem has also been developed to provide a basis to further optimize the G/S repositioning process. The conception of the technique, its experimental and theoretical development, its implementation and most significant implications have been presented in this thesis.

In addition to the G/S repositioning application, the numerical technique can be directly applied to analyse the electromagnetic field problem involved in various electromagnetic metal forming applications. A particularly interesting application is the assembly of the P/T into the end fitting and the C/T into the tube sheet via electromagnetic forming of these tubes instead of mechanical rolling. Electromagnetic metal forming applications in flat

geometries can also be handled by this technique, provided that some minor changes are introduced in the computer program. Another interesting application that can be analysed by this technique is the compaction of metallic powder.

The most important conclusions that can be drawn from the extensive amount of information established throughout this project can be summarized as follows:

1. The concept of the electromagnetic technique to reposition remotely a thin non-magnetic spacer located outside a thick metallic tube, made of the same material as the spacer, from within the tube has been demonstrated theoretically and experimentally. Several difficulties related to the shielding effect of the tube, poor electrical properties of the spacers, direction of the required spacer displacement and dimensional restrictions were overcome in a relatively short period of time to provide a timely solution to a significant engineering problem.

2. The urgency for a solution to the G/S repositioning problem precluded the performance of any rigorous theoretical analysis before the implementation of the

technique. Parameters of the necessary time-varying currents, electromagnetic coils and equipment were established experimentally. The influence of numerous important parameters related to the system design and repositioning process has been established in terms of G/S displacements. Several practical problems related to efficient implementation of the technique, preservation of the fuel channel integrity and development of necessary system components have been resolved. Compact pulse power coils, capable of withstanding over 5000 high-current pulses, and special pulse power cables have been successfully developed and utilized during the G/S repositioning program.

3. A rigorous and accurate theoretical model, based on finite elements, has been developed to analyze the electromagnetic field problem involved in the G/S repositioning process. The validity of the developed numerical solution and associated computer program has been verified by investigating several cases for which analytical solutions exist, and by comparing some of the numerical and experimental results. The accuracy of the numerical results, for the cases of infinitely long current sheets, was found to be within 1% of the analytical results in the region of interest (ie, near

the G/S, away from the axis of the coil). In the case of a short solenoid, some inaccuracy in the magnetic field distribution inside the coil and around the coil leads and reinforcing metallic bolts is introduced because the coil leads and bolts are neglected in this model. However, the calculated axial force on the G/S is not affected by the presence of the leads or the bolts because of their position with respect to the G/S.

4. The simulation technique developed has been used extensively to assess the influence of some of the most important parameters on the G/S displacement. Consistently, the numerical results were in general agreement with the experimental results. The numerical solution provided accurate assessment of the role of each parameter separately: an objective that was not experimentally possible since variation of one parameter in most cases was accompanied by variation of one or more other parameters in the system. Information related to the presence of the C/T and P/T was readily obtainable from the numerical solution.

5. The numerical results have confirmed that the axial impulse force exerted on the G/S is sufficient to cause it to move. The profiles of the radial and axial force

densities in the coil have been substantiated by the observed coil deformations, prior to the development of the final "field" coils. The capability of the developed model to provide the force profiles, exerted on the coil, P/T, C/T and G/S, in the space and time domains is of paramount importance.

6. The method used to correlate the finite element solution of axisymmetric vector field problems to two-dimensional field problems in cartesian coordinates eliminated the need for a lengthy derivation of the finite element equations pertinent to axisymmetric vector fields. This method negated the presence of a singular term in the respective energy functional and made use of the well developed finite element matrices for the planar case, with some minor modifications. This has enlarged the scope of the numerical solution and the developed computer program to cover problems in both the axisymmetric and planar cases.

7. The theoretical simulation method developed to analyze the electromagnetic field problem can be used to investigate and optimize a wide range of coil designs and electric current input waveforms. The computer program developed to implement the numerical solution

has the capability to address various transient and steady state cases without any modification in the program itself.

8. The theoretical and experimental findings established during the development and implementation of this technique laid the foundation for further optimization of the technique and its application under different reactor conditions.

9. The development of this technique along with the various additional developments, such as the theoretical model, strong compact coils and low resistance pulse power cable, have significant implications and advantages in various other applications related to the pulse power industry in general and specifically to the electromagnetic metal forming, compaction of metal powders and fusion technologies.

10. Development of this technique alleviated the need to perform large scale fuel channel retubing operations in five non-commissioned CANDU reactors at Ontario Hydro. The saving in reactor repair cost, interest charges and energy replacement cost was very great.

BIBLIOGRAPHY

1. D. Mosey, "Tube Failure at Pickering Nuclear Generating Station", Energy Newsletter, Vol. 5, No. 2 - June 1984, ISSN 0711-3366, pp. 56-65, published by The McMaster Institute for Energy Studies.

2. W.A. Wolfe And Liberty Pease, "Concentric Tube Structure", United State Patent No 3,106,520, October 8, 1963.

3. Joseph H. Dableh, "Method of Repositioning Annular Spacers in Calandria Structures and Apparatus Therefor", Canadian Patent Application No. 443,095, Filed December 12, 1983. This patent was allowed in February 1986.

   United States Patent Application No. 591,907, Filed March 22, 1984. This patent has been in position for allowance since December 31, 1985.

   European Patent Application No. 8480318.0, Filed June 27, 1984.

   Korean Patent Application No. 84-4124, Filed July 13, 1984.

   Argentina Patent Application No. 297,338, Filed July 25, 1984.

   India Patent Application No. 750/MAS/84, Filed October 1, 1984.

   Romania Patent Application No. 116624, Filed December 11, 1984.

4. Joseph H. Dableh, "Novel Electromagnetic Technique for Repositioning of Coolant Tube Spacers in CANDU Nuclear Reactors", paper submitted to the Review of Scientific Instruments, a publication of the American Institute of Physics, October 1985.

5. H. Hayt, Jr., "Engineering Electromagnetics", Third Edition, McGraw-Hill Book Company, New York, 1974.

6. J.A. Stratton, "Electromagnetic Theory", McGraw-Hill Book Company, New York, 1941.

7. J.H. Ham and G.R. Slemon, "Scientific Basis of Electrical Engineering", John Wiley and Sons, 1961.

8. D.B. Montgomery and R.J. Weggel, "Solenoid Magnet Design, The Magnetic and Mechanical Aspects of Resistive and Superconducting Systems", Robert E. Krieger Publishing Company, Huntington, New York, 1980.

9. W.H. Gray and J.K. Ballou, "Electromechanical Stress Analysis of Transversely Isotropic Solenoids", Journal of Applied Physics, Vol. 48, No. 7, July 1977.

10. K. Baines, J.L. Duncan and W. Johnson, "Electromagnetic Metal Forming", Proc. Instn. Mech. Engrs 1965-66, Vol 180, pt 1, No 4.

11. R.E. Reinovsky, D.L. Smith, W.L. Baker, J.H. Degnan, R.P. Henderson, R.J. Kohn, D.A. Kloc and N.F. Roderick, "Inductive Store Pulse Compression for Driving High Speed Plasma Implosions", IEEE Trans. on Plasma Science, Vol PS-10, No. 2, June 1982.

12. M.H.S. El-Markabi and E.M. Freeman, "Electromagnetic Shielding Effect of a Set of Concentric Spheres in An Alternating Magnetic Field", Proc. IEE, Vol. 126, No. 12, December 1979.

13. P. Krason and W. Lipinski, "Analysis of Electromagnetic Screen By Using Integral Equation Method", IEEE Trans. on Magnetics, Vol. MAG-17, No. 6, November 1981.

14. E. Thornton, "Electrical Interference in Pulsed Power Technology", Proc. IEE, Vol. 126, No. 5, May 1979.

15. V.O. KelHA, J.M. Pukki, R.S. Peltonen, A.J. Penttinen, R.J. Ilmonieni, and J.J. Heino, "Design, Construction, and Performance of a Large-Volume Magnetic Shield", IEEE Trans. on Magnetic, Vol. MAG-18, No. 1, January 1982.

16. E.E. Kriezis and C.S. Antonopoulos, "Low-Frequency Electromagnetic Shielding in a System of Two Coaxial Cylindrical Shells", IEEE Trans. on Electromagnetic Compatibility, Vol. EMC-26, No. 4, November 1984.

17. S.M. Harvey, "Transient EMI Succeptibility of the OH180 Programmable Controller Production Prototype", Ontario Hydro Research Division Report to F.J. Kee, Report No. 81-374-K, File 817.22, November 24, 1981.

18. T.J. Burgess, E.C. Cnare, W.L. OberKampf, S.G. Beard and M. Cowan, "The Electromagnetic Gun And Tubular Projectiles", IEEE Trans. on Magnetics, Vol. MAG-18, No. 1, January 1982.

19. Fritz Herlach, "Explosive-Driven Energy Generators With Transformer Coupling", J. Phys. E: Sci. Instrum., Vol. 12, 1979, Printed in Great Britain.

20. P.N. Murgatroyd, W. Farrer, R.P.D. Hodgkinson And P.D. Mcloughlin, "The Toroidal Cage Coil", IEEE Proc., Vol 127, Pt. B, No. 4, July 1980.

21. E.C. Cnare, "Magnetic Flux Compression by Magnetically Imploded Metallic Foils", Journal of Applied Physics, Vol. 37, No. 10, September 1966.

22. Kenzo Miya, J. Ed Akin and Satoshi Hanai, "Finite Element Analysis of An Eddy Current Induced In Thin Structures of A Magnetic Fusion Reactor", International Journal For Numerical Methods in Engineering, Vol. 17, 1613-1629 (1981).

23. S.C. Tandon and M.V.K. Chari, "Transient Solution of the Diffusion Equation by the Finite Element Method", J. Appl. Phys. Vol. 52, No. 3, March 1981.

24. S. Williamson and J.W. Ralph, "Finite-Element Analysis for Nonlinear Magnetic Field Problems With Complex Current Sources", IEEE Proc., Vol 129, Pt. A, No. 6, August 1982.

25. E.F. Fuchs and G.A. McNaughton, "Comparison of First-Order Finite Difference And Finite Element Algorithms For the Analysis of Magnetic Fields. PART I: Theoretical Analysis, IEEE Trans. On Power Apparatus and Systems, Vol. PAS-101, No. 5, May 1982.

26. M.L. Hodgdon and J.R. Freeman, "Transient Magnetic Field Calculations With TRIDIF", IEEE Trans. on Magnatics, Vol. MAG-18, No. 2, March 1982.

27. Robert D. Pillsbury, Jr., "NMLMAP - A Two Dimensional Finite Element Program For Transient Or Static Linear or Nonlinear Magnetic Field Problems", IEEE Trans. on Magnetics, Vol. MAG-18, No. 2, March 1982.

28. W.F. Mullin, "ABC's of Capacitors" 3rd Edition Indianapolis: Sams, 1980.

29. M. Cenanovic, "Magnetic Metal Forming By Reversed Electromagnetic Forces", Proc. 3rd IEEE International Pulsed Power Conference, Albuquerque, New Mexico, paper 6.4, June 1981.

30. J.D. Kraus, and K.R. Carver, "Electromagnetics" McGraw Hill book company, New York, 1973.

31. Maxwell Laboratories Inc., "Applications for Magneform", Manufacturer's Bulletin, No. 1202, Product Bulletins MLB-2044A and MLB-2012A.

32. K. Jakubiuk, "Analysis of Electromagnetic and Thermal Fields in Exploding Wires" IEEE Trans. on Magnetics, Vol. MAG-19, No. 6, November 1983.

33. P.P. Bennett, "Current Diffusion In Cylindrical Exploding Wires and Fuses During Microsecond Electric Pulses", J. Appl. Phys., Vol. 3, No. 7, 1972.

34. P.V. Phung and D.O. Miles, "Skin Effect in Exploding-wire Physics", J. Appl. Phys., Vol. 46, No. 10, 1975.

35. M. Cenanovic, "High Rate of Energy Release Technique For Nuclear Reactor Repair", Proc. 4th IEEE International Pulsed Power Conference, Albuquerque, New Mexico, Paper 3.3, June 1983.

36. J.H. Dableh, R.D. Findlay, N.T. Nicholson, N.T. Olson, "Experience with High Pulse Power Systems For Remote Repositioning of Concentric Coolant tube Spacers", Jordan International Electrical and Electronic Conference, April 28-May 1, 1985, Aman-Jordan.

37. J.H. Dableh, R.D. Findlay, I.L. Colquhoun, and M.E. Truemner, "Cable for High Pulse Power Applications", IEEE Trans. on Power Apparatus and Systems, Vol. PAS-104, No. 8, August 19, 1985.

38. J.H. Dableh, R.D. Findlay and G.S. Klempner, "Design and Development of Compact, Durable Electromagnetic pulse power coils for Repositioning of Coolant Tube spacers in CANDU Nuclear Reactors", Paper accepted For Presentation at the 1986 IEEE Winter Power Meeting and For Publication in the IEEE Trans. on Power Apparatus and Systems.

39. A.H. Morton, "Advanced Electrical Engineering", published by Sir Isaac Pitman and Sons Ltd., 1966.

40. J.P. Zbasnik, D.N. Cornish, R.M. Scanlan, R.L. Leber, M.R. Chaplin, A.R. Rosdahl and J.E. Johnson, "Operation of the 8-T, 1-m-Diameter Test Facility at Lawrence Livermore National Laboratory", IEEE Trans. on Magnetics, Vol. MAG-17, No. 5, September 1981.

41. E. Hoffman, J. Alcorn, W. Chen, Y.H. Hsu, J. Purcell on R. Schermer, "Design of the BPA Superconducting 30 MJ Energy Storage Coil", IEEE Trans. on Magnetics Vol. MAG-17, No. 1, January 1981.

42. W.M.P. Franken, M.W. Brieko, A.E. Gijze, J.A. Heil, J.A. Roeterdink and H.M. Van Rij, "Design and Construction of An Eight Tesla Insert Coil", IEEE Trans. on Magnetics, Vol. MAG-17, No. 5, September 1981.

43. N. Miki, T. Hamajima, Y. Tonaba, S. Mine, M. Yamaguchi and Y. Sawada, "Structure Analysis of Superconducting toroidal Field Coils for a Tokomak Fusion Experimental Reactor", IEEE Trans. on Magnetics, Vol. MAG-17, No. 5, September 1981.

44. H.F. Vogel and H. Preis, "Study on Diffusion of The Vertical Magnetic Field In The Toroidal Stabilizing Shell And Plasma of The ZT-40M Reversed Field Pinch Device", Compumag - Genoa, May 30 - June 2, 1983, Italy.

45. C.M. Fowler, R.S. Caird, D.J. Erickson and B.L. Freeman, "Pulse Power Applications of Flux Compression Generators", 3rd IEEE International Pulsed Power Conference, Albuquerque, New Mexico, June 1-3, 1981, Paper No. 175.

46. T.N. Olson, J. Bandas and A.C. Kolb, "Design, Performance and Use of a Near Megagauss Pulsed Machine", Megagauss Physics and Technology, Plenum, New York, 1980.

47. W.F. Brown, J. Bandas and T.N. Olson, "Pulsed Magnetic Welding of Breeder Reactor Fuel Pin End Closures", Welding Journal, Vol. 57, No. 5, June 1978.

48. V.M. Mikhailov, V.A. Mironov and V.D. Zemchenkow, "Stripping of Shells From Compacts By Pulse Magnetic Field Forces", 1984 Plenum Publishing Corporation, Translated from Poroshkovaya Metallurgy, No. 10 (250), published in Soviet Powder Metallurgy And Metal Ceramics, Vol. 22, No. 10 (250), October 1983.

49. Hans jörg Jansen, "Some Measurements of the Expansion of a Metallic cylinder with Electromagnetic Pulses", IEEE Trans. On Industry And General Applications, Vol. 1, No. 4, July/August 1968.

50. R.A. Marshall, "Railgun Energy Stores and Systems", 3rd IEEE International Pulsed Power Conference, Albuquerque, New Mexico, June 103, 1981, Paper No. 2.1.

51. R.A. Marshall and W.F. Weldon, "Analysis of Performance of Rail Gun Accelerators Powered by Distributed Energy Stores", 14th Pulse Power Modulator Symposium, Orlando, Florida, June 3-5, 1980.

52. J.H. Dableh and R.D. Findlay, "An Annotated Summary of Analysis and Design Techniques For Pipe-Type Cable Systems", IEEE Trans. On Power Apparatus And Systems, PAS Vol. 103, No. 10, October 1984.

53. N. Flatabo, "Transient Heat Conduction Problems in Power Cables Solved by the Finite Element Method", IEEE Trans. on Power Apparatus and Systems, Vol. PAS 92, No. 1, 1973.

54. A.F. Armor, "Transient, Three Dimensional Finite element Analysis of Heat Flow in Turbine Generator Rotors", IEEE Trans on Power Apparatus and Systems, Vol. PAS-99. No. 3, May - June 1980.

55. O.C. Zienkiewiez & C.J. Parekh, "Transient Field Problems: Two Dimensional and Three Dimensional Analysis by Isoparametric Finite Elements", International Journal for Numerical Methods In Engineering, Vol. 2, 1970.

56. S.C. Tandon, A.F. Armor, M.V.K. Chari, "Nonlinear Transient Finite Element Field computation for Electrical Machines and Devices", IEEE Trans. on Power Apparatus and Systems, Vol. PAS - 102, No. 5, May 1983.

57. E.B. Becker, M.O. Origa, R.D. Pillsbury, H.G. Rylander, W.F. Weldon and H.H. Woodson, "Magnetic Field Calculations for High-Energy pulsed Power Supplies", 1st IEEE International Pulsed Power Conference, Lubbock, Tex., U.S.A., 1976.

58. T. Nakata and Y. Kawase, "Numerical Analysis of Nonlinear Transient Magnetic Field Using the Finite Element Method", Electrical Engineering in Japan, Vol. 104, No. 4, 1984.

59. J. Avila-Rosales and A. Semlyen, "Iron Core Modeling For Electrical Transients", IEEE PES Winter Meetings, New York, N.Y., Feb 3-8, 1985, Paper No. 85 WM 218-3.

60. V.M. Mikhailov, "The Two-Dimensional pulsed Electromagnetic Field of Massive Conductors", Power Eng. (Acad. SCI. USSR) (USA), Vol. 15, No. 3, 1977.

61. O.C. Zienkiewicz, W.L. Wood and N.W. Hine, "A Unified Set of Single Step Algorithms PART 1: General Formulation and Applications", International Journal for Numerical Methods in Engineering, Vol. 20, 1984.

62. A.Y. Hannalla & D.C. MacDonald, "A Nodal Method for the Numerical Solution of Transient Field Problems in Electrical Machines", IEEE Trans. on Magnetics, Vol. MAG-11, pp 1544-1546, Sept. 1975.

63. A.Y. Hannalla & D.C. MacDonald, "Numerical Analysis of Transient Field Problems in Electrical Machines", Proc. IEE, Vol. 123, No. 9, pp. 893-898, Sept. 1976.

64. C.V. Dodd and W.E. Deeds, "Electromagnetic Forces In Conductors", Journal of Applied Physics, Vol. 38, No. 13, December 1967.

65. B. Aldefeld, "Electromagnetic Field Diffusion in Ferromagnetic Materials", Proc. IEE, Vol. 125, No. 4, April 1978.

66. S.P. Verma and S.E. Abo-Shady, "Method of Calculation of Transient Skin-Effect In Conductors Embedded in Slots For Cage Windings", IEEE Trans. on Power Apparatus and Systems, Vol. PAS-99, No. 6, Nov/Dec. 1980.

67. E.F. Fuchs and K. Senske, "Comparison of Iterative Solution of the Finite Difference Method with Measurements as Applied to Poisson's And The Diffusion Equations", IEEE Trans. on Power Apparatus and Systems, Vol. PAS-100, No. 8, August 1981.

68. J.N. Reddy and M.L. Rasmussen, "Advanced Engineering Analysis", John Wiley And Sons, 1982.

69. G.D. Smith, "Numerical Solution of Partial Differential equations", Oxford University Press, 1965.

70. R.D. Findlay and R. Murray, "Application of the Hybrid Finite Elements, Finite Difference Technique to the Solution of Multistrand Conductor Problems, "IEEE Trans. On Magnetics, Vol. MAG-19, No. 6, Nov. 1983.

71. K.R. Davey and W.J. Barnes, "Three-Dimensional Eddy current problems using the T-Ω Method and Fredholm Integral Equations", Trans. on Magnetics, Vol. MAG-19, No. 2, March 1983.

72. J. Simkin, "Comparison of Integral and Differential Equation Solutions of Field Problems, "IEEE Trans. On Magnetics, Vol. MAG-18, No. 2, MAR 1982.

73. S.J. Salon and J.M. Schneider, "A Comparison of Boundary Integral And Finite Element Formulations of the Eddy Current Problem", IEEE PES Summer Meeting, Minneapolis, Minnesota, July 13-18, 1980, Paper No. 80 SM526-4.

74. V.T. Chemeris and A.D. Podol Tsev, "A study of The Magnetic-pulse Interaction of Moving Conductive Bodies in the Presence of A Ferromagnetic Medium (MU=CONST)", TEKH Elektrodin. (USSR) No. 1, Jan-Feb 1980.

75. O.C. Zienkiewicz, D.W. Kelly and P. Bettess, "The Coupling of the Finite Element Method And Boundary Solution Procedures", International Journal For Numerical Methods In Engineering, Vol. 11, 1977.

76. S. Salon and J. Schneider, "A Hybrid Finite Element Boundary Integral Formulation of The Eddy Current Problem", IEEE Trans. on Magnetics, Vol. MAG-18, No. 2, March 1982.

77. S. Cristina and A. DiNapoli, "Combination of Finite and Boundary Elements for Magnetic Field Analysis", IEEE Trans. on Magnetics, Vol. MAG-19, No. 6, Nov. 1983.

78. P. Silvester and M.S. Hsieh, "Finite-Element Solution of 2-Dimensional Exterior Field Problems", Proc. IEE, Vol. 118, No. 12, December 1971.

79. B.H. McDonald and A. Wexler, "Finite-Element Solution of Unbounded Field Problems", IEEE Trans. on Microwave Theory and Techniques, Vol. MTT-20, No. 12, December 1972.

80. S.J. Salon, "Application of Boundary Integral Equation Methods to Electromagnetics", IEEE Trans. on Magnetics, Vol. MAG.21, No. 5, Sept. 1985.

81. R.J. Murray, "FEM Solution of Linear Conductor Problems", M.Sc.E. Thesis, University of New Brunswick, March 1981.

82. M.H.S. El-Markabi and E.M. Freeman, "Analysis of Low-Frequency Circular Cylindrical Induction Devices Having Helical Windings", IEE Proc., Vol. 128, Pt. A, No. 8, November 1981.

83. S.B. Afshartous, P. Graneau, "Current Distribution in the LN_2 Cryocable", Cryogenics, Vol. 10, pp 402-405, 1970.

84. J.A. MacBain, "Solenoid Simulation With Mechanical Motion", International Journal For Numerical Methods, in Engineering, Vol. 21, 13-18 (1985).

85. C. Papageorgiou and E.M. Freeman, "Electromagnetic Field Solution For A Coil of Arbitrary shape Moving Relative to a Set of Ferromagnetic Layers", IEEE Trans. on Magnetics, Vol. MAG-17, No. 6, November 1981.

86. D.E. Merewether, "Transient Currents Induced On a Metallic Body of Revolution By an Electromagnetic Pulse", IEEE Trans. Electromagn. Compat. (USA), Vol. EMC-13, No. 2, May 1971.

87. E.M. Freeman, and M.H.S.EL-Markabi, "2-Dimensional Field Analysis and Input Impedance of A Finite-length Solenoid Coil", Proc. IEEE, Vol. 126, No. 1, Jan. 1979.

88. R. Sikora, P. Krason and M. Gramz, "Synthesis of the Magnetic Field Due To a Thin-Walled Solenoid", IEEE Trans. on Magnetics, Vol. MAG-17, No. 3, 1981.

89. V.M. Mikhailov, "The Surface Effect In a Massive Solenoid When A Powerful Pulsed Magnetic Field is Obtained", Power Eng. (ALAD. SCI. USSR) (USA), Vol. 13, No. 3, 1975.

90. O.C. Zienkiewicz, "The Finite Element Method", McGraw-Hill Book Company, 1977.

91. L.J. Segerlind, "Applied Finite Element Analysis", John Wiley & Sons, 1976.

92. E.M. Freeman and C. Papageorgiou, "The Use of Spatial Fourier Transforms and Parseval's Identity in The Calculation of Magnetic Forces in Linear Induction Devices", Compumag, Genoble, 1978.

93. P.G. Richardson, "Developments and Experience in the Fourier Element Method", IEEE Trans. on Magnetics, Vol. MAG-19, No. 6, Nov. 1983.

94. O.W. Andersen, "Finite Element Solution of Skin Effect and Eddy Current Problems", IEEE PES Summer Meeting, Mexico City, Mex., July 17-22, 1977. Paper No. A77616-6.

95. M.V.K. Chari and Z.J. Csendes, "Finite Element Analysis of the Skin Effect In Current Carrying Conductors", IEEE Trans. on Magnetics, Vol. MAG-13, No. 5, September 1977.

96. Z.J. Csendes and M.V.K. Chari, "Finite Element Analysis of Eddy Current Effects In Rotating Electric Machines", IEEE PES Summer Meeting, Mexico City, Mex, July 17-22, 1977. Paper No. A77615-8.

97. N.A. Dermerdash, D.A. Mohamed, T.W. Nehl, F.A. Fouad and R.H. Miller, "Solution of Eddy Current Problems Using Three Dimensional Finite Element Complex Magnetic Vector Potential", IEEE Trans. on Power Apparatus and Systems, Vol. PAS-101, No. 11, November 1982.

98. J.R. Brauer, "Saturated Magnetic Energy Functional For Finite Element Analysis of Electric Machines", IEEE PES Winter Meeting, New York, N.Y., January 26-31, 1975, Paper No. C75151-6.

99. P. Silvester, H.S. Cabayan and B.T. Browne, "Efficient Techniques For Finite Element Analysis of Electric Machines", IEEE PES Winter Meetings, New York, N.Y. Jan. 28 - Feb. 2, 1973.

100. P. Silvester and P. Rafinejad, "Curvilinear Finite Elements For Two-Dimentional Saturable Magnetic Fields", IEEE PES Winter Meeting, New York, N.Y., Jan. 27 - Feb 1, 1974, Paper No. T74214-3.

101. H.C. Karmaker and G.H. Ardley, "Application of Integral Equation to the Magnetic Field Analysis of Rotating Electrical Machines", IEEE Trans. on Magnetics, Vol. MAG-18, No. 6, November 1982.

102. M.V.K. Chari, "Finite-Element Solution of the Eddy-Current Problem In Magnetic Structures", IEEE PES Summer Meeting of EHV/UHV Conference, Vancouver, B.C., Canada, July 15-20, 1973, Paper No. T73320-9.

103. J. Weiss and Z.J. Csendes, "A One-step Finite Element Method For Multiconductor Skin Effect Problems", IEEE Trans. on Power Apparatus And Systems, Vol. PAS-101, No. 10, October, 1982.

104. P.P. Silvester and R.L. Ferrari, "Finite Elements for Electrical Engineers", Cambridge University Press, Cambridge, 1983.

105. M.V.K. Chari and P.P. Silvester, "Finite Elements in Electrical and Magnetic Field Problems", John Wiley & Sons, 1980.

106. H.C. Martin and G.F. Carey, "Introduction to Finite Element Analysis, Theory and Application", McGraw-Hill Book Company, 1976.

107. G. Strang and George J. Fix, "An Analysis of The Finite Element Method", Prentice Hall, Inc., 1973.

108. E. Hinton and D.R.J. Owen, "Finite Element Programming", Academic Press Inc (London) Ltd., 1977.

109. M. Hattori and K. Asano, "Finite Element Analysis of Magnetic Field of Cylindrical Solenoid With Open Boundaries", Electrical Engineering in Japan, Vol. 104A, No. 1, 1984.

110. K. Preis, H. Stogner and K.R. Richter, "Calculation of Eddy Current Losses in Air Coils By Finite Element Method", IEEE Trans. on Magnetics, Vol. MAG-18, No. 6, November 1982.

111. R.D. Findlay, "Cross-Field Losses In a Solenoid", A B.A.Sc. Thesis, University of Toronto, November 1962.

112. J. Weiss and Z. Csendes, "Efficient Finite element Solution of The Multipath Eddy Current Problems", IEEE Trans. on Magnetics, Vol. MAG-18, No. 6, November 1982.

113. O.W. Andersen, "Finite Element Solution of Skin Effect And Eddy Current Problems", IEEE PES Summer Meeting, Mexico City, Mex., July 17-22, 1977, Paper No. A77616-6.

114. M.J. Turner, R.W. Clough, H.C. Martin and L.J. Topp, "Stiffness and Deflection Analysis of Complex Structures", Journal Aeronautical Science, Vol. 23, pp. 805-824, 1956.

115. B.A. Szabo and G.C. Lee, "Derivation of Stiffness Matrices for Problems in Plane Elasticity by Galerkin's Method", International Journal of Numerical Methods in Engineering, Vol. 1, pp. 301-310, 1969.

116. O.C. Zienkiewicz, "The Finite Element Method in Engineering Science", McGraw Hill, London, 1971.

117. A. DiNapoli and R. Paggi, "Sizing of Magnetic Shields in Saturated Conditions, For Large Transformers Calculated By Means of The Finite Element Method", IEEE PES Summer Meeting, Mexico City, Mex., July 12-22, 1977. Paper No. A77663-8.

118. J.R. Brauer and A.O. Smith, "Finite Element Analysis of Electromagnetic Induction In Transformers", IEEE PES Winter Meeting, New York, N.Y., Jan. 30 - Feb 4, 1977, Paper No. A77122-5.

119. E. Tarasiewicz, R.D. Findlay and J.H. Dableh, "Finite Element Approach to the Solution of Axisymmetric Vector Field Problems", accepted for presentation at Intermag '86 Conference, Phoenix, AZ, April 14-17, 1986. (Also submitted to IEEE Trans. on Magnetics).

120. E. Tarasiewicz, J.H. Dableh and R.D. Findlay, "Accurate Computation of Axisymmetric Vector Potential Fields with the Finite Element Method", submitted to IEEE PES Summer Meeting, Mexico, July 20-25, 1986.

121. W.T. Thomson, "Theory of Vibrations with Applications" Printice-Hall Inc., Englewood Cliffs., N.J., 1981.

122 M.A. El-Kady, "A Sparsity-Controlled, Block Band Matrix Technique with Applications to Power System Analysis", SIAM Conference on Applied Algebra, Raleigh, U.S., March 1982.

APPENDIX A

EXPERIMENTAL RESULTS

This appendix summarizes typical experimental data, related to G/S displacements, obtained throughout the development and implementation of the electromagnetic technique. Its objective is to supplement the information given in Chapters 2 and 3. The G/S displacements presented below represent the motion of an actual G/S placed around a short section (1 to 2 m) of an actual P/T. Section of the C/T was used in a limited number of experiments to avoid wasting time for setting the G/S in the desired location and to minimize the error in measuring its displacement. C/T was normally used when all the preliminary and intermediate experiments had been performed to assess the influence of various parameters. Also note that the current levels or values used always refer to the first peak in the current inpulse.

The first capacitor bank used in this program was the 60 kJ bank. Using this bank and a hand-wound coil made of a grounding cable and having 5-6 turns with wide spacing between turns (6.3 mm), the following G/S displacements

(Table A.1) were obtained as a function of coil current, for a ringing frequency of 2000 Hz and current reversal of about 85%.

TABLE A.1

G/S displacement as a function of current (using the most "primitive" driving coil)

Charging Voltage	Coil Current (Calculated)	Maximum G/S Displacement
1 kV	10 kA	No motion
2 kV	21 kA	G/S swung but no displacement
3 kV	31 kA	1 mm
4 kV	41 kA	2 mm
6 kV	62 kA	4 mm
7 kV	72 kA	5 mm
8 kV	82 kA	10 mm
10 kV	103 kA	26 mm

The second capacitor bank system used was the 1818 μF bank (91 kJ, when charged to 10 kV); the total inductance in the discharge circuit was approximately 5.5 μH, the ringing frequency was 1600 Hz and the current reversal was maintained at about 85%. Using an eight-turn coil made of rectangular copper strip (6 × 12 mm) and having 4 mm spacings between turns, the G/S displacements shown in Table A.2 were achieved. When the two banks mentioned above were connected together (in parallel) to have a total capacity of 150 kJ (3000 μF), the ringing frequency was

reduced to 1300 Hz for the same load coils (8 turns with 4 mm spacing between turns). The results shown in Table A.3 were obtained using this bank and an eight-turn coil.

TABLE A.2

G/S displacement using the 1818 μF capacitor bank and a good driving coil

Charging Voltage	Coil Current (Calculated)	Maximum G/S Displacement
1 kV	12.7 kA	No motion
2 kV	25.4 kA	1 mm
3 kV	38.1 kA	2 mm
4 kV	50.8 kA	3 mm
5 kV	63.5 kA	11 mm
6 kV	76.2 kA	25 mm
7 kV	88.9 kA	55 mm
8 kV	101.6 kA	91 mm

TABLE A.3

G/S displacement using the 3000 μF capacitor bank and a good driving coil

Charging Voltage	Coil Current (Calculated)	Maximum G/S Displacement
1 kV	17 kA	1 mm
2 kV	34 kA	2 mm
3 kV	51 kA	5 mm
4 kV	68 kA	10 mm
6 kV	85 kA	25 mm
7 kV	102 kA	56 mm
8 kV	119 kA	135 mm

The maximum G/S displacement achieved with the C/T present, using the above system at the current level of

120 kA, was 115 mm. This indicated that the G/S displacement is reduced by about 20% due to the additional friction associated with the presence of the C/T. Larger reductions were observed when the G/S was positioned at an inclined plane with respect to the vertical plane that is normal to the axis of the P/T.

The 200 kJ capacitor bank was used next. This system differed from the previous one in its arrangement and connection. The bank was subdivided into 6 modules each having four capacitors and an ignitron rated for 100 kA. Six coaxial cables were used to connect the bank to the coil via an interface block. This arrangement reduced the inductance of the capacitor bank and coaxial cables to about 0.1 μH. Typical results obtained using this bank at various frequencies and with two different coils are presented in Figure 3.3 (Chapter 3).

The current waveform delivered by the "field" capacitor bank systems with the original TL (21.3 long) and a typical field coil prototype is shown in Figure A.1. The current reversal was increased by eliminating one section of the TL and using only the section that had to be inserted into the fuel channels. Figure A.2 shows a typical current waveform that was achieved in this arrangement.

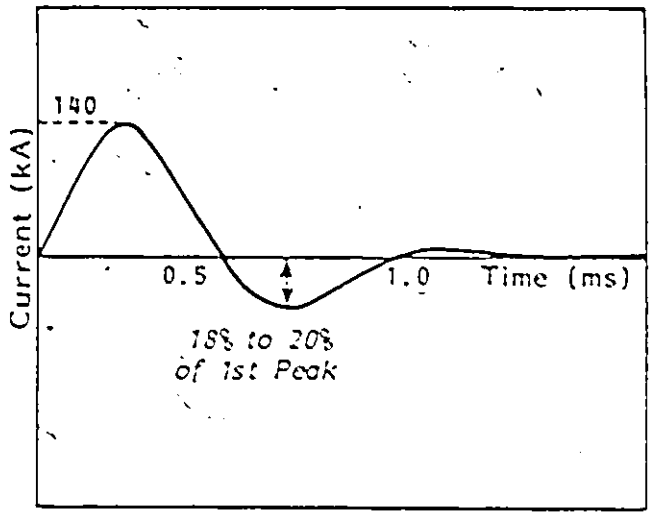

Figure A.1

Typical current waveform delivered by the "field" capacitor bank system with the original transmission line (21.3 m long).

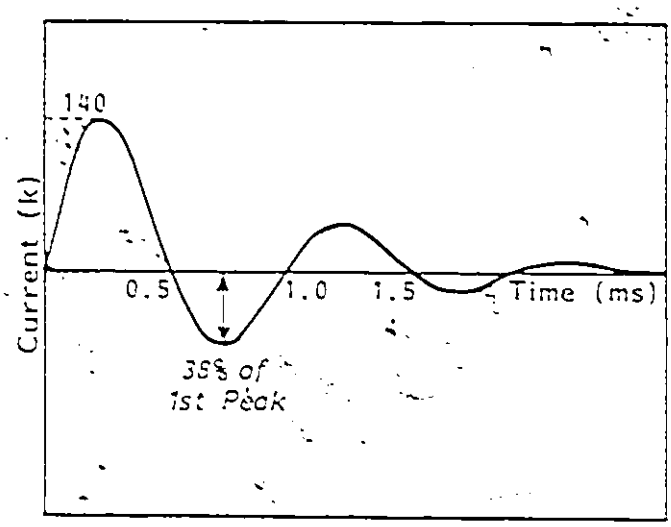

Figure A2

Typical current waveform delivered by the "field" capacitor bank system with 10.7 m long transmission line (made of high-resistance coaxial cables).

Several experiments were carried out to establish acceptable design parameters for a new flexible coaxial cable to build a TL with low resistance. Tables A.4 to A.7 show typical results at various frequencies, current reversals and for various current magnitudes.

Subsequent to the introduction of the new TL and other corrective measures to the capacitor bank systems, the current reversal was brought to the 72% level. Figure A.3 shows a typical current waveform of the achieved pulses.

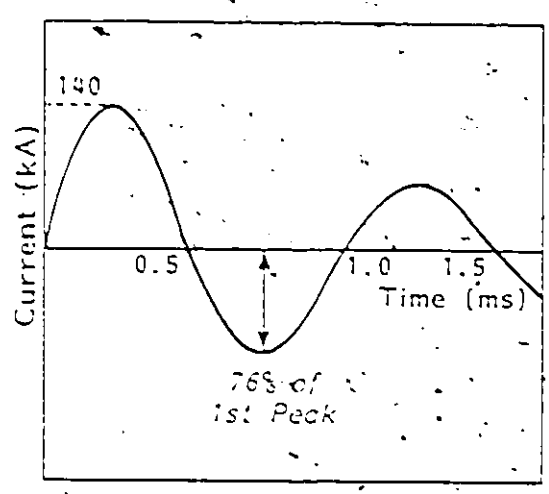

Figure A.3

Typical current waveform achieved with the modified "field" capacitor bank systems and new TL (10.7 m long)

TABLE A.4

Results of tests performed using a 10.7 m TL, 4 coaxial cables in parallel (tuning inductor included)

Shot No	% Energy	1st Current Peak in kA	2nd Current Peak in kA	% Reversal	Frequency	Garter Spring Displacement	
						Front Of The Coil (mm)	Back Of The Coil (mm)
1	40	122.5	48.5	39.6	1064	12	12
2	50	136.5	50.6	37.1	1075	20	19
3	60	150.0	56.7	37.8	1053	28	29
4	70	162.0	64.0	39.5	1042	40	40
5	75	168.0	69.5	41.3	1064	46	45

TABLE A.5

Results of tests performed using 10.7 m TL, 4 coaxial cable in parallel (tuning inductor bypassed)

Shot No	% Energy	1st Current Peak in kA	2nd Current Peak in kA	% Reversal	Frequency	Garter Spring Displacement	
						Front Of The Coil (mm)	Back Of The Coil (mm)
1	20	-	-	-	-	3	3
2	30	144.7	35.3	24.4	1563	8	10
3	40	163.6	36.2	22.0	1492	25	23
4	45	175.0	40.7	23.3	1515	31	25

TABLE A.6

Results of tests performed using A 6.1 m rigid TL with 1.83 m flexible link (tuning inductor included)

Shot No	% Energy	1st Current Peak in kA	2nd Current Peak in kA	% Reversal	Frequency	Garter Spring Displacement	
						Front of the Coil (mm)	Back of the Coil (mm)
1	20	–	–	–	–	1	3
2	25	–	–	–	–	4	7
3	30	111.5	60.0	53.8	1016	11	8
4	35	118.6	65.1	54.8	1000	12	15
5	45	134.4	78.3	58.3	984	19	23
6	55	145.9	85.2	58.3	962	35	42
7	60	154.2	94.0	61.0	980	40	59
8	65	163.6	96.6	59.0	990	66	62
9	70	169.0	105.0	62.1	970	80	83
10	75	174.1	106.4	61.1	970	100	97
11	80	181.3	115.1	63.5	943	110	116

TABLE A.7

Results of tests performed using A 7.6 m TL, 4 coaxial cable in parallel (tuning inductor included)

Shot No	% Energy	1st Current Peak in kA	2nd Current Peak in kA	% Reversal	Frequency	Garter Spring Displacement	
						Front of the Coil (mm)	Back of the Coil (mm)
1	45	136.0	58.3	42.9	1064	18	16
2	55	149.0	62.6	42.0	1068	23	27
3	60	155.0	66.2	42.7	1082	36	32
4	65	162.0	68.5	42.3	1059	40	49
5	70	168.0	73.2	43.6	1059	51	61
6	75	174.0	79.7	45.8	1050	62	64
7	80	180.0	77.9	42.3	1061	75	84
8	85	188.0	91.4	48.6	1046	89	93
9	90	192.0	95.4	49.7	1075	118	117

The contribution of the low-resistance TL to the improvement of the current reversal can be seen from the current measurements, recorded in Table A.8, using one of the modified capacitor bank.

In the last two capacitor bank systems, the tuning inductors were made of copper instead of aluminum, which resulted in increasing the current reversal further to approximately 74%. Typical G/S displacements achieved with one of these systems are summarized in Table A.9.

One of the modified capacitor banks was used in the components buildings at Pickering 'B' NGS, in conjunction with a full-scale fuel channel mock-up, to establish statistically the most suitable procedure for field operation. The objectives were:

a) To determine the optimum location of the electromagnetic coil with respect to the eddy-current probe reading, which indicates the location of the center of mass of the G/S, to account for the statistically varying amount of tilt.

TABLE A.8

Measurements of the impulse current using a modified capacitor bank with the original and the new 10.7 m long TL

Capacitor Bank Energy Setting (%)	Charging Voltage (kV)	Original TL (supplied by Maxwell Laboratories)		New TL Made of the Low-Resistance Cable	
		1st Current Peak (kV)	Current Reversal (%)	1st Current Peak (kV)	Current Reversal (%)
40	6.32	112.7	49	127.1	71
50	7.07	125.9	50	141.5	71
55	7.42	–	–	148.7	71
60	7.75	136.7	53	155.8	72
65	8.06	148.7	47	160.6	72
75	8.66	157.0	50	–	–

TABLE A.9

G/S displacements achieved with a modified capacitor bank having a tuning coil made of copper.

Shot No	% Energy Setting of the 200 kJ Capacitor Bank	1st Current Peak (kA)	% Current Reversal	G/S Displacement	
				Front of the Coil (mm)	Back of the Coil (mm)
1	10	60	72	4	6
2	20	86	72	13	15
3	30	103	76	25	31
4	40	122	72	43	63
5	50	136	74	58	95
6	55	144	72	97	95
7	60	153	71	125	115
8	60	153	72	109	135

b) To determine the amount of coil advancement between successive shots when the eddy-current inspection is performed after two or more shots.

The first sequence of tests consisted of applying a single shot, at a first current peak of 142 kA, and of performing an eddy-current inspection after each shot. The amount of G/S tilt was assumed to be 4 cm, hence the reference point of the electromagnetic coil was located at 2.0 cm from the reading of the eddy-current probe. Two G/S located in the full-scale full channel mock-up, one near the middle of the channel, the other at about quarter length of the P/T from the rolled joint, were used to simulate various pinching conditions. The results of ten shots on each G/S using a coil built at Bruce GS 'B' are shown in Table A.10.

The second sequence of tests was performed as described above except that the amount of G/S tilt was assumed to be 2.0 cm, ie, the electromagnetic coil was located at 1.0 cm from the reading of the eddy-current probe. Table A.11 shows the G/S displacements achieved in this sequence. Other sequences of tests assuming different G/S tilt resulted in an overall G/S displacement less than 29 mm per shot. Therefore, the 2.0 cm tilt was adopted as a

TABLE A.10

G/S displacement in the full-scale fuel channel mock-up at 142 kA, 72% current reversal, 950 Hz, with an eddy-current inspection after every shot (assumed TILT = 4 cm)

Shot No	Displacement of G/S #1 (located near the middle of the P/T) (mm)	Displacement of G/S #2 (located at ~ 1/4 length of the P/T) (mm)
1	40	40
2	20	30
3	10	30
4	20	30
5	20	40
6	20	30
7	20	30
8	20	20
9	20	30
10	20	30
Average Displacement	21 mm/shot	31 mm/shot
Overall Average Displacement	26 mm/shot	

TABLE A.11

G/S displacement in the full-scale fuel channel mock-up at 142 kA, 72% current reversal, 950 Hz, with an eddy-current inspection after every shot (assumed TILT = 2.0 cm)

Shot No	Displacement of G/S #1 (located near the middle of the P/T) (mm)	Displacement of G/S #2 (located at ~ 1/4 length of the P/T) (mm)
1	20	60
2	10	40
3	20	40
4	20	40
5	60	30
6	10	30
7	10	40
8	20	30
9	10	40
10	20	40
Average Displacement	20 mm/shot	38 mm/shot
Overall Average Displacement	29 mm/shot	

base line to specify the initial position of the electromagnetic coil.

In a sequence of tests where a second shot was applied on each G/S after advancing the electromagnetic coil by 25 mm toward the G/S (without performing an eddy-current inspection), the overall average G/S displacement was found to be 22.5 mm per shot. Hence it was recommended that an eddy-current inspection be made after every shot if the objectives were to maximize the average G/S displacement per shot. This recommendation would become more important if the current level was increased to 160 kA or more, since the G/S displacement achieved at 160 kA was approximately double the G/S displacement achieved at 142 kA.

APPENDIX B

FINITE ELEMENT PROCEDURE - SUPPLEMENTARY INFORMATION

This appendix presents the important intermediate steps involved in developing the finite element solution described in Chapter 4. The details summarized refer to the simplex triangular element in two-dimensional Cartesian coordinates. The developed finite element matrices are modified slightly and used for the analysis of axisymmetric vector field problems via the formulation described in Chapter 4.

As indicated earlier, the finite element method is based upon the concept of approximating a continuous function by a discrete model comprised of a set of piecewise continuous functions which are defined over each element in the region [91]. The most popular form of the element function is the polynomial. The triangular elements used in this study have straight side, three nodes, and a first order approximating polynomial of the form (simplex function):

$$A_\phi = \alpha_1 + \alpha_2 x + \alpha_3 y \qquad \text{(B-1)}$$

where α_1, α_2 and α_3 are constants. Note that the nodal values of the variable A_ϕ are denoted by A_i, A_j and A_k (without the ϕ subscript for simplicity). The labeling of the nodes in this thesis consistently proceeds counter-clockwise from node i which is arbitrarily specified. The coordinates pairs of the three nodes (i, j and k) are (x_i, y_i), (x_j, y_j) and (x_k, y_k). The interpolating polynomial of equation (B-1) takes the following values at each node:

$$\begin{aligned} A_i &= \alpha_1 + \alpha_2\, x_i + \alpha_3\, y_i \\ A_j &= \alpha_1 + \alpha_2\, x_j + \alpha_3\, y_j \\ A_k &= \alpha_1 + \alpha_2\, x_k + \alpha_3\, y_k \end{aligned} \qquad \text{(B-2)}$$

Solution of the above equations for α_1, α_2 and α_3 yields:

$$\begin{aligned} \alpha_1 &= \frac{1}{2\Delta}\left[(x_j y_k - x_k y_j)A_i + (x_k y_i - x_i y_k)A_j + (x_i y_j - x_j y_i)A_k\right] \\ \alpha_2 &= \frac{1}{2\Delta}\left[(y_j - y_k)A_i + (y_k - y_i)A_j + (y_i - y_j)A_k\right] \\ \alpha_3 &= \frac{1}{2\Delta}\left[(x_k - x_j)A_i + (x_i - x_k)A_j + (x_j - x_i)A_k\right] \end{aligned} \qquad \text{(B-3)}$$

where 2Δ is twice the area of the triangular element and is given by the determinant

$$2\Delta = \begin{vmatrix} 1 & X_i & Y_i \\ 1 & X_j & Y_j \\ 1 & X_k & Y_k \end{vmatrix}$$

Substitution of the equations for α_1, α_2 and α_3 into equation (B-1) and rearrangement produce the following element equation which has three shape functions, one for each node:

$$A_\phi = N_i A_i + N_j A_j + N_k A_k \qquad \text{(B-4)}$$

where

$$N_i = \frac{1}{2\Delta}\left[a_i + b_i x + c_i y\right]$$

$$N_j = \frac{1}{2\Delta}\left[a_j + b_j x + c_j y\right] \qquad \text{(B-5)}$$

$$N_k = \frac{1}{2\Delta}\left[a_k + b_k x + c_k y\right]$$

and

$$a_i = x_j y_k - x_k y_j \;,\quad b_i = y_j - y_k \;,\quad c_i = x_k - x_j$$

$$a_j = x_k y_i - y_k x_i \;,\quad b_j = y_k - y_i \;,\quad c_j = x_i - x_k$$

$$a_k = x_i y_j - x_j y_i \;,\quad b_k = y_i - y_j \;,\quad c_k = x_j - x_i$$

The evaluation of N_i at node i produces:

$$N_i = \frac{1}{2\Delta} (a_i + b_i x + c_i y) = 1$$

while evaluation of N_i at nodes j and k and at all points on the line passing through these nodes yields $N_i = 0$.

The variable A_ϕ is a function of a set of shape functions which are linear in x and y. Therefore, the gradients in either the x or y directions is constant. This means that many small elements have to be used to approximate a rapid change in the value of A_ϕ.

The determination of the system of equations for the nodal values of A_ϕ by the minimization of the energy functional (equation (4.44)), involves the integration of the shape functions or their derivatives or both over the element. It is easier to perform this integration when the interpolation equation is written in terms of an element coordinate system, located on or within the boundaries of the element. A particularly useful local coordinate system for the triangular element is the well known area coordinate system [68,90,91,104-107]. This system consists of three coordinates L_1, L_2 and L_3, each defined as the ratio of a perpendicular distance from one side to the altitude of that

same side. Hence each of these length ratios vary between 0 and 1. The name area coordinates was given to L_1, L_2 and L_3 because their values give the area of sub-triangles relative to the total area of the considered element; thus they obey the following relationship

$$L_1 + L_2 + L_3 = 1 \tag{B-7}$$

Examination of the properties of L_1, L_2 and L_3 reveals that these coordinates are also the shape functions for the simplex linear element. It can be easily shown that A_ϕ can be expressed by:

$$A_\phi = L_1 A_i + L_2 A_j + L_3 A_k \tag{B-8}$$

The real advantage of using the area coordinates is the existence of integration equations [91], which simplify the evaluation of length and area integrals. These are:

$$\int_\ell L_1^a L_2^b \, d\ell = \frac{a!b!}{(a + b + 1)!} \ell \tag{B-9}$$

$$\int_\Delta L_1^a L_2^b L_3^c \, d\Delta = \frac{a!b!c!}{(a + b + c + 2)!} 2\Delta \tag{B-10}$$

where ℓ is the distance between two nodes. It defines the edge under consideration. The use of area coordinates is also useful to prove the existence of continuity between triangular elements. Reference 91 presents the proof of this continuity and shows that the criteria for convergence of the finite element method toward the correct answer is satisfied.

Having developed the necessary interpolating polynomials for an individual element, development of a set of equations for the entire domain can be initiated. More specifically, the objective is to embed each element into the region and to express the interpolation equation in terms of the global coordinates and the global nodal values. The end result can be represented by the relation:

$$A_\phi = \sum_{e=1}^{E} A_\phi^{(e)} \qquad \text{(B-11)}$$

where E is the number of elements. Details on this collection process are abundant in the literature on finite element.

The energy functional given in equation (4.44) must be minimized with respect to the set of nodal values

$\{A_\phi\}$. This minimization can be performed before evaluating the integrals of this functional:

$$F(A_\phi) = \frac{1}{2} \iint \frac{1}{\mu} [(\frac{\partial A_\phi}{\partial x})^2 + (\frac{\partial A_\phi}{\partial y})^2] dxdy + \iint A_\phi(\sigma\frac{\partial A_\phi}{\partial t} - J_0) dxdy \quad \text{(B-12)}$$

Two matrices can be defined as follows:

$$\{g\}^T = [\frac{\partial A_\phi}{\partial x} \; \frac{\partial A_\phi}{\partial y}] \quad \text{(B-13)}$$

and

$$[D] = \begin{bmatrix} \frac{1}{\mu} & 0 \\ 0 & \frac{1}{\mu} \end{bmatrix} \quad \text{(B-14)}$$

where T denotes transpose and μ is the magnetic permeability ($\mu = \mu_r\mu_0$; $\mu_r = 1$). Equation (B-12) can now be written as:

$$F(A_\phi) = \iint \frac{1}{2} [\{g\}^T[D]\{g\}] dxdy - \iint A_\phi(J_0 - \sigma \frac{\partial A_\phi}{\partial t}) dxdy \quad \text{(B-15)}$$

Recalling that the defined functions for A_ϕ are continuous over individual elements ($A^{(e)}$) and not over the region, the integrals in equations (B-15) must be separated into integrals over the elements, yielding:

$$F(A_\phi) = \sum_{e=1}^{E} \iint \frac{1}{2} \left[\{g^{(e)}\}^T [D^{(e)}] \{g^{(e)}\}\right] dxdy - \iint A_\phi^{(e)} \left(J_0^{(e)} - \sigma^{(e)} \frac{\partial A_\phi^{(e)}}{\partial t}\right) dxdy \tag{B-16}$$

This equation can also be written in the symbolic form as:

$$F(A_\phi) = F(A_\phi)^{(1)} + F(A_\phi)^{(2)} + \text{-----} + F(A_\phi)^{(E)} = \sum_{e=1}^{E} F(A_\phi)^{(e)} \tag{B-17}$$

where $F(A_\phi)^{(e)}$ is the contribution of a single element to $F(A_\phi)$. The minimum of $F(A_\phi)$ occurs when:

$$\frac{\partial F(A_\phi)}{\partial \{A_\phi\}} = \frac{\partial}{\partial \{A_\phi\}} \sum_{e=1}^{E} F(A_\phi)^{(e)} = \sum_{e=1}^{E} \frac{\partial F(A_\phi)^{(e)}}{\partial \{A_\phi\}} = 0 \tag{B-18}$$

In order to evaluate the derivatives in equation (B-18) the integrals in (B-16) have to be written in terms of the nodal values $\{A_\phi\}$. Using the general form of the interpolating polynomial:

$$F(A_\phi)^{(e)} = [N^{(e)}] \{A_\phi\} = [N_i^{(e)}, N_j^{(e)}, N_k^{(e)}] \begin{Bmatrix} A_i \\ A_j \\ A_k \end{Bmatrix} \tag{B-19}$$

we can evaluate (B-13), which along with (B-19) can be substituted into (B-16). Starting with $\{g\}$ yields:

$$\{g^{(e)}\} = \begin{Bmatrix} \dfrac{\partial A_\phi^{(e)}}{\partial x} \\ \dfrac{\partial A_\phi^{(e)}}{\partial y} \end{Bmatrix} = \begin{bmatrix} \dfrac{\partial N_1^{(e)}}{\partial x} & \dfrac{\partial N_2^{(e)}}{\partial x} & \dfrac{\partial N_3^{(e)}}{\partial x} \\ \dfrac{\partial N_1^{(e)}}{\partial y} & \dfrac{\partial N_2^{(e)}}{\partial y} & \dfrac{\partial N_3^{(e)}}{\partial y} \end{bmatrix} \begin{Bmatrix} A_i \\ A_j \\ A_k \end{Bmatrix} \quad \text{(B-20)}$$

or

$$\{g^{(e)}\} = [B^{(e)}]\ \{A_\phi\} \quad \text{(B-21)}$$

where $[B]$ contains information related to the derivatives of the shape functions. Using (B-19) and (B-21) allows the integrals in (B-16) to be written as:

$$F(A_\phi)^{(e)} = \iint \frac{1}{2}\ \{A_\phi\}^T[B^{(e)}]^T[D^{(e)}][B^{(e)}]\{A_\phi\}dxdy - \iint [N^{(e)}]\ \{A_\phi\}J_0\ dxdy + \iint \sigma[N^{(e)}]\ \{\dot{A}_\phi\}\ [N^{(e)}]\ \frac{\partial\{A_\phi\}}{\partial t}\ dxdy \quad \text{(B-22)}$$

The differentiation of (B-22) with respect to $\{A_\phi\}$ can now be accomplished; it yields:

$$\frac{\partial F(A_\phi)^{(e)}}{\partial\{A_\phi\}} = \iint [B^{(e)}]^T [D^{(e)}] [B^{(e)}] \{A_\phi\} dxdy -$$

$$\iint [N^{(e)}]^T J_0 \, dxdy + \iint \sigma [N^{(e)}]^T [N^{(e)}] dxdy \frac{\partial\{A_\phi\}}{\partial t}$$

(B-23)

This set of integrals can be written in the condensed form:

$$\frac{\partial F(A_\phi)^{(e)}}{\partial\{A_\phi\}} = [k^{(e)}]\{A_\phi\} + \{f^{(e)}\} + [c^{(e)}] \frac{\partial\{A_\phi\}}{\partial t} = 0 \quad \text{(B-24)}$$

where

$$[k^{(e)}] = \iint [B^{(e)}]^T [D][B^{(e)}] dxdy \quad \text{(B-25)}$$

$$[f^{(e)}] = - \iint J_0 [N^{(e)}]^T dxdy \quad \text{(B-26)}$$

$$[c^{(e)}] = \iint \sigma [N^{(e)}]^T [N^{(e)}] dxdy \quad \text{(B-27)}$$

The final system of equations has the form:

$$[K]\{A_\phi\} + \{F\} + [C] \frac{\partial\{A_\phi\}}{\partial t} = 0 \quad \text{(B-28)}$$

where

$$[K] = \sum_{e=1}^{E} [k^{(e)}] \quad , \quad \{F\} = - \sum_{e=1}^{E} \{f^{(e)}\} \text{ and } [C] = \sum_{e=1}^{E} [C^{(e)}].$$

[K] is known as the global stiffness matrix, [C] as the capacitance matrix and {F} is the forcing vector. To evaluate the integrals in equations (B-25) to (B-27), the gradient matrix [B] is written as:

$$[B] = \frac{1}{2\Delta} \begin{matrix} b_i & b_j & b_k \\ c_i & c_j & c_k \end{matrix} \qquad \text{(B-29)}$$

and equations (B-14), (B-19) and (B-29) are used to write:

$$[k^{(e)}] = \iint \frac{1}{4\Delta^2} \begin{matrix} b_i & c_i \\ b_j & c_j \\ b_k & c_k \end{matrix} \begin{matrix} \frac{1}{\mu} & 0 \\ 0 & \frac{1}{\mu} \end{matrix} \begin{matrix} b_i & b_j & b_k \\ c_i & c_j & c_k \end{matrix} \, dxdy$$

which yields:

$$[k^{(e)}] = \frac{1}{4\Delta\mu} \begin{matrix} (b_i b_i + c_i c_i) & (b_i b_j + c_i c_j) & (b_i b_k + c_i c_k) \\ (b_j b_i + c_j c_i) & (b_j b_j + c_j c_j) & (b_j b_k + c_j c_k) \\ (b_k b_i + c_k c_i) & (b_k b_j + c_k c_j) & (b_k b_k + c_k c_k) \end{matrix} \qquad \text{(B-30)}$$

The integral in forcing vector is also easily evaluated if area coordinates are employed. Assuming that J_0 is constant within the element yields:

$$[f^{(e)}] = -J_0 \iint \begin{bmatrix} L_1 \\ L_2 \\ L_3 \end{bmatrix} dxdy = \frac{J_0 \Delta}{3} \begin{bmatrix} 1 \\ 1 \\ 1 \end{bmatrix} \qquad \text{(B-31)}$$

Using the relation in (B-10) in evaluating (B-27) yields:

$$[c^{(e)}] = \frac{\sigma \Delta}{12} \begin{bmatrix} 2 & 1 & 1 \\ 1 & 2 & 1 \\ 1 & 1 & 2 \end{bmatrix} \qquad \text{(B-32)}$$

Equations (B-30) to (B-32) can be used according to standard collection procedures to assemble the global matrix and forcing vector.

APPENDIX C

GENERAL DESCRIPTION OF THE COMPUTER PROGRAM

The general algorithm for the numerical solution has been described briefly in chapter 4 (section 4.7). This algorithm was implemented according to the general flow diagram shown in Figure C.1. The flow chart summarizes the major tasks to be performed by the computer program.

The computer program developed to execute the above algorithm was designed in a modular form to ensure a high degree of flexibility and to take advantage of some available subroutines that solve large sets of linear algebraic equations in a highly efficient and economical fashion. The program consisted of one main routine (the main program) and several subroutines. The main program only contained a set of instruction to invoke the required subroutines in the appropriate sequence. Figure C.2 illustrates the organization of the computer program and highlights the functions performed by each subroutine.

Detailed description of each subroutine is too long to be included in this thesis. However, the following comments summarize the main features of the computer program:

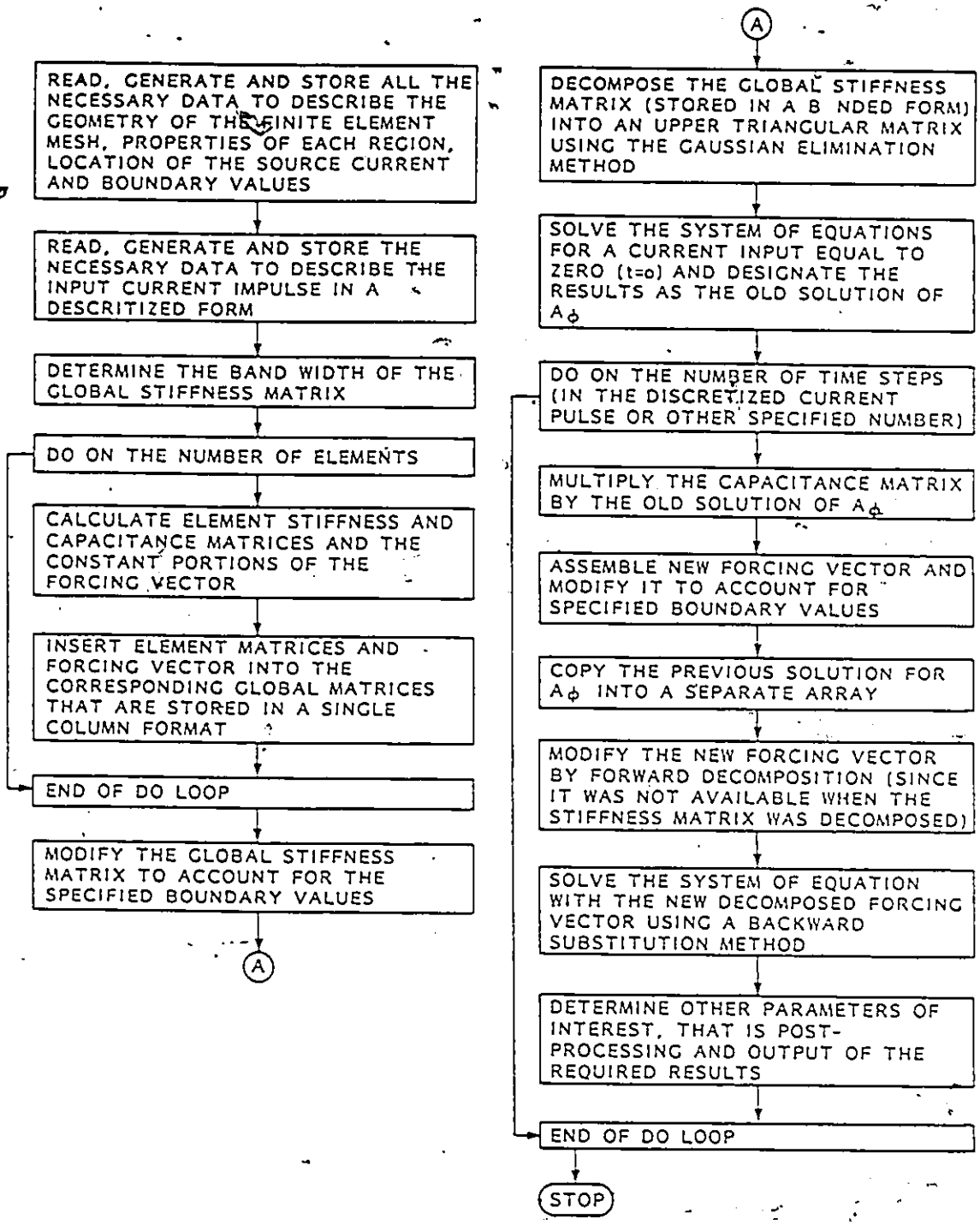

Figure C.1

General flow diagram for the numerical solution algorithm.

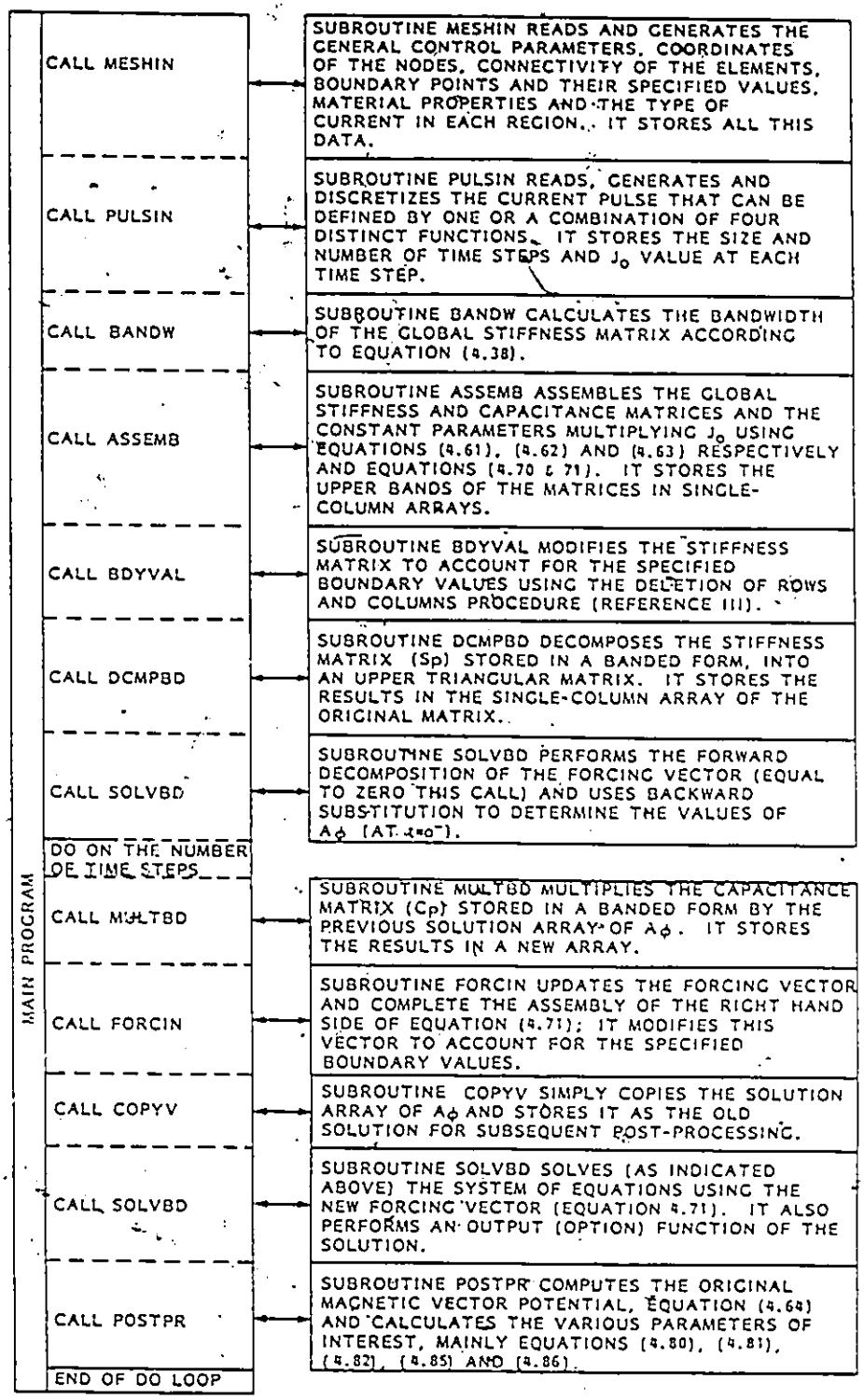

Figure C.2

General organization of the computer program.

1. Subroutine MESHIN is a semi-automatic finite-element mesh generator; it generates most of the input data needed to describe the subdivision of the considered configuration. For example, on any line segment having equally spaced nodes only the node number and coordinates of the first and last node have to be read, data for the nodes in between is generated by the program. Similarly, in any sequence of elements located in a particular region of the configuration only the data defining the first and last element of the sequence is read while data defining the other elements is generated by the program. The boundary nodes and their values are also treated in a similar fashion.

   In addition to reducing the amount of labour involved in defining the geometry of the finite element mesh, this subroutine facilitates the task of checking the correctness of the input data considerably.

2. Subroutine PULSIN has the capability to describe current pulses of practically any shape and to discretize them using a specified number of time steps. The current pulse can be divided into a specified number of main segments; in each segment one

of four functions can be used to describe the variation of the current. These functions are: constant (or a step function), sinesoidal, exponential and exponentially decaying sinewave. Other functions can be easily added to the subroutine. The current density distribution in the coil turns is calculated and stored for all of the constituent time steps. The main advantage of this subroutine is that it allows the program to deal with basically any type of current input simply by preparing appropriate input data file.

3. Subroutine ASSEMB uses the efficient "direct stiffness" method [91] to assemble the stiffness matrix [Sp] (see equations (4.70) and (4.71)). All of the coefficients in the system of equations are stored in a single column vector {M} as shown below:

$$M = \begin{Bmatrix} \{A_\phi\} \\ \{F\} \\ [S_p] \end{Bmatrix}$$

where $\{A_\phi\}$ is the array of unknown variable, $\{F\}$ is the right hand side or the forcing vector of the system of equations, and $[S_p]$ is the global stiffness matrix. This technique eliminates the need to

dimension the individual components $\{A_\phi\}$, $\{F\}$ and $[S_p]$, and greatly reduces the probability of committing mistakes. The banded matrix concept is also incorporated into this subroutine to reduce the amount of required computer storage. Further reduction of the storage requirement can be obtained by using the technique outlined in reference 122. This technique avoids storing the non-significant zero entries within the bands of the matrix and uses special arrays to store the location of these entries. For this study, it was felt that the amount of additional saving in memory storage offers only a marginal advantage when the additional required arrays and programming efforts are considered.

4. Subroutine BDYVAL modifies the stiffness matrix $[S_p]$ and the preliminary forcing vector (for $t = 0^-$), to account for the specified boundary values using the procedure of deletion of rows and columns [91].

5. Subroutines DCMPBD and SOLVBD perform the three main steps involved in solving the system of finite element equations. Subroutine DCMPBD decomposes the band matrix $[S_p]$ into an upper triangular matrix using the Gaussian elimination procedure. SOLVBD first

decomposes the forcing vector and then solves for A_ϕ using the procedure of backward substitution described in detail in reference 91.

This computer program was developed and tested using various cases for which analytical formulae are available before it was used to analyze the G/S repositioning problem, as outlined in chapter 5.